



8-2019

**Modern Data Acquisition, System Design, and Analysis
Techniques and their Impact on the Physics-based Understanding
of Neutron Coincidence Counters used for International
Safeguards (draft)**

Angela Moore
University of Tennessee

Follow this and additional works at: https://trace.tennessee.edu/utk_graddiss

Recommended Citation

Moore, Angela, "Modern Data Acquisition, System Design, and Analysis Techniques and their Impact on the Physics-based Understanding of Neutron Coincidence Counters used for International Safeguards (draft)." PhD diss., University of Tennessee, 2019.
https://trace.tennessee.edu/utk_graddiss/5956

This Dissertation is brought to you for free and open access by the Graduate School at TRACE: Tennessee Research and Creative Exchange. It has been accepted for inclusion in Doctoral Dissertations by an authorized administrator of TRACE: Tennessee Research and Creative Exchange. For more information, please contact trace@utk.edu.

To the Graduate Council:

I am submitting herewith a dissertation written by Angela Moore entitled "Modern Data Acquisition, System Design, and Analysis Techniques and their Impact on the Physics-based Understanding of Neutron Coincidence Counters used for International Safeguards (draft)." I have examined the final electronic copy of this dissertation for form and content and recommend that it be accepted in partial fulfillment of the requirements for the degree of Doctor of Philosophy, with a major in Nuclear Engineering.

Jason P. Hayward, Major Professor

We have read this dissertation and recommend its acceptance:

Charles L. Britton, Howard Hall, Lawrence Heilbronn, Stephen Croft

Accepted for the Council:

Dixie L. Thompson

Vice Provost and Dean of the Graduate School

(Original signatures are on file with official student records.)

**Modern Data Acquisition, System Design, and Analysis Techniques
and their Impact on the Physics-based Understanding of Neutron
Coincidence Counters used for International Safeguards**

A Dissertation Presented for the
Doctor of Philosophy
Degree
The University of Tennessee, Knoxville

Angela Simone Moore
August 2019

Copyright © 2019 by Angela Simone Moore
All rights reserved.

Acknowledgements

I would first like to thank my major advisor, Dr. Jason Hayward, for helping make this accomplishment possible. You have been a great support throughout this process. I appreciate your continuous willingness to listen and offer feedback, your generous assistance to make participating in valuable courses and conferences possible, for teaching, and nominations of my work, and for being the kind man that you are.

I would also like to thank my mentor Dr. Stephen Croft for all of his help, knowledge, patience, and perfectly balanced sarcasm over the last four years. You have taught me more than I will ever remember, and you have directed and shaped my skills to support interests that I am excited to make into a career. I am thankful for your friendship, consideration, and witty remarks— without any of which would have made this a more trying journey.

Thank you to my second laboratory mentor, Dr. Louise Worrall, for her thoughtfulness, kindness, and willingness to support my ideas as this dissertation developed. Your project management skills have helped me greatly and I am grateful for all the opportunities you laid out for me and included me in. Through your backing and input I was able to form a successful dissertation topic and pull together the resources to make it all possible.

A special thank you to the Oak Ridge Safeguards and Security Technology group for always welcoming me as a respected member of the group, teaching me, assisting me, sitting with me in the labs so I could take measurements, and laughing with me at lunch. A special thank you to Bob McElroy for grounding my work with your extensive practical knowledge and ensuring I knew what I was talking about. Thank you to Nance Ericson for finding the time to address my questions and concerns even when you were stretched incredibly thin. Thank you to Chuck Britton for your attempts to turn me “to the dark side” of EE.

Thank you to my committee members for providing meaningful feedback throughout the preparation of the presentation of this work and for sparking ideas for my studies with your insightful courses and throughout the laboratory during my academic career.

A sincere thank you to my previous teachers, professors, and undergraduate advisor, Dr Stephen Padalino, who fostered my goals by granting me the opportunity to participate in research early on, while inspiring me with their dedication to the subject. This journey has been a long one, and without them, I would not have started, or been encouraged to continue, along this path.

Thank you to my girls for always encouraging me, supporting me, and being my escape when I am stressed.

An immense thank you to my family for always being there for me, no matter the distance or challenge faced. Your support and encouragement have helped me realize my goals, and your humor and love have been a source of strength. Thank you for always being my #1 fans and never doubting me.

Lastly, thank you to my incredible husband, Mike. You are my rock when I’m doubtful, my sounding board when I’m stressed, and the best part of every day. Your encouragement, criticism, counsel, and love have allowed me to complete my dissertation with pride and excitement. Thank you for always believing in me and making me believe in myself. And for fixing my flipped fractions. PC4L!

This material is based upon work supported by the US Department of Energy (DOE) National Nuclear Security Administration (NNSA) Office of Defense Nuclear Nonproliferation R&D, and through the Nuclear Science and Security Consortium under Award Number DE-NA0003180.

Abstract

Neutron coincidence counting is a technique widely used in the field of international safeguards for the mass quantification of a fissioning item. It can exploit either passive or active interrogation techniques to assay a wide range of plutonium, uranium, and mixed oxide items present in nuclear facilities worldwide. Because neutrons are highly penetrating, and the time correlation between events provides an identifiable signature, when combined with gamma spectroscopy, it has been used for nondestructive assays of special nuclear material for decades. When neutron coincidence counting was first established, a few system designs emerged as standards for assaying common containers. Over successive decades, new systems were developed for a wider variety of inspection assays. Simultaneously, new system characterization procedures, data acquisition technologies, and performance optimizations were made. The International Atomic Energy Agency has been using many of these original counters for decades, despite the large technological growth in recent years. This is both a testament and an opportunity.

This dissertation explores several topics in which the performance of neutron coincidence counting systems is studied such that their behavior may be better understood from physical models, and their applications may be expanded to a greater field of interest. Using modern list mode data acquisition and analysis, procedures are developed, implemented, and exploited to expand the information obtained of both these systems and sources in question in a common measurement. System parameters such as coincidence time windows, dead time, efficiency, die-away time, and non-ideal double pulsing are explored in new ways that are not possible using traditional shift register logic. In addition, modern amplifier electronics are retrofitted in one model, the Uranium Neutron Coincidence Collar, to allow for a count rate-based source spatial response matrix to be measured, ultimately for the identification of diversion in a fresh fuel assembly. The testing, evaluation, and optimization of these electronics is described; they may serve as a more capable alternative to existing electronics used in IAEA systems. Finally, with a thorough understanding of the system characteristics and performance, neutron coincidence counters may be used to self-certify calibration sources with superior precision to national metrological laboratories.

Table of Contents

Chapter 1 Introduction.....	1
1.1 Neutron Coincidence Counting	4
1.1.1 Nondestructive Analysis	9
1.1.2 Counting System Characterization Parameters	15
1.2 International Safeguards	15
1.2.1 The International Atomic Energy Agency	15
1.2.2 State Obligations Regarding Safeguarding Nuclear Material	18
1.2.3 The Nuclear Fuel Cycle	20
1.2.4 Neutron Coincidence Counting Used in an Inspection	22
1.3 Approved Neutron Coincidence Counters for Nondestructive Assays	22
1.3.1 Coincidence Counters Studied	27
1.3.2 Current Data Acquisition Technologies	29
1.4 Current Limitations of Neutron Coincidence Counting	32
1.5 Addressing the Concerns, A Dissertation Overview	33
Chapter 2 List Mode Data Acquisition and Analysis	35
2.1 Abstract	35
2.2 Introduction	35
2.3 Shift Register Analysis and Detector Characterization Parameters.....	37
2.4 Instrument Setup.....	39
2.5 JCC-71 Characterization using PTR-32	42
2.5.1 High Voltage Characteristic	42
2.5.2 Predelay and Gate width Determination	48
2.5.3 Neutron Die-away Time.....	53
2.5.4 Absolute Efficiency.....	55
2.5.5 Dead Time Determination.....	55
2.5.6 Discussion	57
2.6 Conclusions	58
Chapter 3 Modern Preamplifier, Amplifier, Discriminator Electronics	59
3.1 The Amptek A111 Charge Sensitive Preamplifier and Discriminator Chip	59
3.1.1 The Canberra JAB-01 Preamplifier/Amplifier/Discriminator Boards	61
3.2 ORNL Design Implemented on the JCC-71 Neutron Coincidence Collar, Original Prototype	64
3.2.1 Revealing PTR-32 HV Instabilities	68
3.2.2 Comparison to Standard JAB-01 Preamplifier/Amplifier/Discriminator Boards	73
3.3 ORNL Design Implemented on the JCC-71 Neutron Coincidence Collar, Modified Prototype.....	77
3.3.1 System Testing and Optimization	79
3.4 Discussion.....	83
Chapter 4 Spatial Response Measurements in a new List Mode Neutron Coincidence Collar	84
4.1 Source Position Resolution Using Original JAB-01 Banks	87
4.2 Source Position Resolution Using ORNL Electronics	92
4.2.1 Measurements Using Iteration 1 Electronics	92
4.2.2 Full System Retrofit Measurements Implementing Iteration 2 Electronics	94
4.3 MCNP Simulations.....	99
4.4 Conclusions and Further Work.....	108
Chapter 5 Double Pulsing in the Amptek A111 Charge Sensitive Preamplifier & Discriminator Board-³He Proportional Counter Combination Used in Common Safeguards Neutron Coincidence Counters.....	111
5.1 Investigating the Non-Ideal Behavior Using LMDA	111
5.1.1 Abstract	111

5.1.2	Introduction.....	111
5.1.3	Neutron Coincidence Counting Systems.....	113
5.1.4	Non-Ideal Behavior: Double Pulsing.....	114
5.1.5	Isolating the Behavior: A Comparison between Systems.....	120
5.1.6	ORNL Preamplifier Design.....	122
5.1.7	Double Pulsing Correction for Common A111-based Systems.....	124
5.1.8	Discussion.....	127
5.1.9	Conclusions.....	127
5.2	Methods for Diagnosing and Quantifying Double Pulsing Using Shift Register Logic.....	128
5.2.1	Abstract.....	128
5.2.2	Introduction.....	128
5.2.3	Established Methods of Identifying Double Pulsing.....	130
5.2.4	Double Pulsing Fractions Determined for Various Time Gate Settings.....	134
5.2.5	Double Pulsing Disguised in Traditional Shift Register Measurements.....	137
5.2.6	Double Pulsing Revealed with Non-Traditional Shift Register Measurements.....	144
5.2.7	Double Pulsing Fractions Determined Using a Comparison of High Voltage Characteristics 149	
5.2.8	Conclusion.....	152
Chapter 6 Neutron Coincidence Counting System Dead Time Calculations.....		153
6.1	A Comparison of Methods Using a Boron Coated Straw-Based, High-Level Neutron Coincidence Counter.....	156
6.1.1	Dead Time as a Function of Preamplifier Number.....	161
6.2	A Difference in Values Due to Double Pulsing Using a JCC-71 Neutron Coincidence Collar....	163
Chapter 7 Absolute Source Measurements.....		167
7.1	Absolute Source Measurement ²⁵² Cf Certification Procedure.....	168
7.2	Neutron Pulse Train Extrapolation to Zero Predelay and Infinite Gate Width using PTR-32 List Mode Data Acquisition and Analysis.....	173
7.3	Comparison of Neutron Coincidence Counting Absolute Source Measurements to NIST Certificate Values.....	181
7.4	Uncertainty Determination.....	183
7.5	Conclusion.....	187
Chapter 8 Summary of Research Findings.....		188
8.1	Recommendations for Future Work.....	190
8.1.1	Absolute Source Measurements.....	190
8.1.2	The List Mode Response Matrix.....	190
8.1.3	A New List Mode Data Acquisition System.....	190
8.1.4	Modern Electronics and Advanced System Designs.....	191
8.1.5	Dead Time Modelling Using Monte Carlo Simulation Codes.....	191
References.....		195
Vita.....		202

List of Figures

Figure 1.1. A pulse height spectrum example of a ^3He tube response, indicating the gamma response signal, wall effects, and the thermal capture peak contributions that would be present [6].	3
Figure 1.2. (a) A diagram of a general neutron coincidence counter containing ^3He tubes and a central assay cavity. The different processes that neutrons undergo with relation to detection are shown. (b) An example neutron pulse train illustration showing how correlated neutron events would ideally appear solely from fission events, compared to a typical pulse train with randomly distributed background convoluting these fission events.	6
Figure 1.3. (a) A neutron pulse train illustration indicating which time correlation gates are applied for analysis. (b) A Rossi-alpha distribution showing how this correlation analysis builds a histogram of neutron coincidence events based on these timing windows. [5] (c) An example correlation analysis performed on the neutron pulse train using varying timing gate lengths.	7
Figure 1.4. The nuclear fuel cycle. [25]	21
Figure 1.5. Timeline of IAEA publications containing the list of detectors used in field measurements and their respective applications.	24
Figure 1.6. (a) JCC-71 UNCL (b) N2701 UNCL (c) JCC-51 Large volume variant AWCC (d) Boron coated straw HLNC.	28
Figure 1.7. (a) The Mirion Technologies JSR-12. (b) JSR-14 (c) JSR-15 [28].	31
Figure 2.1. A Rossi- α distribution demonstrating the relevant timing gates for a number of neutron pulses. [5]	38
Figure 2.2. (a) Side view of the JCC-71 Neutron Coincidence Collar with input/output wires connected (b) Illustration and (c) photo of a top-down view of the UNCL showing a ^{252}Cf source placed on a metal stand in the center of the detector body.	41
Figure 2.3. (a) Singles count rate as a function of high voltage with individual channel rates on the left vertical axis and the total detector signal rates on the right vertical axis; (b) Doubles count rate as a function of high voltage.	44
Figure 2.4. Singles count rate as a function of HV shown for data acquired by Canberra using a JSR-15 shift register [68] and data acquired by ORNL using a PTR-32 LMDA system. Differences in count rate are due to 2 different activity ^{252}Cf sources used.	45
Figure 2.5. The ratio of double neutron counts to single neutron counts squared as a function of increasing HV.	47
Figure 2.6. The Rossi- α distribution produced using an uncorrelated neutron AmLi source. The counts recorded in the (R+A) and (A) gates should be approximately equal.	49
Figure 2.7. Bias percentage as a function of predelay for varying gate widths.	49
Figure 2.8. Relative standard deviation of the doubles count rate as a function of gate width for varying predelay values using a ^{252}Cf source.	51
Figure 2.9. (a) Rossi- α distribution through 1024 μs . The channel width is 100 ns. (b) Expanded portion of the Rossi- α distribution between 0 and 6 μs to show non-ideal behavior structure below 2.5 μs .	52
Figure 2.10. A single detector channel Rossi- α distribution with the red exponential fit applied.	54
Figure 2.11. Doubles count rate data obtained by the JSR-15, with a saturating exponential fit applied.	54
Figure 3.1. A photograph of the Amptek A111 chip, with metal housing.	60
Figure 3.2. A diagram illustrating the general pulse processing chain used to analyze the ^3He charge collection signals [75].	60
Figure 3.3. (a) The JAB-01 Board positioned next to the (b) ORNL prototype board (c) the original JCC-71 junction box containing 1 JAB-01 board for 6 ^3He tubes and (d) the new retrofit JCC-71 bank containing 6 ORNL boards for the 6 ^3He tubes.	63

Figure 3.4. (a) Modified JCC-71 junction box to accommodate the new ORNL electronics. The “HV in” position has been moved along with the “+5 V in” and the “Signal in”, “Signal out”, “HV out”, and “+5 V out” have been removed, as seen when compared to the original junction box (b)	63
Figure 3.5. (a) A diagram illustrating the traditional electronics chain used in the original JCC-71. (b) A diagram illustrating the ORNL electronics chain as implemented on the modified JCC-71. (c) A basic illustration of the ORNL electronics retrofit design and placement on 6 ³ He tubes in 1 bank of the JCC-71. [77].....	65
Figure 3.6. An oscilloscope trace of both the unipolar shaper output (brown) and the preamplifier output (green) using in the ORNL circuit. The preamplifier output indicates that the charge was collected quickly in this instance, resulting in a sharp, quick-rising pulse. Note that the vertical scales for these pulses are different, as given on the oscilloscope display [77].	67
Figure 3.7. (a) The two JCC-71 banks with the ORNL electronics on the left and JAB-01 boards on the right. A ²⁵² Cf source is suspended equidistant between the banks for simultaneous comparative measurements. The 6 ORNL LVDS channel outputs are sent to the converter board (b) where they are changed into TTL pulses and output by BNC connections so that they may be recorded using the PTR-32 (c)	67
Figure 3.8. The singles (a) and the doubles HV characteristic (b) measured using the PTR-32 HV supply from 1200-1980 V.....	69
Figure 3.9. The singles (a) and the doubles HV characteristic (b) measured using the PTR-32 HV supply for the range of 1200-1980 V, with all channels from the ORNL preamplifiers disconnected. No HV settings measured an erroneous 0 cps result.....	71
Figure 3.10. The singles (a) and the doubles HV characteristic (b) measured using an Ortec 556 HV supply module and manually changing the HV settings while simultaneously acquiring the signals from the JAB-01–based bank and ORNL–based bank through the PTR-32.....	71
Figure 3.11. (a) A comparison of HV outputs for various settings as studied using a HV probe and oscilloscope. An unstable ripple can be noted between 1260 V and 1420 V. The output signal is relatively clean beyond this region. (b) An oscilloscope trace measured of the PTR-32 HV supply measured at 1340 V on a 1 mV scale. This average shows a ~0.25 mV increase from baseline caused by instabilities in the HV supply.	72
Figure 3.12. The singles (a) and doubles HV characteristic (b) of a ²⁵² Cf source produced using a JSR-15 supply bias, while the data was collected and analysed using PTR-32. The performance between the two banks with differing electronics is matched.	74
Figure 3.13. The singles (a) and doubles HV characteristic (b) produced using a ¹³⁷ Cs source to test the threshold settings of the ORNL electronics. There are no gamma events measured before 1800 V. 74	74
Figure 3.14. The singles (a) and doubles HV characteristic (b) produced by simultaneously using a ¹³⁷ Cs and ²⁵² Cf source to test the threshold settings of the ORNL electronics. The singles HV characteristic supports the threshold setting is sufficient for the operational HV. The doubles HV characteristic has a sporadic behavior that prompted further optimization in a second iteration.....	76
Figure 3.15. The full JCC-71 active system retrofit with iteration 2 electronics (a) , shielded converter boards (b) , and PTR-32 18 channel inputs (c)	78
Figure 3.16. The measurement setup used to measure the 18 channel iteration 2 retrofit.	80
Figure 3.17. The singles (a) and doubles HV characteristic (b) of a ²⁵² Cf source produced using PTR-32 and the full JCC-71 system retrofit with iteration 2 ORNL electronics.....	81
Figure 3.18. The singles (a) and doubles HV characteristic (b) produced by simultaneously using a ¹³⁷ Cs and ²⁵² Cf source. The singles HV characteristic supports the threshold setting is sufficient, with the modifications made between iteration 1 and 2. The doubles HV characteristic is more stable within the operational HV than Figure 3.14, but shows a downward trend beyond 1760 V.....	81
Figure 3.19. The doubles HV characteristic produced using a ¹³⁷ Cs and ²⁵² Cf source. This figure compares the results for both the initial JAB-01–based measurement and the iteration 2 ORNL prototype measurement to highlight how both characteristics have a downward trend beyond ~1760 V.....	82

Figure 4.1. (a) A map of fission events occurring in an example fresh fuel assembly as a function of distance from the AmLi source. (b) List mode response matrix illustrating the coincidence count rate due to AmLi-induced fissions as a function of ^3He tube number from 1–18.	86
Figure 4.2. The experimental setup using the JCC-71 in passive mode, with ^{252}Cf source resting on an axially centralized source stand. The radially center position is shown.....	88
Figure 4.3. The doubles count rate measured in the front detector bank (#2) to the doubles count rate measured in the back detector bank (#4) as the ^{252}Cf source location varied through 9 positions.....	88
Figure 4.4. The doubles count rate measured in the left detector bank (#3) to the doubles count rate measured in the right detector bank (#1) as the ^{252}Cf source location varied through 9 positions.....	89
Figure 4.5. The measured doubles count rates obtained for the 4 original banks of the JCC-71 as a function of ^{252}Cf source position, in addition to the total system output doubles count rate signal... ..	89
Figure 4.6. The measured doubles count rates obtained for various combinations of logic coincidences between the 4 original banks of the JCC-71 as a function of ^{252}Cf source position.....	91
Figure 4.7. The design, and fabricated, XYZ source stand as implemented on the JCC-71.....	93
Figure 4.8.(a) Singles count rate data as a function of applied HV illustrated for each channel. Preliminary indication of spatial response capabilities with additional preamplifiers for each detector bank are shown (b) The source was placed between detector Channels 3 and 4.	93
Figure 4.9. A measured doubles count rate response across all 18 ^3He tubes with a ^{252}Cf source placed in the center of the well of the modified JCC-71.	95
Figure 4.10. A measured doubles count rate response across all 18 ^3He tubes with a ^{252}Cf source placed near banks 1 and 2 (tubes 6 and 7) of the modified JCC-71.	96
Figure 4.11. A measured doubles count rate response across all 18 ^3He tubes with a ^{252}Cf source placed near bank 3 (tube 18) and the active HDPE slab of the modified JCC-71.	97
Figure 4.12. The measured doubles count rates in Tubes 1-18 for ^{252}Cf source positions 0-9 within the JCC-71 well.....	98
Figure 4.13. A comparison of MCNP simulated data and (a) measured singles count rate data and (b) measured doubles count rate data using a ^{252}Cf source placed at the center Position 0 of the modified JCC-71. The MCNP output data has been normalized to the experimental source strength.	101
Figure 4.14. A comparison of MCNP simulated data and (a) measured singles count rate data and (b) measured doubles count rate data using a ^{252}Cf source placed at the top left Position 3 of the modified JCC-71. The MCNP output data has been normalized to the experimental source strength.	102
Figure 4.15. A comparison of MCNP simulated data and (a) measured singles count rate data and (b) measured doubles count rate data using a ^{252}Cf source placed at the bottom right Position 4 of the modified JCC-71. The MCNP output data has been normalized to the experimental source strength.	103
Figure 4.16. A comparison of MCNP simulated data and (a) measured singles count rate data and (b) measured doubles count rate data using a ^{252}Cf source at Position 3. The data has been normalized to the singles count rate measured and simulated for the central position 0 response.	105
Figure 4.17. A comparison of MCNP simulated data and (a) measured singles count rate data and (b) measured doubles count rate data using a ^{252}Cf source at Position 4. The data has been normalized to the singles count rate measured and simulated for the central position 0 response.	105
Figure 4.18. The comparison between LMDA measured data and MCNP simulated data used to determine the (a) neutron die-away time using the doubles count rate trends as a function of gate width and the (b) optimal operational gate width using the relative standard deviation as a function of gate width for the center source position. These values were verified for the other two source positions.	107
Figure 4.19. A MCNP model of the JCC-71 in active mode with Cd liners, the AmLi interrogation source, and a standard 17x17 pressurized water reactor fresh fuel assembly.	110

Figure 5.1. (a) Canberra Industries JCC-71 Neutron Coincidence Collar. (b) Variant on the Canberra Industries JCC-51 Active Well Neutron Coincidence Counter, the large-volume Active Well Coincidence Counter. (c) AnTech N2071 Neutron Coincidence Collar.....	114
Figure 5.2. (a) Measured doubles count rate HV characteristic of the UNCL with individual channel count rate scale on the left and the total detector signal with scale on the right. (b) A measured HV characteristic for a well-behaved neutron coincidence counting system. (c) RAD for a ^{252}Cf measurement with the UNCL for HV range 1560–2000 V, revealing non-ideal behavior centered about 1 μs . (d) A measured RAD characteristic for a well-behaved neutron coincidence counting system.....	116
Figure 5.3. (i) An exaggerated representation of various pulse shapes collected on the central anode wire of a ^3He tube, caused by the positional dependence of the p and T-induced charge collection from the $^3\text{He}(n,p)\text{T}$ reaction. (a) Triton ionization trajectory is closer to the anode; collection of the triton-induced charge cloud is smaller and collected earlier in time than the charge cloud generated by the proton. (b) Charged particle trajectories at an intermediate angle; it is more difficult to resolve the two individual charge collection peaks. (c) The particles' trajectories are parallel to the anode; charge collection time is the same. (d) Proton ionization trajectory is closer to the anode; collection of the proton-induced charge cloud is larger and collected earlier in time than the charge cloud generated by the triton. (ii) An example neutron pulse train with red double pulsing, events highlighting the possible false counts that could be measured [48].....	117
Figure 5.4. Oscilloscope captures of two different neutron events measured in the JCC-71 with ORNL preamplifiers before their optimization. These captures highlight the difference in the effects that pulse shape and amplitude can have on the number of events measured by the system, dependent on pulse shaping time and threshold settings. (a) The charge collection peaks for the proton and triton are distinguishable; however, because the measured voltage does not drop below the set threshold between the peaks, a single neutron event is measured. (b) The charge collection peaks for the proton and triton are marginally distinguishable and have a lower voltage amplitude than the previous pulse. Because the voltage signal dips below the threshold between charge collection peaks, two events are measured instead of one.	119
Figure 5.5. (a) A comparison of the RAD of the large volume JCC-51 AWCC compared with that of the JCC-71 UNCL. The spike is again measured at 1 μs . (b) A comparison of the RAD of the AnTech N2071 compared with that of the JCC-71. The spike is again measured at 1 μs , but it drifts in time as the HV is increased.	121
Figure 5.6. The RAD obtained from one bank of the JCC-71 retrofitted with ORNL-designed preamplifiers shown for HVs from 166 to 1980 V. (a) A 0–20 μs subsection of the 0–1024 μs bin range shown at the right (b)	121
Figure 5.7. (a) Original JAB-01 board within the JCC-71 junction box. (b) A comparison between the JAB-01 circuit board and the new ORNL board (right). (c) Six ORNL boards placed within the JCC-71 junction box.....	123
Figure 5.8. (a) The HV characteristic comparison between the JAB-01 boards and the ORNL boards. (b) A RAD produced for both electronic systems at 1720 V to highlight the lack of double pulsing measured in the ORNL boards.	123
Figure 5.9. (a) RAD for several HVs within the operating regime and beyond, illustrating the effect of double pulsing. (b) RADs normalized to the RAD at 1640 V without double pulsing.....	125
Figure 5.10. (a) RADs produced for a range of HVs RAD within the operating regime and beyond, illustrating the effect of double pulsing (Section 5.1). (b) A HV characteristic produced using the JCC-71 UNCL and PTR-32 LMDA module. The expected “plateau” region is depicted for a coincidence system without double pulsing.	133
Figure 5.11. The measured doubles count rate values as a function of increasing predelay, with set gate width of 64 μs for 1680 V, 1720 V, and 1840 V.....	138

Figure 5.12. The measured doubles count rate values as a function of increasing gate width, with set predelay of 4.5 μs for 1680 V, 1720 V, and 1840 V. Counting statistic error bars are smaller than the data points. The calculated die-away times are also reported for each fit.....	139
Figure 5.13. The calculated bias from the RAD (R+A) and A gates, of 64 μs , across a range of HVs... 143	143
Figure 5.14. The ratio of double neutron count rate to single neutron count rate squared as a function of increasing HV, illustrating inconsistencies in system response due to double pulsing. [89]	145
Figure 5.15. The measured doubles to singles squared count rate ratio values as a function of increasing predelay, with set gate width of 64 μs for 1680 V, 1720 V, and 1840 V.....	145
Figure 5.16. The doubles count rate measured with a 0.5 μs predelay, and 1.5 μs gate width for both a ^{252}Cf source and an AmLi source to reveal double pulsing. Error bars are smaller than the data points.....	147
Figure 5.17. The doubles count rate measured with a 4.5 μs predelay and 64 μs gate width for an AmLi source, as determined through LMDA RAD values and shift register based analysis using PTR-32 timing windows.....	148
Figure 5.18. The HV characteristic (Section 5.1) produced for a simultaneous measurement of one JCC-71 bank with A111 electronics and another bank with ORNL electronics with the given experimental setup. The difference in performance across the HV range is attributed to double pulsing in the A111 and lack of double pulsing in the ORNL boards.....	150
Figure 5.19. The difference in count rate measured between the double pulsing bank and non-double pulsing bank of the JCC-71 for various HVs.....	150
Figure 6.1. An illustration exaggerating the response of a neutron coincidence counting system to separate fission event neutrons. An example neutron coincidence counter is drawn here with 6 separate banks, each with their own preamplifier, separated by the dark gray lines. The yellow and red highlights indicate that the specific bank has captured a neutron and its associated preamplifier electronics are busy processing that event. For the red highlight, the preamplifier was already busy when the second neutron was captured, therefore this event will not be recorded. In reality, dead time may be induced through multiple fission events, or the detection of multiple neutrons from one fission event.....	155
Figure 6.2. The BCS HLNCC showing (a) the six detector bank outputs; (b) the BCS HLNCC-specific conversion box containing electronics to shape and amplify the output signals, resting on the external power supply used for the +5 V; (c) the output signal cables of the conversion box; and (d) PTR-32.....	159
Figure 6.3. A plot of the measured doubles-to-singles count rate ratio as a function of the measured singles count rate. An empirical fit used to determine the dead time parameters is shown as the dotted red curve. The error bars are smaller than the markers.....	159
Figure 6.4. The dead time determined using the statistical analysis approach is shown for a variety of channel combinations in the BCS HLNCC.....	162
Figure 6.5. The RADs produced for the four individual JCC-71 banks and the total summed signal. The dotted black line indicates where the measured count rate stabilizes.....	165
Figure 7.1. (a) Extrapolated doubles count rate estimated for a 0 μs predelay with set gate width by fitting a range of measured data, ignoring charge collection and electronic effects. The structure seen between successive predelay settings is described in the next section. (b) Extrapolated doubles count rate estimated for a 1024 μs gate width with set predelay.....	169
Figure 7.2. (a) Doubles count rate values over a range of predelays, including the PTR-32 calculated value at 0 μs illustrating non-physical behavior. (b) Doubles count rate values from 0.25 μs -10 μs , showing an expected count rate trend.....	174
Figure 7.3. The PTR-32-calculated doubles count rate for various predelays. The orange and blue data points show the oscillating values as given by PTR-32: orange is for every 0.25 and 0.75 μs predelay setting, blue is for every 0.50 and 1.00 μs predelay setting. Their extrapolation difference for the zero predelay intercept is highlighted.....	178

Figure 7.4. (a) Doubles count rate data as a function of increasing predelay setting with a fit applied from 2.0 μ s- 10.0 μ s and extrapolated backwards to determine the intercept for D(0,64). **(b)** Doubles count rate data with a fit applied from 5.0 μ s- 10.0 μ s. **(c)** The deviation of intercepts generated by different fits applied between a starting predelay range of 2.0 μ s and 5.0 μ s to 10.0 μ s. 180

Figure 7.5. (a). The measured doubles count rates obtained for various predelay settings for all three ^{252}Cf sources. A linear fit is applied to each source's data from which the $D_{0,64}$ count rate value is calculated. **(b).** The measured doubles count rate data obtained for an infinite gate width, $D_{4.5,1024}$, for all three ^{252}CF sources. 182

Figure 7.6. (a). The doubles count rate data for various predelay settings reported for twenty cycles of one hour acquisitions. The cut away investigates the scatter in the calculated doubles count rates over these multiple cycles for two specific predelay values. **(b).** The doubles count rate data for various gate width settings reported for twenty cycles of one hour acquisitions. The spread in the calculated doubles count rates increases with increasing gate width. 186

List of Tables

Table 1.1. A list of given IAEA–approved neutron coincidence counters used in inspections to assay non-irradiated samples, as given in [8] [9]. These systems are listed with their commercial model numbers, as available from Mirion Technologies [28] and Antech Inc [29]. [10].....	25
Table 2.1. Calculated Die-Away time and Efficiency for all channels	53
Table 2.2. Dead time values calculated for all four detector channels and the total detector signal	56
Table 2.3. Summary of system characterization parameters obtained through the JSR-15 and PTR-32...	57
Table 3.1. A comparison of settings for iteration 1 and 2 ORNL electronics	77
Table 4.1. A comparison of experimental to simulated calculated system die-away times and fit parameter R_0	106
Table 5.1. Canberra JCC-71 Collar Double Pulsing Normalized to 1640 V, measured source strength: ~40, 500 nps	126
Table 5.2. AnTech Collar double pulsing normalized to 1660 V, measured source strength: ~26, 000 nps	126
Table 5.3. LV AWCC variant on the Canberra JCC-51 double pulsing normalized to 1820 V, measured source strength: ~8,000 nps.....	126
Table 5.4. Canberra JCC-71 Collar Double Pulsing RAD approach, no timing settings (Section 5.1) ...	131
Table 5.5. JCC-71 UNCL Double Pulsing Normalized to 1640 V for various predelays; HV: 1680 V, T _g : 1024 μ s- T _p	136
Table 5.6. JCC-71 UNCL Double Pulsing Normalized to 1640 V for various predelays; HV: 1720 V, T _g : 1024 μ s- T _p	136
Table 5.7. JCC-71 UNCL Double Pulsing Normalized to 1640 V for various predelays; HV: 1680 V, T _g : 64 μ s	136
Table 5.8. JCC-71 UNCL Double Pulsing Normalized to 1640 V for various predelays; HV: 1720 V, T _g : 64 μ s	136
Table 5.9. RAD–based Double Pulsing Percentage, with 4.5 μ s predelay and 64 μ s gate width	136
Table 5.10. JCC-71 UNCL Double Pulsing Normalized to 1640 V for various gate widths; HV: 1680 V, T _p : 4.5 μ s.....	136
Table 5.11. JCC-71 UNCL Double Pulsing Normalized to 1640 V for various gate widths; HV: 1720 V, T _p : 4.5 μ s.....	137
Table 5.12. HV Characteristic–based Double Pulsing Percentage, with 4.5 μ s predelay and 64 μ s gate width, subtraction of singles neutron count rate values	150
Table 5.13. HV Characteristic–based Double Pulsing Percentage, with 4.5 μ s predelay and 64 μ s gate width, subtraction of doubles neutron count rate values	151
Table 6.1. Total detector dead time values calculated using the second order factorial moment.	161
Table 6.2. Comparison of total detector dead time values using the traditional method and the statistical approach.	161
Table 6.3. The dead time values calculated for the JAB-01–based JCC-71 using the statistical analysis method.....	165
Table 7.1. LV AWCC characterization parameters.....	172
Table 7.2. The different doubles count rate values estimated for an approximately zero predelay	175
Table 7.3. Doubles count rates for various predelay settings in 0.05 μ s increments	176
Table 7.4. Doubles count rates for various predelay settings in 0.25 μ s increments	177
Table 7.5. The effective doubles count rate estimated for fits to the measured data in different predelay intervals.....	179
Table 7.6. Absolute source measurement yield comparison to the NIST certificate value	181

Table 7.7. A summary of the different doubles count rates of FTC-CF-1830 and associated yields
calculated for various predelay range fits..... 184

Table 7.8. Doubles count rate values for two effectively infinite gate width settings at 4.5 μ s predelay 184

Chapter 1

Introduction

Neutron coincidence counting is a well-established technique used for the nondestructive quantification of special nuclear material (SNM) and other fissioning isotopes of interest during international safeguards inspections. Neutrons are characteristically highly penetrating particles and are, therefore, quite difficult to shield from detection in either a security or safeguards scenario. Neutrons are also not commonly produced in nature. The sources of neutrons are cosmic rays, nuclear fission, and (α , n) reactions. Therefore, neutrons serve as a strong signature of the presence of fissioning material that is of interest in safeguards, especially when they may be detected in coincidence or higher multiplicities. The gross number of neutrons may be acquired for a source intensity measurement or to locate a neutron source in a search and find application. Time correlation methods may be applied for a more detailed quantification analysis of a known source such as in neutron coincidence or multiplicity analysis. When coupled with gamma spectroscopy, a correlated neutron signal may identify the isotopes present in an item.

However, it is a challenge to measure neutrons. They are neutral particles, and may be born with approximately 2 MeV of energy from a fission reaction. In one method of detecting a neutron, it must be slowed by elastic collisions with nuclei of similar mass, such as high-density polyethylene, to a point where the neutron may be captured by a medium such as ^3He . This hydrogenous moderator is selected in order to have the largest possible scattering cross section so that the maximum amount of energy is deposited by a neutron per interaction. This thermalization, to an energy of 0.025 eV, takes hundreds of microseconds. At this energy, the ^3He will have a maximized neutron capture cross section, which will allow a greater detection efficiency for the system. The transition from fast to detectable speeds occurs at times of 10-100 μs in three phases: slowing down, thermalization, and migration. Slowing down and thermalization occur in only a few microseconds, but the migration, or diffusive, phase follows a $1/e$ time relationship of approximately 20-50 μs in typical counters. This restricts the ^3He detector response time. Due to the numerous collisions, the original locations of these neutrons are obscured. Because of this, most safeguards neutron systems do not rely on spatial resolution or spectroscopy, but rather a neutron count rate. Neutron coincidence counting, in addition to gross neutron counting, relies on the conversion of these captured neutrons into charged particles such that a current may be used to indicate an interaction event. These signals are then analyzed as a function of time to relate the number of trigger events to the number of neutrons produced from the item measured.

^3He gas has been used as the gold standard for neutron detection for decades because of its high thermal neutron absorption cross section and robust performance in high rate applications over long durations. ^3He proportional counters are used in a wide variety of fields including nuclear scattering, nuclear and particle physics, health physics, medical physics, security, and oil well logging, in addition to nuclear safeguards. These tubes have been shown to have a long-lasting reliable performance even when exposed to high radiation. They operate on a relatively low working voltage setting with high gain abilities and they can be used in high rate scenarios.

Gas proportional counters tend to consist of an aluminum or copper cylindrical container housing pressurized gas mixtures, and an inner biased wire of tens to hundreds of micron diameter. The gas-filled proportional detectors function by applying a potential difference between the central anode wire and the wall of the container which is effective as a cathode. The bias may be supplied by a preamplifier, and the resulting charge collection signal is amplified and shaped into a signal that can be analyzed using a lower level discriminator to eliminate noise, such as gamma interactions and wall effects, from true neutron capture events. These logic pulses can then be analyzed in coincidence time windows to determine their relationship to a fissioning event in the material under question.

Neutron coincidence counters are commonly designed with a high-density polyethylene annular body, centered about an inner well for item assay, and are populated with a number of ^3He proportional counting tubes connected to a varying number of preamplifiers. ^3He gas is selected as the preferred detection material for these fission neutrons due to its high thermal neutron cross section paired with excellent gamma–neutron pulse height discrimination. When a neutron interacts with the ^3He gas within the proportional counter, the neutron is captured in the $^3\text{He} (n,p) \text{T}$ reaction. This capture reaction, with a thermal neutron cross section of 5333 barns, releases two charged particles: a proton with 573 keV and a triton having 191 keV with back-to-back trajectories to conserve energy and momentum. These heavy charged particles interact with the surrounding gas through collisions which further ionize the inert ^3He into free electrons and positive ions in a Townsend Avalanche [1]. The electron-ion pairs are created in a number directly proportional to the energy deposited by the neutron; the number of pairs is also directly related to the number of capture reactions, and thereby, neutrons. The ^3He tubes are specifically biased to operate in the proportional counting voltage region of a gaseous detector, above the ion chamber region and below the Geiger region [1]. By operating the ^3He detector in the proportional mode, each avalanche is created independently from the others, and the signal produced by each interaction is proportional to the energy absorbed from the capture of the neutron. Therefore, the incident radiation is able to be measured in distinct interaction events resulting in individual pulses.

Due to the cylindrical geometry of these tubes and the back-to-back release of the primary charged particle pairs, some capture reactions result in the absorption of one of the two heavy charged particles by the tube wall. When this happens, the remaining energy of that particle is absorbed, and not transferred to the ionization of the ^3He gas, which affects the charge collection response. This phenomenon is known as the wall effect, and it creates low energy noise in the pulse height spectrum in the form of a continuum between the full triton energy deposition and the full proton energy deposition (see **Error! Reference source not found.**). Because gamma rays are also produced during fission events but have a low interaction probability with the low density gas, gamma interactions will be measured simultaneously with neutron interactions, due to their ionization of the aluminum or copper in the proportional counter wall, but the energy deposition between the two interactions differs greatly. The energies deposited by these gamma interactions are only tens of keVs compared to the 191 keV of the triton and 573 keV of the proton (**Error! Reference source not found.**). The discriminating threshold value would be ideally set such that all energies on the pulse height spectrum beginning at the triton edge and ending after the full neutron energy peak will indicate a neutron interaction, but any gamma events will not be incorporated into the gross counting performed using these tubes; in reality this is difficult for high rate applications, but it can be optimized to the best ability.

The track lengths of these primary charged particle pairs through the tube will vary based on the gas composition and pressure, which can be calculated using stopping power programs such as TRIM for specific tube characteristics. Typically, the gas is a mixture between ^3He and a quench gas such as CO_2 or Ar/CH_4 . The quench gas helps reduce the range of the proton and triton through the detector's volume by introducing higher Z elements for the primary charged particle pairs to collide with, thereby increasing the stopping power. This reduces the fraction of particles striking the wall, improving the signal to noise ratio, while also improving the electron drift velocities to the anode. Commonly in ^3He proportional counters a mixture of 90% Argon and 10% CH_4 is used, commercially known as P-10 gas. It is important to remove all impurities in the gas, as they are likely to absorb electrons and decrease the avalanche chain through de-excitation through photon emission. Quench gas decreases wall effect, but also increases the number of ion-pairs created by a gamma interaction by introducing gases with lower ionization energies. As with many of the other tube design parameters, a good balance between these two effects must be reached for proper system performance.

Near the cathode, the electric field is not strong enough to accelerate the electrons to cause ionization collisions whereas around the anode, the electric field is the strongest. At approximately two times the radius of the anode wire, the electrons gain enough energy in the field to cause an ionization in a collision with the gas [2]. Due to the avalanche process, most electrons are produced very near to the anode, and therefore do not travel a large distance, preventing the gain of a large amount of energy,

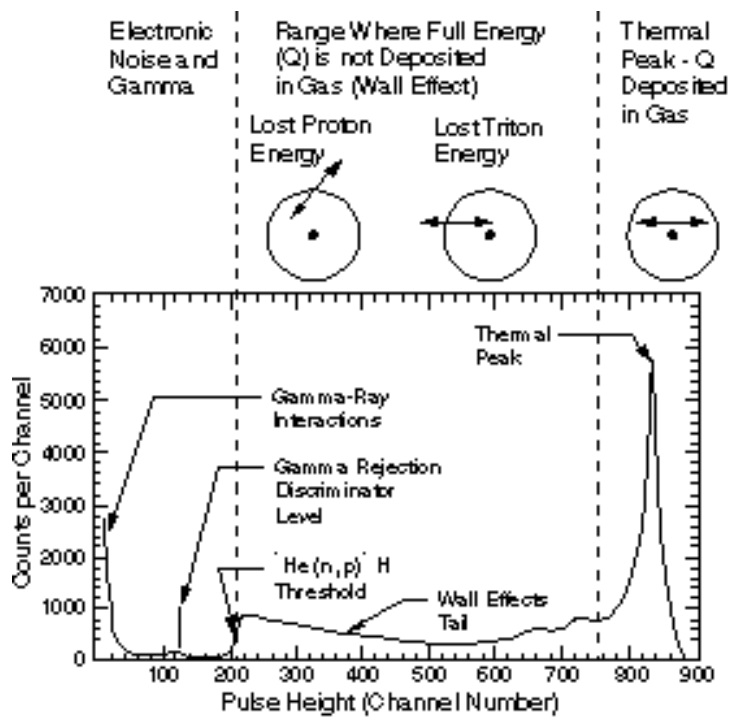


Figure 1.1. A pulse height spectrum example of a ^3He tube response, indicating the gamma response signal, wall effects, and the thermal capture peak contributions that would be present [6].

before reaching the anode. This generates a low amplitude charge collection signal from the electrons.

The reciprocal positive ions travel to the cathode on a much slower timescale, approximately 1000 times slower than the electrons. Because the electrons are produced very near to the anode, the positive ions travel across a majority of the tube's radius before reaching the cathode, thereby gaining much more energy across the electric field. Therefore, the induced charge caused by the movement of the positive ions is what is used to collect a large amplitude signal of the neutron interactions within the gas. This current may be distinguished from the primary current based on the particle drift timescales (nanoseconds compared to microseconds).

The resulting current is input to the preamplifier, which maximizes the signal-to-noise ratio and creates the linear tail pulse such that it may be further integrated, shaped, and amplified by the amplifier circuit to modify the signal into a useable shape and pulse height for the discriminator [1]. The signal has a fast rise time component generated by the induced charge collection of the electrons near the anode, convoluted with the slower component generated by the induced charge collection of the ions as a function of distance from the cathode. The charge collection time of the ion-induced current on the anode has a long signal tail of hundreds of microseconds. Therefore, the shaping time used in the charge integration circuit of the ^3He tubes must encompass at a minimum the rise time of the signal, but should omit some of the long component of the tail to reduce pulse pileup and improve detection efficiency [3]. If a number of counters are connected in parallel to a common preamplifier/amplifier/discriminator then the gamma pile-up is worsened because the pulses are additive.

Typically, a shaping time of 1-4 μs is selected for neutron coincidence counting in order to resolve the separate fission neutron events while minimizing the number of gamma events recorded and minimizing dead time effects. The typical charge collection time of the positive ion drift extends from several microseconds up to the order of milliseconds depending on many different parameters [2] [4]. The charge collection time of the electrons is approximately 1000 times faster. In general, for high rate applications such as with large items or spent nuclear fuel, a shorter shaping time is preferred for sufficient gamma discrimination in order to minimize pulse pileup. For neutron spectroscopy longer shaping times are necessary to ensure the entirety of the pulse's energy is collected, from the full charge collection of the neutron interaction, in order to properly bin the interaction events into an energy spectrum. In addition, the collection of the induced charge cloud as a function of time is related to the orientation of the back-to-back trajectory of the primary charged particle pairs relative to the anode and cathode, and therefore the ionization clouds caused by their interactions with the ^3He gas. Variations in this initial trajectory, ranging from parallel to perpendicular to the anode wire, cause variations in the rise times and long tail component of the signal response. The shaping time must be long enough to integrate over the charge clouds generated by both primary charged particles such that the discriminator does not register two neutron events from a single interaction. Various systems should have an optimized shaping time for their specific geometry, application, and rate application.

As the shaped pulses are evaluated by the discriminator, if their amplitudes cross the set threshold, logic pulses are generated. A record of these logic pulses as a function of time is kept in associated software, indicating the number of neutron interactions in the system during a measurement in addition to their relationship over time. These logic pulses are then analyzed with specified time windows for correlations to produce a single, coincidence, and higher order multiplicity neutron event count rate.

1.1 Neutron Coincidence Counting

The burst-like nature of neutron release from spontaneous and induced fission in SNM allows for multiple neutrons to be detected from a single originating fission event. The fission timescale is less than a picosecond, typically releasing between one and three prompt neutrons. However, background and (α , n) reactions also contribute to the total number of fission events [4] [5]. In addition, not all neutrons produced during a fissioning event will be thermalized or captured; some will leak out of the system and go undetected (**Figure 1.2 a**). For neutron coincidence counting, in order to determine the mass of the

fissioning material, an item is centralized in the counter, and the emitted neutrons are captured by surrounding ^3He -filled tubes. Neutrons from the same fission event are detected close to each other in time, whereas neutrons from non-fission processes are randomly distributed in time (**Figure 1.2 b**). Using time-correlation methods allows these counters and associated software to discriminate against this background and distinguish between events. The highly time-correlated neutron distributions do not obey Poisson statistics, unlike many other types of radioactive decay. Neutron coincidence counters must possess high enough efficiencies to detect correlated events while still distinguishing between successive fission events.

When the item undergoes fission, a random number of neutrons are released, varying from zero to upwards of ten, forming a neutron multiplicity distribution. These detected neutron events are recorded and used to perform time-correlation analysis to ultimately determine the mass of the fissioning material [4] [5]. Each isotope has a unique signature through this analysis. In traditional neutron coincidence counters, only the number of one (totals or singles) and two (pairs, reals or doubles) time-correlated neutron events (defined by shift register logic) are recorded. Meanwhile in neutron multiplicity analysis, the software counts the 0, 1, 2, 3, 4... multiples of neutrons (the multiplicity histogram) within the event-triggered correlation-timing windows. Neutron multiplicity counting requires significantly more efficient counters such that triples (3 correlated neutron events) may be detected in a timely fashion. It is a highly useful technique for mass quantification in some more advanced inspection scenarios, but it will not be discussed here.

Traditionally, shift register acquisition methods are used to collect the neutron signals from the coincidence counters. The shift register is based on a number of clock-driven flip-flop circuits linked together in a number of stages [4] [5]. The incoming pulses shift through the different stages, over the circuits' characteristic time. During this length of time, the electronics are busy and will not be able to process future events. Events that are registered during this time are stored in a buffer to then be processed after the circuit is no longer busy to prevent dead time and a high loss of events; if the buffer capacity is sufficient for the count rate, this introduces a marginal dead time for the full system. These pulses can then be compared with every other pulse to perform this time-correlation analysis with respective timing windows. The associated up/down counter keeps a record of the number of events being processed in the circuit over time. When another pulse is detected, the counter is incremented, and when the pulse passes through the final stage, the counter is decremented. This keeps a running tally of the number of pulses measured. From this time correlation analysis, the number of singles and doubles may be calculated for each acquisition. Despite the number of preamplifiers used on a system, traditionally the total summed signal from the system is recorded and analyzed using one signal in to the shift register.

These timing windows consist of four gates: a predelay, (R+A) gate width, a long delay, and an A gate (**Figure 1.3 a**). The predelay, T_p , is a short timing gate, typically 4.5 μs for standard neutron coincidence counters, used to account for any electronic artifacts influencing the neutron pulse train.

Following a triggering event, the predelay is open and the system does not record any measured events during this duration. During this time, the system experiences charge collection and dead time effects from the processing time of the electronics. However, during this time, there is a greater probability of detecting another correlated neutron event relative to the trigger event. Therefore, it is important to balance the length of this time window between mitigating the dead time and charge collection effects and losing correlated neutron events. Following the predelay, the (R+A) gate width, T_g , opens for a typical length of 64 μs .

The (R+A) gate is derived from the Rossi-alpha distribution (**Figure 1.3 b**). This distribution was initially developed for reactor noise analysis [7] and is commonly used in neutron coincidence counting analysis. The Rossi-alpha distribution is a histogram of the doubles count rate measured in the coincidence system as a function of time. It is produced through the neutron pulse train record time stamps, and it provides a great deal of information about the counting system. After an initial triggering neutron event is measured, the frequency at which another neutron is measured relative to that trigger is recorded over a range of time for selected time bins. Every measured neutron event acts as a trigger;

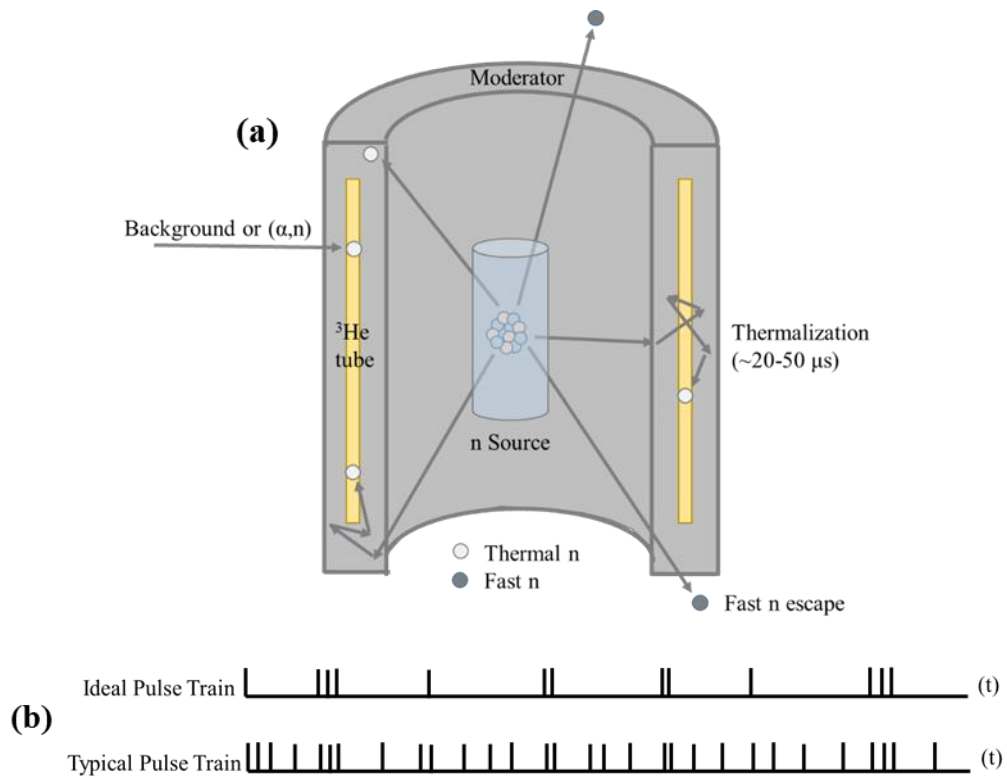


Figure 1.2. (a) A diagram of a general neutron coincidence counter containing ^3He tubes and a central assay cavity. The different processes that neutrons undergo with relation to detection are shown. (b) An example neutron pulse train illustration showing how correlated neutron events would ideally appear solely from fission events, compared to a typical pulse train with randomly distributed background convoluting these fission events.

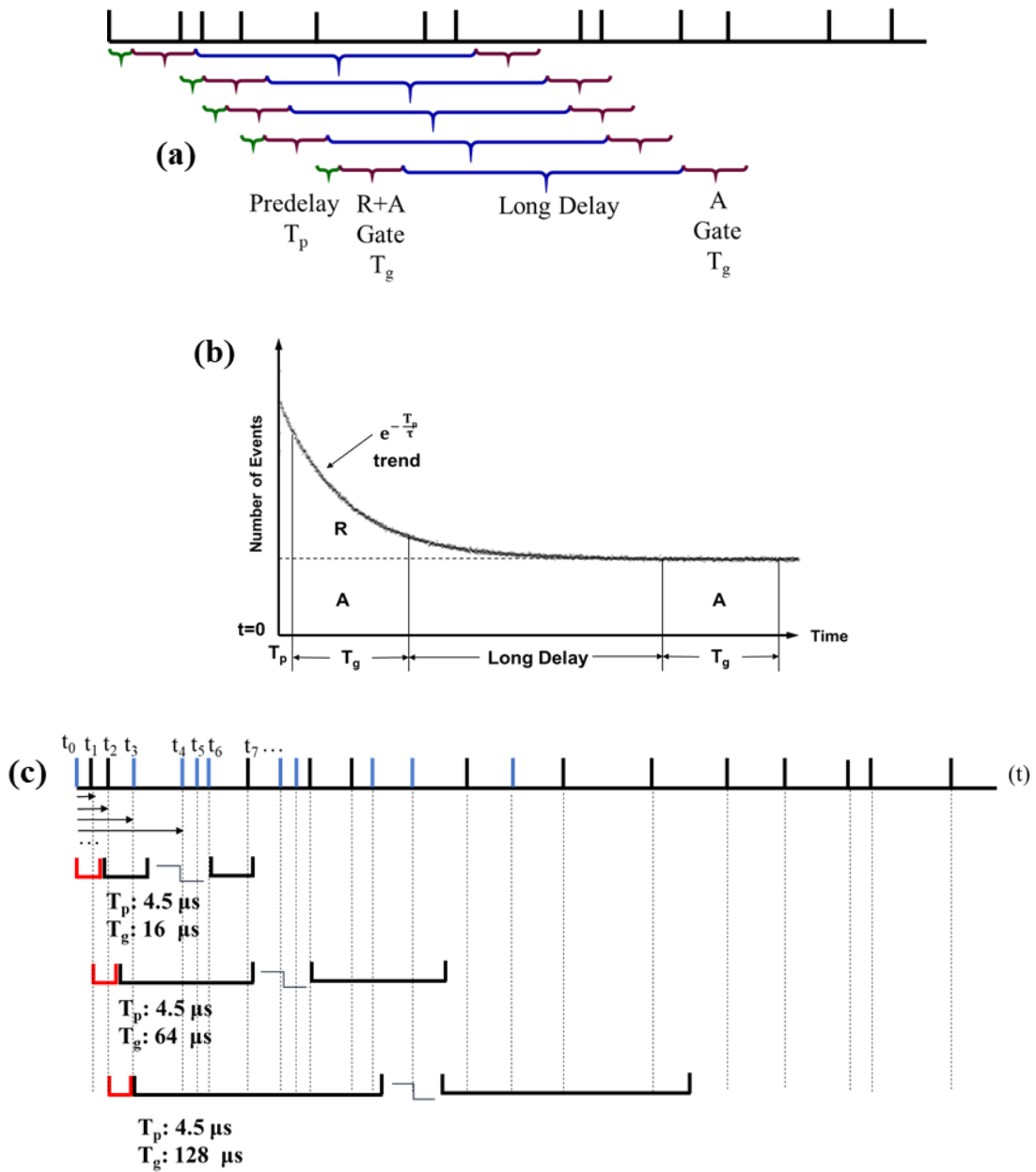


Figure 1.3. (a) A neutron pulse train illustration indicating which time correlation gates are applied for analysis. (b) A Rossi-alpha distribution showing how this correlation analysis builds a histogram of neutron coincidence events based on these timing windows. [5] (c) An example correlation analysis performed on the neutron pulse train using varying timing gate lengths.

therefore, this analysis is conducted for every measured event. Ultimately, the total number of coincident events is collected and reported in the Rossi-alpha distribution for the full duration of a measurement. Typically, a Rossi-alpha distribution ranges from $t=0$ to $t=1024 \mu\text{s}$, and it can have bins as small as $0.1 \mu\text{s}$.

Due to the exponentially decaying nature of this histogram, the (R+A) gate of length T_g encompasses a majority of the true doubles count rate (R for reals). However, in combination with these true neutron events, background neutron events and (α, n) events are also recorded as coincidences with the triggering event (A for accidentals). A long delay of $4096 \mu\text{s}$ follows the (R+A) gate to allow sufficient time for all correlated neutrons relative to the trigger to be detected or escape the system, including any room return events. After this long delay the same gate width, T_g , is opened to count the number of accidental coincidences. A subtraction is then done in software to determine the true number of coincidences, (R+A)-A, and the doubles count rate.

An example of this analysis in terms of the neutron pulse train is shown in **Figure 1.3 c**. This drawing is not to scale but it is made to highlight the important components of this analysis. Beginning with the initial trigger event at t_0 , the red gate represents the predelay. The arrows then indicate the distance in time between the trigger event and the individual successive events. The events in blue are the true fission neutron detections and the events in black are the randomly distributed neutron background (Accidentals). Each of these events will have a respective time stamp. Analyzing the neutron pulse train for three different gate widths, $T_g = 16, 64, 128 \mu\text{s}$, the dotted lines indicate where the successive events fall within the respective gates. Starting the analysis from t_0 for the instance where $T_p = 4.5 \mu\text{s}$ and $T_g = 16 \mu\text{s}$, t_1 would fall within the predelay, and not contribute to the coincidence analysis. Both t_2 and t_3 would fall within the (R+A) gate width for a record of 2 different coincidence events with t_0 with their respective time differences being reflected in their binning on the histogram. The (R+A) T_g is followed by the long delay indicated by the break on the diagram. The long delay, in reality, would extend across a large portion of the pulse train ($\sim 4096 \mu\text{s}$) to allow for correlated events relative to the trigger to either be captured by the system or escape. Here, it is drastically shortened to show how the accidental gate subtraction would take place. Following this long delay, the number of events recorded in the second T_g gate for the t_0 case would be 1 neutron coincidence with the trigger. Therefore, the (R+A)-A subtraction would result in 1 true coincidence between t_0 and the successive events. This would be the expected result as there was both one true neutron event and one background neutron event recorded in the (R+A) T_g gate, as indicated by the blue and black pulses, and one background neutron event recorded in the (A) T_g gate, as indicated by the black pulse, for a net result of one true neutron coincidence following the t_0 trigger.

This same analysis is then performed for the t_1 trigger. The t_2 event would fall within the set predelay. For this analysis a gate width of $T_g = 64 \mu\text{s}$ is used to illustrate how more counts will be recorded from the neutron pulse train with a longer time gate. This is also highlighted with the $T_g = 128 \mu\text{s}$ example. It is important to optimize this gate width setting relative to the length of time correlated neutron events will linger within the system to ensure a maximum number of correlated events can be detected, while not introducing a large number of background events in this analysis. For the $T_g = 64 \mu\text{s}$, within the (R+A) gate five neutron coincidence events are recorded relative to the t_1 trigger. However, because the long delay is not to scale, and therefore falls earlier along the pulse train than it would in a real analysis, this subtraction will not work out to the true number of coincidence events in this instance. This is attributed to the fact that in this example true events are still being recorded in the A gate, when in reality the only events being recorded in the A gate would be background and randomly distributed events from (α, n) . This analysis is continued along the neutron pulse train for all trigger events for the respective time gates selected, and the frequency of these coincidences in time relative to their respective trigger build the Rossi-alpha distribution and the net doubles count rate.

1.1.1 Nondestructive Analysis

Neutron coincidence counters are used to perform nondestructive assays (NDAs) on declared fissioning items that may be housed in areas such as a material balance area of a nuclear facility or within the assembly line of a nuclear fuel fabrication plant. The item may be loaded in the central well of a neutron counter that is appropriate for the size, activity, and application of the item. There are many different models of neutron counters reported to be routinely used in the field currently for a wide variety of measurements [8] [9].

These systems can be large, expensive, and sometimes cumbersome. Therefore, typically they remain in house, stored between inspection dates in a location that is easily accessible. They require the presence of an inspector who oversees the movement of the items, operates the counting software, and records the results of the assay. The purpose of the neutron coincidence counting measurement is to verify that the declared mass given by the facility is correct without opening or otherwise altering the item. Gamma measurements are used in combination with neutron coincidence counting to provide the isotopics of the item under question. The same systems and procedures can also be used for domestic safeguards.

A time correlated neutron nondestructive measurement can exploit either passive or active interrogation techniques to assay a wide range of Pu, U, and MOX items [11]. Many of the available neutron coincidence counting systems can be used in both active and passive mode to perform NDAs on items under question. Passive neutron counters have been designed and built for plutonium-bearing items but may be applied to assay uranium; active neutron correlation counting can be used for uranium, plutonium, and mixtures of both. The dynamic range of items is large, extending from milligrams to multiple kilograms for both current passive and active assay techniques.

The selected mode is dependent on if the item has a significantly high spontaneously fission rate or if it needs a neutron source to stimulate fission. Passive assay relies on the natural radioactivity of an item to determine the mass by spontaneous fission; even isotopes such as ^{238}U , ^{238}Pu , ^{240}Pu , and ^{242}Pu undergo spontaneous fission and can be measured without an external source. For nuclides that will not spontaneously fission, like those containing a significant fraction of ^{233}U and ^{235}U , active assay requires bombarding the item with neutrons from an external source to stimulate fission. Current ^3He counters have inserts, typically containing AmLi sources, which can be used for active measurements. Typically, these AmLi sources can also be removed for passive measurements to offer both mode options for a single design.

The neutron coincidence events from a Pu item will be generated from the various even isotopes of Pu. ^{240}Pu is traditionally the most present isotope in either low burnup or high burnup fuel; therefore, a majority of the detected neutrons stem from the ^{240}Pu spontaneous fissions. In terms of nonproliferation, when ^{240}Pu is present in measurable quantities in an item, that item is no longer easily weapons-useable. The spontaneous fission neutrons would prematurely initiate the necessary chain reaction for a successful implosion, thereby significantly decreasing the yield. So, ^{240}Pu is a clear indicator of peaceful uses of that material, and its presence is verified during an inspection. Therefore, it is the focus for quantification during a passive NDA. Since it is not possible to separate when neutrons come from ^{240}Pu compared to ^{238}Pu or ^{242}Pu , an effective ^{240}Pu mass must be calculated by incorporating the other constituents contributing to the measured coincidence rate [4] [5]. The effective mass is the mass of ^{240}Pu that would be necessary to generate the same coincidence response as that that is measured with a mixed item. The coefficients are used to account for the different spontaneous fission yields in Pu metal.

$$^{240}\text{Pu}_{eff} = 2.52 \cdot ^{238}\text{Pu} + ^{240}\text{Pu} + 1.68 \cdot ^{242}\text{Pu} \quad (1.1)$$

When combined with gamma spectroscopy or previously declared isotopics of the item, the total Pu mass may be calculated from the $^{240}\text{Pu}_{eff}$ value by:

$$Pu_{total} = \frac{^{240}\text{Pu}_{eff}}{2.52 f_{238} + f_{240} + 1.68 f_{242}} \quad (1.2)$$

where $f_{238}, f_{240}, f_{242}$ are the weight fractions of the respective isotopes within the item. The $^{240}\text{Pu}_{eff}$ value would be given through an NDA analysis and these further calculations can then be performed.

In a measurement, though, it is more likely that the effective weight would be calculated in place of the $^{240}\text{Pu}_{eff}$, obtained from the mass fractions declared in the isotopics in place of the weight fractions given in Equation 1.1. Then, the neutron coincidence counting would be used to produce an effective mass value, which would be used on Equation 1.2 with the effective weight, to determine the total Pu mass.

For an active measurement, assay of the odd numbered isotopes of uranium and plutonium is of interest. However, active measurements focus primarily on uranium. The neutron coincidence events from a U item will be generated from inducing fission in ^{233}U and ^{235}U ; spontaneous fissions rates are very low. The singles count rate cannot be used due to the random-in-time neutrons dominating this signal, produced from the interrogation source such as AmLi. Instead, the neutron coincidence rate is used to isolate the induced fission neutrons from the singles background. The spontaneous fissions occurring with ^{238}U also convolute the signal and therefore must be subtracted out using passive analysis in combination with the active interrogation analysis. Since ^{233}U is not produced in nature, but is made by bombarding ^{232}Th in an accelerator or reactor, it is not present in fresh fuel assemblies for Light Water Reactors. It has a high specific activity and is challenging to handle. Because of this, it would not be common to find ^{233}U in items under question during an inspection. Therefore, the primary signal acquired during an active measurement is of the neutron coincidences produced from the induced fission in ^{235}U .

Some systems can be adapted to operate in fast or thermal mode. In the former mode, cadmium is used within the walls of the detector to prevent thermal neutrons from scattering back into the item and inducing more fissions later in time. Thermal mode does not use cadmium liners within the system. The use of cadmium simplifies the interpretational model used to convert rates to reported or assayed mass. Fast mode is used more readily when high-mass items are being assayed. Fast neutrons are more likely to penetrate into the center of the high mass items. Because high-mass items will naturally have a higher count rate due to the presence of more nuclei that can undergo fission, the associated lower capture cross section of the nuclei provides a suitable balance to prevent large dead time effects overwhelming the system. Thermal mode is used for low-mass items since the thermal energy neutrons will be more readily captured by the item due to the high fission cross section, thereby improving the statistical precision of the measurement. However, if thermal mode is used on high mass items, the neutrons will not penetrate deeply into the item, resulting in fission events mainly near the surface of the item. These options allow these systems to have a wide range of applications in the field with ease of use for operators.

An NDA neutron coincidence measurement may take anywhere between several minutes to tens of minutes, but it does not traditionally extend beyond a half hour. The measurement is conducted for the length of time necessary to achieve good statistics on both the singles and doubles neutron count rate, so it is source rate and system dependent. Better statistics yield better assay precision. The item under question is placed within the central well of the respective neutron coincidence counter, and a shift register is used to acquire the neutron pulse train over the length of the measurement. The time correlation analysis is performed automatically using associated internal software of the connected data acquisition hardware and the results may either be read directly from the shift register or using INCC software.

For in-field use, the data is analyzed using INCC. INCC is the IAEA Neutron Coincidence Counting software created by Los Alamos National Laboratory (LANL) [12], and it is used for all neutron coincidence counting NDAs. It is a user-friendly program that works on Windows operating systems and it provides information like the singles, doubles, and triples count rates, background values, (R+A) and A values, associated errors, cycle data, calibration curves, known-alpha curves, etc., and ultimately assists in performing an NDA. A background measurement is always conducted prior to data acquisition of the item and again following the acquisition to ensure no changes have occurred. These files are stored and a background subtraction is performed on successive data. It is also important to ensure the system is performing as it was the last time it was used to verify that it has not been tampered with, nor has the system malfunctioned. All acquired rates must be dead time corrected based on the respective correction factor equations of the system used.

Before a measurement can be performed, however, the counting system must be calibrated to understand that specific system's response to a source relative to what it will be used to measure. In a laboratory or manufacturing setting, it is common to measure multiple sources of different neutron output activities that are characteristically similar to those unknown items that will be measured in the field. This is done by using various source standards that may have a similar geometry, composition, and/or neutron count rate. Typically, these are certified sources, whose neutron output is known to approximately 0.1% precision. If the standards used to calibrate the system are representative of what items will be measured, the multiplication, M , and ratio of (α, n) neutrons to spontaneous fission neutrons, α , will be known, for a straightforward assay. Multiplication, also known as leakage multiplication, can be defined as the number of neutrons leaving the item divided by the number of neutrons produced from a combination of spontaneous fission and (α, n) reactions. This will allow a successful NDA coincidence measurement to be performed with confidence. However, in the field these standards are not readily available. Instead, normalization procedures across different systems and different sources are necessary to allow for practical field verification measurements to be conducted in a timely manner. Or, instead, neutron multiplicity counting and analysis may be used with the appropriate systems where all system parameters and several source parameters are taken into consideration for an in-depth analysis. There are three calibration and assay methods used with neutron coincidence counters which will be discussed below.

Nondestructive analysis is dependent on many potentially unknown parameters, some of which include: 1) the spontaneous fission rate, 2) the induced fission, or item self-multiplication, and its variation across the item, 3) the (α, n) reaction rate in the item, 4) the spatial variation in neutron detection efficiency, 5) the energy spectrum effects on detection efficiency, 6) the neutron capture in the item, and 7) the neutron die-away time in the detector [4]. These parameters must be well understood such that their influence on an NDA may be corrected. It has become common practice to use empirical methods for calibration of a system in the field out of necessity due to measurement and analysis limitations, and to bundle these possibly unknown parameters into less complex semi-empirical "effective" correction factors. In doing so, however, information about the counting system and source may be lost. The known-alpha method assumes the chemical composition of the item is known (in part also compensating for other uncertainties), which allows the α value to be calculated from the isotopic composition using nuclear data of known (\square, n) and spontaneous fission yields for those isotopes. Pure metal items have an $\alpha = 0$, meanwhile oxides and fluorides and impurities have varying (α, n) reaction rates that can be referenced in documents such as the Passive Non-Destructive Assay Manual (PANDA) manual [11], which is a powerful reference for this field. For the example of a ^{240}Pu source under question, the alpha value is calculated for pure Pu oxide; a scaling factor, the alpha weight, is then used for other Pu compounds relative to the pure oxide alpha value. The alpha weight is 1 for pure plutonium oxide and 0 for pure plutonium metal. A library of different doubles to singles count rate ratios must be built for various mass items, with this set known alpha. Using the known α , and the measured doubles to singles count rate ratio,

the doubles count rate can be corrected for item multiplication of the unknown item to determine its mass. The doubles to singles count rate ratio must have been previously calculated or measured for a non-multiplying item of pure ^{240}Pu metal to provide a ρ_0 value. Using

$$r = \frac{\left(\frac{D}{S}\right)(1 + \alpha)}{\rho_0} \quad (1.3)$$

with the quadratic equation

$$2.166(1 + \alpha)M^2 - [2.166(1 + \alpha) - 1]M - r = 0 \quad (1.4)$$

to solve for the item multiplication, M , the doubles rate for that specific item composition's may be determined [13].

This analysis is done internally to INCC where the user must input the material type, alpha weight, and ρ_0 parameters. This can be done for an active or passive measurement by selecting the appropriate box. For an inspection, there would be a stored library from previous use of this system using known sources, or from historical reference that would be used as the comparison to the new measurement data. A fit through the measured doubles to singles count rate ratio against the declared mass would have a straight line, on which the new measurement should fall, within statistical error. If this new measurement point deviates greatly from this fit, it may be assumed that the known alpha is not correct and another method may be necessary.

In this instance, the system dead time, the item chemical composition, the respective (α, n) rate and spontaneous fission rate nuclear data, and the doubles to singles ratio for a non-multiplying item of pure metallic item of the same isotopics as the item under question, must be known for an accurate assay. Knowing all of these components is oftentimes difficult, and, without them, this method is not reliable.

Another method relies on forming a calibration curve and referencing that data against the item under question. Calibration sources of known activities and compositions are recorded in separate measurements. The item types may be selected from INCC or input manually with the respective known isotopics. Their rates are then recorded. The calibration curve is a representation of the measured doubles count rate compared against the declared mass. As the mass of the item increases, however, multiplication will increase due to introducing induced fissions in addition to the spontaneous fissions within the matrix. This causes a non-linear relationship between this ratio. The difference between a passive calibration curve and an active calibration curve is the behavior at these high mass ranges. For a passive curve, the behavior will be an increasing non-linear trend; meanwhile, for an active curve, the behavior will be a saturating trend due to increasing self-shielding of the neutrons due to short mean free paths within the high mass item. The fit is applied through INCC by selection of the desired curve equation across the relevant data sets. For most items inspected, this method suffices because these items fall within the linear region of this relationship and not the non-linear regions. The item under question is then measured using a verification measurement in INCC and the calculated assay mass, using the designated fit equation, is reported alongside the entered declared mass. The assay mass should be in agreement with the declared mass within the predetermined error.

This measurement relies solely on the doubles count rate, and it has a higher error than the known-alpha method that relies on the ratio of the doubles to singles. It requires that several calibration source standards similar to the source in question are available for measurement. This is not always accessible during an inspection, and high mass and high multiplication items are less accessible. In certain instances, a proper calibration curve cannot be produced if the important characteristics of the items to be assayed are not well known. The correct fit equation must also be selected. Fast and thermal mode

operations of the same system have very different calibration curves. Different materials also have significantly different calibration curves since the penetration of the neutrons varies based on the mass of the item, and the neutron multiplication in the items is sensitive to the density and geometry of the item.

It is more efficient, convenient, and commonly selected to use normalization procedures for a system, exploiting empirical calibration approaches. To do this, one model of the neutron coincidence counting system type is calibrated in a manufacturing or laboratory setting using the appropriate category of material over a wide range of mass standards. The calibration parameters necessary for this system are then fixed, and the response from any other model of that system type is normalized to those fixed parameters in a scaling factor. That specific calibration curve is then used as the “gold standard” for that configuration and application against which all other models are normalized. This is typically successful in calibrating and performing an NDA, but it leaves behind a large amount of unrecorded information about the source and system with many empirical correction factors.

The final, and more mathematically direct, approach includes the system parameters and source nuclear data in a detailed analysis rather than an empirical approach. The observable rates are described in terms of the item properties and detector characteristics in the framework of a point kinetics model (Equations 1.5-1.7). In the case of neutron coincidence counting, this is typically solved or inverted in the known (α, n) and known efficiency approximation. This holds the assumptions that the material is known so that the (α, n)-to-spontaneous fission rate ratio can be calculated from the isotopic composition and nuclear data, like with the known-alpha method. Also, it is assumed that the neutron counter efficiency (and gate factor) is not strongly influenced by the presence of the item, so this value would be known through a previous system characterization. Using the measured, dead-time-corrected singles and doubles count rate values, Equations 1.5 and 1.6 can be solved for the mass and multiplication of the item. This is a robust and mathematically complete solution, as there are two equations (for singles and doubles) and two unknowns (mass and multiplication). In the case of neutron multiplicity counting, the triples rate is also acquired, and the three point model equations are solved for three unknowns: the effective ^{240}Pu mass, item self-multiplication, and the (α, n) reaction rate when this is not well-known. However, in practice, this is much more sensitive to model bias, and some of the previously listed point-model parameters are treated as effective rather than physical values. Work is consistently ongoing to improve this understanding.

In using the point kinetic equations, more information is recorded about the measurement and the system used [4]. These equations, when used for passive neutron coincidence counting, are:

$$S = F\varepsilon M v_{s1} (1 + \alpha) \quad (1.5)$$

$$D = \frac{F\varepsilon^2 f_d M^2}{2} \left[v_{s2} + \left(\frac{M-1}{v_{i1}-1} \right) v_{s1} (1 + \alpha) v_{i2} \right] \quad (1.6)$$

and if multiplicity counting were to be used, the triples equation would be:

$$T = \frac{F\varepsilon^3 f_t M^3}{6} \left\{ v_{s3} + \left(\frac{M-1}{v_{i1}-1} \right) [3 v_{s2} v_{i2} + v_{s1} (1 + \alpha) v_{i3}] + 3 \left(\frac{M-1}{v_{i1}-1} \right)^2 v_{s1} (1 + \alpha) v_{i2}^2 \right\} \quad (1.7)$$

where

- F : spontaneous fission rate for ^{240}Pu
- ε : detector efficiency
- f_d : doubles gate fraction
- f_t : triples gate fraction
- M : leakage self-multiplication

α : ratio between the number of (α, n) reactions to spontaneous fission neutrons (varies from item to item depending on its composition)
 ν_{in}, ν_{sn} : n order reduced factorial moment of induced/spontaneous fission neutron distribution

The gate fractions are calculated using the time correlation gates, assuming an ideal system with a pure exponential decaying behavior, following:

$$f_d = e^{-\frac{T_p}{\tau}} \left(1 - e^{-\frac{T_g}{\tau}} \right) \quad (1.8)$$

$$f_t = f_d^2 \quad (1.9)$$

where T_p is the pre-delay, T_g is the gate width, and τ is the known neutron die-away time of the system.

The equations used for the active measurements consist of [14]:

$$S = S_0 + B + S_S + F\epsilon M\nu_{s1} \quad (1.10)$$

$$D = \frac{F\epsilon^2 f_d \nu_{s2}}{2} \cdot C_d \quad (1.11)$$

$$T = \frac{F\epsilon^3 f_t \nu_{s3}}{6} \cdot C_t \quad (1.12)$$

where the same parameters exist as above, in addition to:

S_0 : singles count rate from the AmLi sources without an item present in the well

B : background singles rate in the room

S_S : the change to S_0 due to scattering and absorption of AmLi neutrons by the item

C_d : correction factor for the self-multiplication contribution to the doubles

C_t : correction factor for the self-multiplication contribution to the triples

Self-multiplication must then be solved using a cubic equation. Coupling between the AmLi source and the item must also be taken in account. Due to the complexity of these equations, traditionally the more empirical methods are used with active neutron counting. For a fresh fuel NDA, five correction factors are applied to the “gold standard” calibration curve to accommodate any differences in the coincidence counters, AmLi sources, electronics, assembly sizes, and burnable poisons between the reference model and the model being used [15].

The point kinetics model NDA analysis requires an in-depth understanding of the system behavior and the sources used, from physics first principles. Various source standards will be used to determine the system-specific parameters in a characterization and calibration approach prior to system operation in the field. Although this method is time consuming and requires detailed analysis of each of the terms included, it is the ideal analysis method for system evaluation and detailed reporting. In using each of these parameters, system designers may be able to study which characteristics may be better optimized to minimize the error on an NDA while maximizing the count rate obtained during a measurement. In addition, if a discrepancy were to arise between the declared mass of an item and the calculated mass through this analysis, it would be easier to identify the source of error contributing to this discrepancy compared to using empirical normalization analysis methods. This approach is not currently ideal for time-restricted inspection measurements, but NDA scientists have been focusing their efforts on making this more efficient such that it may be more widely implemented in the future. The development of modern neutron coincidence counting procedures and analysis techniques in support of the point kinetic equation NDA method will be the focus of this work.

1.1.2 Counting System Characterization Parameters

Referencing the nondestructive analysis methods discussed in the previous section, it is obvious that the system's parameters have a large influence on the final analysis. In order to perform a reliable and accurate NDA, the neutron coincidence counting system that is used in this measurement must be well characterized and its behavior must be very well known. Specifically, for the point kinetics model an in-depth system characterization must be performed prior to the system's use where the predelay, T_p , and the gate width, T_g , must be optimized, and the neutron die-away time, τ , the dead time, and the efficiency, ϵ , of the system must be well understood.

A neutron coincidence counting characterization procedure begins by verifying the operational high voltage (HV) through the HV characteristic (or Geiger Plateau Curve [1]). The HV characteristic is a visual representation of the neutron count rate across a range of HV settings. The singles count rate is typically used for this analysis, but it is possible to also study the doubles trend across a range of HVs. This is done to ensure proper performance and accurate gain settings of the preamplifiers within the system, matching the measured trend to historical data of the same model systems. For most neutron coincidence counting systems, the operational HV selected is between 1680 V and 1720 V. This setting is selected based off the stability of the count rate across different HVs. With the optimized HV setting, the predelay and gate width settings must then be optimized to ensure a balance between the collection of true neutron coincidences and the inclusion of background and electronic events in the analysis.

The neutron die-away time of a system is the length of time it takes a neutron to either be thermalized and captured in the system, or escape. Verifying the neutron die-away time will support the gate width selection as it should be approximately 1.27 times the neutron die-away time [4]. These values are then used to calculate the gate fractions in the point kinetic equations. The gate fractions are used to account for the fact that not all correlated neutron events fall within the selected timing windows, resulting in some inefficiency. It adjusts the rate equation to accommodate this decreased measured value from the true emitted value. In addition, the system's detector efficiency must also be well known to correct the point kinetic equations for the true emitted source rate. Most neutron coincidence counting systems have a system efficiency of 15-30%. Therefore, a majority of the emitted neutrons will not be captured and measured by the counter. In order to calculate the correct mass of the item, this effect must be taken into account. Finally, due to the properties of the charge collection in the ^3He tubes and the electronic pulse processing chain, dead time effects will be inherent within the pulse train. These effects decrease the number of measured neutron events. Because of this, the measured rates will need to have an accurate dead time correction applied to them for the true singles and doubles rates to be evaluated. It is crucial to accurately represent these parameters in the point kinetics equation for each system. Each of these parameters has an associated uncertainty that propagates through to the final calculated assay mass, so minimizing the uncertainty on these parameters will have a significant impact in final assay precision.

1.2 International Safeguards

1.2.1 The International Atomic Energy Agency

As the work of neutron coincidence counting research and development directly supports the International Atomic Energy Agency (IAEA), its attributes, duties, and limitations must be considered. The IAEA is, as the name implies, an international agency comprised of representative from many different countries around the world, which is responsible for the promotion of peaceful uses of nuclear

energy. It ensures that nuclear technology is not used for military purposes, including nuclear weapons. The Agency is autonomous, but it does report to both the UN General Assembly and Security Council.

The IAEA is broken down into three bodies: the Board of Governors, the General Conference, and the Secretariat. The Board of Governors is responsible for making most of the policy of the IAEA. It selects the Director General, interprets the Safeguards Agreements, determines the non-compliance of a State, approves the budget, and also decides what to report to the UN Security Council, which is the only body with power to enforce the repercussions of non-compliance. The General Conference is comprised of 171 member states that participate in the annual meetings held to approve the actions and budgets passed on from the Board of Governors. The conference serves as a forum for debate on current issues and policies in which each state may voice its concerns and opinions. The Secretariat is made up of the staff working for the IAEA such as the inspectors, analysts, and scientists.

It has three main missions on which it operates: safeguards and verification, safety and security, science and technology. For the safeguards and verification mission the IAEA works to prevent the further spread of nuclear weapons through the deployment of inspectors who work to verify that safeguarded nuclear material and activities are not used for military purposes in nuclear facilities worldwide. For the safety and security mission the IAEA works to protect people and the environment from harmful radiation exposure through helping countries upgrade their nuclear safety standards and procedures and prepare for, and respond to, emergencies. For the science and technology mission the IAEA works to support the peaceful applications of nuclear science and technology in its member states such as in developing countries.

The IAEA received governance from its Statute [16], a treaty, which came into effect in 1957. The Statute has since been amended in 1963, 1973, and 1989. The agency was developed following President Eisenhower's "Atoms for Peace" address to the General Assembly of the United Nations in 1953, concerned with atomic warfare and the implications it could have on society. Several articles to highlight are: Article II which outlined the objectives of the Agency, Article III which set forward the functions of the Agency and what it is authorized to do, and Article XII which established the rights and responsibilities of the Agency in terms of applying safeguards and conducting inspections in various States. In 1961 "The Agency's Safeguards", INFCIRC/26 was issued, which was applicable primarily to research facilities [17]. In 1965 INFCIRC/66 was issued, "The Agency's Safeguards System (1965)," revising INFCIRC/26 and creating an extensive and comprehensive set of safeguards covering reactors of all sizes. In addition, revisions were successively made to include reprocessing plants (Rev. 1) and fuel fabrication plants (Rev. 2) in 1967 and 1968.

In 1970 the Treaty on the Non-Proliferation of Nuclear Weapons (the Non-Proliferation Treaty or NPT) entered into force [18]. The NPT was created to prevent the spread of nuclear weapons and weapons technology, promote cooperation in exploiting peaceful uses of nuclear energy, and work towards achieving nuclear disarmament. It also provides security against the threat of a nuclear devastation, through the nuclear umbrella, for non-nuclear weapons states that gave up the option to pursue nuclear weapons by signing the treaty. The treaty has since been extended indefinitely. There are currently 191 signatories. North Korea has withdrawn, and four UN States have not signed: Israel, Pakistan, India, and South Sudan. Four of these five States are believed, or known, to have nuclear weapons.

The NPT ideals expressed throughout the preamble and eleven articles are interpreted in the form of three iconic pillars: non-proliferation, disarmament, and the right to peaceful use of nuclear technology. There is an intrinsic balance between these matters that form the pillars and each is mutually reinforcing for the other two. Article I of the NPT states that every nuclear-weapon state pledge not to transfer nuclear weapons to any recipient, or in any way assist, any non-nuclear-weapon state in manufacturing or acquiring a nuclear weapon. Then, Article II states that each non-nuclear weapon state

will not attempt to acquire, manufacture, or seek assistance in the manufacturing of, any nuclear weapons. These two articles address the non-proliferation concerns. In order to verify that these obligations are met, a procedure for inspection and drawing conclusions to this end, had to be developed. Article III establishes that each non-nuclear weapons state will reach an agreement with the IAEA for the application of its safeguards to all nuclear material in all of the state's peaceful nuclear activities, and to ensure there is no diversion this material to nuclear weapons.

The right to peaceful uses of nuclear energy for both nuclear weapons states and non-nuclear weapons states is established in Article IV of the NPT. It clarifies that every signatory to the treaty has an inalienable right to develop research for the production and use of nuclear energy technologies, and it states that they may benefit from international cooperation in this area, in conformity with their non-proliferation obligations. International cooperation for the spread of nuclear energy may be used to further the development of the applications of nuclear energy for peaceful purposes, with consideration for the needs of the developing areas of the world. Because of this article, many countries have since implemented, while other countries have helped assist with building, securing, and regulating, nuclear reactors for energy needs. Each of these reactors then must fall in an IAEA safeguards agreement with the respective State, which requires IAEA resource investments for the inspections and assessments of their peaceful uses.

In addition, the nuclear weapons states agree to pursue good-faith negotiations on effective measures relating to general and complete disarmament under Article VI. Although this article has generated great dispute over the decades between various countries, the process of disarming has produced additional safeguards concerns. The material made available through the dismantling of nuclear weapons has been incorporated under the respective State–IAEA agreements, and peaceful uses for that material have been investigated, ensuring it is not used for proliferation.

The NPT defines nuclear-weapon states as those that have tested a nuclear explosive device before January 1, 1967 through Article IX. The weapons states are then the United States, Russia, the United Kingdom, France, and China. Again, the four other states, Pakistan, India, North Korea, and Israel, are known or believed to possess nuclear weapons but have not signed and ratified the NPT. Israel is deliberately ambiguous regarding its nuclear weapons status. All other signatories are considered non-nuclear weapons states.

In 1972 INFCIRC/153 was issued [19], in support of the NPT Article III requirement that all non-nuclear weapon state signatories must establish an agreement with the IAEA for application of its safeguards with the State to ensure peaceful use of nuclear material. This INFCIRC defines the general structure and content of these agreements for the States, through Comprehensive Safeguards Agreements (CSAs). The weapons states have different arrangements with the IAEA than non-nuclear weapons states regarding their nuclear material. They are not obligated under the NPT to hold safeguards agreements with the IAEA. Instead, they have all voluntarily made other arrangements. This is practical as there is no longer a concern for these weapons states that they will obtain nuclear weapons; they already have them. So, inspection resources should not be dedicated to verifying the peaceful uses of nuclear technology, but instead they should be used to verify that these States are not proliferating. In addition, five treaties have been ratified from 1967- 2006 regarding regional Nuclear Weapons Free Zones in Latin America and the Caribbean, the South Pacific, Southeast Asia, Africa and Central Asia [20]. The NPT supports the creation of these nuclear weapons free zones by explicitly stating that any group of States has the right to issue regional treaties to assure “the total absence of nuclear weapons in their respective territories.” These treaties require the signatories to uphold a CSA with the IAEA. Safeguards are also required for the European Atomic Energy Community (Euratom), which was created by a treaty passed in 1957. Euratom is an organization formed between the members of the European Union to share nuclear energy and technology, and it has its own safeguards that is performed in close partnership with the IAEA.

INFCIRC/153 acknowledged the existence of Euratom safeguards, and inspections of their respective facilities are performed in collaboration between Euratom and the IAEA [21]. A binational safeguards agency exists between Argentina and Brazil (ABACC) to also verify its own peaceful uses of nuclear technology. ABACC works in direct support of IAEA concerns.

Following the discovery of clandestine nuclear weapons activity in both Iraq and North Korea, the IAEA decided it needed enhanced verification measures for its safeguards that extended beyond declared nuclear material and declared facilities. This discovery proved that the IAEA safeguards worked well with verification activities on declared nuclear material and facilities, but it was not well-equipped to detect undeclared nuclear material and activities in States with CSAs. Therefore, in 1997 INFCIRC/540 was issued that outlined an Additional Protocol (AP) for the IAEA. It includes provisions for information about, and access to, all parts of a State's nuclear fuel cycle, from mines to nuclear waste facilities, including decommissioned sites and locations outside facilities. It was designed for States that have any type of safeguards agreement with the IAEA. The AP provides broader information and broader access. The broader information comes from the right to inspect nuclear fuel cycle research and development components that do not house nuclear material, such as the development of centrifuge technology, in addition to the manufacturing and export records of sensitive nuclear-related equipment and material. This information must be revealed by the State if prompted. The broader access allows complementary access to any building on a nuclear site with a short notice of 2 hours, or 24-hour access, visits to any State-declared locations as part of the nuclear fuel cycle from mining to waste, and access to any other locations for the collection of environmental samples. With the AP inspectors also receive multiple entry/exit visas so they may show up on short notice to a facility such that the State may not have time to hide its activities. This introduction sparked a great restructuring and investment of new resources in terms of non-destructive assay systems for various new applications, data analysts, information scientists, and more staff to execute these new requirements. In implementing an AP in combination with a CSA, the IAEA can reach more certain conclusions that a State's activities are for peaceful uses only.

1.2.2 State Obligations Regarding Safeguarding Nuclear Material

Because of these different treaties and conditions, the IAEA concludes three types of safeguards agreements: CSAs with non-nuclear weapon state parties to the NPT, Voluntary Offer safeguards agreements with the nuclear weapon state parties to the NPT, and item-specific safeguards agreements with non-NPT States. Each of these agreements may be complemented with an AP. A small quantities protocol may be concluded in conjunction with a CSA for States that have minimal or no nuclear material and no nuclear material in a facility.

“The objective of IAEA Safeguards is to deter the spread of nuclear weapons by the early detection of the misuse of nuclear material or technology. This provides credible assurances that States are honouring their legal obligations that nuclear material is being used only for peaceful purposes.” [22] Safeguards are based on assessments of the correctness and completeness of a State's declared nuclear material and its nuclear-related activities. The IAEA verification measures combine inspections and ongoing monitoring and evaluation. To draw a conclusion about a State complying with its obligations under the NPT, the IAEA must conduct a sufficient level of safeguards activities and also perform a comprehensive evaluation of all safeguards-relevant information available. It also needs to have addressed anomalies, questions, or inconsistencies identified by its safeguards activities, and have assessed whether there are any indications that would constitute a safeguards concern. Therefore, the responsibilities and actions of the IAEA follows an annual cycle with four main processes. These processes are intertwined and form a constant recycling of duties and obligations. They consist of

developing safeguards approaches; planning, conducting, and evaluating safeguards activities; drawing safeguards conclusions; and collecting and evaluating information [23].

For the collection and evaluation of safeguards-relevant information, the IAEA reviews all available open source, 3rd party, publications, satellite imagery, patents, and media information to evaluate its consistency with the State's declarations about its nuclear program. In developing a safeguards approach for a State, acquisition path analysis, material balance accountancy, design information verification, environmental sampling, NDA/DA sampling, weighing, containment, and remote surveillance procedures are outlined to physically verify the State's declarations. The IAEA then evaluates these technical findings and identifies if any inconsistencies exist in terms of compliance or noncompliance ruling, or if a Complimentary Access visit is necessary. Finally, the safeguards conclusion is drawn and reported each year to the Board of Governors in the Safeguards Implementation Report.

Each State has its own respective agreement with its own inspectors, data analysts, and information scientists. It will be evaluated based on its agreement with the IAEA. For all non-nuclear weapons states that are signatories to the NPT, a CSA must be performed. The CSA declares that the IAEA has the right and obligation to ensure that safeguards are applied on all nuclear material in the territory under control of the State, for the exclusive purpose of verifying that such material is not diverted to nuclear weapons or other nuclear explosive devices. As of June 2018, 174 States have a CSA with the IAEA. For the nuclear weapons states, all five (China, France, Russia, United Kingdom, United States) have voluntarily signed Voluntary Offer Safeguards Agreements with the IAEA. These agreements allow the IAEA to apply safeguards to nuclear material in State-selected facilities to verify that that nuclear material remains in peaceful activities and is not withdrawn from safeguards, except as provided for in their respective agreements. This covers civilian nuclear material and sites. Three States not party to the NPT (India, Pakistan and Israel) have item-specific agreements they have concluded with the IAEA. Item-specific agreements are based on the safeguards procedures established in INFCIRC/66, where only the nuclear material, non-nuclear material, facilities and other items directly specified in the safeguards agreements can fall under inspection. The States undertake not to use their nuclear material, facilities or other items subject to the agreement for the manufacture of any nuclear weapon or to further any military purpose. States with minimal or no nuclear activities can conclude a Small Quantities Protocol (SQP) with the IAEA if the material is used in locations called 'locations outside facilities,' defined in the Model Additional Protocol as "any installation or location which is not a facility, where nuclear material is customarily used in amounts of <1 effective kg. As of December 2018, 88 States have SQPs [24]. The AP may be applied in addition to any of these agreements. As of June 2018, 132 countries and Euratom have concluded APs that are now in force; 16 other States have signed their AP agreements but have not entered them into force. All five nuclear weapon states have concluded APs to their voluntary offer safeguards agreements.

The States must then develop their own system for Material Control and Accountability in compliance with their respective agreement, typically falling under domestic safeguards. This supports the State-Level Concept for integrated safeguards, which will tailor the IAEA activities to each specific State. The entire State is treated as one entity by the IAEA, such that material balances must exist across the entire State, rather than on a facility by facility approach. Each facility may have several material balance areas where nuclear material is kept. These facilities then report to the State that keeps a record of these balances. Logs of all nuclear material transactions, inventory adjustments, material losses and gains, and system access must be kept and reported to the IAEA during the annual inspection or during a complimentary access. This information, in combination with the information directly collected by the IAEA, helps form the State evaluation. A statistical sampling is then performed by inspectors in material balance areas at chosen facilities during the annual inspection. These measurements, in combination with the other facets of the inspection, are evaluated such that if discrepancies above a set value were to exist

from what was declared by the State, further investigation would be necessary to draw a safeguards conclusion.

1.2.3 The Nuclear Fuel Cycle

With the extension of inspections spanning across the entire nuclear fuel cycle with the ratification of the AP, many new facilities and procedures have come into play for IAEA inspections. The nuclear fuel cycle begins at the mining stage to harvest uranium ores. It then progresses to milling, conversion, enrichment, and fuel fabrication stages as illustrated by **Figure 1.4**. After the lifetime of the fuel in the reactor, it must “cool” in the spent nuclear fuel pond, and then be transferred to storage and either remain there or be sent to a fuel reprocessing plant. All of these stages have relevant safeguard concerns which need to be addressed due to the material handled and the processes involved.

The nuclear material may begin as one of the many ore chemical forms: Autunite, Coffinite, Davidite, Töbernite, Uraninite (pitchblende), Zeunerite, etc. This ore composition is typically less than one percent uranium in the total mass of material harvested. The uranium is then milled to chemically purify and condition it into U_3O_8 yellow cake. The material balance between what is mined as ore to what comes out in the form of U_3O_8 must be verified. This mining and milling procedure also leaves behind tailing, or waste, that may include small amounts of uranium that must be accounted for. The U_3O_8 is then converted into UF_6 gas through a number of eligible processes. The mass balance between this conversion procedure must be in agreement. The UF_6 gas is then enriched to the desired ^{235}U percent value. In addition to verifying a mass balance within this facility, it is crucial to ensure the uranium used during these stages remains below the IAEA-specified threshold between low-enriched uranium (LEU) and high-enriched uranium (HEU), at 20%. Typically, commercial reactors use enrichments anywhere between 3-5% and research reactors can use upwards of 19.9% enriched fuel. This is related to the amount of separative work units (SWU) necessary to reach that enrichment threshold. SWU is the work, or effort, needed to be put into this process in order to separate ^{235}U from ^{238}U . Beyond a 20% enrichment, there is little gain in SWU necessary to reach weapons grade uranium; therefore, the IAEA restricts all peaceful uses of nuclear material to below a 20% enrichment to ensure there is no malicious clandestine activity.

The enriched UF_6 gas is then loaded into large storage cylinders which are typically used to move the material from the enrichment facility to the fuel fabrication facility. The UF_6 gas is then unloaded and typically converted to UO_2 for use in Light Water Reactors (LWRs), although other fuel forms exist for different reactor types worldwide. The enriched UF_6 gas undergoes another conversion to get it into UO_2 . This UO_2 powder is ground and sintered into individual pellets, which are then loaded into the respective fuel assembly fuel rods. This process contains many different stages and sources of loss of material that must be confidently measured to ensure there is no diversion of material. The advancement of these nuclear fuel assemblies, such as the inclusion of burnable poisons, complex configurations, and varied enrichment pellets throughout an assembly, complicate safeguards verification measures.

Following the fuel fabrication into an assembly, it is important for safeguards to ensure that same amount of material goes in to the reactor, and comes out, less for burnup. After the lifetime of the fuel within the reactor, the spent nuclear fuel must be safeguarded during cooling, and then transport, to ensure no material is diverted. Depending on the country in question, that spent fuel is either reprocessed, which is placed under heavy safeguards due to the presence of ^{239}Pu , or stored in dry casks that also require monitoring for diversion. All material must be accounted for throughout this process to adhere to the agreements made between the respective State and the IAEA.

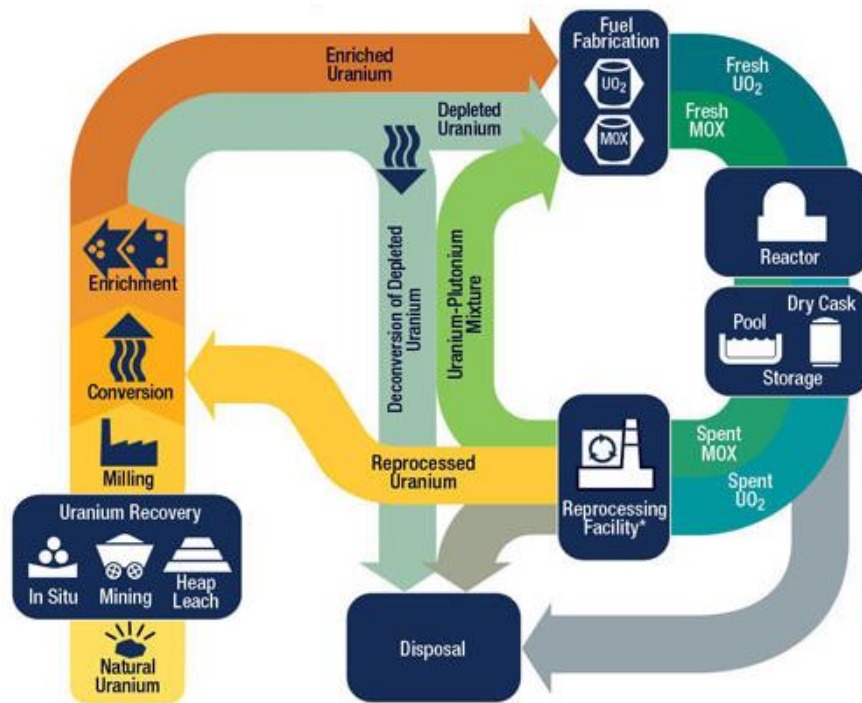


Figure 1.4. The nuclear fuel cycle. [25]

1.2.4 Neutron Coincidence Counting Used in an Inspection

Neutron sources of interest for NDA exist across the entire nuclear fuel cycle. However, for neutron coincidence counting of non-irradiated materials, the focus ranges primarily across the different aspects of the fuel fabrication stage due to the presence of uranium, and in some State cases, plutonium. Neutron coincidence counting is also essential in material balance areas within laboratories or other facilities that may house fissioning nuclear material kept under IAEA safeguards. Items of varying masses, activities, geometries, and chemical compositions need to be assayed. This requires a variety of neutron coincidence counters that can accommodate these differences.

The primary applications of neutron coincidence counting are measuring both uranium and plutonium metals and oxides, in scrap samples produced throughout the fuel fabrication process, fuel pellets, fuel rods, fuel assemblies, laboratory and research samples, and HEU quantities. Solid scrap may be contained in complex geometries filled with other non-nuclear waste produced from manufacturing in the UF_6 to UO_2 conversions, sintering of the UO_2 into fuel pellets, any unsuitable production quality pellets, any excess metal, substantial build-up of material tails from machining, or unrecoverable material from any of the processes. If plutonium is part of the State's nuclear fuel cycle PuO_2 , Pu metal, Pu solutions from the separation of Pu from waste and for fuel fabrication, may also be assayed. The assayed items across the numerous systems range from milligrams to multiple kilograms. They may be contained in large 55 gallon waste drums, waste crates, shipping crates, in gloveboxes, or cans and containers housing any combination and concentration of liquids, powders, and pellets. [26]

Once the fuel assemblies are loaded into the reactor, they no longer fall under the pre-irradiation neutron coincidence counting NDA jurisdiction. Instead, other safeguards measures come into play such as unattended monitoring and surveillance, containment, Cerenkov viewing devices, and spent fuel measurement systems. Muon tomography may be used to ensure spent fuel assemblies remain in their dry cask storage.

1.3 Approved Neutron Coincidence Counters for Nondestructive Assays

Many IAEA-approved neutron coincidence counters have been imagined and developed into prototypes by LANL and its collaborators over the last several decades [11]. The more widely applicable prototypes then become commercialized through various companies. For those systems that may have very niche applications, industry may provide custom orders for interested customers, but they are not highly advertised for reference. AnTech Incorporated and Canberra Industries (now Mirion Technologies) are the two main commercial suppliers of neutron coincidence counters to the IAEA. Both manufacturers must follow strict guidelines and system performance requirements in each of their designs, as dictated by the Agency. Therefore, there is no significant variation between detector models to guarantee similar performance. The IAEA has released several public documents [27] over the last twenty years containing the glossary of terms used by the Agency, the policies behind the evolution of safeguards, and the comprehensive list of detectors used in various field measurements worldwide [8] [9] (**Figure 1.5**). This incorporates the integrated safeguards approach instated in the 1990's, including the added requirements and resources needed for an AP. The IAEA/NVS/I Safeguards Techniques and Equipment [8] [9] lists and describes the coincidence neutron detector systems for the nondestructive analysis of non-irradiated fissile fuel, which is the focus of this work. These documents are the main references the greater community has to what technology is being used to realize the goals of the IAEA in routine measurements. About twenty versions of coincidence detector systems are currently in use for nuclear safeguards, with design features optimized for specific item sizes, shapes, or plutonium mass ranges

(**Table 1.1**). The associated commercial systems produced by Canberra and Antech have been compiled in this table as well as reference examples. Other systems exist beyond the twenty; through private communication with a previous system designer [10], it has become clear that not all systems that are used by safeguards customers are included in this list. Some of these systems have niche applications, so they are not widely deployed, meanwhile it is unknown why others are not listed.

It is clear that each of these systems has its own application and item range that lends itself useful to particular assay situations. It is typical that these systems remain within the set facility where an inspection will take place, due to their size and niche. Therefore, during an IAEA inspection, previous calibrations and characterizations will be used in the current analysis to perform an NDA. Inspectors are trained on how to use each system, with associated electronics and data acquisition software, and how to interpret the data acquired to reach conclusions on their NDAs. Large resource investments are associated to these measurements, and because of that, these systems are not easily replaced or interchanged. Most of these systems were designed in the late half of the 20th century and have been used since. As facilities continue to advance and the items under question become more complex, these systems may be challenged. However, since 2003, no new systems have been widely deployed, as is shown with referencing **Table 1.1**.

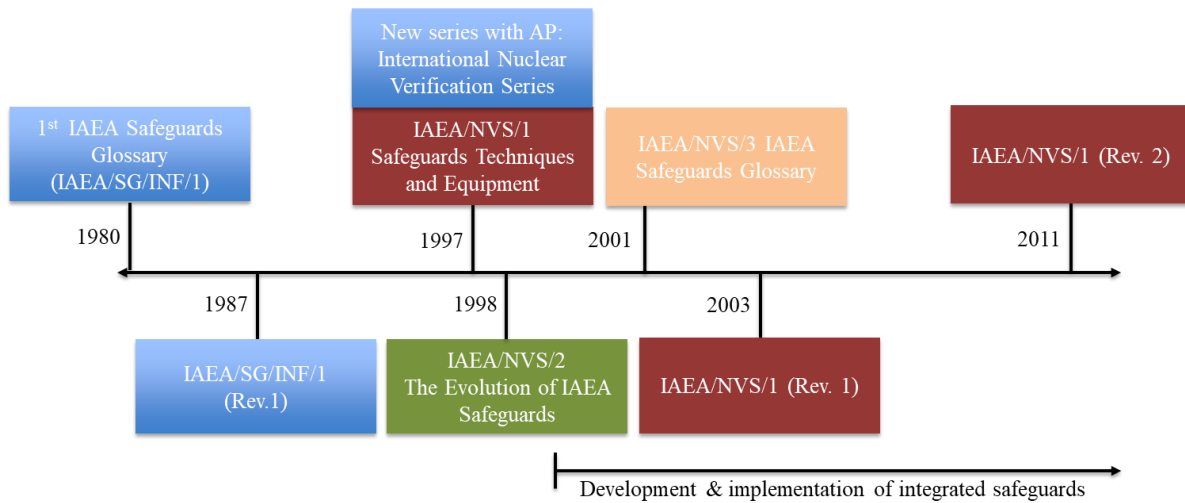


Figure 1.5. Timeline of IAEA publications containing the list of detectors used in field measurements and their respective applications.

Table 1.1. A list of given IAEA–approved neutron coincidence counters used in inspections to assay non-irradiated samples, as given in [8] [9]. These systems are listed with their commercial model numbers, as available from Mirion Technologies [28] and Antech Inc [29]. [10]

Counter Name	Counter Description	IAEA NVS Listing	Mirion Technologies Model #	Antech Model #
<i>Passive Counting</i>				
Bird Cage Counter (BCNC)	Verification of Pu mass in fast critical assembly fuel plates that are stored in containers called birdcages	2003, 2011	---	---
Compact Neutron Coincidence Counter (CNCM)	Verification of MOX fuel assemblies in shipping crates	2003	---	---
Drawer Counter (DRNC)	Verification of Pu mass in facility specific containers	2003, 2011	---	---
Fuel Assembly/Capsule Assay System (FAAS)	Verification of Pu mass in MOX fuel assemblies	2003, 2011	---	---
Fuel Pin/Pallet Assay System (FPAS)	Verification of Pu mass in MOX fuel pins in facility specific storage trays	2003, 2011	---	---
Glovebox Assay System (GBAS)	Semi-quantitative determination of Pu hold-up in gloveboxes	2003, 2011	Available	Available
Hold-up Blender Assay System (HBAS)	Semi-quantitative determination of Pu hold-up in facility blenders	2003, 2011	---	---
High Level Neutron Coincidence Counter (HLNC)	Verification of Pu in 20-2000 g canned samples (pellets, powders, scrap)	2003, 2011	JCC-31	N2018
Inventory Sample Counter (INVS)	Verification of Pu in 0.1-300 g samples. Modified version can be attached to gloveboxes	2003, 2011	JCC-12	---
Large Neutron Multiplicity Counter (LNMC)	Verification of Pu in contaminated/impure items	2003, 2011	LEMC, multiple	Available
Glovebox Counter (MAGB)	Verification of Pu mass in facility gloveboxes	2003, 2011	Available	---
Canister Counter (PCAS)	Verification of Pu mass in MOX canisters	2003, 2011	Available	Available
Plutonium Neutron Coincidence Collar (PNCL)	Verification of Pu mass in MOX fuel assemblies	2003, 2011	JCC-71, 72, 73	N2023-M, N2044, N2071

Table 1.1. Continued.

Counter Name	Counter Description	IAEA NVS Listing	Mirion Technologies Model #	Antech Model #
Plutonium Scrap Multiplicity Counter (PSMC)	Verification of Pu in 1-300 g (1-5000 g)* canned samples of scrap	2003, 2011	PSMC-01, multiple	N2098
Passive Well Coincidence Counter (PWCC)	Verification of Pu mass in CANDU MOX fuel bundles	2003, 2011	JCC-51, 41, multiple	N2442
Universal Fast Breeder Counter (UFBC)	Verification of Pu in Fast Breeder reactor fuel, up to 16 kg	2003, 2011	JCC-61, 62	---
Underwater Coincidence Counter (UWCC)	Underwater verification of Pu in fresh MOX fuel assemblies	2003, 2011	---	N2106, N2108
<i>Active Counting</i>				
Active Well Coincidence Counter (AWCC)	Verification of ²³⁵ U in high enriched U samples	2003, 2011	JCC-51	N2442
Uranium Neutron Coincidence Collar (UNCL)	Verification of ²³⁵ U in low enriched U fuel assemblies	2003, 2011	JCC-71, 72, 73	N2023-M, N2044, N2071
Waste Crate Assay System (WCAS)	Verification of waste materials, mg-kgs	2003, 2011	WCAS	N2940-2552
Waste Drum Assay System (WDAS)	Interrogation of low level waste drums for Pu mass	2003, 2011	WM3100, 3400	N2240 Series, N2223-220, N2221-220

1.3.1 Coincidence Counters Studied

The Safeguards laboratory at Oak Ridge National Laboratory houses several standard neutron coincidence counters. These include: a Canberra Industries/Mirion Technologies JCC-71 Neutron Coincidence Collar that represents the Uranium Neutron Coincidence Collar, an Antech N2071 Neutron Coincidence Collar, a large volume variant on the Mirion JCC-51, Large Volume Active Well Coincidence Counter, and a modern ^3He replacement prototype a boron-coated-straw-based High Level Neutron Coincidence Counter. Characteristics on each of these systems will be discussed below.

The Uranium Neutron Coincidence Collar (UNCL)

The Neutron Coincidence Collar was designed to measure ^{235}U content in fresh fuel assemblies used in pressurized water reactors, boiling water reactors, or Canada Deuterium Uranium reactors. It can also measure plutonium content in MOX fuel. The size of the counter's assay cavity can also be altered to better accommodate these different fuel assembly types. The rectangular detector body is comprised of four individual banks each containing six ^3He tubes with 2.54 cm diameters pressurized at 4 atmospheres (atm) embedded in a single row within HDPE moderating slabs.

The Neutron Coincidence Collar is designed to operate in two modes: active and passive. In active mode, three ^3He detector banks are connected with a fourth hinged HDPE bank (**Figure 1.6 a**), containing no ^3He tubes, whose central hole contains an AmLi source encased in a tungsten pot. In passive mode, the HDPE slab is replaced by a fourth detector bank containing ^3He tubes. This fourth bank is hinged to ensure easy placement of a fuel assembly within the cavity. Cadmium sheets can also be inserted, if desired, to reduce neutron reflections back into the system and therefore decrease the neutron die-away time.

For the JCC-71 (**Figure 1.6 a**) [30], the tubes and HDPE assembly are connected to a junction box panel containing a single preamplifier board per bank designed around an Amptek A111 charge sensitive preamplifier, discriminator, & pulse shaper chip [31]. Each bank is then capable of producing a signal. The Mirion electronics used in each of their junction boxes is named the JAB-01 Preamplifier/Amplifier/Discriminator board which houses the A11 with additional shaping and OR logic. The junction box transfers HV between the connected banks through "HV in" and "HV out" connections, and it contains "Signal in" and "+5 V in" inputs and "Signal out" and "+5V out" outputs to interconnect the banks and communicate with an external data acquisition system. For the N2071 (**Figure 1.6 b**) [32], these junction boxes house the Amptek A111 chip and the necessary low voltage, signal and HV distribution networks. It has the same connections on the box faces as the JCC-71, and they are both compatible with the same data acquisition technologies.

The Active Well Coincidence Counter (AWCC)

The LANL design standard version of the AWCC, manufactured by Canberra as model JCC-51, uses 42 ^3He tubes with 2.54 cm diameters pressurized at 4 atm. These tubes are arranged in two concentric rings of 21 tubes each, embedded in HDPE, for a total system diameter of 50 cm; they extend throughout the 70 cm height of the cylindrical body with an active length around 51 cm [33]. The central cavity dimensions can be altered from as small as 23 cm in diameter and 21 cm in height to as large as 23 cm in diameter and 35 cm in height by removing the nickel ring and spacers within the end plugs to accommodate larger items. The AWCC uses two AmLi sources for active interrogation. The system can be operated in active fast, active thermal, and passive thermal configurations by adding or removing the AmLi and Cd inserts.

The ORNL Large Volume Active Well Coincidence Counter (LV AWCC) is a variant of the JCC-51 but with a larger cavity (**Figure 1.6 c**). This model uses 48 ^3He tubes with 2.54 cm diameters

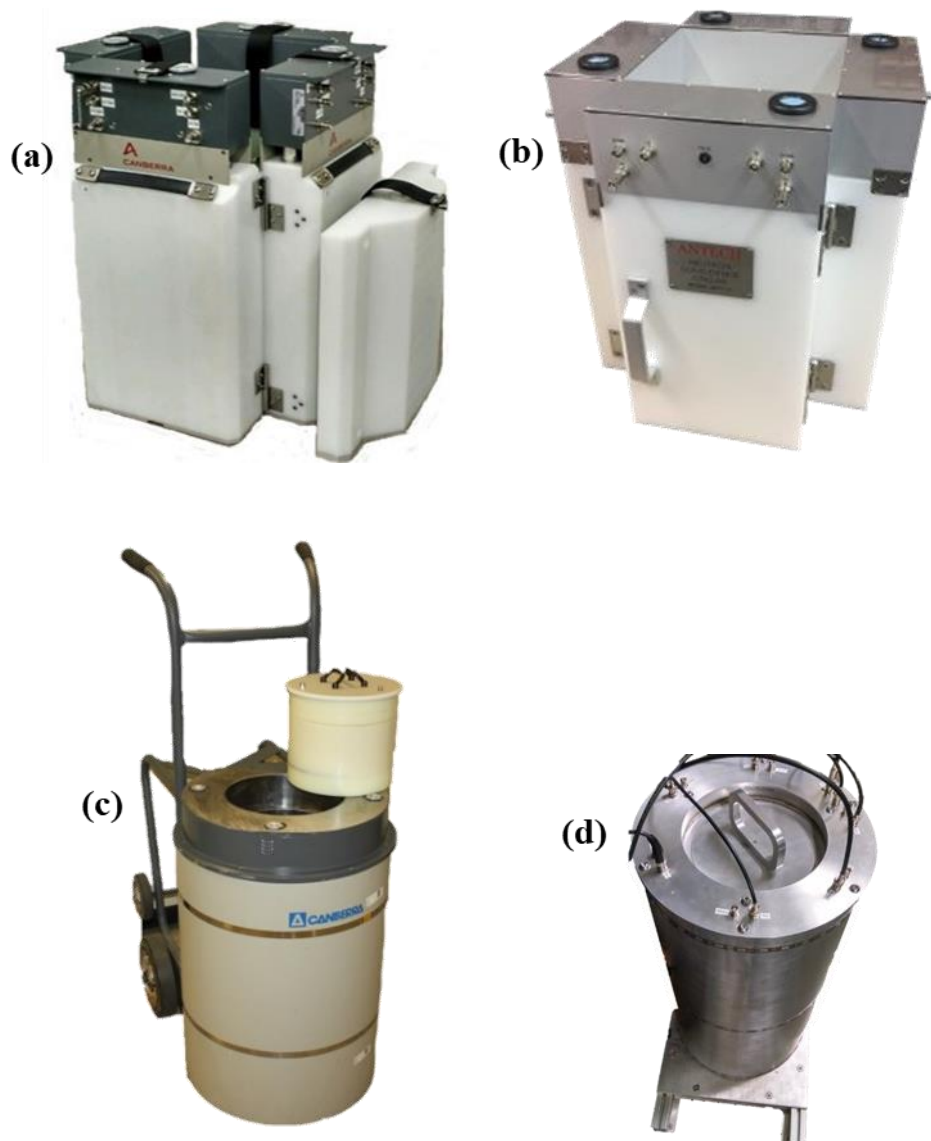


Figure 1.6. (a) JCC-71 UNCL (b) N2701 UNCL (c) JCC-51 Large volume variant AWCC (d) Boron coated straw HLNC.

pressured at 4.5 atm and arranged in two concentric rings encompassing a 27.94 cm diameter by 38.10 cm tall assay measurement cavity. The tubes are organized into eight groups with each group connected to a Canberra JAB-01 Preamplifier/Amplifier/Discriminator board. The top of the system has a “HV in”, “+5 V in” and three signal output connections; one for each of the two rings plus a total summed signal output.

A Boron-Coated-Straw-Based High Level Neutron Coincidence Counter (HLNC)

A boron-coated-straw-based (BCS) counter was built by Proportional Technologies Incorporated (PTI) as a direct replacement to the HLNCC-II for a previous project at ORNL [34]. The BCS-based HLNCC-II is composed of 804 ^{10}B straws, each 4.4 mm in diameter, allowing for a tight packing within the geometry to help improve detection efficiency by compensating for the lower neutron capture cross section compared to ^3He . $^{10}\text{B}_4\text{C}$ at 96% enrichment is sputtered along the inside of an aluminum or copper straw with a thickness of approximately 2 μm and filled with a mixture of P-10 gas at 1 atm. The dimensions of the ^3He HLNCC-II are preserved, although there is an increase in mass of 6 kg; it consists of a cylindrical HDPE body with 34 cm diameter and a height of 68.2 cm (**Figure 1.6 d**). The sample cavity is 17 cm in diameter and 41 cm in height and is sealed with top and bottom end plugs made of HDPE and aluminum. There are six detector banks, of 134 tubes each, connected together and processed by six amplifiers made in-house at PTI. The 804 straws are uniformly dispersed within the moderator for thermalization of neutrons. Six signal connections are available on the top face of the system. This signal can then be read out with standard acquisition software.

1.3.2 Current Data Acquisition Technologies

Neutron coincidence counters almost exclusively operate in combination with a shift register logic module when used in the field. The shift register provides HV to the system and a low voltage to the preamplifier boards, it acquires the neutron pulse trains from the connected signal(s), and then it performs the data analysis in combination with an affiliated software, INCC, as discussed in Section 1.1. Today, the IAEA uses the Mirion JSR-12 model, the Neutron Coincidence Analyzer, paired with a laptop using the INCC software and a printer during its measurements using these coincidence systems [9]. The JSR-12 (**Figure 1.7**) was designed by LANL and first produced commercially by Canberra in the early 1990s. It was made as an upgrade from the previously used JSR-11. This module included a new LCD screen compared to the JSR-11, a 4 MHz internal clock, and a serial port to connect it to a computer. The JSR-12 counts and records pulses from neutron events and their time-correlations for coincidence counting.

In addition, Mirion has also produced commercially available JSR-14 Neutron Analysis Shift Register and a JSR-15 Handheld Multiplicity Register modules (**Figure 1.7**). These shift registers have since introduced further improvements to the data acquisition hardware and software such that the interface between the inspector and the module are now easily done through the computer, and multiplicity rates can be recorded. Both modules are more easily portable and battery powered for ease of use, and their internal clocks are significantly faster than the JSR-12.

The JSR-15 is used throughout this work as the comparison for all data acquisition and analysis as it is the most modern shift register available to the Agency. It was designed by LANL and made commercially available by Canberra in 2011. It has a large LCD screen face paired with push buttons that allow easy option selection independent from a computer. It may be plugged in but also holds a sufficient charge for various measurements. It provides the HV, LV, and can acquire 3 inputs simultaneously: one in the signal in port, and 2 others in the auxiliary 1 and 2 ports. A measurement summary can be written out on the LCD screen for the signal in port listing the cycle data, singles rate, doubles rate, triples rate and associated uncertainties, (R+A) values, A values, and a background value. A count rate value can be

produced for the two auxiliary ports. The JSR-15 has a 50 MHz internal clock so it may handle higher count rate applications. Despite the added capabilities and benefits offered by JSR-15, due to the cost of replacing the JSR-12 in many facilities worldwide, it is still widely used for inspections. This prevents any acquisition from recording a measured triples rate and it operates on a lower internal clock speed for incoming pulses to be processed.



Figure 1.7. (a) The Mirion Technologies JSR-12. (b) JSR-14 (c) JSR-15 [28]

1.4 Current Limitations of Neutron Coincidence Counting

Neutron coincidence counting works. It has been applied in hundreds of thousands of NDAs to successfully verify a State's compliance to the obligations of its respective safeguards agreement. It accomplishes the relevant tasks of an inspection and has for decades. However, through the use of these systems, several limitations and weaknesses have become apparent from a fundamental perspective.

The process in which an NDA is carried out with these systems contains many different correction factors that are not based on system characteristics that can be understood from physics first principles, as discussed in Section 1.1.1. The known-alpha and calibration curves involve empirical fits that are dependent on the system used, the item in question, and the representative sources previously measured. These empirical fits are completed at the time of the measurement and are subject to inspector decisions. A passive NDA using the point kinetics equations uses an approach much more grounded in physical parameters, but it still suffers from the challenges of a reliable system characterization. Representative source standards are not easily accessible, and the system parameters oftentimes are selected based on historical values, resulting in sizeable uncertainties. This analysis also contains calculated gate fractions, which are dependent on the timing gates selected for neutron coincidence counting analysis, and other correction factors that cannot be broken down into fundamental properties.

The data acquisition hardware used with these systems, such as a commercial-off-the-shelf shift register, has a limited number of input signals for analysis, and it reports the total summed results from all connected channels, rather than each individual counter bank's results. This limits the amount of information obtained from the system- constraining it to a single neutron pulse train analysis. If one of the banks of these systems is malfunctioning at the time of measurement, the only indication would be a decreased count rate measured from the source relative to previously measured values. This may not be easily identified, depending on the change in count rate, empirical fit uncertainty, or other environmental factors. A lesser mass may be determined from this NDA, raising further compliance questions. In addition, with models such as the Canberra JSR-12, only the singles and coincidence values are reported, which limits the use of any neutron multiplicity counters for a three-parameter assay. Finally, when data is acquired using a shift register such as the JSR-12, there is no saved record of measurement of the neutron pulses as a function of time for offline replay and analysis if a measurement is called into question. A measurement would need to be repeated through means of another visit from inspectors.

Most of these systems were designed in the late half of the 20th century and have been used since. Both commercial suppliers, Mirion and Antech, implement similar electronics in their systems based on the Amptek A111 charge sensitive preamplifier, discriminator, & pulse shaper chip [31]. This A111 was designed in the 1960's for x-ray applications, and it was adopted for use in neutron coincidence counters in 1984 by Swansen [35]. Since this adoption, the A111 has been applied in all successive neutron coincidence counters. However, over the last few decades there has been a very large advancement in the realm of pulse processing electronics. This means that not only are electronic circuit designs and components developed in the 1960's powering and processing the signals from these counters, but the same A111s are paired across a wide range of neutron coincidence counters in a variety of geometries, tube lengths, fill pressures, and rate applications. This occasionally causes the response of the system to not operate at its optimal performance.

Today, the amount of nuclear material and the number of nuclear facilities under IAEA safeguards is growing steadily [36]. More nuclear power plants are being built and used in nations worldwide, and the demands are also increasing as more facilities are decommissioned, generating additional needs to verify nuclear material packaging, movement, and disposition. The IAEA resources are stretched extremely thin to ensure they can complete all required tasks in a timely fashion. There have been two revisions on the Safeguards Techniques and Equipment publications in 2003 [8] and 2011 [9].

During these 8 years, no new coincidence counting systems were openly adopted. The sole change between Rev. 1 and Rev. 2 for coincidence systems was the removal of the Compact Neutron Coincidence Counter (**Table 1.1**). This, however, does not reflect the efforts of the safeguards community; there have been large movements to develop and test novel system models, data acquisition technologies, and the recent movement to build and characterize systems utilizing ^3He alternatives as drop-in replacements to address the reported ^3He shortage. Despite this effort, an updated revision has not been released within the last 7 years to reflect new adoptions of these systems. This statement is not acknowledging the advancements incorporated in other realms of the safeguards field, including differential die-away self-interrogation and remote sensing; but for neutron coincidence counting, the hope of wide-spread adoptions of new systems to replace pre-existing functioning counters is not well-grounded.

The main difficulties associated with attempting to replace current neutron coincidence counting technology are that ^3He gas has optimal performance over other neutron capture reactions, and the current systems fulfill all required tasks of an inspection. The different neutron coincidence counting system models are deployed worldwide with existing infrastructure, and IAEA inspectors have many hours of experience and training on them. In order to begin replacing these systems, the IAEA would need to significantly alter their annual budgets, and for an organization with limited budgets to fulfill all obligations, the perceived benefits and tangible improvements would need to be far-reaching and guaranteed; at this moment, they are not. As the pressure on IAEA resources continues to grow, there's a drive to do more with less. New ways of using existing systems and the data collected with them are needed, combined with ensuring the continued functionality of the current safeguards instrumentation fleet.

1.5 Addressing the Concerns, A Dissertation Overview

How do we then get more information out of the same system? My current drive to advance the field of neutron coincidence counting for international safeguards is to improve the functionality of currently deployed systems in the measurement capabilities, data acquisition, and analysis fronts. This will minimize costs, while still modernizing and advancing the field. In using modern data acquisition, advanced data analysis techniques, and improved system design, neutron coincidence counting may be more widely applied to measure complicated items, with modern electronics and better calibration procedures; ultimately leading to improved performance and more confidence in a system's reliability.

This can be accomplished by obtaining an in-depth physical understanding of the system performance using additional capabilities of List Mode Data Acquisition (LMDA) paired with multichannel analysis using updated modern electronics. The Hungarian Institute of Isotopes/ Centre for Energy Research Pulse Train Recorder-32 (PTR-32) LMDA hardware and software module [37] is the only commercial-off-the-shelf LMDA module approved for use by the IAEA. LMDA provides a complete record of the measurement taken, with offline analysis options. Using LMDA allows a careful inspection of the system parameters, with low associated uncertainties, through detailed analysis of the neutron pulse train- which is grounded in true physical parameters. The PTR-32 is also directly compatible with existing neutron coincidence counters through its 32 channel input BNC connections, for a drop-in replacement. It was approved for use in 2014, but its use has not since been well characterized. In addition, more signal outputs may be added to existing counters by introducing additional preamplifiers into the system. The footprint of these systems, and signal output format, may also be maintained. Each preamplifier is then capable of producing a measurable signal from its respective grouping of ^3He tubes. The more preamplifiers used, the smaller the groupings, and the more detailed information may be obtained. In doing so, modern commercial electronics may also be introduced. This

not only would help mitigate costs associated with introducing more electronics, but it would help move these existing systems into current day and provide additional pulse processing capabilities.

In order to implement these changes, LMDA technology and its associated analysis procedures must be used with preexisting neutron coincidence counters. Today, list mode capabilities are not being fully utilized in safeguards neutron counting systems or by corresponding analysis methods. To make this possible, it was necessary for me to develop a characterization and measurement method that translates between various counting systems and achieves the same (if not better) results as shift register-based analysis. This is done in Chapter 2. This allows for an understanding of each system's behavior for diagnostic, characterization, acquisition, and analysis purposes for in-field and in-laboratory measurements.

In addition, I had to expand upon current neutron coincidence counting procedures, theory and equations to exploit this greater knowledge granted by LMDA. To do this, I had to obtain a high-fidelity physics-based understanding of these systems, and have an in-depth understanding of all of the characterization parameters and their sources of error. System parameters such as coincidence time windows, dead time, efficiency, die-away time, and non-ideal double pulsing are explored in new ways that are not possible using traditional shift register logic. This is done in Chapter 2, 3, 5, 6 and 7.

Finally, the feasibility of replacing present electronics with modern prototype electronics on smaller groupings of tubes was evaluated in support of a Department of Energy National Nuclear Security Administration Defense Nuclear Nonproliferation Research and Development funded project, the "List Mode Response Matrix for Advanced Correlated Neutron Analysis for Nuclear Safeguards." The List Mode Response Matrix project consisted of electronics design and development, experimental, and simulation tasks performed by a large team with various skill sets over four years. This dissertation research directly supported, and provided, the experimental objectives of the project in developing and implementing the procedures for LMDA system characterization and comparative analysis, testing and evaluating the ORNL-developed preamplifiers, presenting work at international conferences and project reviews, collecting and analyzing the spatial response data for the various stages of the project, and simulating the system's response to a ^{252}Cf to compare and evaluate the MCNP model's performance to physical measurements. These details are discussed in Chapter 4. Working alongside the designers at ORNL, I tested these prototype electronics, implemented on all 18 ^3He tubes of the JCC-71 Neutron Coincidence Collar, with the relevant safeguards analysis approaches and software in several iterations to understand, evaluate, and optimize their performance. This work is described in Chapters 3 and 4.

The List Mode Response Matrix generated a need for the implementation and testing of these new technologies, with a focus on source positioning location using a maximum number of counter system channel outputs. It also led to the diagnoses of several non-ideal behaviors within the A111 electronics, the prototype electronics, and the PTR-32 module. In doing so, the signatures of these historic counters were investigated to provide a much more detailed understanding of the system performance and limitations; meanwhile their capabilities and applications were also extended. With a thorough understanding of the system characteristics and performance, and access to the full neutron pulse train with offline analysis options, neutron coincidence counters may be used to perform an absolute source measurement to self-certify calibration sources on the same order of precision as national metrological laboratories. This could help expand the use and interest of neutron coincidence counting, and assist with nuclear data concerns. The relationship of uncertainties in these parameters are studied for their influence on the final precision of the certification in Chapter 6. These topics will be studied using the systems described in Section 1.3.1, 1.3.2, and the PTR-32 LMDA.

Chapter 2

List Mode Data Acquisition and Analysis¹

2.1 Abstract

There is a perceived trend toward augmenting or interchanging current international safeguards shift register-based data acquisition systems with list mode data acquisition systems because of their greater versatility. Neutron list mode data analysis offers comparable analytical results to the more widely used shift register analysis in nuclear material quantification applications. In addition, it offers several instrument diagnostic benefits that are specifically useful to in-laboratory characterization and calibration measurements such as identification of non-ideal behavior, optimization of operational parameters from a single measurement, and a better understanding of the physics-based behavior for a more precise system representation and more confident assay results. In this work, two commercial-off-the-shelf International Atomic Energy Agency-supported technologies are used for a typical detector characterization procedure. Specifically, a ³He-based Canberra Industries JCC-71 Neutron Coincidence Collar is characterized using the Hungarian Institute of Isotopes' Pulse Train Recorder-32 (PTR-32) list mode data acquisition system, and the results are compared to those found using the standard Canberra Industries JSR-15 model shift register. The quantitative results from the two systems are in agreement, which demonstrates that the PTR-32 is a technically viable alternative to conventional shift register electronics for this task. A suitable procedure for full instrument characterization is described, and the added benefits of list mode for characterization and data collection are discussed. This is an important step toward establishing a procedure for the routine use of list mode data acquisition and analysis for system characterization in safeguards field applications.

2.2 Introduction

Shift register data acquisition systems are well-established in international safeguards where they are used to measure and record detected neutron events. When coupled to neutron coincidence counters, shift registers help perform nondestructive assays on nuclear material samples using time-correlation counting techniques [4]. There are several other plausible analysis options beyond time-correlation analysis that allow nondestructive assays to be performed, but this paper will focus on this approach since it is the most commonly used approach in current field measurements. Shift register circuits are composed of a series of clock-driven flip-flops linked together in a number of stages. These stages are driven by a set frequency of the internal clock to process the incoming stream of electronic pulses, where each pulse represents a detected neutron event, with a preset timing gate. Through this logic circuit, time-correlated neutrons can be detected and related to the effective mass of a nuclear material sample undergoing spontaneous or induced fission. The accurate measurement of these neutrons is crucial to the successful quantification and verification of the declared mass of nuclear material within a material control or

¹This chapter was originally published in a peer reviewed journal under the original title “Using the JCC-71 neutron coincidence collar as a benchmark for detector characterization with PTR-32 list mode data acquisition,” A.T. Simone, S. Croft, J.P. Hayward, L.G. Worrall, Nuclear Instruments and Methods in Physics Research Section A: Accelerators, Spectrometers, Detectors and Associated Equipment, 908, pp.24-34. It is printed here with permission from the editors in its original form.

international safeguards program. Therefore, it is imperative that the instrumentation used for these verification measurements operates as designed, without artifacts, so all parties have confidence in the results of an assay. Additionally, the ability to confirm correct setup and operation of a nondestructive assay system is a desirable acquisition feature, improving the effectiveness and efficiency of safeguard inspections.

In general, list mode data acquisition (LMDA) systems, as applied in international safeguards applications, are based on a common field programmable gate array (FPGA) circuit with multichannel signal inputs. They function by recording neutron arrival times for each channel on an event-by-event basis, within a specific timing resolution, for the entirety of a measurement. Typically, a timing resolution of tens to hundreds of nanoseconds is provided, which is generally acceptable for typical neutron coincidence counters that have characteristic neutron lifetimes in the few tens of microseconds range. In a post-measurement analysis of the pulse train, various timing gate windows can be applied to the same data set to optimize statistical precision and to exploit various modes of analysis. This type of analysis has been proven to have comparable precision to shift register analysis [38] [39], while offering several detector system diagnostic benefits not available with existing shift register acquisition platforms.

The European Safeguards Research and Development Association (ESARDA) Nondestructive Analysis Working Group organized several benchmark measurements in 2009 for a comparison between then-available list mode acquisition modules for use with neutron coincidence counting systems [40] [41] [42]. In parallel to this benchmark, individual laboratories and companies have continued investigating, improving, and implementing list mode models for use with various neutron coincidence systems [38] [43] [44] [45] [46]. Although it is an old concept, there is renewed interest in list mode systems that have progressively benefited from the reduced size and increased functional density of electronics (e.g., FPGAs) and storage media, in addition to increased computing power available; i.e. list mode analysis is continuously reformulated as each generation of electronics is better than the previous, and thereby the same concepts may be reapplied to a wider range of applications. Although the IAEA has recently approved a LMDA system for use, current list mode analysis for in-field safeguards inspections is still limited by the lack of straightforward, user-friendly analysis interfaces, the relatively large file size associated with high count rates, and limited processing power. However, its additional capabilities have expanded the scope of detector characterization and calibration in the laboratory setting. The use of list mode has extended the investigation of physical parameters including optimal gate width and gate utilization factors [47], double pulsing [48], neutron correlation analysis [49], detector dead time [50], and differential die-away self-interrogation [51].

List mode has also expanded steadily to benefit other fields such as high energy physics, medical imaging and homeland security, in addition to international safeguards. Since safeguards is not the driving field for list mode development, we are able to draw inspiration from these developments and reengineer and expand these methods of analysis for our own purposes. Our intention here is not to provide a comprehensive summary of this technology, since the applications of list mode are vast, but instead to discuss some established and emerging examples in which list mode analysis is relevant. The advantages provided by offline analysis of the full system also pertain to coincidence spectroscopy [52] and imaging arrays [53] using various scintillators, positron emission tomography reconstruction in medical applications [54], and measuring accelerated particle flux-induced reactions from ion beams [55], to provide some examples. The full-time record of measurement and post-processing options of these data allow for simultaneous multiparameter acquisition, gamma rejection in false coincidence events under varying timing windows, optical fiber resolution and linearity tests, and complex image reconstruction analysis. Both commercially available systems and in-house designed [56] [57] [58] data acquisition systems are frequently used in experimental setups, depending on the needs and complexity of the measurement; the FASTComTec Multiparameter TOF Acquisition System [59] has been chosen by some in the literature for use with scintillators and spectrometers, and the Hungarian Institute of Isotopes' Pulse Train Recorder-32 (PTR-32) [37] has commonly been used for neutron multiplicity counters in international safeguards.

Ultimately, with a full record of the measurement, an enhanced physics-based understanding of coincidence counting system characteristics can be achieved using LMDA. The use of list mode permits second order effects on neutron correlation analysis to be examined, for more a precise system representation and more confident assay results. Analyzing the pulse train offline with various gating parameters allows flexibility for the system; although this same analysis could be performed using shift register data acquisition systems, LMDA reduces the hurdle by utilizing a single pulse train rather than independent pulse trains for each timing window. Monitoring the behavior of the system for the duration of data acquisition using time-tagged list mode techniques also allows for greater information on the state-of-health of the system and of each individual detector bank. If a bank malfunctions, the full data acquisition is not compromised, and can be amended offline. In addition, due to the multichannel input capability, spatial patterns and cross-correlation may be used in the future for complex systems (e.g., a fuel assembly), which cannot be supported by current shift register technology. As they exist now, list mode systems are most applicable to in-laboratory safeguard instrument characterization measurements, where their extended capabilities are most beneficial to a characterization and calibration regimen on a more flexible timeline. However, efforts are underway to make list mode more streamlined for practical field applications.

Because of this, nondestructive assay measurements using neutron coincidence counters remain limited by the constraints of the shift register approach. To better the general understanding of the applications of LMDA and ease the transition to this data-rich system, an accepted procedure for a full detector calibration and its use must be outlined, and the accuracy of the measurement results for systems currently used in the field must be demonstrated. This paper serves as an in-depth characterization procedure for a representative ^3He -based neutron coincidence counter, the Canberra Industries² JCC-71 Neutron Coincidence Collar [30], which is used in conjunction with the advanced LMDA options made available by the PTR-32. We select the Neutron Coincidence Collar to be used with the PTR-32 first in part due to the lower count rate associated with measuring fresh fuel and the efficiency of the system. The resulting file sizes will be smaller than with other detector systems, and therefore, more easily handled by everyday computers. The results obtained through the PTR-32 are compared to the results obtained using the JSR-15 Handheld Multiplicity Register [60], and the additional capabilities of LMDA are described in the context of international safeguards measurements. We suggest that the measurements and information described herein may be extended for use with other ^3He -based neutron coincidence or multiplicity counters.

2.3 Shift Register Analysis and Detector Characterization Parameters

When a fission takes place in a measurement item, a number of neutrons are released essentially simultaneously [61]. These time-correlated neutrons are slowed in the moderating body of a detection system, spreading out the distribution over a longer period of time, related to the characteristic neutron die-away time, τ . The thermalized neutrons captured by the ^3He tubes may be registered, after shaping and amplification, as electronic logic pulses (e.g. TTL or LVDS) by the shift register software, which are then translated into coincidences and higher order multiplicities using appropriate timing gates driven by flip-flop circuitry.

In addition to recording the incoming pulse train, the shift register module performs a signal-triggered coincidence measurement. The action of the shift register can be thought of in the following

² Canberra Industries has recently become Mirion Technologies.

way. It is designed to count pairs (or coincidences) with respect to each incoming event using a gating structure and logic that naturally records the second reduced factorial moment [4]. Each pulse triggers, and thus marks, the opening of a time gate called the predelay, T_p (see **Figure 2.1**), which is a set duration of time when the shift register does not record subsequent correlated events. During this short time interval following a pulse, the amplifiers are biased by pulse pileup and electronic dead time, and the count rate cannot be accurately measured. Consequently, the shift register waits for these effects to stabilize before beginning to collect coincidence data. Having a predelay that is too long in duration causes true neutron counts to be missed, so determining the optimal time duration is essential. Once the predelay time has ended, a longer gate width, T_g , is opened to collect neutron event pulses. All succeeding neutron events detected within the set gate width are recorded as a histogram (2 time-correlated neutrons for coincidence counting, and greater numbers such as 3, 4, and 5 for multiplicity counting). This gate width must be large enough (e.g., 64 μ s) to ensure collection of correlated neutron events without allowing background neutron events to dominate; this distribution of true fission neutrons as a function of time approximately follows an exponentially decaying trend. After the pulse collection for the set gate width has completed, a long delay is set where no events are recorded (commonly on the order of thousands of μ s). After the long delay, a second gate of width, T_g , is opened, and neutron events are recorded (as Accidentals) for this duration. This is repeated for every neutron event acting as the initial trigger. The pulse shifting process through all stages of the register is related to the number of stages and the clock speed of the module (e.g., JSR-15: 50 MHz), which is typically on the order of tens of microseconds. This process could produce a Rossi- α distribution through list mode analysis [4] (**Figure 2.1**) which can be used in part to describe the characteristics of the instrument such as neutron die-away time.

The total number of neutron events measured during an acquisition is recorded as the singles count tally. The doubles count tally corresponds to the number of times two neutrons were measured together during the acquisition, with each pair including the trigger event as one of the pair. Higher multiplicities, such as triples, are not measured quantities, but derived quantities, obtained from factorial moments calculated using the techniques outlined by Hage and Cifarelli [62] [63]. These are not used for the assay of fresh fuel in the Uranium Neutron Collar (UNCL) [64]. The detected events are tabulated according to the number of 1 registered neutron events and 2 registered correlated neutron events to form a neutron count distribution; that is if 2,000 1s (single neutron events) and 700 2s (double neutron events) were recorded, then multiplicities of 1 and 2 would have 2,000 counts and 700 counts, respectively. However, in addition to truly time-correlated fission neutrons, background and (α , n) neutrons are also detected within these timing gates. These “Accidentals” (A) generate artificial coincidences which must be subtracted.

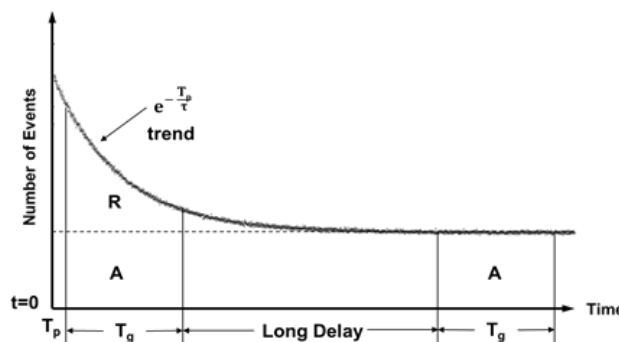


Figure 2.1. A Rossi- α distribution demonstrating the relevant timing gates for a number of neutron pulses. [5]

The likelihood of higher order events being measured during these timing gates is related to the detector efficiency, neutron die-away time, and the dead time of the detector plus electronics system, in addition to background cosmic ray spallation events causing false multiplicities to be measured due to a simultaneous increase in count rate relative to the neutrons produced by the fissioning source. The accurate characterization of these parameters for an instrument is crucial to a successful verification measurement of special nuclear material. The single neutron efficiencies of various neutron coincidence and multiplicity counters differ greatly, ranging from approximately 10% [65] up to 65% [66], and are mostly dependent on system geometry and the number of ^3He tubes used in the design. Because neutron die-away time is a measure of the time it takes for an emitted neutron to thermalize and be detected by the system, a short neutron die-away time is desired to improve measurement precision through a lower accidental rate. The dead time is related to the charge collection and pulse processing recovery time of the ^3He tube plus electronics system. It depends on the distribution of charge throughout the individual amplification chains and varies based on the number of preamplifiers used in the system. During this characteristic dead period, individual neutron interactions cannot be distinguished, so they do not contribute to the neutron pulse train and information is lost. The total system dead time is therefore less than an individual channel's dead time because there are multiple amplification chains (i.e., if one channel is dead, the other remaining channels may still detect a neutron event). The resulting count rate within this timing regime is decreased approximately by the percentage this detector bank would contribute to the total rate. The dead time contribution from either a shift register or LMDA system is considered negligible. It is necessary to have high confidence in these parameter values prior to using a counter for an assay, therefore proper characterization procedures and methodology are required.

2.4 Instrument Setup

The JSR-15 Handheld Multiplicity Register was designed by Los Alamos National Laboratory and built by Canberra Industries. The model JSR-15 is a commonly used shift register which has replaced the previous JSR-12 and JSR-14 models. The JSR-15 can output a user-selected high voltage to supply the ^3He tubes, a +5 V output to provide power to the neutron coincidence counter electronics junction box, and it has a "Signal in" BNC connection in addition to two auxiliary scaler inputs that process TTL pulses. The internal clock speed of the JSR-15 is 50 MHz, which allows for pulses separated by at least 20 ns to be recorded. It is typically used in conjunction with the IAEA Neutron Coincidence Counting (INCC) Program [12] through a USB computer connection. A JSR-15 was used by Canberra Industries for an initial detector characterization prior to shipment of a JCC-71 Neutron Coincidence Collar, described below.

The PTR-32 was chosen as the preferred list mode acquisition system for this work since it has already been approved for use by the IAEA. The hardware contains 32 BNC channel inputs and can output a user-selected high voltage and +5 V. It communicates with a separate computer GUI interface through a USB connection. Within the software, the user can set a count time limit, the number of cycles desired, and/or a pulse limit before beginning acquisition. As data is acquired, the window updates a plot showing the number of counts as a function of follow-up time (which is the time between subsequently registered neutron events), the total count rate, and the acquisition time. The system can handle rates up to 3 MHz of periodic pulses, and it can process pulses separated by at least 10 ns. During a measurement, the individual rates measured on each of the detector banks can be monitored using the "Channel Rates" option.

A Canberra Industries-built JCC-71 Neutron Coincidence Collar (used as an UNCL) was characterized using the PTR-32. This instrument was built and shipped to Oak Ridge National Laboratory (ORNL) after it was factory tested by Canberra for performance evaluation. The Neutron Coincidence Collar was designed to measure ^{235}U content in fresh fuel assemblies used in pressurized water reactors (PWRs), boiling water reactors (BWRs), or Canada Deuterium Uranium (CANDU) reactors. It can also measure plutonium content in mixed oxide (MOX) fuel.

The rectangular detector body (**Figure 2.2**) is comprised of four individual banks each containing six ^3He tubes, with 2.54 cm diameters and active length of 33 cm [30], embedded in a single row within high-density polyethylene (HDPE) moderating slabs. The tubes and HDPE assembly are connected to a junction box panel containing a single JAB-01 preamplifier/amplifier/discriminator board per bank. This Canberra amplifier/discriminator board is designed around an Amptek A111 preamplifier chip. The junction box transfers high voltage (HV) between the connected banks through “HV in” and “HV out” connections, and contains “Signal in” and “+5 V in” inputs and “Signal out” and “+5V out” outputs to interconnect the banks and communicate with an external data acquisition system. This entire assembly has a height of 52.4 cm and weighs approximately 38 kg.

The Neutron Coincidence Collar is designed to operate in two modes: active and passive. The former mode is used to measure U fresh fuel, and the latter mode is used to measure ^{240}Pu in MOX. In active mode, three ^3He detector banks are connected with a fourth hinged polyethylene bank, containing no ^3He tubes, whose central hole contains an AmLi source encased in a tungsten pot. In field applications, four measurements must take place for an accurate active interrogation assay: 1) no AmLi source, nor fuel assembly is present, a background measurement is conducted, 2) no AmLi source, the fuel assembly is present, the doubles count rate background measurement is conducted, 3) an AmLi source is present, no fuel assembly, the singles count rate background measurement is conducted, and 4) an active measurement is taken. The active measurement uses the AmLi source to interrogate the ^{235}U in the fuel assembly by inducing fissions, and the neutrons released are then detected by the ^3He tubes. From the combination of both the background and the active measurements, the linear density of ^{235}U in a fresh fuel assembly can be calculated. In passive mode, the polyethylene slab is replaced by a fourth detector bank containing ^3He tubes. This configuration is used to measure ^{240}Pu -effective content in MOX by detecting neutrons emitted from the spontaneous fissions of the Pu isotopes. This fourth bank is hinged to ensure easy placement of a fuel assembly within the cavity. Cadmium sheets can also be inserted, if needed, to reduce neutron reflections back into the system and therefore decrease the neutron die-away time.

The size of the counter’s assay cavity can also be altered to better accommodate different fuel assembly types. The Neutron Coincidence Collar is designed to accommodate either PWR fuel assemblies or smaller BWR assemblies within the cavity. The larger configuration measures 23.4 cm x 23.4 cm, and the smaller configuration measures 16.5 cm x 23.4 cm; the geometrical change is made by sliding one of the detector banks inward to fit an inner screw position. To allow all four detector banks to be characterized simultaneously, the passive mode configuration was selected for this work. The Neutron Coincidence Collar will further be referenced as the UNCL. The UNCL was arranged and fixed in the passive, PWR configuration without cadmium inserts for these measurements.

The UNCL “High voltage” and “+5 V” ports were daisy-chained between banks using BNC cables connected to their appropriate inputs and outputs; both the incoming high voltage and +5 V were supplied by the PTR-32 module. Each of the four detector bank “Signal out” channels were connected to an input channel on the PTR-32.

The PTR-32 software provides various offline analysis options. When a pulse train is recorded, the summation of all channel inputs connected to the board at the time of measurement is saved as a single file. Each of the channels can be extracted from this summed pulse train using either the “Unfold” option, which will produce 32 individual files—one per channel including unused channels—or using the “Subtract” option. Subtraction allows the user to manually select which channels to remove from the current pulse train. This is particularly useful if post-measurement a problem has been identified with a tube or bank and the measurement is not able to be repeated. The problematic bank’s pulse train can be subtracted and the remaining pulse train will be intact for analysis, albeit a non-ideal analysis, but not all of the measured data would be lost. Any number of channels can be placed in coincidence using the simple “Channel Coincidence” submenu, which combines pulse trains into a single file reporting coincidence events. Additionally, the neutron count distribution can be produced using the “INCC export” option (which saves data in an output with similar format to INCC), the Rossi- \square distribution can be produced and saved using the “Rossi Alpha” menu, the data can be fit using the “Fit exponential” function, and a portion of the pulse train as a function of time can be omitted using the “Chopper” menu.

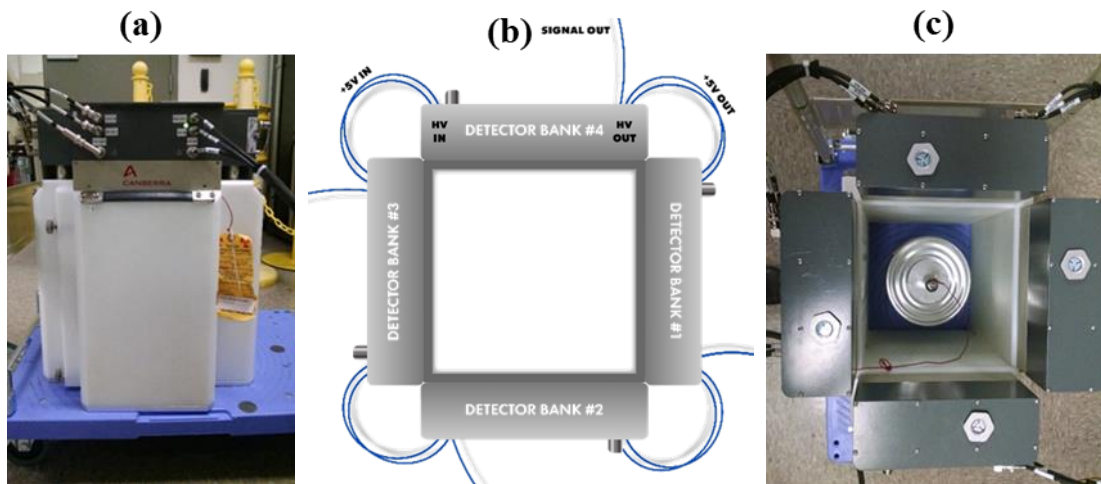


Figure 2.2. (a) Side view of the JCC-71 Neutron Coincidence Collar with input/output wires connected (b) Illustration and (c) photo of a top-down view of the UNCL showing a ^{252}Cf source placed on a metal stand in the center of the detector body.

Ultimately, these built-in features of the PTR-32 list mode analysis provide additional capabilities with a potential for improved system diagnostics.

2.5 JCC-71 Characterization using PTR-32

When the UNCL was received at ORNL, all four detector banks were connected to the inputs of PTR-32 and basic source response checks were conducted. After this, a full characterization of the system was performed. These characterization measurements are described in detail below and include the determination or optimization of the operating HV characteristic, timing gate parameters, neutron die-away time constants, absolute efficiency, and finally dead time estimation. All list mode acquisition results are compared with the Canberra-measured values reported using their own JSR-15 shift register at their facility. These values were given in the shipping documents accompanying the system, which incorporate the standard system functionality tests and their associated calibration performed prior to shipment. This checklist report is a 34 page document detailing the ^3He tube serial numbers and their associated characteristics, along with the electronic settings used within the system, and all successive characterization measurement results. Inclusion of a checklist report is customary with the purchase of a new system from a vendor such as Canberra to show the system is functioning as expected; however, the measurements may not always have the finest precision or the greatest detail included. One would typically repeat these same tests in the facility or laboratory once the system has been delivered as a test to ensure there was no damage during shipping. Further tests beyond what is reported in the checklist report were also completed using the PTR-32.

2.5.1 High Voltage Characteristic

The optimal operational voltage was verified by acquiring the neutron count rate as a function of HV to produce a HV characteristic. The HV characteristic functions as a visual diagnostic of the optimal operational HV by plotting the neutron count rate as a function of increasing HV; the count rate will begin at 0, increase with a certain slope, and then reach a plateau. It is common practice to operate the counter 40 V above the “knee” where the count rate changes from increasing to level to accommodate any HV drift over the operational time. A ^{252}Cf source of approximately $3 \cdot 10^5$ nps emission was placed on an aluminum stand positioned at the center (within 5 mm) of the UNCL cavity. Data were collected using the PTR-32 “HV plateau” option in software. The HV range and the voltage increment were specified between measurements, along with the duration of the count time. For this measurement, 300 s measurements were performed at 20 V increments between 1560 V and 2000 V. The program recorded the pulse train in these specified steps and produced a live-time plot of singles count rate and doubles count rate as a function of HV.

The pulse train from the total input signal for each HV setting was saved inherently as an individual binary and channel file. PTR-32 software reads in the binary file to perform successive analysis on the neutron pulse train. The channel file is crucial if any unfolding or subtractions on the original acquired pulse train are desired. Using the PTR-32 software main screen, each of the channels’ pulse trains were unfolded from the total file offline. Employing this method for each HV setting, the characteristics for each channel, in addition to the total detector signal, were evaluated. Often the HV operating point is set based solely on the singles HV characteristic. However, since the principal assay of fresh fuel is based on the doubles count rate, it is good practice to also measure the doubles HV characteristic; yet, it is not currently done since it is not automated in shift register software. Because PTR-32 software plots the doubles HV characteristic in live time alongside the singles HV characteristic, it is now possible to utilize the doubles HV characteristic as a diagnostic without additional analysis. Thus, the “SDT” function in PTR-32 (which provides the Singles, Doubles, and Triples count rate values for the acquisition) was used to determine the multiplicity rates for each HV setting. The uncertainty in these values is reported by PTR-32, with no explanation of their determination. Therefore, the error

analysis described in [67] is used for our reported values; these errors differ slightly from those given by the PTR-32. The count rates were then compiled externally to produce a HV characteristic.

The HV characteristic was produced for both the singles neutron count rate and the doubles neutron count rate (see **Figure 2.3**). Each of the four detector channels follow very similar trends as a function of HV: increasing from 1560 V to approximately 1660 V, reaching a plateau between 1680 V and 1780 V, increasing again between 1800 V and 1900 V, and then decreasing through 2000 V. The total signal also follows this trend. This structure has been proposed to be an indication of non-ideal behavior in the JAB-01 boards, such as double-pulsing [48]. It is thought that this effect becomes evident as HV increases because the gain is effectively increased, which means the discriminator is more likely to re-trigger on structure in the pulse shape. Double pulsing is primarily caused by the difference in collection and shaping times within the electronic charge collection process; it is exacerbated as the trajectory angle of the charged particles relative to the anode wire increases from 0° to 90°. Varying the pulse shaping time in the preamplifier boards would allow this effect to be studied. A concurrent work has focused on studying and describing these effects.

The HV data obtained at ORNL was compared with the data reported by Canberra (**Figure 2.4**). Both data sets follow the same trend; however, they reflect different count rates because different activity ²⁵²Cf sources were used. The JSR-15 is not capable of easily producing a doubles HV characteristic. To produce the HV characteristic for the total detector signal and reproduce the singles HV characteristic for all four individual detector banks (**Figure 2.3**), five separate data acquisitions would be necessary with the shift register.

For the UNCL, the doubles HV characteristic is more relevant than the singles HV characteristic, since when operated in the standard active mode to assay fresh fuel, the singles count rate will be flooded with uncorrelated scattered neutrons from the AmLi interrogation source; therefore, it cannot be used quantitatively in the assay. Looking at the doubles HV characteristic obtained from the list mode data, the double plateau structure is more pronounced. This is because the doubles scales with the square of the efficiency of the system, whereas the singles scales directly with the system efficiency. Canberra selects 1680 V as the operational HV based on the singles HV characteristic, but we have decided to operate slightly higher at 1720 V in a more stable count rate region. It is essential to operate the system in a stable region not only to accommodate HV drift without compromising the efficiency, but also to remain below any gamma breakdown that may occur in the ³He tubes. Because the UNCL is not used in high gamma field fluxes, nor is the fresh fuel count rate high, the system is simple to calibrate. This voltage can be set by simply entering the value in the “Set HV” menu option in the PTR-32 software. For all future measurements the UNCL was operated at 1720 V.

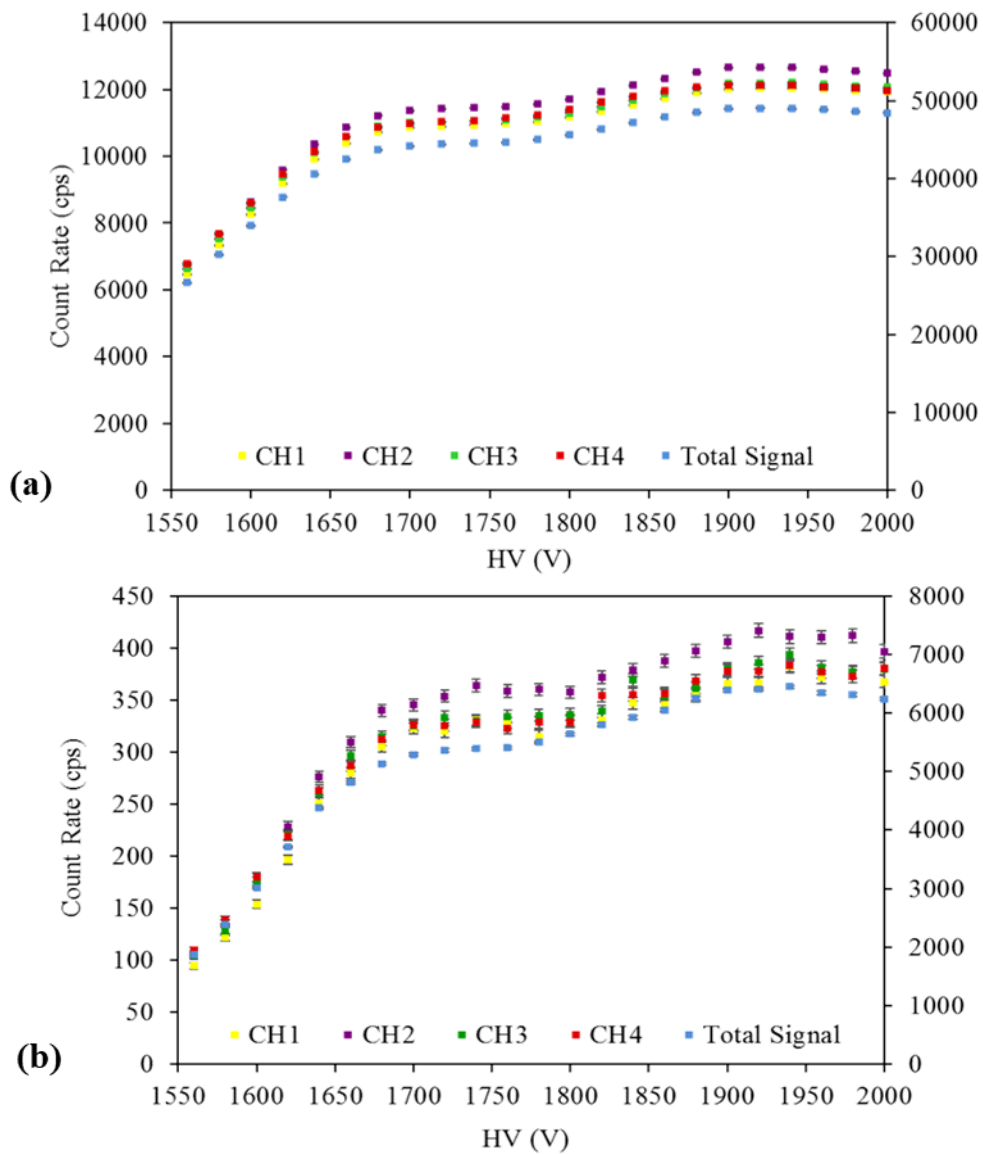


Figure 2.3. (a) Singles count rate as a function of high voltage with individual channel rates on the left vertical axis and the total detector signal rates on the right vertical axis; (b) Doubles count rate as a function of high voltage.

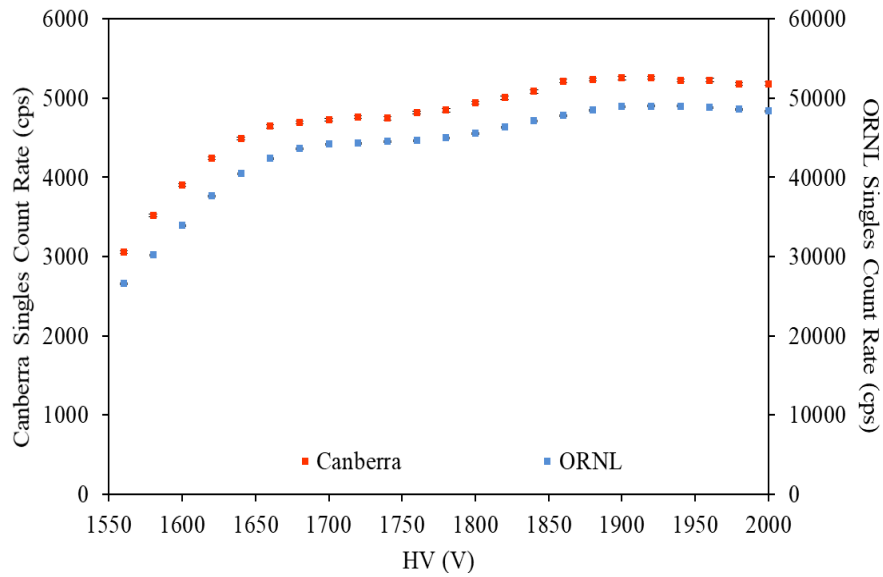


Figure 2.4. Singles count rate as a function of HV shown for data acquired by Canberra using a JSR-15 shift register [68] and data acquired by ORNL using a PTR-32 LMDA system. Differences in count rate are due to 2 different activity ^{252}Cf sources used.

In addition to producing a HV characteristic for all attached channels, the list mode data allows for an in-depth study of the doubles to singles squared ratio as a function of increasing HV as a diagnostic of the system's behavior (**Figure 2.5**). This ratio should be proportional to efficiency squared over efficiency squared from the point kinetic model equations, ultimately reducing this relationship to be independent of the count rate increase effects as the HV increases. For a properly operating system, this should produce a constant value across an increasing HV; deviation from this behavior may indicate some form of non-ideal behavior in the system where the doubles count rate may not scale with the singles count rate. If electronic artifacts are causing the preamplifiers to re-trigger on the same event, non-physical representations will appear in this study. We see this behavior across a range of commonly-used instrument types, and yet it is a feature that has typically been ignored. This effect is not significant for the current applications and general operation of these instruments within their predetermined timing windows. However, it would be relevant for any absolute measurements or extraction of count rate values at extreme timing windows. Because of the simplicity of this analysis, the inclusion of this test in a standard laboratory characterization procedure would be of great benefit to future system diagnostics.

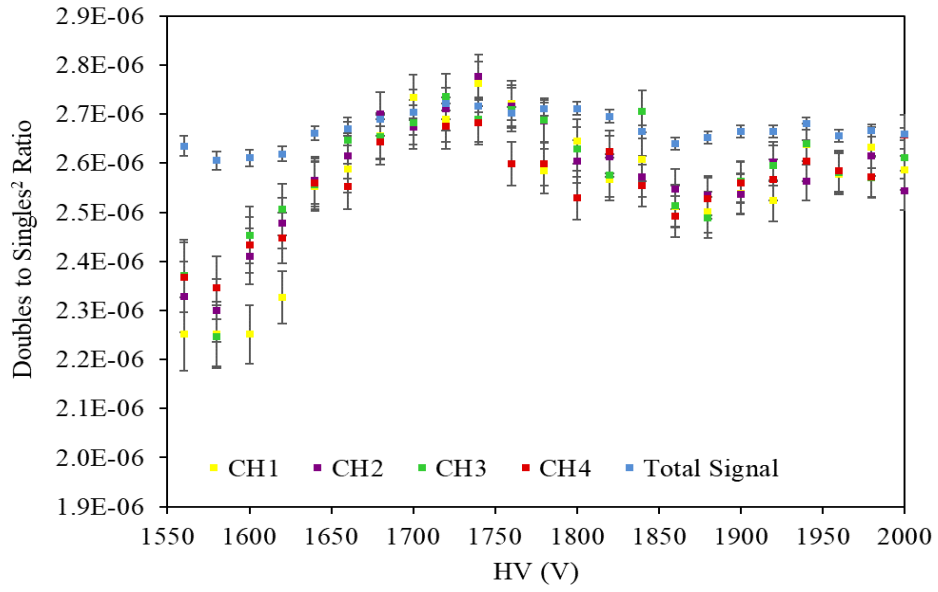


Figure 2.5. The ratio of double neutron counts to single neutron counts squared as a function of increasing HV

2.5.2 Predelay and Gate width Determination

Once the operational voltage was established, the predelay and gate width were investigated. Four AmLi sources, two with strengths of approximately 7,300 cps with a relative standard deviation of 0.11% and two with strengths of approximately 10,200 cps and relative standard deviation of 0.11%, were centered in the detector body, and a 7,200 s data acquisition was obtained using 24 cycles of 300 s each.

Because an uncorrelated neutron source was used for these data, the typical decaying trend illustrated in a Rossi- α distribution (**Figure 2.1**) is no longer present, and there is statistically no difference in mean neutron count number, $\langle i \rangle$, between the (R+A) and (A) gate (**Figure 2.6**). This means that because an AmLi source was used, these measurements are in the domain where the Accidentals rate (the singles count rate squared multiplied by the gate width) dominates the net doubles count rate. If the count distributions are not equal between these gates, non-ideal behavior in the system may be present, and the predelay gate selection may help mitigate this effect.

The PTR-32 “INCC export” function was used to produce neutron count distributions for the 24 cycles in order to match the INCC software format. A preamplifier re-triggering event not related to a true neutron event (e.g., non-ideal behavior and charge collection artifacts) could then be identified by a calculation of the bias, where

$$Bias = 100 \left[\frac{\langle i \rangle_{R+A}}{\langle i \rangle_A} - 1 \right] \% \quad (2.1)$$

A bias of 0% is desired. A study of the calculated bias, using the neutron count distributions for all predelay and gate width combinations, reveals the regimes where this is achievable. A predelay of 2.5 μs or longer will suffice for all gate widths for the UNCL (**Figure 2.7**). It has long been established that the timing gates of the UNCL are 4.5 μs for the predelay and 64 μs for the gate width, and these have been standardized for routine operational use. There is no expected difference in bias between 2.5 μs and 4.5 μs predelays over the dynamic range of the UNCL fresh fuel count rates, so it would be possible to shorten the predelay value to include more counts during an acquisition. Yet to allow for an unbiased comparison between others’ measurements with the UNCL, the standard 4.5 μs was selected for further measurements. Note, these values are instrument-specific and could be altered by design.

The ^{252}Cf source of approximately $3 \cdot 10^5$ n/s emission replaced the four AmLi sources, and a 7,200 s data acquisition run was taken. The PTR-32 software can be used to produce the singles and doubles count rates for a wide range of gate widths and predelay values. The single file was loaded offline and the “SDT” function was used to generate singles and doubles rates for predelays varying from 0.5 μs to 6.0 μs in 0.5 μs steps. Gate widths of 16 μs , 32 μs , 48 μs , 56 μs , 64 μs , 72 μs , 86 μs , and 128 μs were used to provide a wide range for comparison. As previously discussed, the reported neutron count rate will vary based on the timing gates. Because of this, a comparison of the relative standard deviation (rsd) in the doubles count rate was able to be determined as a function of gate width for all selected predelays (**Figure 2.8**). The uncertainties used in this calculation are generated using the format provided in [67], which utilizes the count time, predelay, gate width, and count rates.

The rsd reaches a minimum between 32 μs and 64 μs , and is marginally less for shorter predelay times. Despite the lower rsd measured at 48 μs , a 64 μs gate width was preserved both for historical reasons and to ensure a substantial count rate for good statistics in a short collection period. This is consistent with the expectation that the gate width should be approximately 1.27 times the neutron die-away time [4] for pure exponential behavior.

Canberra provides both a Reals count rate and an Accidentals count rate as a function of gate width with a constant predelay value of 4.5 μs . With these data, an uncertainty on each of these rates can be back-calculated from standard deviations and calculated gate fractions [67]. Because of the difference in source strength, and the 90 s acquisition time per measurement, the shift register-determined rsd is over an order of magnitude greater, and the significance of these rsd values is questionable. Since the list mode data was acquired over 7,200 s, with a source that was approximately nine times stronger than the source

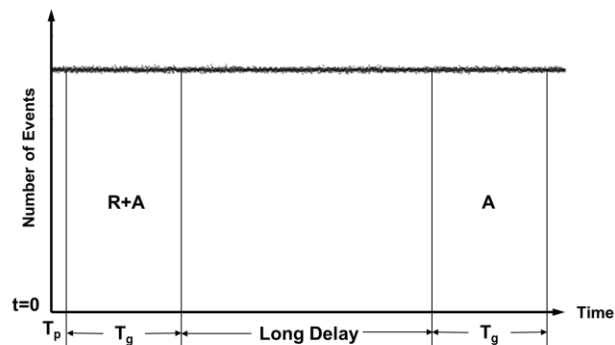


Figure 2.6. The Rossi- α distribution produced using an uncorrelated neutron AmLi source. The counts recorded in the (R+A) and (A) gates should be approximately equal.

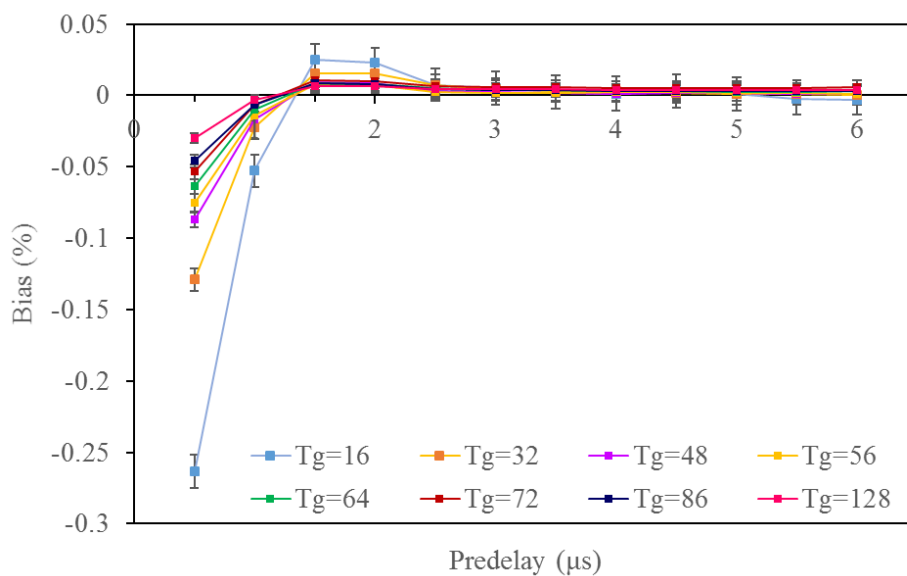


Figure 2.7. Bias percentage as a function of predelay for varying gate widths.

Canberra used, the *rsd* values offer greater confidence. What is evident between the comparisons, however, is that both the shift register-analyzed data and the list mode-analyzed data follow a comparable trend. Both analyses justify a gate width setting ranging from 32 μs to 64 μs .

The ability to analyze an acquired pulse train multiple times, while varying parameters, is unique to list mode and has advantage over repeating measurements for every parameter change, as is necessary when using a shift register-based approach. The significance of this application is that within 7,200 s of acquisition and post analysis, an entire parameter space can be surveyed for optimal calibration in the laboratory. Another benefit of using LMDA is that a measurement can be taken of a source before specifying the timing gates. Therefore, the unadulterated pulse train is recorded and offline analysis can be performed later if the optimal settings are not known, which is a useful tool for characterizing new systems.

PTR-32 can record the number of pulses in 100 ns bins up to 1,024,000 ns under the “Rossi Alpha” option. This file was exported as a .csv for manipulation. By adjusting the gate width to 1 μs , the doubles count rate for 1,024 bins yielded Rossi- α distributions (see **Figure 2.9**) for each of the detector channels and the total signal. Again, a single measurement with PTR-32 produces all of this information. In **Figure 2.9**, the full distribution for the 1,024 μs is shown on the top, and an expanded window between 0 μs and 6 μs is shown on the bottom.

The expanded window reveals structure in the count rate behavior consistent with the previously calculated bias below 2.5 μs . Although the source of this bias has not been fully determined beyond speculation of double pulsing in combination with standard charge collection effects in the Canberra JAB-01 boards, the Rossi- α distribution provides another, and rather direct, visual justification that operating the UNCL at a 4.5 μs predelay will mitigate any of these undesirable effects.

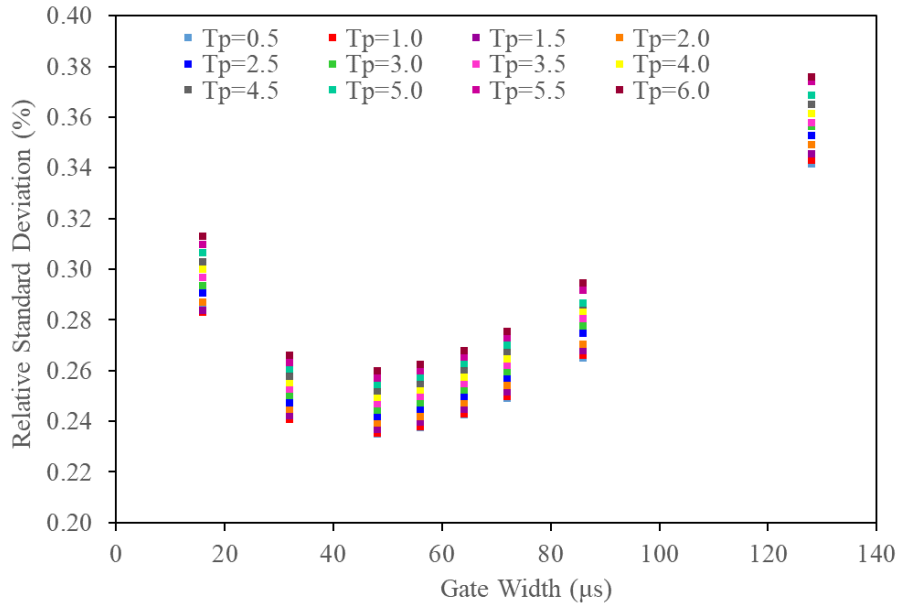


Figure 2.8. Relative standard deviation of the doubles count rate as a function of gate width for varying predelay values using a ^{252}Cf source.

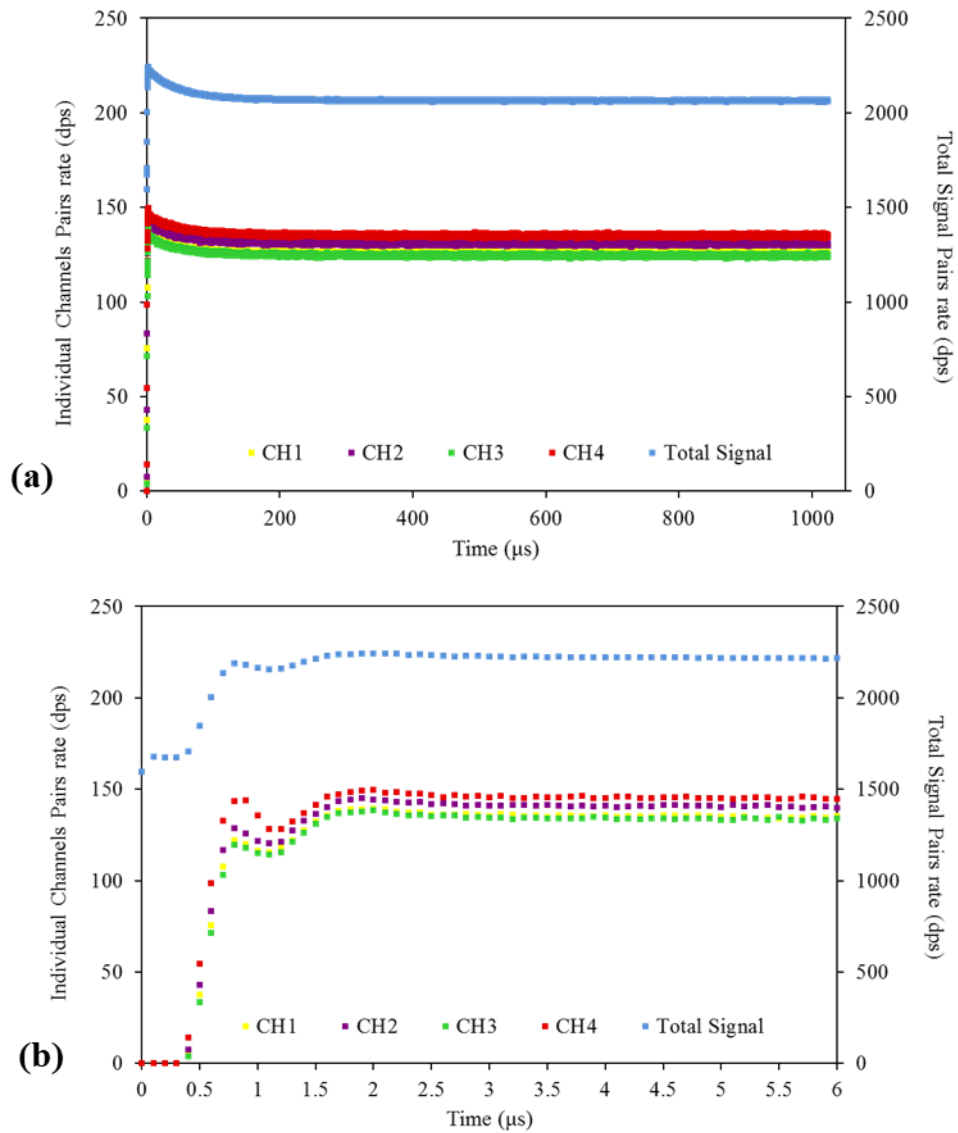


Figure 2.9. (a) Rossi- α distribution through 1024 μ s. The channel width is 100 ns. (b) Expanded portion of the Rossi- α distribution between 0 and 6 μ s to show non-ideal behavior structure below 2.5 μ s.

2.5.3 Neutron Die-away Time

Using the previous measurement of the ^{252}Cf source and the Rossi- α distribution produced, the die-away time for each of the four detector banks and the total detector signal were determined. An exponential fit was independently applied to the distribution between 2.5 μs and 1024 μs (**Figure 2.10**) using

$$A e^{-T_p/\tau} + b \quad (2.2)$$

where A is a scaling factor, T_p is the pre-delay gate value, and τ is the die-away time. Both A and τ were determined by chi-squared analysis minimizing the sum of squared errors between the data and the exponential fit. This equation also includes a background term, b , into the fit rather than initially subtracting out the Accidentals. This approach is unique to list mode analysis as the Rossi- α distribution must be used for this analysis.

This procedure was completed for each of the channels, and the results are summarized in **Table 2.1**. Channel 4 was the bank closest to the cement wall, and, therefore, the calculated die-away time is slightly longer due to associated neutron scatter. A single exponential does not fully and accurately describe the neutron die-away time of the instrument based on differences in shape, fill pressure, tube location, position of Cd liners, etc.; however, this expression can approximate it. The die-away time may vary slightly as different intervals of time are fit, and as multiple fits are applied together over different ranges. PTR-32 software assists in this analysis as the pulse train may be trimmed to different time lengths using the ‘‘Chopper’’ function. The ‘‘Rossi Alpha’’ menu must then be selected for the file to produce a die-away time value. There is also a simple ‘‘Fit Exponential’’ option that allows the user to select the range for the fit to be applied over. It then draws the fit alongside the data and the trend of that fit can be compared to adjust the range accordingly. PTR-32 does not calculate a value of the die-away time, however.

Table 2.1. Calculated Die-Away time and Efficiency for all channels

Channel	Die-Away (μs)	Efficiency (%)
1	48.76 ± 0.20	3.371 ± 0.047
2	49.45 ± 0.19	3.440 ± 0.048
3	49.53 ± 0.19	3.357 ± 0.047
4	51.20 ± 0.20	3.496 ± 0.048
All	50.657 ± 0.058	13.66 ± 0.15

An alternative approach to determine the neutron die-away time with shift register logic uses the doubles count rate (R_G) as a function of increasing gate width (T_G), rather than fitting the Rossi- α distribution. By performing chi-squared analysis using

$$R_G = R_0 \left(1 - \text{Exp} \left(-\frac{T_G}{\tau} \right) \right) \quad (2.3)$$

and minimizing the sum of squared errors, both R_0 (the maximum count rate) and τ may be calculated. The doubles count rates measured with the JSR-15 (provided by Canberra), were used with this fit to calculate a total detector system die-away time of 50.89 μs , with a fit uncertainty of 0.66 μs (see **Figure 2.11**). The die-away time analyzed by both methods, with data acquired through the PTR-32 and the JSR-15, are in agreement. Slight deviations and sources of error may be attributed to differences in the measurement environment (i.e., the individual channels or total detector body may have been subjected to

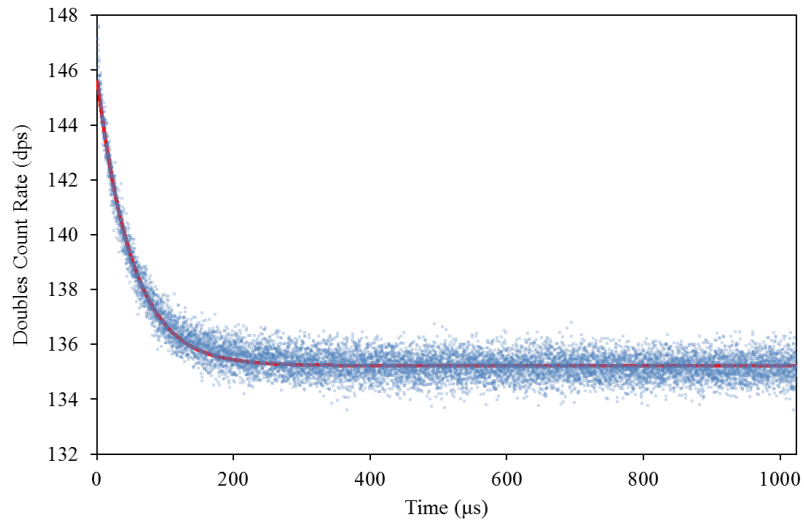


Figure 2.10. A single detector channel Rossi- α distribution with the red exponential fit applied.

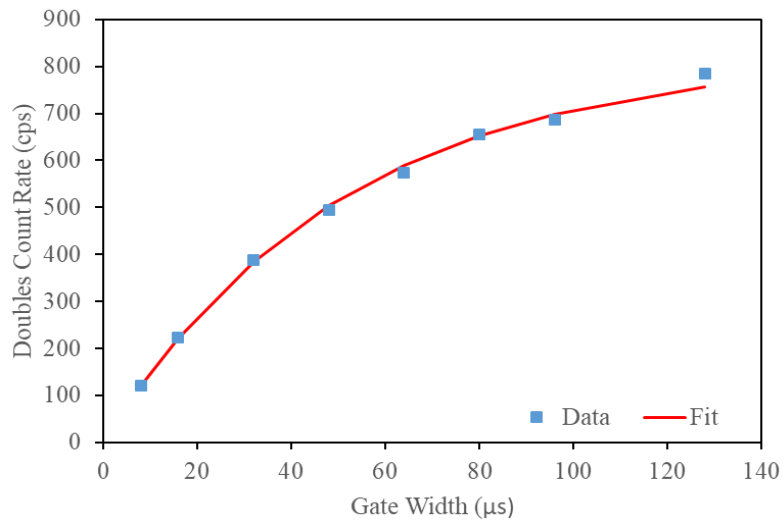


Figure 2.11. Doubles count rate data obtained by the JSR-15, with a saturating exponential fit applied.

more scatter and/or reflection in one of the two facilities where measurements were conducted), measurement time, the time window to which the exponential fit was applied, and the associated fit error.

It should be noted that a similar analysis may also be performed by fitting the doubles count rate as a function of increasing predelay value with

$$R_G = R_0 \left(\text{Exp} \left(-\frac{T_p}{\tau} \right) \right) \quad (2.4)$$

but this is not completed in the scope of this paper. Both of these analyses may be completed, as well as the analysis described by Equation 2.2, using the list mode neutron pulse train data by selecting the specific timing windows and performing count rate analysis. However, the results for each time setting would be correlated due to sampling the same pulse train for each setting rather than performing separate measurements as is the case with the shift register. These results also integrate over a wide range of gate widths which tends to smooth out and mask finer structure in the behavior of the system.

2.5.4 Absolute Efficiency

A simple efficiency calculation was applied to each of the four detector channels in addition to the total detector body using separate pulse trains produced through the “Unfold” option. The same 7,200 s data acquisition file from the ^{252}Cf source measurement, of known strength and relative standard deviation of 1.02%, was analyzed to determine the efficiencies (counts per source neutron) of the channels, as reported in **Table 2.1**. The efficiency calculated from the Canberra reported values is 13.6% using an independent ^{252}Cf source. The minor channel efficiency variations may have been slightly influenced by the instrument placement near a concrete block wall that caused scatter and reflection of neutrons. The same analysis may be performed using a shift register, but multiple measurements, or additional shift registers, would be needed to determine the individual channel efficiencies due to the limited number of channel inputs.

2.5.5 Dead Time Determination

The dead time of each of the four channels was calculated using the previously described 24 cycles of 300 s acquisition data obtained by measuring the four uncorrelated neutron AmLi sources. The total detector pulse train measured in PTR-32 was unfolded into the pulse trains for each of the four detector channels and each file was exported to INCC format for analysis.

To perform the “INCC export” function in PTR-32 for similar analysis to that done with the shift register, the predelay and gate width parameters were changed to match the 4.5 μs and 64 μs gates of the UNCL. We iterated through all of the acquired cycle files to produce a final result file containing the neutron count distribution. This procedure was repeated for each channel. Then, the neutron count distribution was analyzed to determine the dead time using the neutron count number and its frequency, the affiliated variance across all 24 cycles, and the known gate width as derived in [69]. The dead time was calculated individually for the (R+A) and (A) neutron count distributions, checked for bias (as previously described), and then combined into a 48 cycle data set to determine a combined dead time value exploiting the fact that the uncorrelated AmLi sources would have statistically equal (R+A) and (A) distributions (Section 4.2).

The dead time values found for the (R+A) and (A) gates are in agreement for all channels, as expected when using an uncorrelated neutron AmLi source with a bias consistent with 0 (**Table 2.2**). Although this procedure differs from the one used by Canberra [70], which is currently the most widely-used method in the field, a recent work [71] has proven the two methods return very similar results when the list mode data is analyzed in software to simulate the output of a shift register. Both methods only

return experimental approximations for the dead time values of the system. The benefit of using the neutron count distribution to determine the dead time is the simplicity of the acquisition and analysis, and the reduced associated uncertainties.

Table 2.2. Dead time values calculated for all four detector channels and the total detector signal

Channel	$\delta_{(R+A)}$ (μs)	$\delta_{(A)}$ (μs)	$\delta_{(\text{Combined})}$ (μs)	Bias (%)
1	0.699 ± 0.012	0.666 ± 0.014	0.6824 ± 0.0092	-0.022 ± 0.032
2	0.685 ± 0.012	0.688 ± 0.014	0.6865 ± 0.0091	0.033 ± 0.026
3	0.717 ± 0.011	0.701 ± 0.013	0.7091 ± 0.0085	0.043 ± 0.025
4	0.615 ± 0.010	0.622 ± 0.011	0.6187 ± 0.0075	-0.017 ± 0.023
Total	0.1648 ± 0.0021	0.1635 ± 0.0022	0.1641 ± 0.0015	0.0028 ± 0.0047

The a and b parameters listed by Canberra ($a=1.07 \mu\text{s}$, $b=0.53 \text{ ps}$, with a/b ratio set at $2 \cdot 10^6$) were tested using the standard dead time correction equations (Equations 2.5–2.7) with the given shift register-measured source count rates (S_m, D_m)

$$CF_D = e^{\delta_R \cdot S_m} = e^{(a+b \cdot S_m) \cdot S_m} \quad (2.5)$$

$$CF_S = e^{\delta_T \cdot S_m} = e^{\frac{1}{4}(a+b \cdot S_m) \cdot S_m} = CF_D^{1/4} \quad (2.6)$$

$$S_{DTC} = CF_S \cdot S_m, D_{DTC} = CF_D \cdot D_m \quad (2.7)$$

The total detector doubles dead time found with these values was $1.1 \mu\text{s}$. When this analysis was repeated, and b was set to be equal to $a^2/4$ [72], the dead time was again found to be $1.1 \mu\text{s}$, showing negligible dependence on the b term at these relatively low count rates. The dead time parameter for the singles count rate can therefore be approximated as $a/4$ in this instance, resulting in a system dead time of $0.27 \mu\text{s}$. These data were analyzed four ways: the two previously described methods, along with b set to 0, and finally eliminating a data point from the fit to study the sensitivity. This study of generated dead time values revealed that this data set did not generate a highly precise result, with final dead time values ranging approximately 20%. This study indicates that the five sources used by Canberra for this determination are not sufficient to produce a reliable fit that is robust against model choice or the number of data points included. Due to the magnitude of this discrepancy, and the sources of uncertainty just discussed, we are inclined to refer to the neutron count distribution-determined dead time values performed at ORNL. This approach has been previously verified with multiple ^3He - based neutron coincidence counters [73] and the standard error-associated uncertainty generated from this method is smaller due to the nature of minimal user-dependent manipulation.

The neutron count distribution-determined dead time results can be justified by referencing the previously discussed Rossi- α distribution in **Figure 2.9**. When examining the individual detector bank responses, an increasing structure is evident between $0 \mu\text{s}$ and $0.7 \mu\text{s}$. From $0 \mu\text{s}$ to approximately $0.4 \mu\text{s}$, there is no measured count rate; this is consistent with dead time, where no coincidence events can be registered. Then, between $0.4 \mu\text{s}$ and roughly $0.7 \mu\text{s}$, the drastic increase in count rate signifies the recovery of the preamplifier system combined with charge collection effects in the ^3He tubes. After this artifact, more structure can be observed until the signal stabilizes around $2 \mu\text{s}$. This may be related to ultimate charge drifting and collection effects and the further stabilization of the electronics. Investigating the pulse train behavior of the total detector signal reinforces these claims. Between 0 and $0.4 \mu\text{s}$, there is approximately $3/4$ of the total count rate measured, which is in agreement with one of the four detector banks being dead. Because the total signal relies on all four channels, it will still register neutron events in three out of the four banks while a neutron event is being processed in the last bank; therefore, the dead

time of a system is much less than the dead time of a single preamplifier chain. Then, following the same trend as each individual channel, there is a drastic increase in count rate between 0.4 μs and 0.7 μs . The undershoot that is present in the individual signals is also much less drastic in the total signal.

Using LMDA and analysis to produce a Rossi- α distribution provides a cursory visualization of the dead time and electronic stability of a system. It is a simple approach to gain relevant insight into this behavior, and can be used as a quick diagnostic of the characterization parameters and timing windows. Again, both calculation methods return experimental approximations for the dead time values, and therefore may be slightly different than what is observed in the Rossi- α distribution. It is important to note, however, that since the UNCL is designed for low count rate applications (which is standard for fresh fuel assembly assay), there is no dead time correction applied in the field. Rather, the dead time effect is included empirically in the doubles versus ^{235}U g/cm calibration curve, alongside the efficiency and die-away time values. This test and characterization is strictly relevant to laboratory measurements, so this deviation is not significant to its application.

2.5.6 Discussion

Although a shift register data acquisition system has many of the same characterization capabilities as a list mode acquisition system, often the complexity of the required measurements to achieve similar results hinders its extended use. A JSR-15 shift register, in combination with a neutron coincidence counter and in this instance INCC, is capable of performing a live time singles HV characteristic, and is capable of recording neutron count rates used to determine optimal gating parameters, neutron die-away time, system efficiency, and dead time. However, by using list mode acquisition and analysis, many channels may be studied simultaneously and a single data acquisition can be analyzed to produce these values. A summary of these parameters found by both data acquisition systems is provided in **Table 2.3**. In terms of the JSR-15 and the PTR-32, one signal input in combination with two auxiliary inputs may be connected to the shift register, whereas 32 channel inputs may be connected to the list mode system. The stability of individual channels over the duration of a measurement may easily be investigated and compared to the total detector output signal. In addition, more in-depth studies may be performed using PTR-32 such as an investigation into non-ideal behavior done by examining the doubles HV characteristic and the doubles to singles count rate ratio, or the more readily available visual representation of the pulse train in a Rossi- α distribution.

Table 2.3. Summary of system characterization parameters obtained through the JSR-15 and PTR-32

Parameter	JSR-15 Shift Register Values		PTR-32 LMDA Values			
	Total	Channel 1	Channel 2	Channel 3	Channel 4	Total
Neutron die-away time	50.89 $\pm 0.66 \mu\text{s}$	48.76 $\pm 0.20 \mu\text{s}$	49.45 $\pm 0.19 \mu\text{s}$	49.53 $\pm 0.19 \mu\text{s}$	51.20 $\pm 0.20 \mu\text{s}$	50.657 $\pm 0.058 \mu\text{s}$
Absolute efficiency	13.6%	3.371 $\pm 0.047 \%$	3.440 $\pm 0.048 \%$	3.357 $\pm 0.047 \%$	3.496 $\pm 0.048 \%$	13.66 $\pm 0.15 \%$
Dead time	0.27 μs	0.6824 $\pm 0.0092 \mu\text{s}$	0.6865 $\pm 0.0091 \mu\text{s}$	0.7091 $\pm 0.0085 \mu\text{s}$	0.6187 $\pm 0.0075 \mu\text{s}$	0.1641 $\pm 0.0015 \mu\text{s}$

2.6 Conclusions

List mode has long been established in a variety of fields; however, it has not been readily implemented in international safeguards. Efforts are currently underway to streamline list mode for more practical field applications. Meanwhile, new versions of INCC are being developed to resolve some outstanding issues. This paper ultimately serves to provide an in-depth characterization of a standard neutron coincidence counter in which the extended capabilities of list mode data acquisition (LMDA) are highlighted in comparison to traditional shift register data acquisition. Some of these capabilities include an automated doubles HV characteristic, individual channel analysis options, a Rossi- α distribution for specific neutron die-away time calculations, and offline analysis where an acquired pulse train can be studied multiple times, while varying parameters, to optimize settings.

In this work, we described the characterization of a JCC-71 Neutron Coincidence Collar (UNCL) using a Pulse Train Recorder-32 LMDA system. The results of these list mode measurements/analyses are compared with JSR-15 shift register-based measurements/analyses on the same system, or in some cases, compared to the parameters reported by the manufacturer. The HV characteristic, predelay, gate width, neutron die-away time, detector efficiency, and system dead time were analyzed through measurements and detailed offline analysis. Operating at the determined HV of 1720 V, the traditionally accepted predelay and gate width parameters of 4.5 μs and 64 μs were validated, respectively. Using these timing settings, the neutron die-away time for the each of the four UNCL channels was discovered to range between 48.76 and 51.20 μs , with a total detector system die-away time of 50.66 μs , which is similar to the shift register-determined die-away time of 50.89 μs , as shown in **Table 2.3**. In addition, the absolute efficiency for each of the channel banks was determined to range between 3.36% and 3.50%. When analyzing the total UNCL response, the system efficiency was calculated to be 13.66%, which is in agreement with the shift register-calculated value of 13.6% found using an independent ^{252}Cf source. Finally, using the neutron count distribution provided by PTR-32 in the specific timing windows, the dead time was found to range between 0.62 μs and 0.71 μs for the four channels, and 0.16 μs for the total system response. The total detector system dead time determined using the shift register is 0.27 μs . The cause and the effect of this discrepancy on a final assay value will be investigated as a part of future work.

The use of LMDA in its current state better suits laboratory characterization and calibration efforts than in-field measurements. Future work toward a more universal safeguards implementation will need to include automating more of this process through scripts and GUIs to provide a more user-friendly interface. In addition, at high rates up to the megahertz range for various safeguards applications, the main drawback of the LMDA format is the large and variable file size. This can be tolerated in laboratory measurements to a degree, but it can be prohibitive for routine field use. Therefore, for the time being with current computer storage and data processing limitations, full LMDA in its current form is best suited for low rate applications. However, because the extended capabilities of LMDA provide a better understanding of the physics-based behavior for a more precise system representation and more confident assay results, establishing a characterization procedure for the routine use of list mode data acquisition and analysis is an important step toward its full implementation in the safeguards field.

Chapter 3

Modern Preamplifier, Amplifier, Discriminator Electronics

3.1 The Amptek A111 Charge Sensitive Preamplifier and Discriminator Chip

After Swansen's adaptation and adoption of the Amptek A111 hybrid charge sensitive preamplifier, discriminator, & pulse shaper [31] for neutron coincidence systems in 1984 [35], it has been almost exclusively used in all Antech and Canberra Industries' commercial systems used by the IAEA (**Table 1.1**). The Antech electronics board is based on the Amptek A111 chip. The Canberra JAB-01 preamplifier/amplifier/discriminator board implements the Amptek A111 chip with a 74221 dual monostable multivibrator integrated circuit and a 74-S140 50-ohm line driver integrated circuit [30]. The A111 was developed in the mid-20th century for high-rate applications implementing short shaping times and radiation hardness while adhering to specific design parameters for its original x-ray measurement application. It was designed for use with charge-producing fast detectors operating in the pulse counting mode [31]. Over the last several decades the commercially available chip has been adopted for use in the safeguards field, among many other fields, such as aerospace and portable instrumentation, mass spectrometers, particle detection, imaging, laboratory and research experiments, medical electronics and electro-optical systems, due to its reliable performance in a range of different count rates. It is a self-contained amplifier, shaper, and discriminator unit (**Figure 3.1**) that produces a digital output. The unit requires a single + 5 V supply, and can perform in count rates up to 10^6 cps without saturation of the preamplifier [31].

Precision Data Technology (PDT) also produces electronics directly compatible with ^3He systems [74]. PDT shaping times are generally $\sim 0.5 \mu\text{s}$, and are, therefore, slower than the A111 [75]. They also have a lower charge sensitivity than the A111. Some counting systems developed by LANL have been designed using these 110A preamplifier/discriminators in place for the A111; however, they have not yet been widely adopted by neutron coincidence counting manufacturers such as Canberra or Antech for use by the IAEA.

The A111 uses bipolar shaping, with a time constant much shorter than the full charge collection duration to mitigate the long dead times characteristic of ^3He counters. Currently, two types of shapers are used in detection circuits: unipolar shapers and bipolar shapers. As **Figure 3.2** illustrates, the preamplifier signal is integrated and differentiated by the selected shaper to produce the respective pulse shape, which is then evaluated by a discriminator with a set lower level threshold, producing logic pulses to be read by counting software. These shapers use a number of CR-RC combinations in order to integrate and differentiate this signal. The CR stage is a high-pass filter differentiator, while the RC stage is a low-pass filter integrator. This combination cuts out large amounts of electronic noise in frequencies where there is little signal energy. However, it also adds to the duration of the pulse due to the long exponential decay component. To mitigate these effects, several stages of these filters may be used in combination to create a Gaussian filter whose resulting pulse does not suffer from the long, exponentially decaying tail. However, since the pulse width of a Gaussian filter is longer than with a unipolar or bipolar shaper, pileup is more common in high rate applications, which makes this filter less desired for safeguards applications.

The A111 has a CR-RC-CR circuit typical of all bipolar shapers with time constant $0.15 \mu\text{s}$ [35]. However, its final pulse output appears unipolar when probed from the pulse monitor since this original pulse is not externally available. A problem with the A111 chip is that it is housed in a self-contained circular metal casing that cannot be modified or probed (**Figure 3.1**). Whatever timing properties it is



Figure 3.1. A photograph of the Amptek A111 chip, with metal housing.

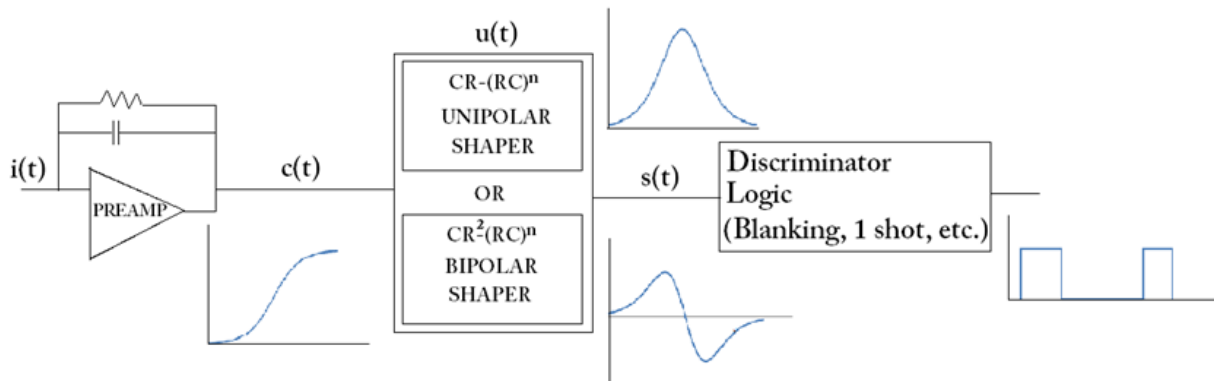


Figure 3.2. A diagram illustrating the general pulse processing chain used to analyze the ^3He charge collection signals [75].

manufactured with are what the chip will operate with. In a way, these systems are black boxes; as the documentation on their components is minimal, access to different parts of the circuit is restricted, and proprietary information is controlled. The threshold is adjusted externally by a potentiometer which controls the gain, rather than a comparator threshold. The gain is set during the manufacturing of a neutron coincidence system by matching the performance across all channels and then increasing or decreasing the value of the gain to match the desired count rate performance of the system at the operating setting. It is specifically selected such that the threshold will fall in the valley of the ^3He pulse height spectrum between the gamma and neutron regions (Chapter 1).

Bipolar shapers do not suffer from large baseline shifts, unlike unipolar shapers, due to their balance of both a positive and negative pulse lobe centered about zero. Therefore, no additional baseline restorer is necessary in a bipolar circuit. When a unipolar shaper is exposed to high rate fields, counting losses become more prominent as their characteristic undershoots in pulse amplitude, generated by a pulse's long decaying tail [1], effectively increase the threshold for any subsequent pulses stacked on this negative amplitude baseline. Because of this effectively increased threshold, lower amplitude pulses at the lower end of the pulse height spectrum, such as wall effect events, may not be counted. However, at lower rates, unipolar shapers have the advantage, since bipolar pulses have a comparably longer duration for the same charge collection, increasing the system's dead time. Bipolar signal-to-noise characteristics are also typically worse than unipolar shaping because the resulting pulse amplitude is lower. However, through their decades of use, the A111 has proven that it has sufficient gain and adequate signal-to-noise to be used with ^3He detectors— at the expense of realizing full count-rate capability, which is accounted for in analysis.

Due to the physics of charge collection from the $^3\text{He}(n,p)\text{T}$ reaction in the tubes, the collected and shaped pulses have a large variation in shape and duration. The location of the capture event, and subsequent charged particles' ionization tracks relative to the anode wire, generate a shorter fast charge collection component joined with a longer slow charge collection component that must both be accounted for in the shaping time. If the shaping time is not sufficient to collect both peaks this charge, not only could the system retrigger on the two ionization cloud's components (known as double pulsing and discussed in detail in Section 5), but it could also cause a large variation in the measured pulse height for a given energy interaction due to ballistic deficit, that may not allow the true number of measured pulses to cross the set threshold. Ballistic deficit is the degree to which a shaped pulse's amplitude is decreased compared to the expected amplitude that could be obtained with an effectively infinite time constant [1]; it is especially significant for spectroscopy. Since the spectrum does not matter in coincidence counting, these counters are operated in a shorter pulse shaping time regime (hundreds of nanoseconds up to microseconds) compared to the charge collection time of the positive ions (several microseconds up to the order of milliseconds for the full collection time) to decrease dead time effects, which in turn causes pulse height distribution distortions. This is not problematic as long as the separation between gamma events and neutron events in the pulse height spectrum remains sufficient.

The shaping time of the A111 chip is 150 ns, meanwhile the rise time is listed at 25 ns (electron collection time is 1000 times faster than the positive ion collection time) [31]. Because the same settings are selected for all A111s, and then paired across a wide range of neutron coincidence counters used in a variety of geometries and different count rate applications, occasionally the performance of the system is compromised to incorporate this commercially available component; e.g. double pulsing may be present in some systems using the A111 where it is not present in others.

3.1.1 The Canberra JAB-01 Preamplifier/Amplifier/Discriminator Boards

The Canberra Industries' neutron coincidence counters employ an in-house designed Preamplifier/Amplifier/Discriminator Board that is built around the A111 chip. The JAB-01 Preamplifier/Amplifier/Discriminator Boards uses the amplification, shaping, and discrimination provided by the Amptek A111 chip. It also incorporates a 74221 dual one-shot to modify the output

signal to a set 50 ns width, and a 74-S140 50 Ω line driver to provide a single signal output from the system containing multiple boards [30]. The 74-S140 also functions as an OR gate that can combine logic pulses produced from other banks used in a daisy-chain fashion to supply a single neutron pulse train. The components are integrated on a 1.5 x 2.2" printed circuit board (PCB) [35] which is housed in a junction box and connected to the ^3He tube groupings (**Figure 3.3** a and b). This double-sided PCB is divided into two sections: all HV components are placed on one side of the board, and all low voltage components are placed on the other side of the board. The tube signal is fed through a pin jack to an insulating standoff to prevent any signal feedback generated by impedance mismatch through the exposed anode connections, which could lead to multiple pulsing or oscillations. The output monitor LED lamp flashes for any pulse that exceeds the set threshold in the A111 (**Figure 3.4** b). Dessiccant plugs are placed on each junction box to reduce the humidity and minimize any HV breakdown across the capacitors which would cause electrical noise [30].

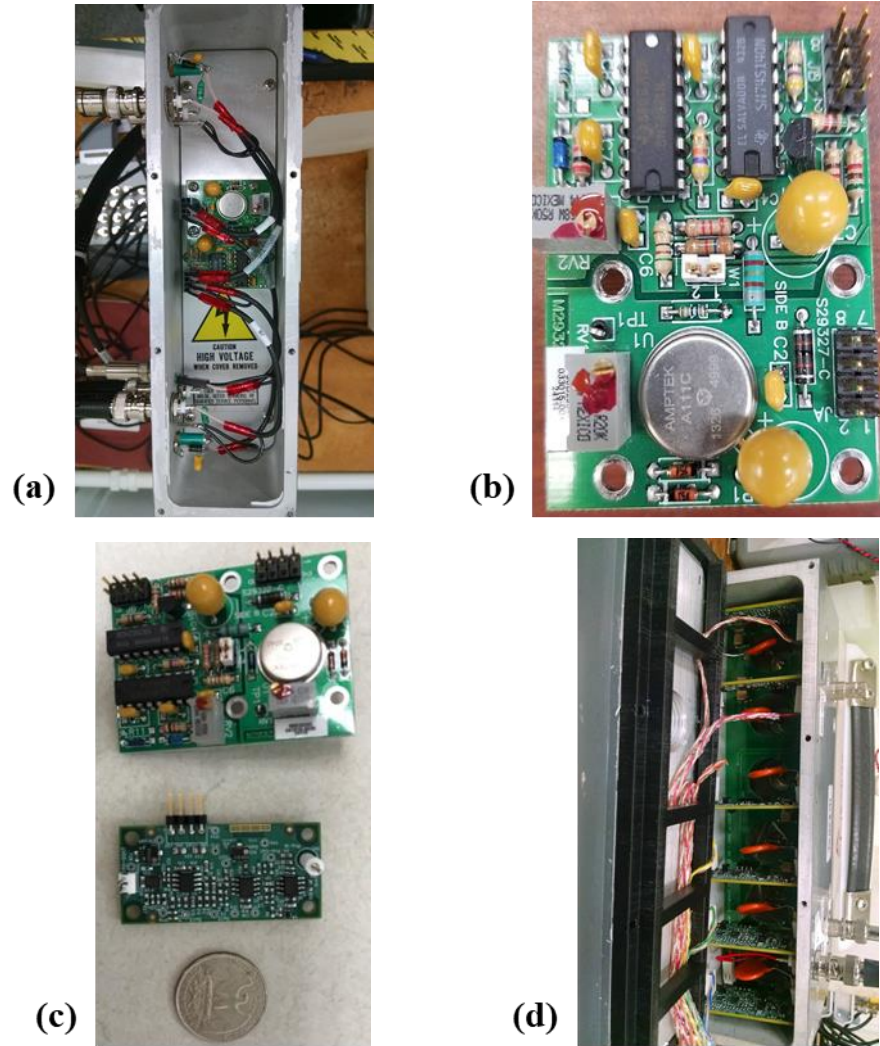


Figure 3.3. (a) The JAB-01 Board positioned next to the (b) ORNL prototype board (c) the original JCC-71 junction box containing 1 JAB-01 board for 6 ^3He tubes and (d) the new retrofit JCC-71 bank containing 6 ORNL boards for the 6 ^3He tubes.

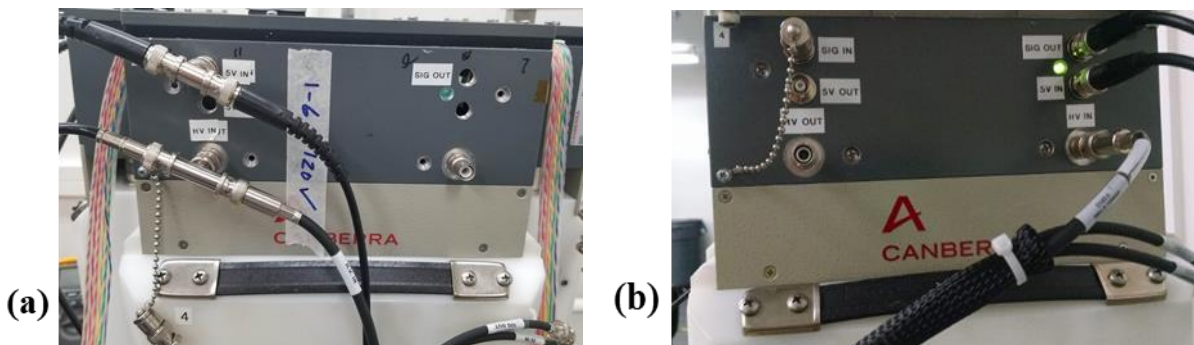


Figure 3.4. (a) Modified JCC-71 junction box to accommodate the new ORNL electronics. The “HV in” position has been moved along with the “+5 V in” and the “Signal in”, “Signal out”, “HV out”, and “+5 V out” have been removed, as seen when compared to the original junction box (b).

3.2 ORNL Design Implemented on the JCC-71 Neutron Coincidence Collar, Original Prototype³

New neutron counting electronics were designed and built by Chuck Britton, M. Nance Ericson, and R. Bruce Warmack, electrical engineers at ORNL, as an alternative to the Canberra Industries/Mirion Technologies JAB-01 preamplifier/amplifier/discriminator boards under a NA-22 funded project titled the “List Mode Response Matrix for Advanced Correlated Neutron Analysis for Nuclear Safeguards.” The results of my testing, evaluation, and optimization of these electronics in support of this project are discussed here.

The goal of the new electronics for this project is to provide the same neutron processing functionalities as the JAB-01 boards and extend the capabilities of the JCC-71 system by placing a preamplifier on each of the 18 ³He tubes. Each ³He tube is then capable of producing an individual signal output to be analyzed using a LMDA system. This project aims to use all 18 signal channels to produce a spatial response matrix to ultimately assay fresh nuclear fuel assemblies; this will be discussed in detail in the next chapter. It could be possible to use the JAB-01 board for each of the ³He tubes, but they are expensive and too large to place within the existing junction boxes (**Figure 3.3 c**). Instead, the ORNL electronics are used for this project for convenience, cost, and the evaluation of modern electronic components with neutron coincidence counting systems. There are other suitable alternative electronics designed for use in safeguards systems, specifically for high rate applications [75] [76], but to date, they have been used commercially to replace the A111, possibly primarily out of tradition.

The JCC-71, like other standard UNCLs, contains six ³He tubes embedded in a single row within a HDPE moderating slab. Four of these slabs are connected to form the Passive Neutron Collar, and three slabs are used connected to a basic HDPE slab housing an active interrogation source for the Active Neutron Collar, which is most commonly used in inspections. The six tubes in each bank are connected to a junction box panel containing a single JAB-01 preamplifier/amplifier/discriminator board per bank (**Figure 3.3 a**). The junction box transfers HV between the connected banks through “HV in” and “HV out” connections and contains “Signal in” and “+5 V in” inputs and “Signal out” and “+5 V out” outputs to interconnect the banks and communicate with an external data acquisition system (**Figure 3.4**). The JCC-71, like other collars, ORs the signal from six separate ³He tubes to a single JAB-01 board (**Figure 3.5 a**). Then, depending on the data acquisition method, again ORs the output between the number of banks, in this case three, to measure a total system output.

Instead, the modern ORNL design consists of 18 separate preamplifier networks with their individual discriminators to produce pulses for each qualifying neutron event in each tube. Each detector then has its own signal output going to the digital processing unit using a custom external FPGA (**Figure 3.5 b and c**). The preamplifiers are also modular and scalable in design, which could ultimately allow for easy translation between various coincidence counting systems.

To satisfy the goals of the List Mode Response Matrix project and to make these electronics a viable modern alternative option for neutron coincidence counting systems, the new electronics were designed such that they would have the same, or superior, performance to the JAB-01. Therefore, the design was based on low cost commercially-available components. These new electronics include a preamplifier and motherboard design, which fit inside the footprint of the existing junction box (**Figure 3.3 d**), as well as an external FPGA pulse processor board. They leverage advanced electronic components developed for use in other fields such as high-energy physics. This combination is a more cost-effective upgrade than replacing historic systems with other novel systems that may offer multichannel analysis options.

³ This work has been adapted from its current form as presented in the Institute of Nuclear Materials Management Annual Meeting Conference Proceedings, Baltimore, MD, 2018

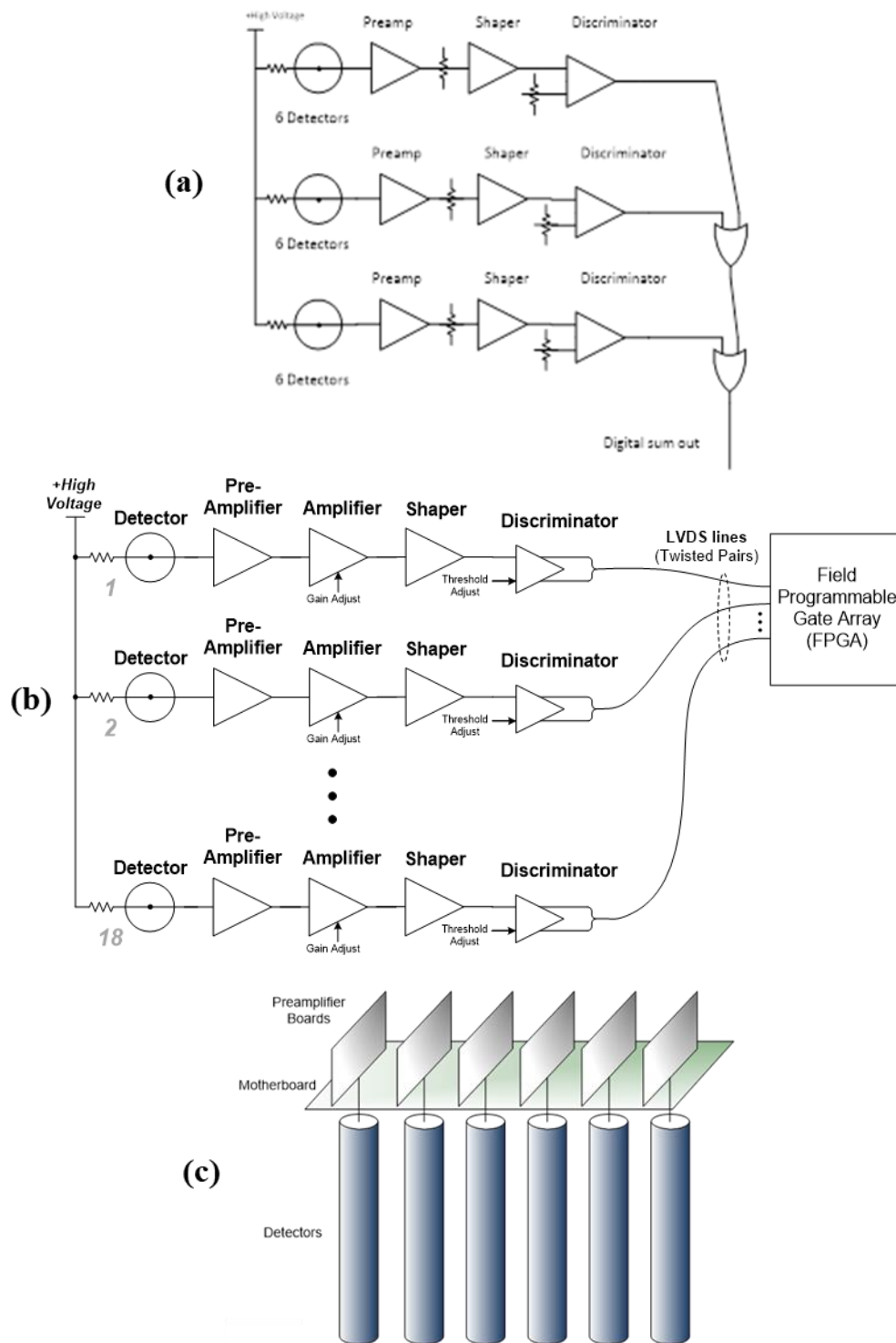


Figure 3.5. (a) A diagram illustrating the traditional electronics chain used in the original JCC-71. (b) A diagram illustrating the ORNL electronics chain as implemented on the modified JCC-71. (c) A basic illustration of the ORNL electronics retrofit design and placement on 6 ^3He tubes in 1 bank of the JCC-71. [77]

The first iteration of the ORNL prototype electronics consisted of six preamplifiers based on PCB technology and a motherboard retrofit in a single bank of the JCC-71, and an external Low Voltage Differential Signal (LVDS) to TTL converter board. This new design uses the latest generation, low-voltage, commercial operational amplifiers. The operational amplifier packages are standard 8-SOIC packages (EIA-481-D), which provide footprint compatibility with future devices to mitigate the risk of component obsolescence, looking toward the use of FPGA-based signal processing. There are minimal hand wiring connections in contrast to the JAB-01 board using the PCB design (**Figure 3.3 d**). The standard BNC “Signal in”, “Signal out”, and “+5 V out” connectors were removed from the face of the junction boxes, as this is no longer needed, or it is handled using external components (**Figure 3.4**). The previous connection locations from the “HV in” and the “+5 V in” were changed, using the preexisting holes in the junction box face, to accommodate the new circuitry. The HV is supplied by an external power source and supplies HV to each board independently, removing the previous “HV out” daisy chain used for the JAB-01 assembly throughout the different banks. The “+5 V in” is supplied from an external power source. The signal is output using ribbon cable.

Fully differential, low-swing logic allows faster signal processing, reduced injected electrical interference, and less ground-induced current noise. This helps make each channel independent of the others, as single-ended TTL signals notoriously feed fast edges back into the circuit from which they came, and also feed those edges into other co-located circuits as cross talk, causing false triggers. LVDS is instead a fully balanced signal that has a low voltage swing which makes it inherently non-interfering in a complex multichannel system. This enables LMDA using many simultaneous channel inputs. LVDS is a standard interface on all modern FPGAs. However, all IAEA-approved neutron coincidence counting data acquisition modules, whether they are shift registers or the PTR-32, are designed to accept TTL pulses of 50 ns widths through BNC connections. The PTR-32 needs input TTL pulses of a minimum of 30 ns wide; a maximum width is not limited [78]. Therefore, for compatibility with current safeguards technology, an external FPGA-based converter board is necessary to take the time-over-threshold signal from each discriminator and convert it to a fixed 50 ns width TTL pulse of approximately 5 V amplitude. During this 50 ns pulse window, the board does not allow retriggering. Using this converter board, the logic pulses may be output using BNC connections, which are directly compatible with existing infrastructure. These outputs may be read as individual channels, or as an ORed sum of six tubes as one bank, as is possible with the JAB-01-based UNCL, or as an ORed sum of the three six-tube banks that are traditionally used. This converter board was unshielded on the benchtop during the first phase of testing.

For this first iteration of the prototype, the gain was optimized at 0.440 V for a system operational HV of 1720 V; the shaping time was selected as 160 ns, the preamplifier comparator (LTC6754) hysteresis was fixed at 4.5 mV (i.e., the difference between the threshold and the retrigger point), and the output was designed as a unipolar signal with 200 ns peaking time (the time it takes for the shaped pulse to go from baseline to its peak value). Both the gain and discriminator threshold were made to be adjustable, and pole-zero compensation was included. A HV input filter of 220 K Ω and 0.1 μ F, followed by a 499 K Ω and 0.1 μ F, near each of the preamplifier connections on the motherboard was used. HV coating was also manually applied to the exposed HV locations on the daughterboard PCB (Super Corona Dope, MG Chemicals).

The initial performance of these electronics was tested on the benchtop using an oscilloscope. The signal from both the unipolar shaper and the preamplifier are shown in **Figure 3.6**. Then, as the electronics were retrofit in the single bank of the JCC-71, I performed side-by-side comparison measurements against a JAB-01-based bank of the same JCC-71 (see **Figure 3.7**).

The six tube LVDS outputs connected to the ORNL preamplifiers were sent to the converter board, and those TTL pulses were read into Channels 1-6 in PTR-32. A single TTL output from the JAB-01 board on the opposing bank was read in as Channel 7 on PTR-32. A ^{252}Cf source was suspended equidistant between the two banks to ensure equal geometric efficiency between the two banks, isolating any differences in measured count rate to a difference in performance of the different electronics. The HV was sent into the ORNL preamplifier board input from the PTR-32 module and split to continue to the

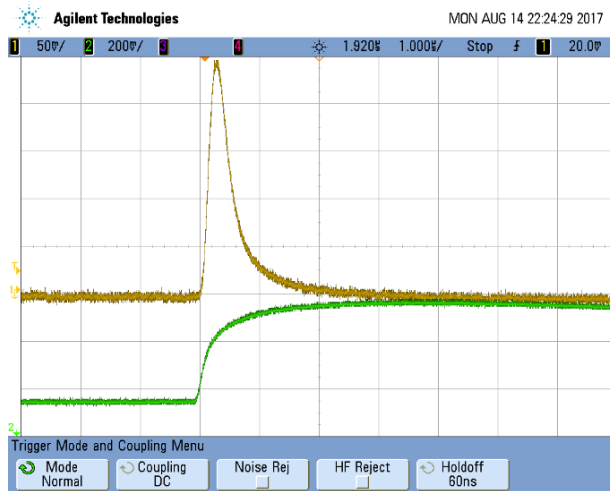


Figure 3.6. An oscilloscope trace of both the unipolar shaper output (brown) and the preamplifier output (green) using in the ORNL circuit. The preamplifier output indicates that the charge was collected quickly in this instance, resulting in a sharp, quick-rising pulse. Note that the vertical scales for these pulses are different, as given on the oscilloscope display [77].

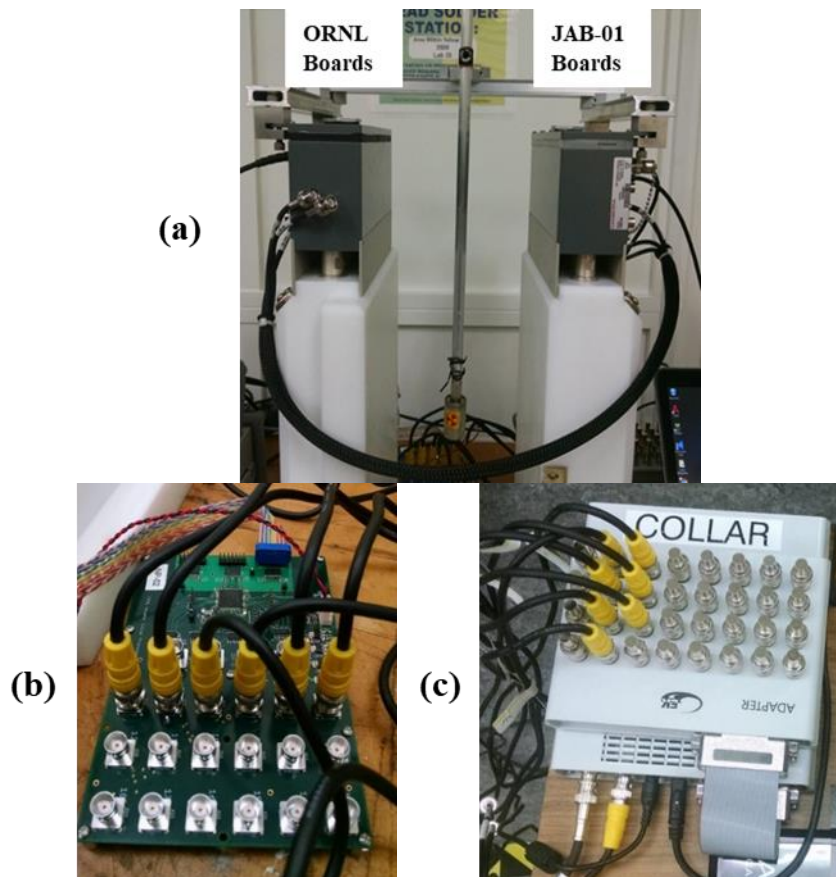


Figure 3.7. (a) The two JCC-71 banks with the ORNL electronics on the left and JAB-01 boards on the right. A ^{252}Cf source is suspended equidistant between the banks for simultaneous comparative measurements. The 6 ORNL LVDS channel outputs are sent to the converter board (b) where they are changed into TTL pulses and output by BNC connections so that they may be recorded using the PTR-32 (c).

JAB-01 HV input. An additional +5 V was supplied to the ORNL preamplifiers from an external power supply, which was also used to supply low voltage to the converter board. Meanwhile, the PTR-32 +5 V output was used to power the JAB-01 board. The events measured in all 6 ORNL–system tubes were summed and compared to the output of the events measured in the JAB-01 bank.

A HV characteristic (see Section 1.1.2) was acquired as a comparison between both systems. The measured singles and doubles count rates of the ^{252}Cf source were recorded, from 1560 V to 1980 V in steps of 20 V, from both banks of the JCC-71 and compared. This initial measurement was used to test the gain and discrimination on each of the preamplifiers to match the count rate response to that of the JAB-01 boards within the relevant operating regime. It was determined that the gain should be set at 0.440 V and the discrimination at 30 mV. The HV characteristic is used in later described measurements as the main source of diagnosing the behavior of the ORNL preamplifiers because it provides the neutron counting rates over the detector’s operational range and, therefore, provides simple performance comparisons across both banks. However, during this testing, the first measurement revealed a peculiar response that resulted in an in-depth testing of the system. An extensive study of this behavior is discussed in the following section.

3.2.1 Revealing PTR-32 HV Instabilities

In a separate measurement, the count rate response was recorded over a HV range of 1200 V-1980 V in 20 V increments supplied by the PTR-32 to also study the system’s behavior outside of the operational regime. More electronic artifacts manifested over this range. For this measurement, as is seen in the singles count rate response of **Figure 3.8**, between 1280 V and 1400 V the ORNL boards registered many more single neutron events than the JAB-01 board. The doubles count rates differ greatly as well between the two boards’ responses in the range of 1280 V-1540 V. This behavior obscures the true performance of the preamplifiers below 1540 V. Another acquisition was taken examining the region between 1200 V and 1400 V in detail for this behavior and for repeatability. The same effect was measured again.

These count rate responses are not physical. If this spurious effect at low HVs was caused by something physical in the setup, the singles and doubles count rates would trend together over the same range since they are not independent of each other, which they do not. The measured doubles count rate should not be of similar magnitude (or greater) to the measured singles count rate. The measured doubles count rate should also not be greater at lower HVs than along the plateau region as well. This is not reflected in the JAB-01 board response. Based on these results, these effects can be assumed to be caused by a persistent electronic artifact intrinsic to the setup.

For this measurement, a value of 0 cps was measured at 1600 and 1620 V in the JAB-01 boards for both the singles and doubles HV characteristics. It is important to note, before this side-by-side comparison campaign, a 0 cps value beyond 1300 V was never recorded with the JCC-71 system, in any bank containing a JAB-01 board. Since the same neutron source, in the same geometry, is present equidistant between both banks, they should both record the same number of events, within statistical error, around 1600 V since their performance was previously matched within the operational regime by setting an appropriate gain.

To investigate the 0 cps response within the 1600 V region, another acquisition was taken of the system using the PTR-32 HV supply for the range of 1550-1675 V in 25 V increments. In this separate measurement, there was no longer any registered 0 cps events in either system where they were previously measured. This conflicting result around 1600 V further confounded the diagnosis of the behavior measured. To diagnose whether this behavior was due to the introduction of the ORNL electronics or not, the JAB-01–based bank was then measured without any connections from the ORNL–based bank using the PTR-32 HV supply from 1200 V-1980 V in 20 V increments. No erroneous 0 cps readings were measured in the 1600 V range (**Figure 3.9**). This investigation incited the notion that the

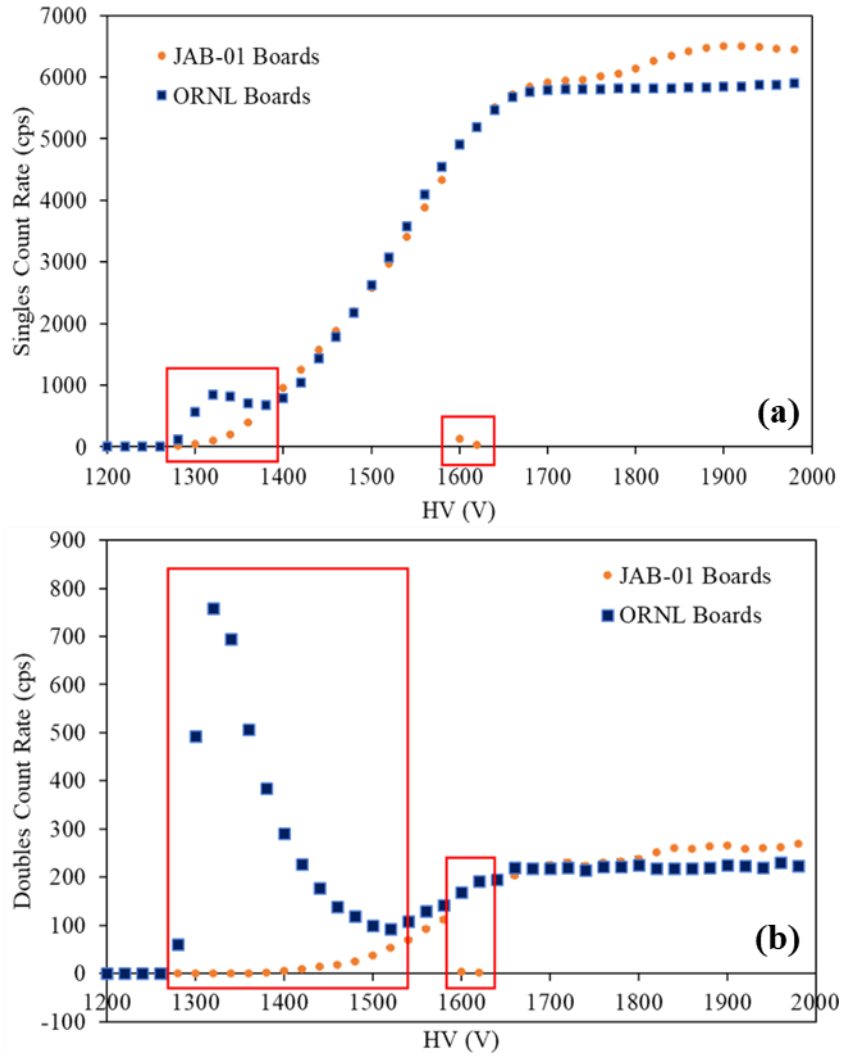


Figure 3.8. The singles (a) and the doubles HV characteristic (b) measured using the PTR-32 HV supply from 1200-1980 V.

problem was caused by an unexpected interaction between the ORNL boards and the JAB-01 board when the full range of HVs were sampled from 1200-1980 V.

The behavior of the response from both the JAB-01-based bank and the ORNL-based bank was then studied at the lower HVs simultaneously using an alternative HV supply rather than the PTR-32 supply. Using an Ortec 556 HV supply from 1200-1650 V in 50 V increments shows no indication of the structure that was seen when using the PTR-32 HV supply (**Figure 3.10**). The count rate response was clean of any electronic artifacts in both the singles and doubles HV characteristics of the ORNL response and the JAB-01 response. This was tested using a JSR-15 shift register HV supply, with the same clean result. Surprisingly, it was revealed that the behavior at low HVs and around the 1600 V region was HV-supply dependent.

To confirm this finding, a HV probe was connected to the HV output of the PTR-32 and the signal was inspected on an oscilloscope for various settings (**Figure 3.11 a**). The scope captures are 1V/division and are looking at the true HV output from the PTR-32 SHV port. It was determined that an instability in the PTR-32 HV power supply in this region was causing the peaks in count rate to be measured in the ORNL electronics at low HVs. This behavior was determined to not be transient; it persists for as long as the applied HV remains at that setting. Looking at an average of the HV output signal measured at 1340 V on a 1 mV scale (**Figure 3.11 b**), this effect results in a ~0.25 mV peak in HV relative to the baseline; 1340 V has the greatest measured increase in singles and doubles count rate. This increase in HV allows for greater charge collection by increasing the electric field, which increases the measured count rate. Beyond 1420 V, these instabilities appear to quiesce, but it is not likely that this instability is no longer affecting the system, as proven by the 0 cps measurement around 1600 V. Simultaneously during these investigations, the supply current drawn from the six ORNL boards was noted to vary between 0.260 A and 0.299 A. This means that the drift in HV is pulling the negative output signal in the ORNL amplifiers closer toward ground, which ultimately decreases the measured counts; which may be part of the cause of the seemingly random 0 cps measurements as a function of HV. Because the HV supplied to the system initially enters the junction box with the ORNL electronics, and is connected to also supply the junction box with the JAB-01 electronics, there may be some cross talk that drives the JAB-01 signal toward zero as well when the HV instability directly affects the ORNL preamplifiers.

It was proposed that this instability was caused by a HV loop instability related to the use of a Cockcroft-Walton generator circuit [79] within the PTR-32. These circuits are used to generate a high DC voltage from a low-voltage AC or pulsing DC input; they are commonly used to supply HV in every day electronic devices so this assumption is reasonable without additional proprietary knowledge. It is a convenient HV supply as the circuit converts low voltage to a higher DC voltage level through a voltage multiplier ladder network of capacitors and diodes. This enables lightweight, inexpensive, supplies that can multiply a low starting voltage up to a very high voltage. Therefore, it is an attractive option for many portable module designers such as the PTR-32. However, based on the circuit design, as the number of multiplying stages increases, voltage ripple becomes significant when supplying an output current; which is likely what is happening here. This effect can be mitigated by using an output filter.

Due to the minimal HV filtering initially applied to these ORNL electronics, this instability was not only revealed, but its effects had significant impacts on the measured HV characteristics. This behavior was masked previously in the laboratory, and likely during the fabrication and testing of PTR-32 by its manufacturer, when using JAB-01 electronics within various neutron coincidence counters due to the heavy filtration networks. Although adding greater HV filtering to the ORNL electronics is not a large burden, the fact that this instability exists within an agency-approved module is significant and should be addressed. Another PTR-32 module of the same model number as the first was brought in to repeat these measurements to investigate if this behavior was module or model-specific. The same results were reflected in the neutron pulse trains acquired using this other PTR-32. Unfortunately, after numerous attempts were made by the author and colleagues to contact the designer and manufacturer of PTR-32, Dr. Jozsef Huszti, over the length of this dissertation, it was discovered that he had recently unexpectedly

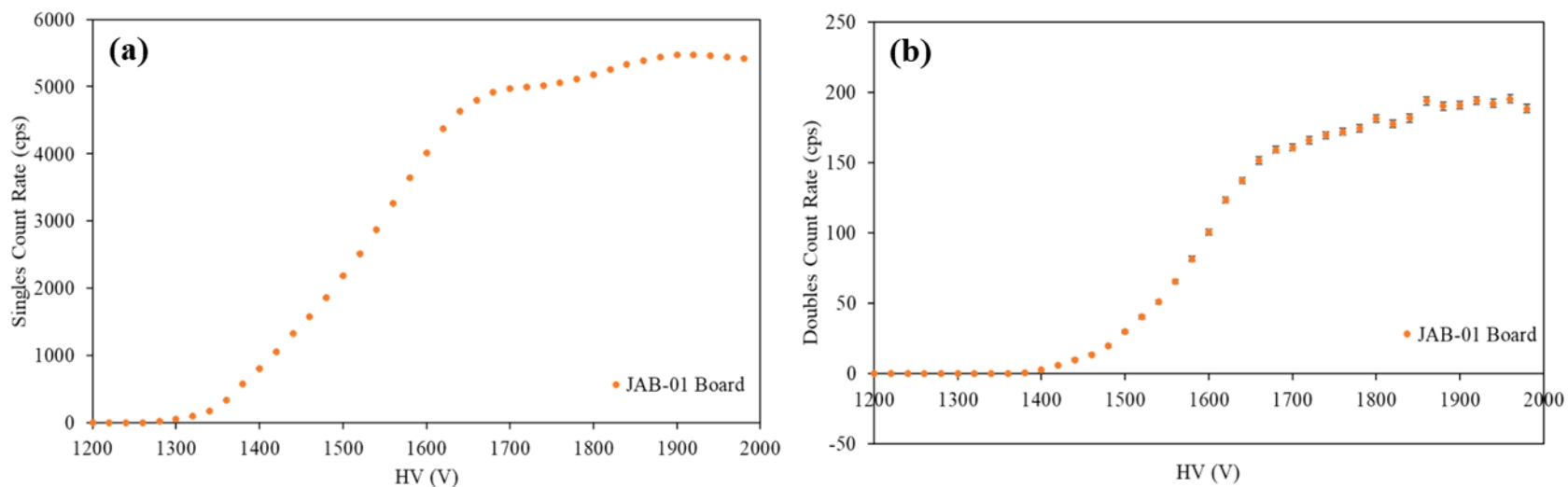


Figure 3.9. The singles (a) and the doubles HV characteristic (b) measured using the PTR-32 HV supply for the range of 1200-1980 V, with all channels from the ORNL preamplifiers disconnected. No HV settings measured an erroneous 0 cps result.

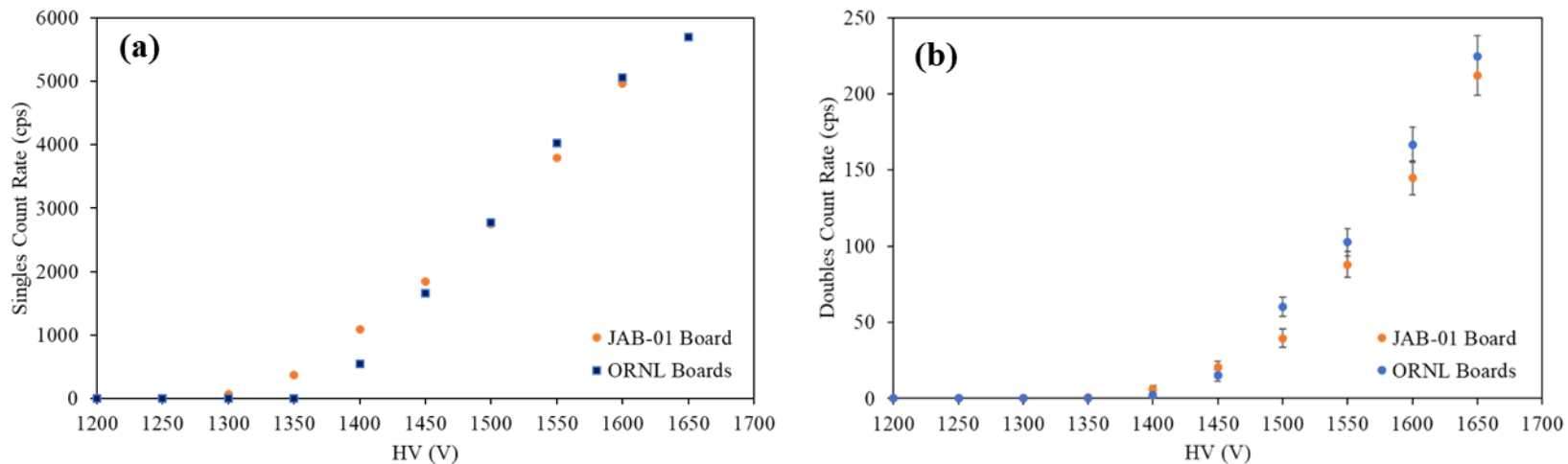


Figure 3.10. The singles (a) and the doubles HV characteristic (b) measured using an Ortec 556 HV supply module and manually changing the HV settings while simultaneously acquiring the signals from the JAB-01-based bank and ORNL-based bank through the PTR-32.

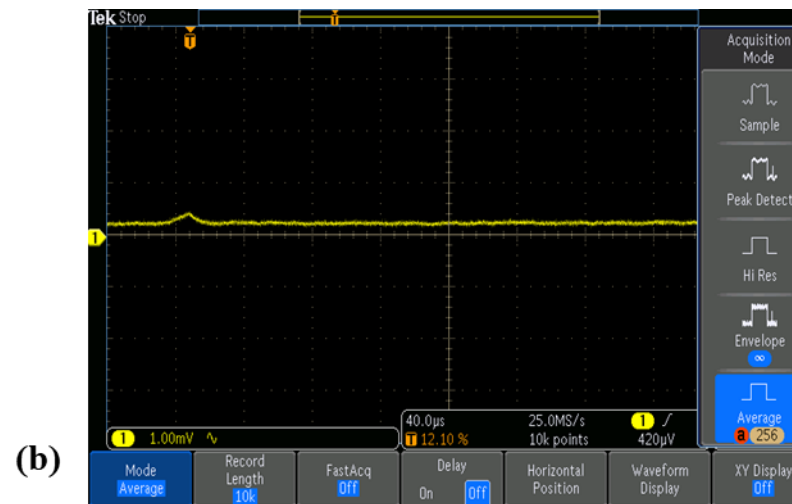
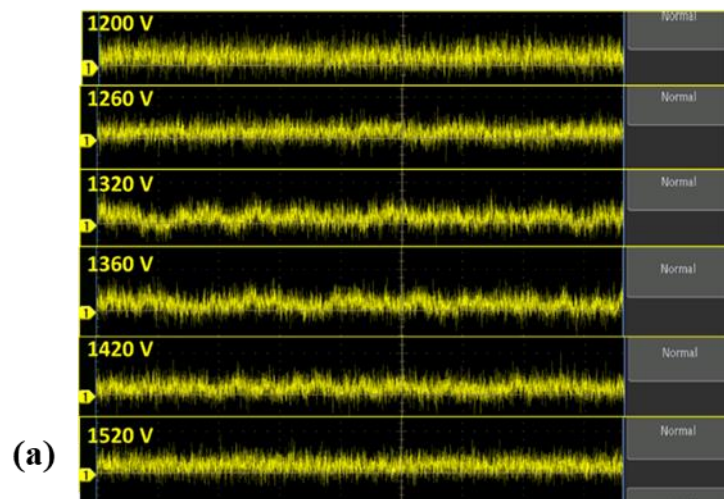


Figure 3.11. (a) A comparison of HV outputs for various settings as studied using a HV probe and oscilloscope. An unstable ripple can be noted between 1260 V and 1420 V. The output signal is relatively clean beyond this region. (b) An oscilloscope trace measured of the PTR-32 HV supply measured at 1340 V on a 1 mV scale. This average shows a ~ 0.25 mV increase from baseline caused by instabilities in the HV supply.

passed. At the time of this work, a new contact is being established. Many questions remain unaddressed regarding the functionality and more detailed processes of the module which need to be pursued.

For this first iteration of electronics, before a more robust HV filtration network could be introduced into the circuit, the challenges this discovery brings is only significant in terms of when multiple data acquisitions are necessary at varying HV settings. Because the PTR-32 HV supply can no longer be used with confidence in this testing, an external HV supply is substituted for biasing the system, meanwhile the PTR-32 is still used to acquire and analyze the channel data. This means that a user cannot take advantage of the automated HV ramping between acquisitions that PTR-32 “HV plateau” subprogram performs, but instead must be present to manually change the HV using their substituted power supply. This is relevant when considering system characterization such as performing the HV characteristic, which was used here extensively for the performance comparison between the different electronics. However, with a characterized system, a simple substitution of an external HV supply can be made for laboratory measurements until the PTR-32 HV supply issues are resolved by the manufacturers or a third party.

3.2.2 Comparison to Standard JAB-01 Preamplifier/Amplifier/Discriminator Boards

To maintain consistency of using an IAEA-approved device for the project, a JSR-15 shift register was substituted for both the PTR-32 HV supply and the Ortec 556 HV supply to provide the bias to both detector banks. The channel data was still obtained and analyzed through the PTR-32 list mode capabilities. The HV characteristic was repeated using the same ^{252}Cf source in the same geometry from 1200 V to 1980 V in 20 V increments for 5 minutes each. As is clear in **Figure 3.12**, there are no obvious indications of HV instabilities influencing the counting rates, and the performance of the ORNL electronics appears to match to the performance of the JAB-01 electronics. The doubles count rate plateau is not as stable as expected within the counting precision, which points to a need for further optimization, but it is sufficient to provide information for this performance comparison.

The threshold setting was verified to be sufficient by placing a 13 mCi ^{137}Cs source between the two banks to provide >100 mR on contact on the slabs. As seen in **Figure 3.13**, the measured gamma response begins at 1800 V due to a sufficiently high gain that is able to amplify the gamma pileup tail on a neutron pulse above the set threshold. This verifies that the 30 mV threshold was adequate for this system at the operational HV setting of 1720 V because there is no gamma response measured within this region. The increasingly negative doubles count rate measured in the JAB-01 board may be related to more Accidental counts being measured than Reals+Accidentals in their respective time gates due to increasing dead time as the HV increases. When the (R+A)-A subtraction is done to determine the doubles count rate, if the dead time extends well into the (R+A) gate, less counts will be measured. The A gate does not suffer from this dead time effect. In addition, another contributing factor to the increasingly negative doubles count rate measured with the JAB-01 board may be that as the exposure rate increases, the pulse height distribution overall broadens, decreasing the amplitude of the neutron pulse, and if the threshold is set too high, some events will drop below the threshold and will not be measured. These effects are important to understand, but are not present at the operating HV setting, and therefore will not influence the performance of the system.

When a simultaneous measurement of the ^{137}Cs and ^{252}Cf sources was conducted, the resulting singles HV characteristic trends as expected and supports the finding that the gamma influence on the count rate is not measured until 1800 V, and is therefore, not of concern within the operating regime (**Figure 3.14**); this threshold setting is applicable for the JCC-71.

However, the doubles count rate response showed troublesome behavior. This response indicates that some aspect of the electronic processing is randomly causing more doubles counts to be measured than are physically present at various HV settings, without pattern. Because the JCC-71 is used in low count rate applications, the unipolar pulse shape suffices and should not cause a sporadic count rate

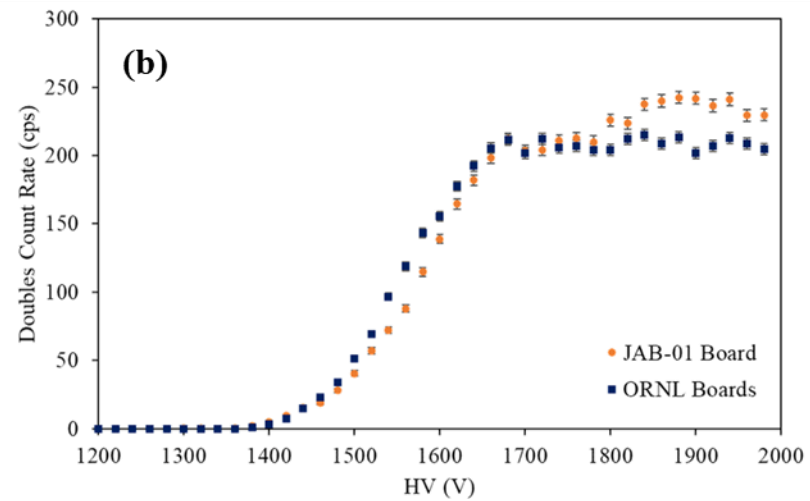
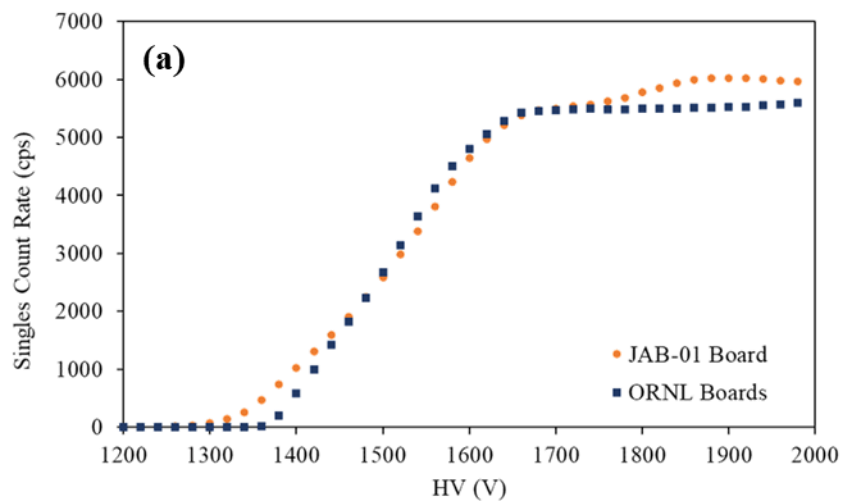


Figure 3.12. The singles (a) and doubles HV characteristic (b) of a ^{252}Cf source produced using a JSR-15 supply bias, while the data was collected and analysed using PTR-32. The performance between the two banks with differing electronics is matched.

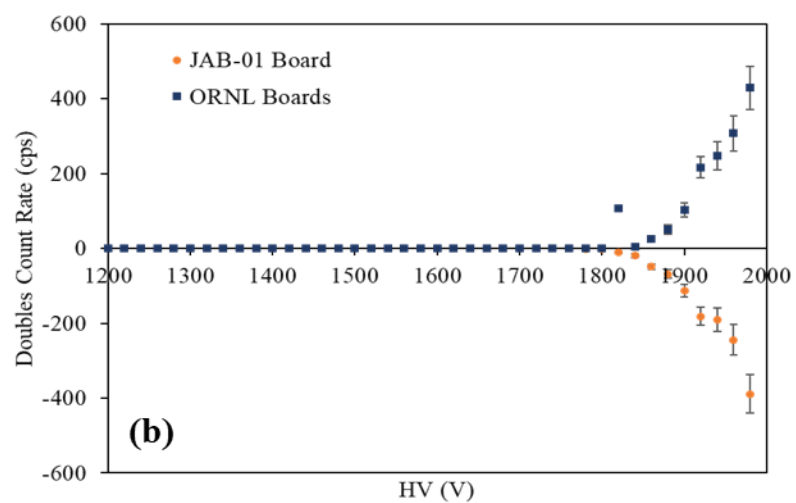
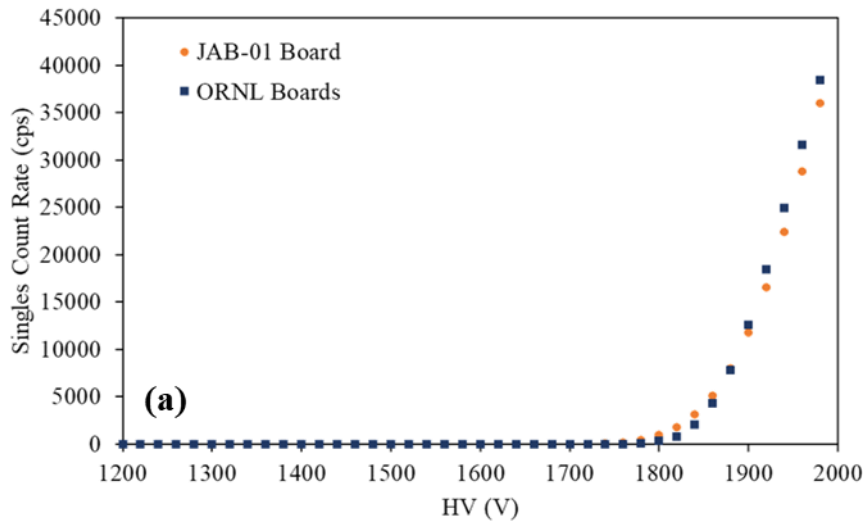


Figure 3.13. The singles (a) and doubles HV characteristic (b) produced using a ^{137}Cs source to test the threshold settings of the ORNL electronics. There are no gamma events measured before 1800 V.

to be measured. If these boards are to be implemented on systems with higher rate applications, the signal should be changed to a bipolar output to avoid baseline shifts. The pole zero compensation included in these circuits is intended to mitigate any undershoot in the unipolar shaper; pole zero restricts the charge signal to a single decaying exponential to ensure the amplitude of a successive pulse is not lowered below threshold if it were to be stacked on this tail. However, it is possible that this could be causing pile-up events that are falsely increasing the count rate depending on their location in time relative to other events. Pole zero will be removed in the optimized prototype. With pole zero removed, and more HV filtering added, this response is expected to stabilize.

For completeness, a longer shaping time of 600 ns was investigated to test if the 160 ns shaping time was causing double pulsing which was contributing to the behavior found in **Figure 3.14**. Double pulsing will be discussed in detail in Chapter 5, but it is an unwanted electronic artifact caused by the physics of charge collection in ^3He tubes. The shaping time must be long enough such that both the proton and triton charge collection peaks can be collected. If it is not, and if the amplitude drops below threshold between the collection of the two peaks, two events will be measured when only one took place. It is a function of HV and the charged particles' trajectories relative to the anode wire. This would falsely increase the measured doubles count rate. Although double pulsing was found to be present at low HVs with the 160 ns shaping time, strictly due to the electric field being strong enough to collect both charge clouds, but not large enough to accelerate them on a similar time scale, there is no double pulsing measured at 1660 V and beyond so it is not a concern for these boards and does not explain the erratic behavior seen in **Figure 3.14**. Double pulsing is, however, clearly exemplified in the operating range of the HV characteristic of **Figure 3.12**; but in the JAB-01 response and not with the ORNL boards. This discovery will be examined and explained in Chapter 5. The increased shaping time did change the ORNL HV characteristic such that counts began to be measured approximately 100 V later than with a 160 ns shaping time, which does not match the performance of the JAB-01 board. In addition, a longer shaping time increases the dead time of the electronics. Therefore, 160 ns shaping time was maintained for the second iteration of these boards.

Through this testing, the optimal gain, threshold, and shaping time were determined for this application. These studies also revealed a HV instability within the IAEA-approved PTR-32 list mode module HV supply. In progressing to the second iteration of these prototype preamplifiers, modifications on the HV filtering and pole zero compensation were made.

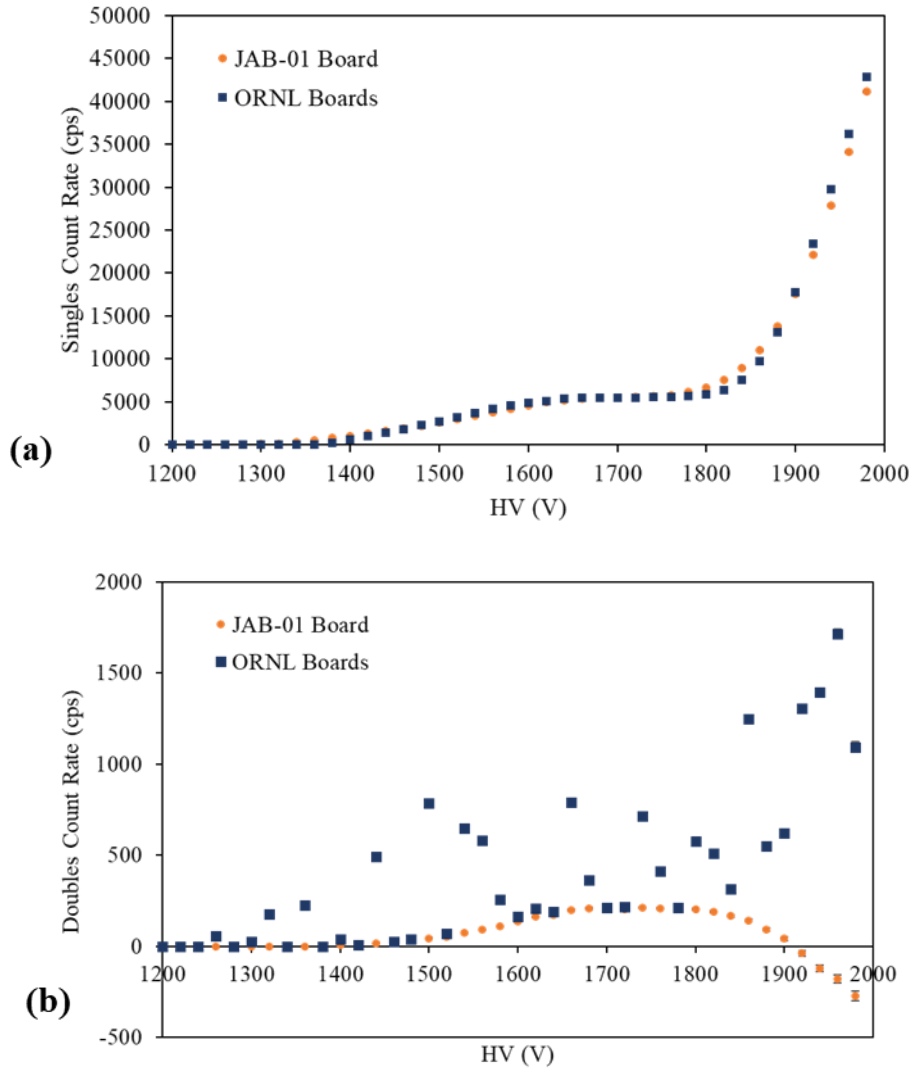


Figure 3.14. The singles (a) and doubles HV characteristic (b) produced by simultaneously using a ^{137}Cs and ^{252}Cf source to test the threshold settings of the ORNL electronics. The singles HV characteristic supports the threshold setting is sufficient for the operational HV. The doubles HV characteristic has a sporadic behavior that prompted further optimization in a second iteration.

3.3 ORNL Design Implemented on the JCC-71 Neutron Coincidence Collar, Modified Prototype

The comparison of settings used on the first prototype of the ORNL boards, as implemented on 6 ^3He tubes, and the second prototype of the ORNL boards, as implemented in the full system retrofit of 18 ^3He tubes (**Figure 3.15 a**), is outlined in **Table 3.1**. The HV filtering was increased to accommodate the PTR-32 HV instabilities, and account for any other systems that may introduce electronic artifacts into the counting circuit. The HV input filter resistance was increased from 220k Ω to 1M Ω , and the preamplifier connection filter was increased from 499 k Ω to 1M Ω . Local voltage regulators were added to each preamplifier's supply voltage as well, and the HV signals were routed for improved isolation. The hole size in the motherboards that center over each of the ^3He tubes was decreased from 0.96" to 0.50" to allow the HV components to be better spaced from the motherboard's edges and the junction box's housing, which improved voltage standoff.

Pole zero compensation was removed for prototype 2 to investigate if this provides a more stable doubles count rate response. Because 18 channels would be used on the full system retrofit, the current supply for the preamplifiers was increased to 1.5 Amps. The converter board was also fit into a housing that provided convenient shielding, while organizing the 18 LVDS signals in and the 18 TTL signals out for a cleaner setup (**Figure 3.15 b**). On the boards, the two potentiometers used for setting the preamplifier gain and comparator threshold for each tube were replaced with same value versions having side adjustments rather than top adjustments for ease of access when working within the constraints of the junction boxes. This change should have no effect on the performance of the preamplifier but only enables adjustments to be made much more easily. The shaping time of 160 ns was maintained, the gain of 0.440 V and threshold of 30 mV were also maintained.

Table 3.1. A comparison of settings for iteration 1 and 2 ORNL electronics

	ORNL Prototype 1: 6 preamplifiers	ORNL Prototype 2: 18 preamplifiers
Shaping time	160 ns	160 ns
HV filtering	HV input filter: 220k Ω and 0.1 μF , Preamp connection filter: 499k Ω and 0.1 μF	HV input filter: 1M Ω and 0.1 μF , Preamp connection filter: 1M Ω and 0.1 μF
Gain	0.440 V	0.440 V
Threshold	30 mV	30 mV
Pole zero	Yes	No

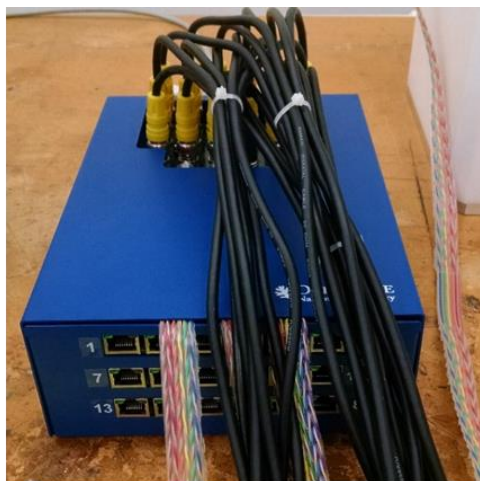


Figure 3.15. The full JCC-71 active system retrofit with iteration 2 electronics (a), shielded converter boards (b), and PTR-32 18 channel inputs (c).

3.3.1 System Testing and Optimization

The full retrofit system containing the 18 iteration 2 ORNL electronics boards were tested in the same way that the iteration 1 boards were. A ^{252}Cf source was suspended equidistant between all banks (**Figure 3.16**) and HV characteristics were obtained for each channel using PTR-32. For these measurements, due to the added HV filtering, PTR-32's HV supply was used; it was previously verified that the use of this HV supply did not affect the measured neutron count rate as it did with the iteration 1 electronics. The combined total signal from all 18 preamplifiers was analyzed to generate the results shown in **Figure 3.17**. The individual channel responses can be seen in the spatial response data provided in the next chapter.

It is clear that with the optimized filtration, the removal of the pole zero compensation, and a longer count time, the stability of the count rate response across a range of HVs has improved, even using the PTR-32 HV supply. These electronics maintain the gamma discrimination behavior previously shown in **Figure 3.14** through the operational HV region. Within the system's doubles count rate response to both a gamma and neutron source, however, there is an unexplained trend beyond the operational region. Beyond 1760 V, a decreasing trend in the measured doubles count rate is evident (**Figure 3.18**). This behavior is not a hindrance to using this system for its intended application as its operational HV ranges between 1680-1720 V, but this is significant in terms of optimizing the final ORNL prototype.

Although this behavior is unexplained, this structure is now seen with both the original JAB-01 board comparison measurement and the iteration 2 ORNL prototype (**Figure 3.19**), where before the iteration 1 ORNL prototype had an increasing trend across this range compared to the JAB-01 response (**Figure 3.13**). Without access to the PTR-32 specific analysis description, since this is not documented for reference, it cannot be determined what the reason for this behavior is. It may be possible that the source of this behavior is the way the internal analysis is performed by PTR-32; or it may be due to electronic behavior such as dead time effects and the broadening of the pulse height distribution in the both preamplifiers, as discussed in Section 3.2.2. Despite this uncertainty, with confidence through these measurements, it is confirmed that the ORNL prototype 2 boards match the performance of the original JAB-01 boards with use in the JCC-71.

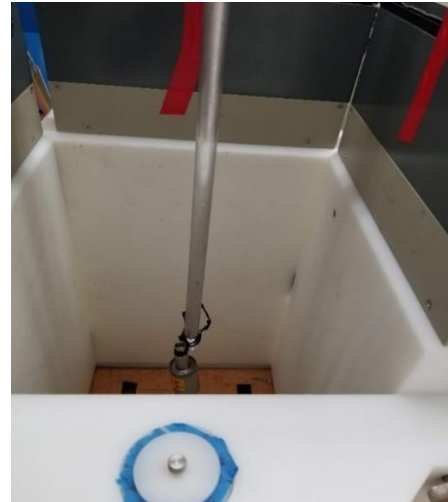


Figure 3.16. The measurement setup used to measure the 18 channel iteration 2 retrofit.

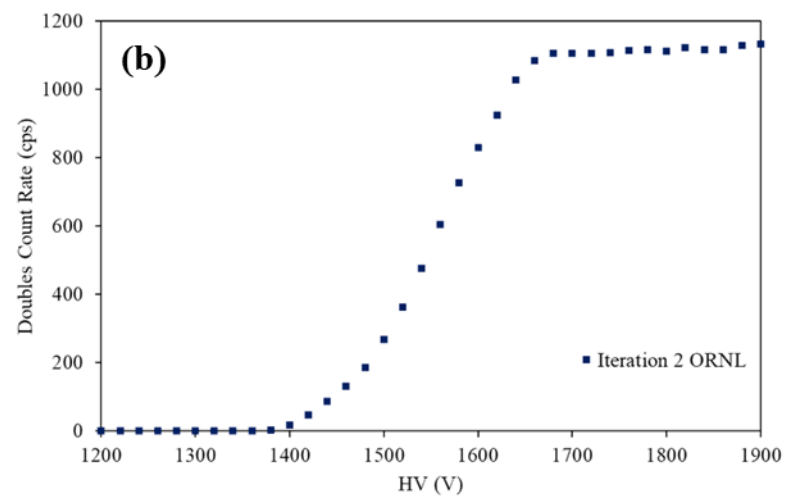
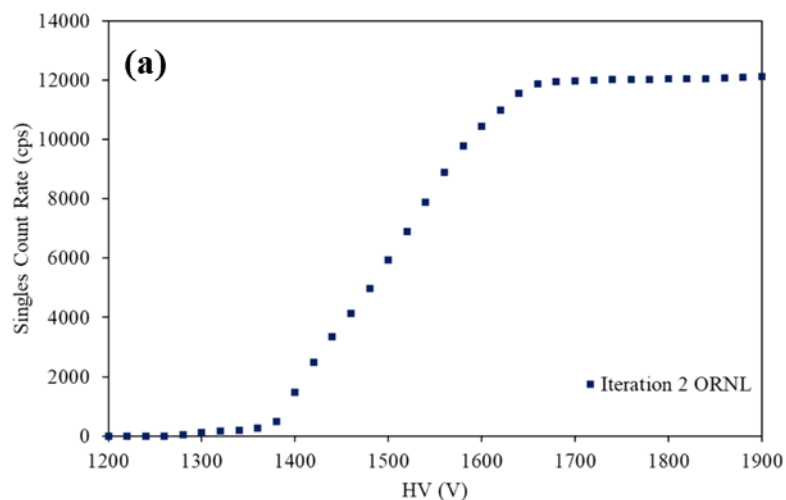


Figure 3.17. The singles (a) and doubles HV characteristic (b) of a ^{252}Cf source produced using PTR-32 and the full JCC-71 system retrofit with iteration 2 ORNL electronics.

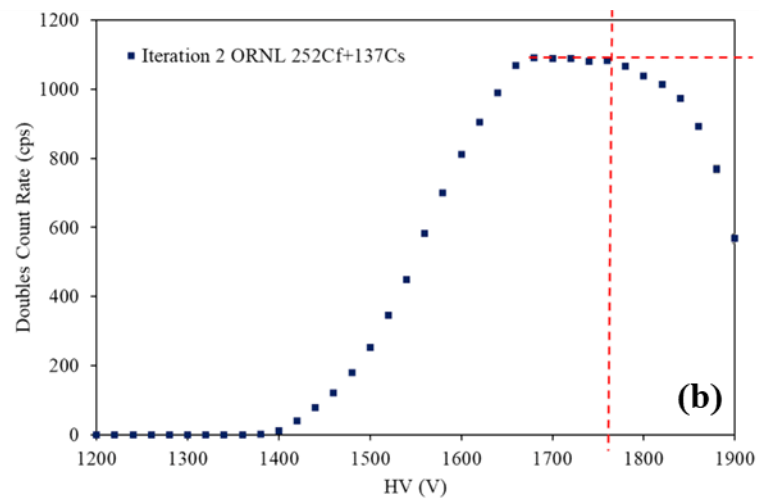
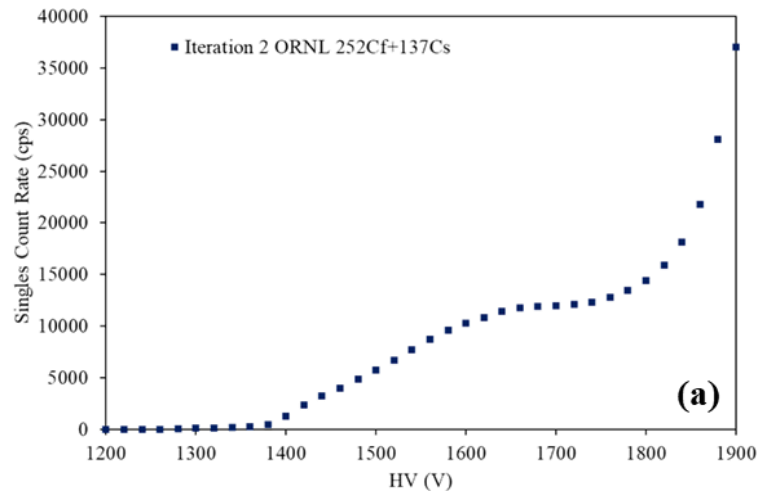


Figure 3.18. The singles (a) and doubles HV characteristic (b) produced by simultaneously using a ^{137}Cs and ^{252}Cf source. The singles HV characteristic supports the threshold setting is sufficient, with the modifications made between iteration 1 and 2. The doubles HV characteristic is more stable within the operational HV than Figure 3.14, but shows a downward trend beyond 1760 V.

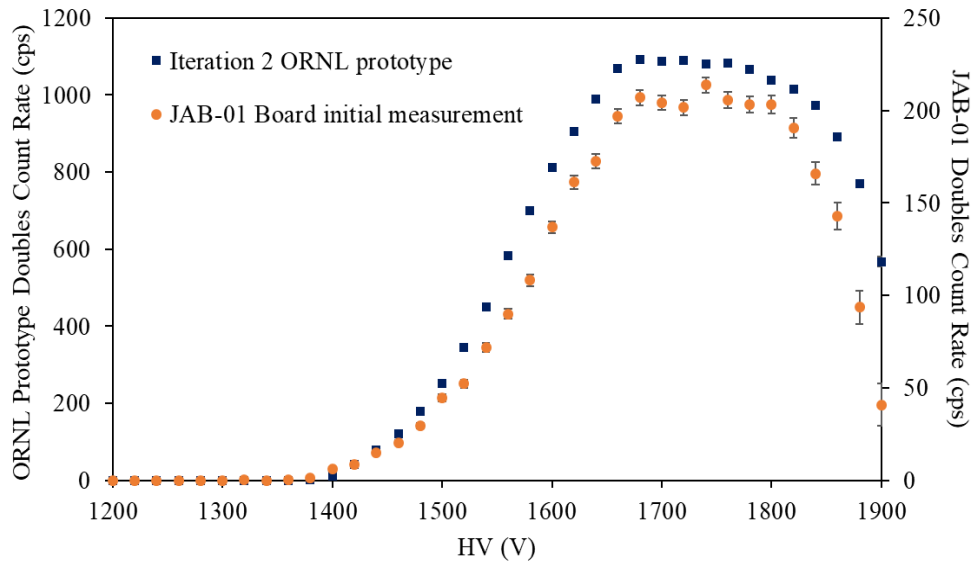


Figure 3.19. The doubles HV characteristic produced using a ^{137}Cs and ^{252}Cf source. This figure compares the results for both the initial JAB-01–based measurement and the iteration 2 ORNL prototype measurement to highlight how both characteristics have a downward trend beyond ~ 1760 V.

3.4 Discussion

It has been shown that the JCC-71 can be retrofitted with the ORNL prototype preamplifiers within the existing counter junction boxes without modification to the system or overall counter form factor. This is an important result in the context of defining an upgrade plan. Each of the 18 ^3He tubes within the JCC-71 were retrofitted with a prototype preamplifier, and their combined signal outputs were studied in detail. These prototype iterations have addressed many concerns in the count rate response, meanwhile achieving similar precision to the JAB-01 Preamplifier/Amplifier/Discriminator boards. They also provide a viable alternative that outperforms the JAB-01 in certain instances due to the discovery of non-ideal behavior measured in the JAB-01, which is discussed in detail in Chapter 5.

The performance of these boards was adjusted to match the performance of the preexisting JAB-01 for this project. However, these settings may be further optimized to exceed the performance of currently available systems with the proper testing and components. In addition, a successive third iteration could provide the final optimization adjustments to make this prototype fieldable. Some of these modifications include an improved version of the printed spacer used on each motherboard to better route the LVDS ribbon cables away from the HV coupling capacitor and HV traces to avoid any possibility of arcs. Securing the components in a robust backbone structure between the motherboard and channel preamplifiers would also be necessary to avoid any wear during shipment and movement of these systems. Better design placement of the components across the PCB would aid in the manufacturing, assembly, and adjustment performed during system testing. Furthermore, increasing the comparator hysteresis, which controls the difference between the threshold and the retrigger point, could improve performance. If these electronics are to be extended to other system models, a higher rated HV cap could provide a lenient buffer to encompass a greater range of applied HV settings. Finally, understanding the PTR-32 LMDA internal analysis could improve any final optimization made on these electronics.

Similarly designed preamplifiers were also produced and tested for use in a neutron counter used in the Neutron Activation Analysis laboratory at the High Flux Isotope Reactor at ORNL. These preamplifiers have similar components as those implemented in the JCC-71 but are again modified in design to fit within counter-specific housing. They are designed to be compatible with a different tube manufacturer, tube diameter and fill gas pressure, operational HV, geometry, form factor, and different readout software. The system is also used in high rate applications with significant gamma exposure, so a shaping time of 400 ns compared to 160 ns was used. Therefore, the performance and pulse processing requirements differed considerably from the JCC-71 electronics. It was my role to test the assembled system for performance optimization using the standard neutron coincidence counting software and appropriate timing windows. Through this testing, these electronics were found to also meet the specified requirements, further justifying that these prototypes may be easily modified to fit various systems for a variety of applications, while remaining compatible with most common neutron coincidence counters.

Chapter 4

Spatial Response Measurements in a new List Mode Neutron Coincidence Collar

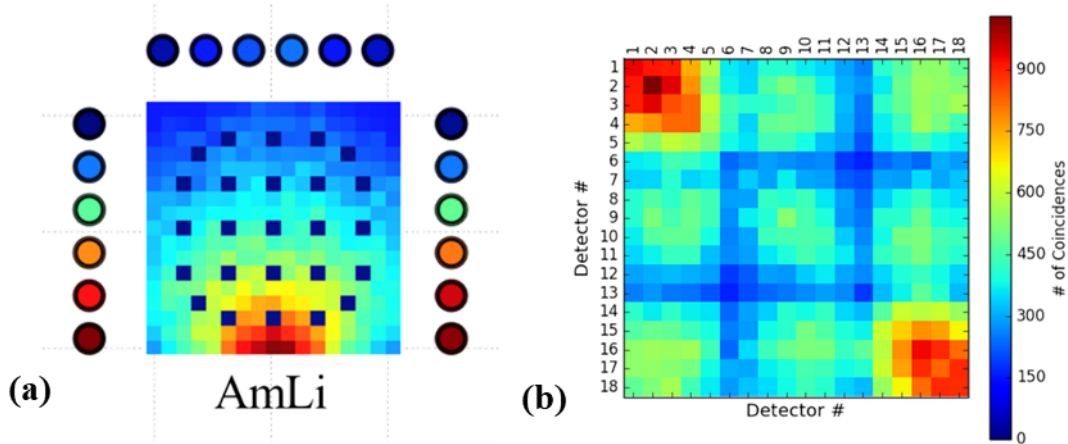
Serving as the experimental lead under the Department of Energy National Nuclear Security Administration Defense Nuclear Nonproliferation Research and Development sponsored project, “A List Mode Response Matrix for Advanced Correlated Neutron Analysis for Nuclear Safeguards,” this chapter presents the various stages of the project in context of the contributions and goals of the experimental measurements and validation I have performed. The ultimate goal of this project, which motivated this research, was to demonstrate the capabilities of a list mode response matrix for the nondestructive assay of fresh nuclear fuel assemblies. To enable partial defect detection of fuel pin locations and absences within an assembly, the project aims to extend well-established correlated neutron analysis techniques on a preexisting Neutron Coincidence Collar by extracting a greater number of useful signatures from the system than are currently generated. LMDA, combined with the addition of multiple preamplifiers, facilitates this capability by increasing the number of simultaneous signals that can be measured due to the many channel inputs on the hardware, while allowing for an in-depth analysis of multi-channel neutron coincidence events to determine a fissioning sample’s location based on the measured doubles count rate in various channel logic coincidence combinations. All of this can be done from a single measurement pulse train in offline analysis, which is the major benefit provided by LMDA.

For the traditional use of the UNCL in the field, one summed neutron pulse train is collected by shift register electronics during an active measurement of the fresh fuel assembly; this acquisition yields a net total system neutron coincidence counting rate when background and passive contributions are subtracted, despite 18 detector channels being potentially available. From the original design, four channels may be measured using LMDA, by terminating each bank’s Signal In connection and measuring each Signal Out when the system is assembled in passive mode. This project has alternatively made use of the 18 independent detector channels in active mode to analyze each signal output to form the spatial response matrix from the doubles count rate. To accomplish this, each of the 18 individual ^3He tubes was retrofit with individual preamplifiers designed and tested at ORNL, which were described in detail in Chapter 3.

As is seen in **Figure 4.1**, at the start of the project campaign, a relative fission rate map was generated to illustrate what count rates would be expected when using the specific JCC-71 UNCL in active mode with a representative AmLi source as the interrogation source. The induced coincidences in the fresh fuel assembly were then used to build a representative spatial response matrix that could ultimately highlight any measurable difference in count rates caused by a lack of fresh fuel within the assembly. This was done by studying the singles and doubles neutron count rate profile on all 18 ^3He tube channels.

The first stage of this dissertation research performed to support the project was to ensure that the JCC-71 performed on delivery to ORNL as was specified during industry testing at Canberra Industries. This was done, as described in detail in Chapter 2, while conducting a comparative system characterization procedure using PTR-32 LMDA to ensure reciprocity of values between the standard JSR-15 shift register and LMDA. It was shown that LMDA does not introduce any bias in the characterization procedure relative to using a shift register for these measurements, and, therefore, it was

verified that using this technology for the project would be suitable. After this characterization, source positioning response measurements were conducted using a ^{252}Cf source placed at various locations within the well of the collar. The count rate response measurements are discussed in Section 4.1, showing the initial capabilities of locating a source's position based on its LMDA measured coincidence rate. These measurements were conducted with the original system, containing a single JAB-01 board in each of the four banks. After the first iteration of the ORNL prototype electronics were shown to have similar functionality as the JAB-01 boards, as outlined in Section 3.2.2, a simple spatial response was compiled from the measured ^{252}Cf data. Using the ORNL electronics in one bank of the JCC-71, the source response profile was used to indicate if individual neighboring tubes were able to discern a measurable difference in count rate, which they were, as described in Section 4.2.1. Finally, with the full system retrofit with the Iteration 2 ORNL preamplifiers, a final stage of this phase of the project was completed by measuring a certified ^{252}Cf source in various positions within the well of the Collar to determine the source spatial response, as discussed in detail in Section 4.2.2. Then, a MCNP6 model of the JCC-71 was modified and evaluated using the measured spatial response data for its performance relative to the physical system, laying the foundation for future analysis work to meet the ultimate goals of the List Mode Response Matrix project.



⁴Figure 4.1. (a) A map of fission events occurring in an example fresh fuel assembly as a function of distance from the AmLi source. (b) List mode response matrix illustrating the coincidence count rate due to AmLi–induced fissions as a function of ³He tube number from 1–18.

⁴ The anticipated performance and response of this proposed system was initially simulated in MCNP6 by Andrew Nicholson and Louise Worrall at ORNL, using an original UNCL-I MCNP model in fast Pressurized Water Reactor mode, developed by Anthony Belian of NA-241 for the separate Neutron Rodeo Campaign, and modified to match the active configuration of the Canberra Industries JCC-71 using their technical drawings.

4.1 Source Position Resolution Using Original JAB-01 Banks

The original JCC-71 Neutron Coincidence Collar UNCL arrived from Canberra Industries with the standard JAB-01 preamplifier/amplifier/discriminator boards within each of the four banks. As the system design describes, a single JAB-01 board is used in each of the four banks to produce a signal output from the 6 tubes in that bank. Unlike in its standard operation, each of these four signals were acquired simultaneously using PTR-32 LMDA to measure the spatial response of the JCC-71 operated in passive mode to a ^{252}Cf source. The $42\ \mu\text{Ci } ^{252}\text{Cf}$ was placed on a stand centralized axially within the well (**Figure 4.2**), the JCC-71 was biased by PTR-32 to 1720 V, and various measurements were taken as the source was moved to 9 different positions. The positions were assigned to show the general variation of the spatial response across the system, and the source was placed by eye. The neutron pulse trains were recorded for all four channels at each of the positions for 5 minutes each. From these 9 measurements all successive comparisons were made offline through use of the replay features in PTR-32 using the traditional timing window settings.

The first comparison evaluates the measured count rates on opposing segments of the detector body. As shown in **Figure 4.3**, the ratio of doubles count rate on the front-to-back detector banks changes with the source position. At position 0 (the center) the ratio is 1, as expected. An even distribution of neutron counts should be incident on all banks from the center position. As the source is moved closer to the front detector bank (#2) as in positions 2, 3 and 6, the ratio increases; when it is moved closer to the back detector bank (#4) as in positions 1, 4 and 5, the ratio decreases. Positions 7 and 8 are intermediate and this is reflected in the response.

The same method of analysis was performed on the ratio of doubles count rate on the left-to-right detector banks. Again, it is evident that the ratio responds to the source position, shown in **Figure 4.4**. The ratio between left-to-right doubles count rate increases at source positions 2, 4 and 8 and the ratio decreases at positions 1, 3, and 7. Positions 5 and 6 provide intermediate count rate ratios.

The four individual 6-tube bank rates were individually analyzed as well to investigate if their measured rates would suffice for source positioning location. This is significant as when the new electronics are retrofit on the JCC-71, the efficiency of each of the 18 tubes will be much less than the combined efficiency of the 6-tubes used in the total summed signal from each bank. If these banks were not able to indicate the source's relative position, it would not be possible to continue to the next stage of testing. Referencing **Figure 4.5**, it is clear that the individual banks measured count rates can indicate the source's relative position. The total doubles signal differs slightly across the different positions due to the slight difference in geometry and manufacturing tolerances within the separate banks.

With a basic proof of concept that each of the four 6-tube banks count rate responses could indicate a relative source's position, the next step in experimental validation was to test the neutron count rate responses for various bank channels in logic coincidences with each other in offline analysis. This feature is crucial for the List Mode Response Matrix as the measured doubles count rate in channel logic coincidences will be higher than the measured doubles rate in individual channels; this will be necessary for active interrogation with fresh fuel assemblies that suffer from characteristic low count rates due to the proportion of fissioning ^{235}U . In addition, to resolve partial defects such as fuel pin removal, positioning of the decreased count rate is key. These channel logic coincidences allow the user to isolate the region in which a lower count rate is measured than expected compared to closely neighboring rates, and prompt further investigation.

PTR-32 has a combination of GUI subroutines available that enable any number of pulse trains from the 32 channel inputs to be put into logic coincidences in any combination. First, the total acquired neutron pulse train must be spliced to contain the combined pulse trains of interest using the "Subtract" subprogram. Then, that pulse train may be analyzed using either the "SDT" subprogram for the Coincidence Rates for which a simple text file is produced, the "Channel Coincidences" subprogram for a more in-depth visual comparison, or the "All Coincidences" subprogram to automatically analyze any number of different files containing combinations of spliced neutron pulse trains which are then read out

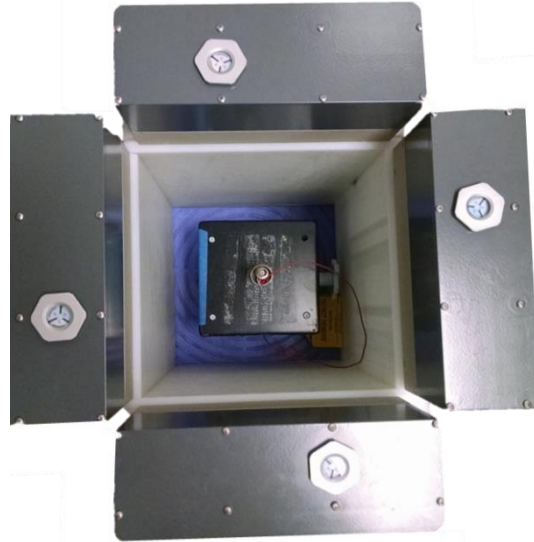


Figure 4.2. The experimental setup using the JCC-71 in passive mode, with ^{252}Cf source resting on an axially centralized source stand. The radially center position is shown.

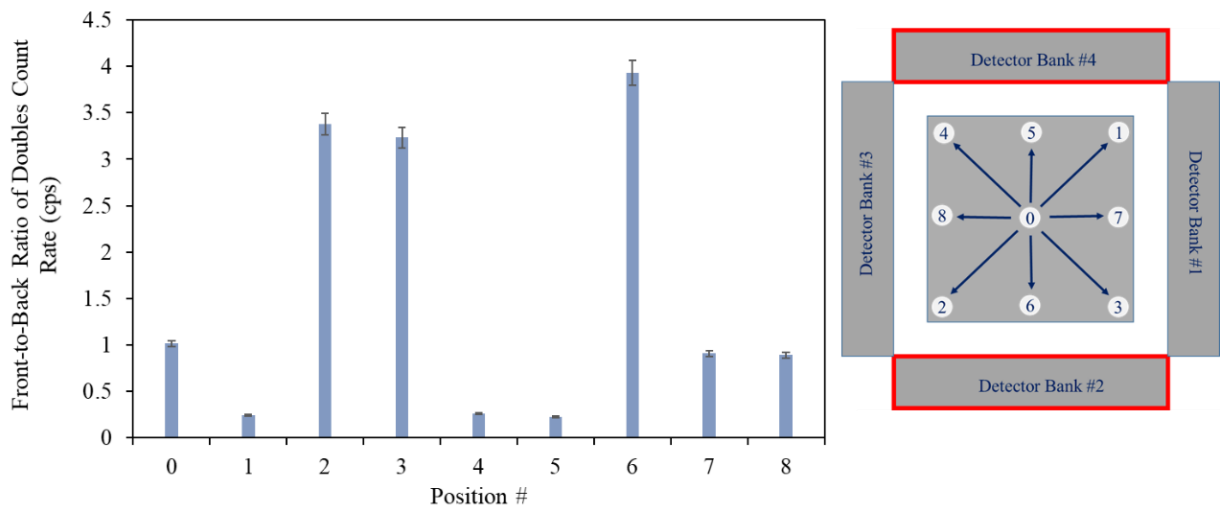


Figure 4.3. The doubles count rate measured in the front detector bank (#2) to the doubles count rate measured in the back detector bank (#4) as the ^{252}Cf source location varied through 9 positions.

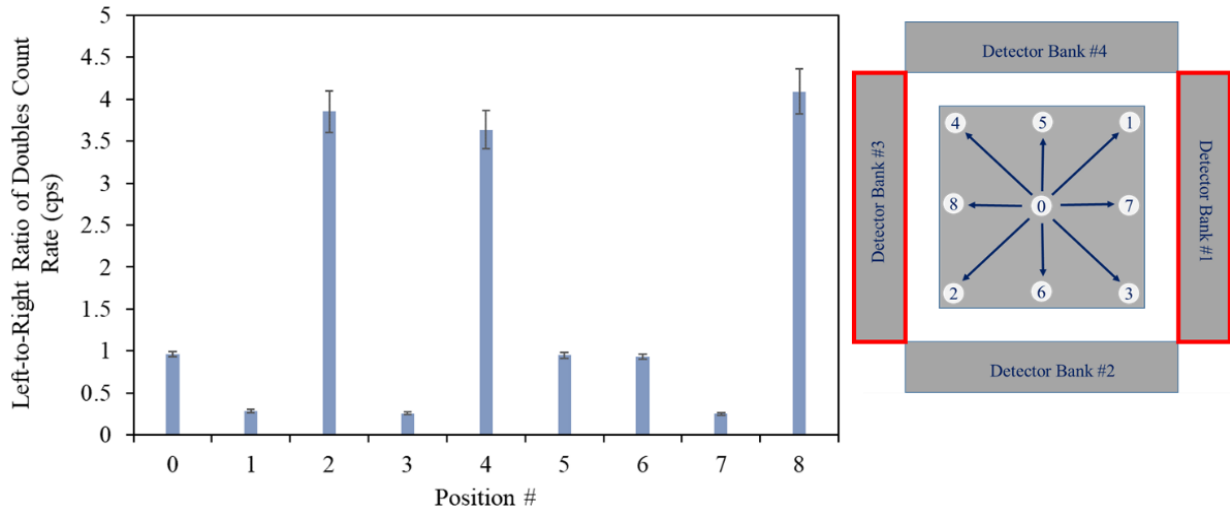


Figure 4.4. The doubles count rate measured in the left detector bank (#3) to the doubles count rate measured in the right detector bank (#1) as the ^{252}Cf source location varied through 9 positions.

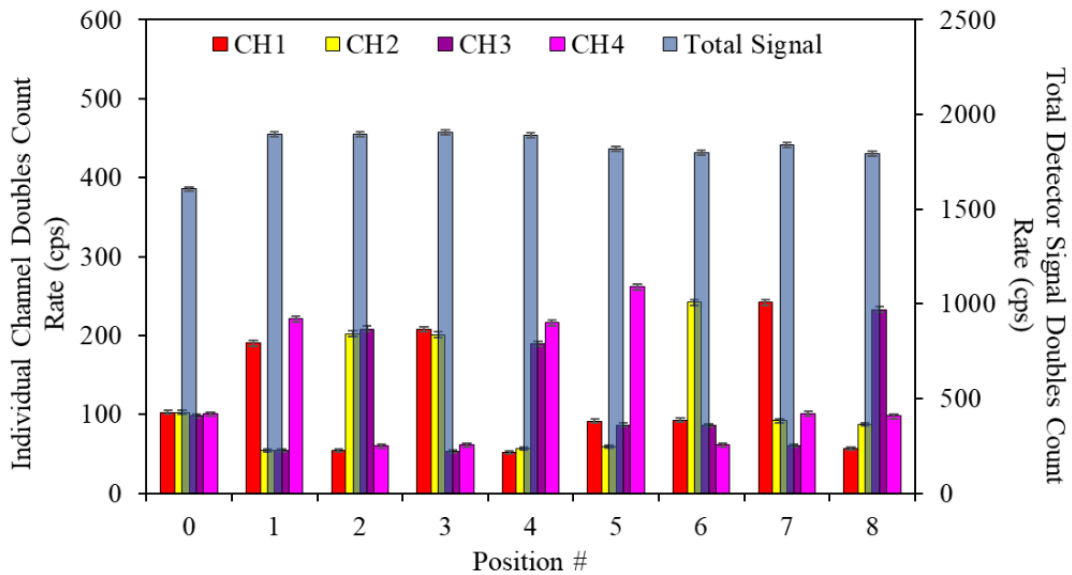


Figure 4.5. The measured doubles count rates obtained for the 4 original banks of the JCC-71 as a function of ^{252}Cf source position, in addition to the total system output doubles count rate signal.

in a simple text file. Each of these subprograms require the user to click and select the input files, designate what channels to keep and remove, and also set the relevant timing windows. This can be done for any and all combinations of the measured input channels. For this work, the “Subtract” was used to produce the modified pulse trains for all combinations of 2 banks. “All Coincidences” was then used for convenience and efficiency purposes for the various files containing the pulse trains of different bank combinations at each position.

However, this approach will not be favorable in terms of time and effort invested to perform this offline analysis when 18 separate channels are used in the full system retrofit and any number of tubes in any number of combinations will need to be analyzed to assay a fuel fresh fuel assembly. Unfortunately, PTR-32 is not an editable program and its code is proprietary so modifications to these scripts must come from the developers. As was previously mentioned in Chapter 3, over the course of this dissertation, the author and colleagues attempted to get in contact with the developer to discuss these concerns, without response. It was only recently that we have learned of Dr. Jozsef Huzsti’s unexpected passing. For the purpose of this project, PTR-32 must be used as it is currently the only IAEA-approved LMDA module, and with attempting to keep these modifications fieldable, new software cannot be introduced at this point in time.

Referencing **Figure 4.6**, the measured doubles count rate produced from the channel logic coincidences reflect the source’s position with a distinguishable count rate, and, therefore, prove that this may be a viable prospect to accomplish when using the full system retrofit. This positive spatial response investigation using the four banks of the JCC-71 with original JAB-01 electronics encouraged the project to progress to its next stage of electronics development, implementation, and testing discussed in the next section.

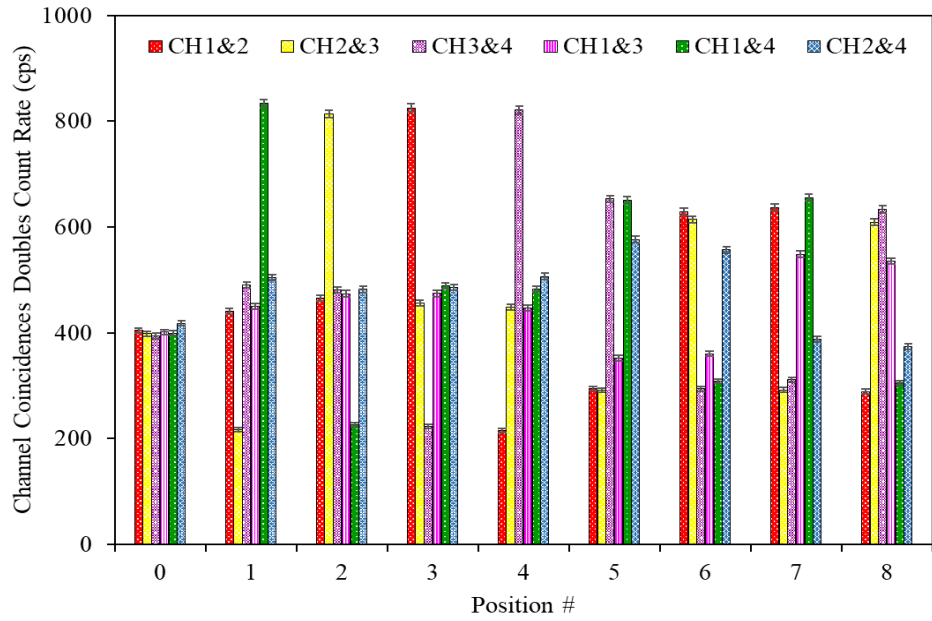


Figure 4.6. The measured doubles count rates obtained for various combinations of logic coincidences between the 4 original banks of the JCC-71 as a function of ^{252}Cf source position.

4.2 Source Position Resolution Using ORNL Electronics

4.2.1 Measurements Using Iteration 1 Electronics

The next stage of this project implemented the 6 ORNL–designed preamplifiers onto 6 tubes in one bank of the JCC-71. These electronics were shown to have equal, if not better, performance to the original JAB-01 preamplifier/amplifier/discriminator boards contained in the JCC-71 (Chapter 3). In addition, to make measurements more precise and repeatable, I designed an XYZ source stand that was fabricated at ORNL (**Figure 4.7**). The source stand allows any source to be suspended, and its position relative to the desired tube(s) in x,y, or z to be chosen and specified. Using the one retrofitted bank of the JCC-71 and the same ^{252}Cf source suspended approximately 15 cm away from the center of the bank, a neutron pulse train was acquired for all 6 channels simultaneously using PTR-32. This pulse train was acquired across a range of HV settings, as part of the electronics evaluation campaign presented in Chapter 3.

Due to the source’s positioning relative to the 6 channels, a simple spatial response was discerned; the positions of channels 1–6 are illustrated in **Figure 4.8**, with the source placed between channels 3 and 4. Channels 3 and 4 are expected to have the highest measured count rate, followed by both channels 2 and 5, then channels 1 and 6. This is reflected in the measured Singles count rate as a function of applied HV (**Figure 4.8**). With these data, the location of the source may be inferred; with the remaining twelve ^3He tubes, this positioning resolution should increase to better pinpoint where the decreased measured count rate is generated from. However, the measured doubles count rate was not as stable, nor as consistent, in providing a distinguishable response profile like with the singles count rate. This was in part due to the measurement duration in addition to the electronic settings selected for testing on the Iteration 1 electronics. The stability of the electronics was improved in Iteration 2.

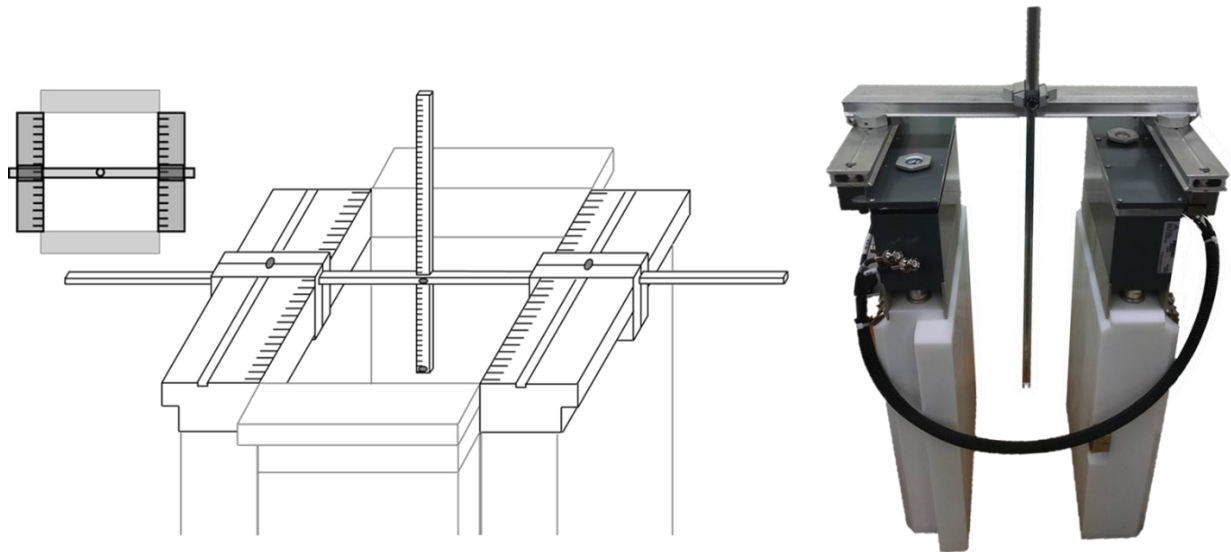


Figure 4.7. The design, and fabricated, XYZ source stand as implemented on the JCC-71.

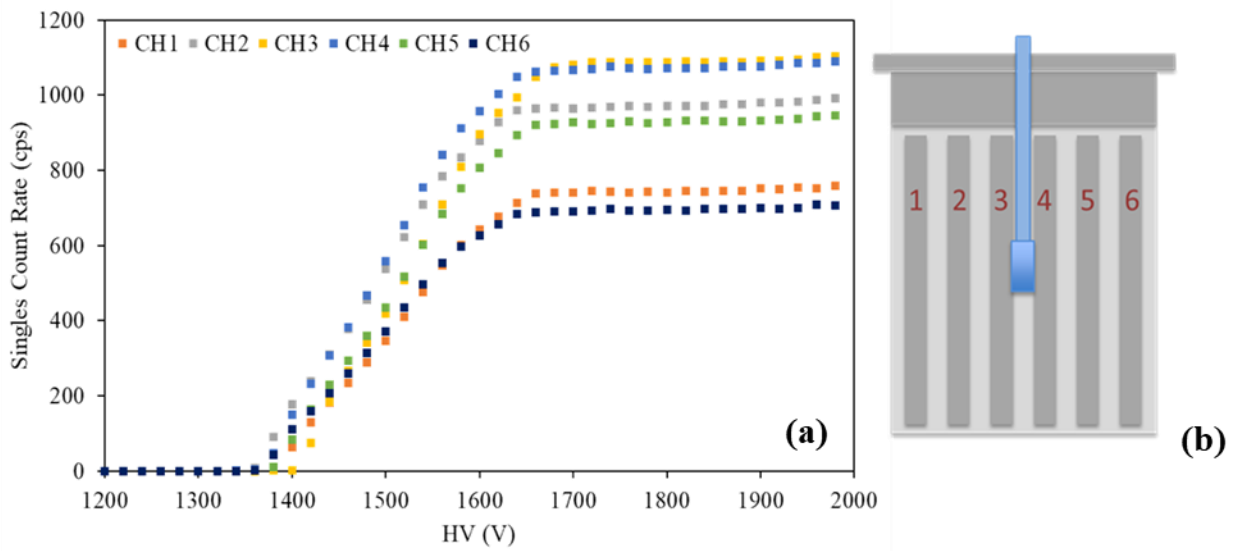


Figure 4.8.(a) Singles count rate data as a function of applied HV illustrated for each channel. Preliminary indication of spatial response capabilities with additional preamplifiers for each detector bank are shown **(b)** The source was placed between detector Channels 3 and 4.

4.2.2 Full System Retrofit Measurements Implementing Iteration 2 Electronics

Once the second iteration of the ORNL preamplifiers was tested, as described in Chapter 3, a spatial response measurement was conducted using the ^{252}Cf source suspended equidistant from the banks of the modified JCC-71 system. The active configuration of the system was used, with no AmLi placed within the active HDPE bank. The system was biased to 1720 V, and the preamplifiers were supplied with the low voltage from an external supply. The data from each of the 18 channels were read into PTR-32. Measurements of the ^{252}Cf source, of a strength of 42 μCi , were conducted for 9 different positions within the well, centralized axially, at 20 minutes each. The neutron pulse trains from each of 18 ^3He tubes were obtained and analyzed to get a net singles and doubles count rate for each. The doubles count rates were then studied relative to each tube to provide a spatial response of measured counts. Three different cases are shown in **Figure 4.9-Figure 4.11**: the first with the ^{252}Cf in the center, the second with the ^{252}Cf in the corner between banks 1 and 2 near tubes 6 and 7, and finally with the ^{252}Cf in the corner between bank 3 and the active HDPE slab near tube 18. It is evident that the addition of the preamplifiers on each ^3He tube has improved the spatial positioning of a point source and the current setup has the ability to indicate a large difference in measurable count rate across the 18 tubes depending on the location of the source.

It is also evident that geometric effects of the system have a role in the measured count rate. In **Figure 4.11** with the source in the center, tubes 6, 7, 12, and 13 have distinguishably lower count rates. This is due to their location; at the corners of the JCC-71 there is less HDPE which decreases the number of neutrons thermalized and captured in this region. This effect is seen reflected in **Figure 4.10** and **Figure 4.11** as well, but it is not as noticeable due to the sources location in those instances. In addition, the tubes more centralized in the HDPE banks such as 3 and 4, 9 and 10, and 15 and 16 measure a greater count rate due to the opposite effect: there is more HDPE in areas both to the left and right of these tubes in which neutrons can be thermalized and then captured in these tubes. As a whole, the system has a very low measured doubles count rate in each tube with the ^{252}Cf placed in the center position.

Using the same strength source, the measured doubles count rate is significantly higher in **Figure 4.10** and **Figure 4.11** where the ^{252}Cf is placed up against the corners of the banks. When the source is instead placed in the corner between banks 1 and 2, the doubles count rate measured in tubes 4-9 is much greater count rate than that measured with the source is at its center position. Due to geometry, the count rate measured in tubes 13-18 are low comparatively as many neutrons will not travel in this direction, but instead escape out of the system. With the same argument, banks 1 and 2 in **Figure 4.11** have a low measured count rate due to the placement of the ^{252}Cf near the active HDPE block that will not detect any events. Tube 18 has the greatest measured count rate due to the thermalization of the neutrons within this block and capture within the ^3He tube.

Finally, the response of the modified JCC-71 for all 9 ^{252}Cf source positions was compared to illustrate the different count rates recorded in every tube at all positions (**Figure 4.12**). This figure is quite complex and contains considerable information within it. The measured doubles count rates are recorded in a histogram format, coupled with a color-coded trend that guides the eye to better interpret the trend of the count rate as a function of tube number. For the instances where the ^{252}Cf is closest to bank 1 (Tubes 1-6) such as in positions 1, 3, and 7, the count rate responses in these tubes are greatest. The exact location can be assumed between these three positions as well. For position 1 the measured doubles rate is greatest in Tubes 1, 2, and 3 with the greatest value measured in Tube 1. For position 3 the measured doubles rate is greatest in Tubes 5, 6, 7, and 8 with the greatest value measured in Tube 7. In position 7 the measured doubles rate is greatest in Tubes 3 and 4. The measured rates in the other tubes then varies based on that source's position relative to them, but they are always less than what is measured in bank 1. The same applies to the other 6 source placements and their neighboring tubes.

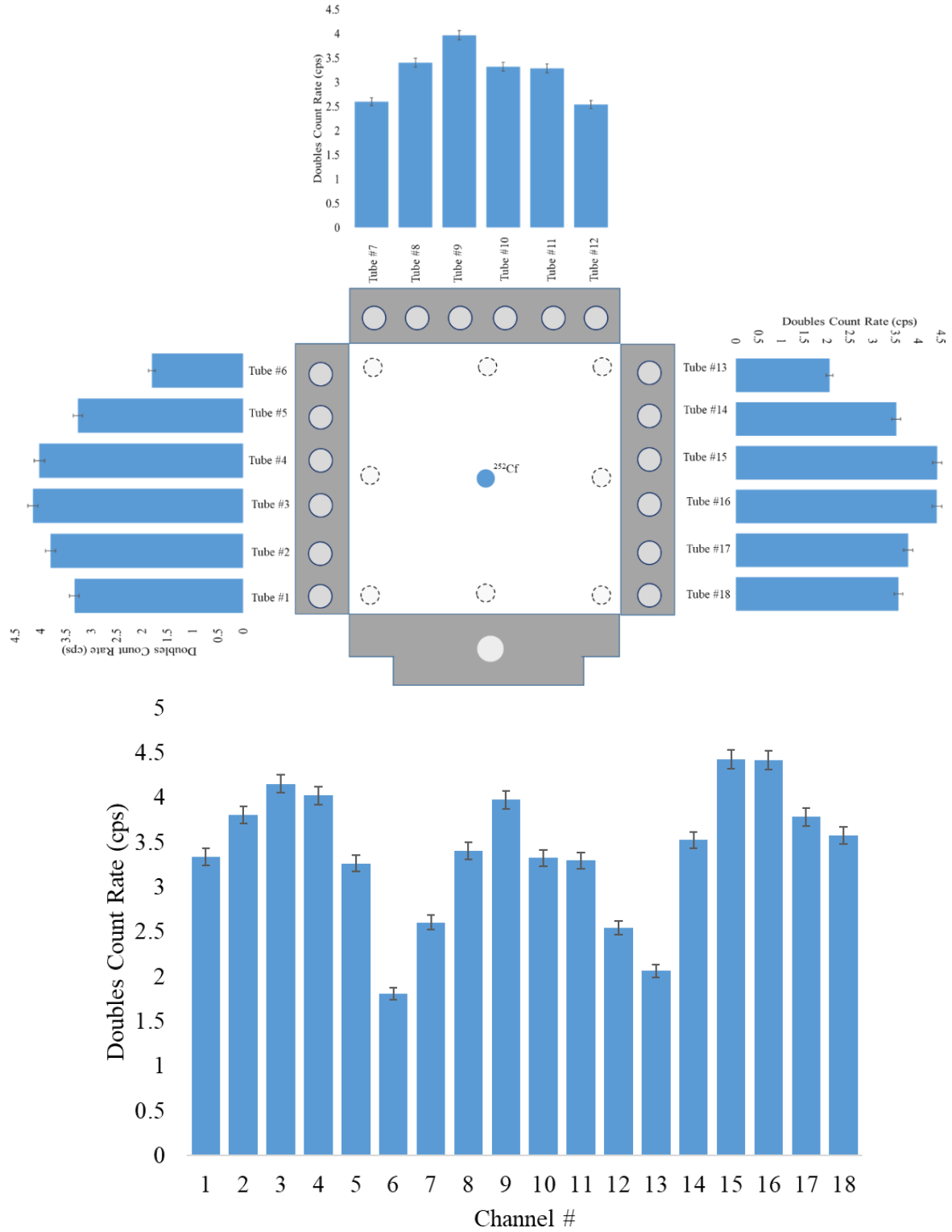


Figure 4.9. A measured doubles count rate response across all 18 ^3He tubes with a ^{252}Cf source placed in the center of the well of the modified JCC-71.

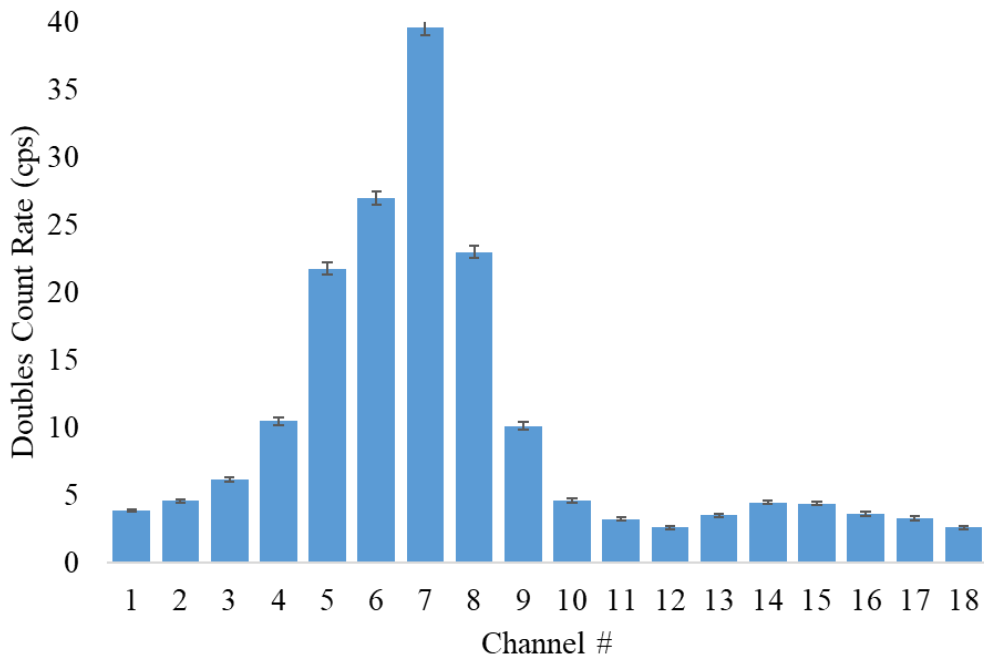
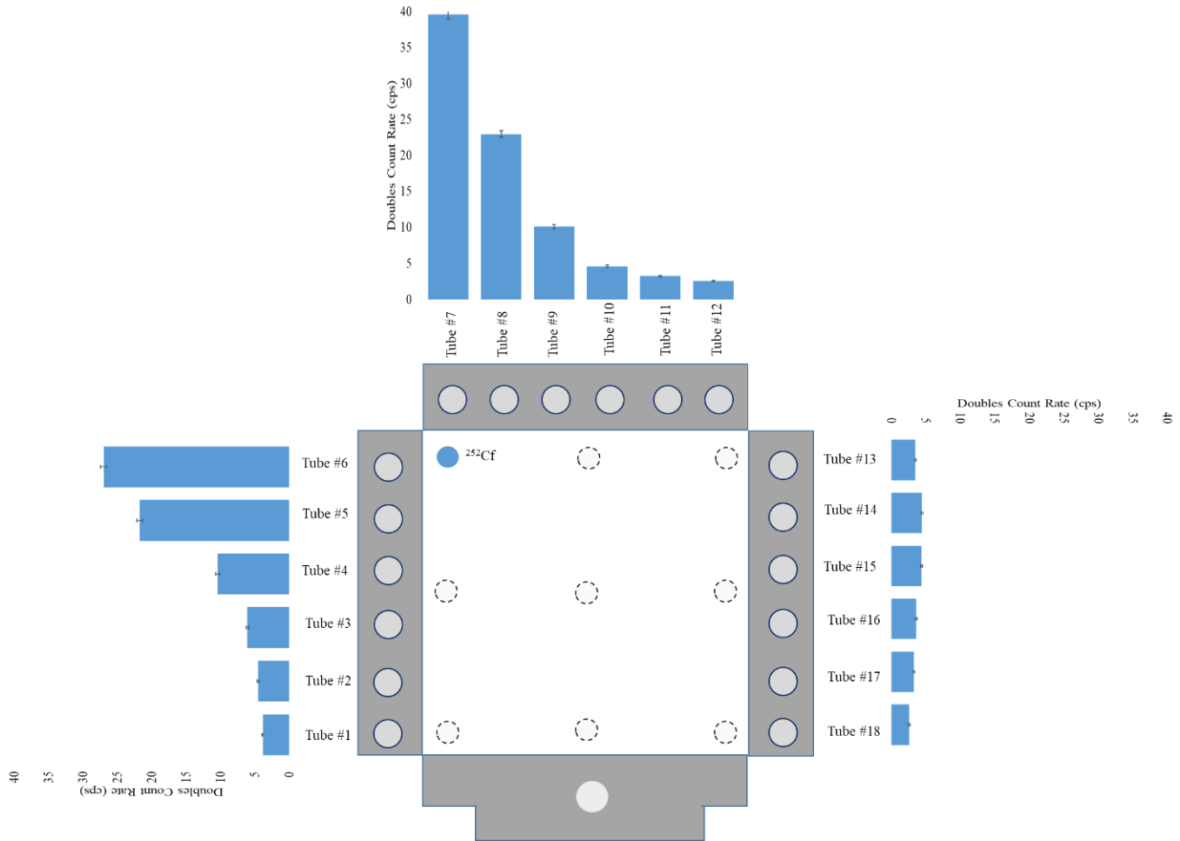


Figure 4.10. A measured doubles count rate response across all 18 ^3He tubes with a ^{252}Cf source placed near banks 1 and 2 (tubes 6 and 7) of the modified JCC-71.

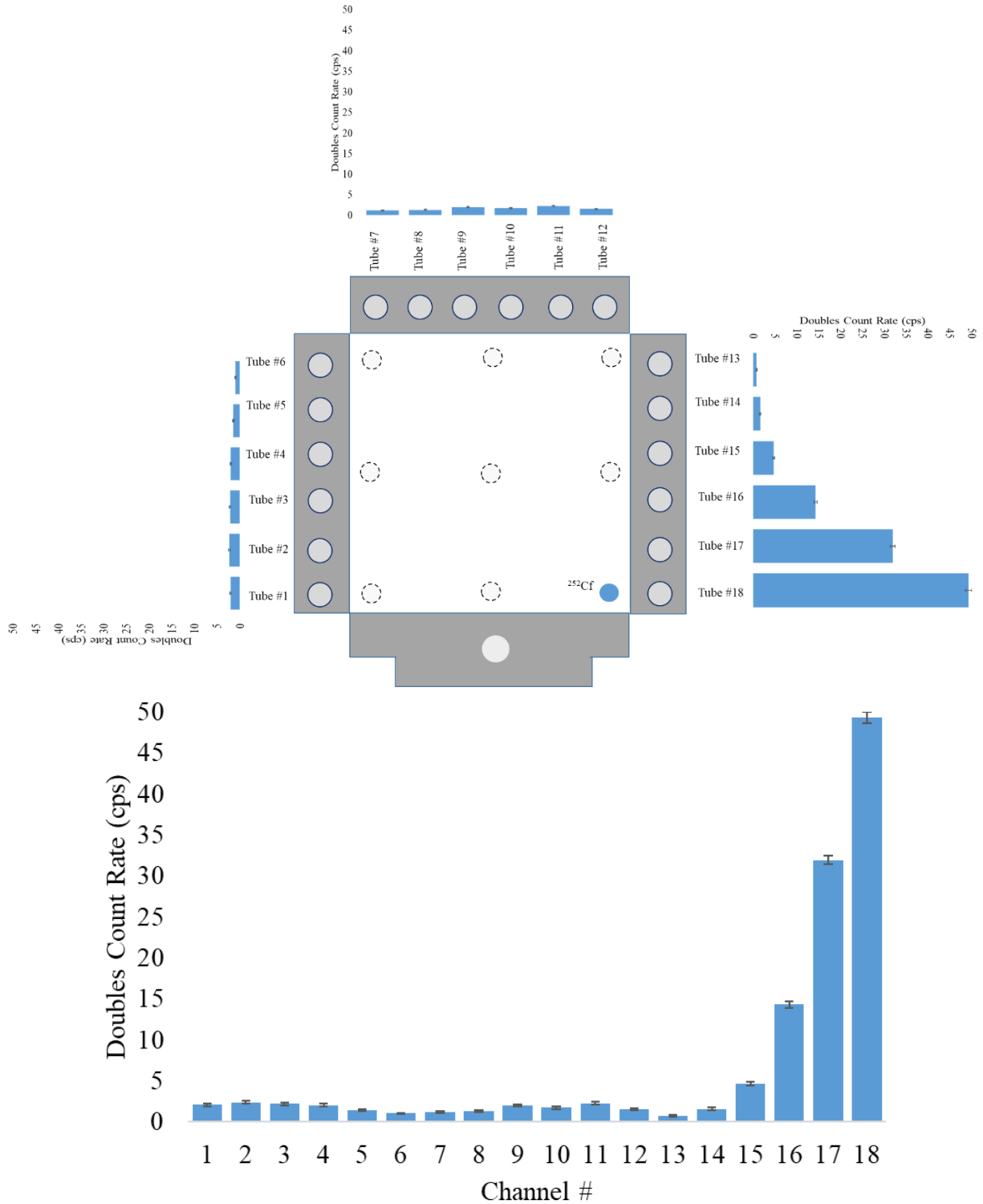


Figure 4.11. A measured doubles count rate response across all 18 ^3He tubes with a ^{252}Cf source placed near bank 3 (tube 18) and the active HDPE slab of the modified JCC-71.

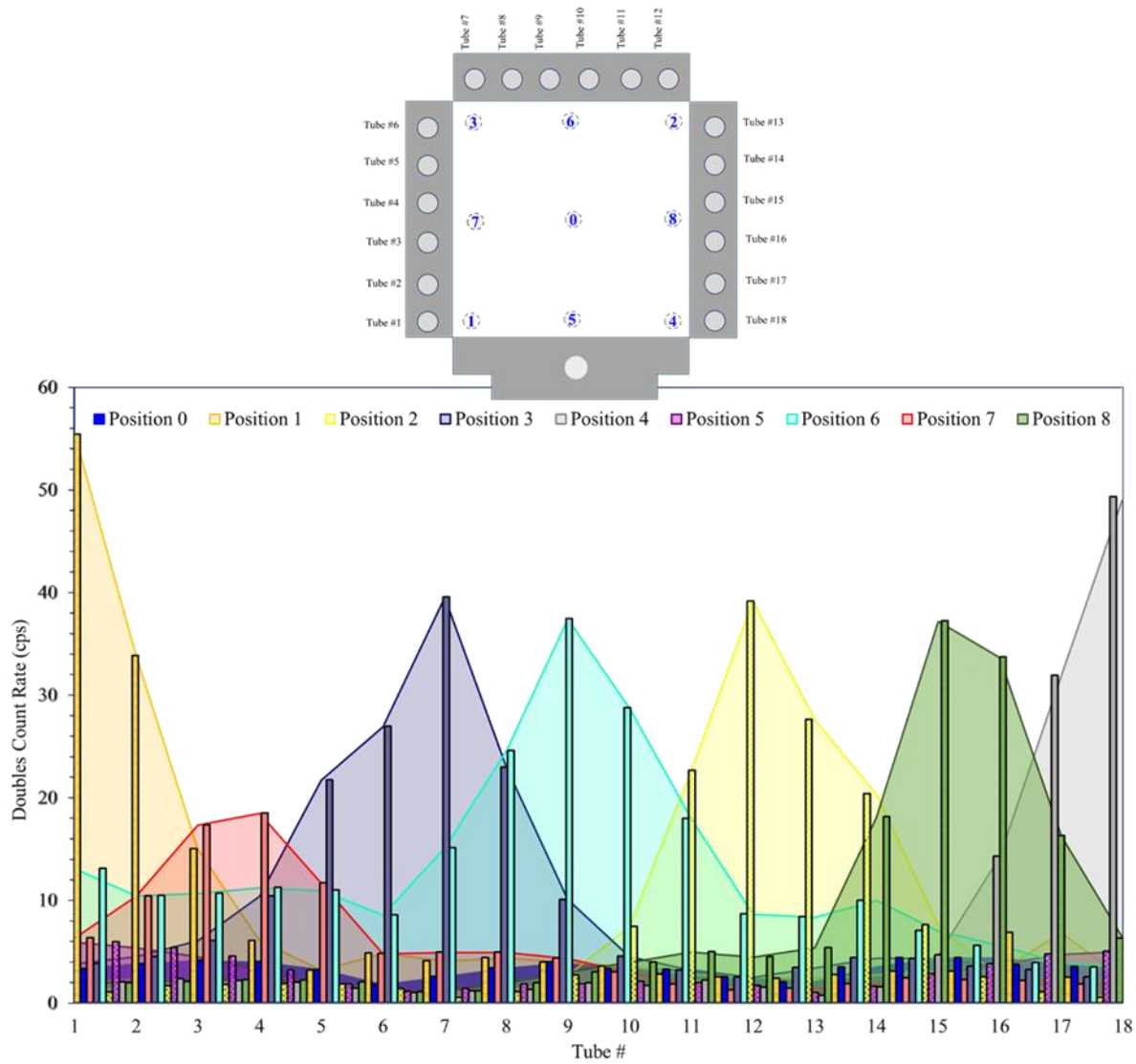


Figure 4.12. The measured doubles count rates in Tubes 1-18 for ^{252}Cf source positions 0-9 within the JCC-71 well.

Essentially, this comparative measurement highlights the greater capability of source positioning based on measured doubles count rates available with the 18 preamplifiers applied to the system. The combination of source strength and tube efficiency was sufficient to measure a varying count rate based on the different positions of the point source within the well.

Due to the complexities of handling these data for all combinations of the 18 tubes in each measurement within PTR-32, as was mentioned in Section 4.1, the logic coincidences are not studied here. This is beyond the scope of this work and would require extensive software development beyond what is available with the PTR-32 software. In order to complete a full tube-by-tube logic coincidence analysis, one would need access to the originally acquired neutron pulse trains taken with a LMDA interface, such as PTR-32 or another, which is not currently possible. Then, an external pulse processing software would need to be developed to not only analyze the individual neutron pulse trains for all 18 tubes but perform all combinations of the logic coincidences offline in a timely fashion that would be useful to in-field measurements. This would, at a minimum, need to support the analysis of all 18 tubes in pair combinations, leading to over 150 analyses in real time. If multiple channel logic coincidences were to be performed for better spatial resolution, this would complicate the analysis further.

4.3 MCNP Simulations

A fresh fuel assembly mockup was not available in the laboratory at ORNL to take experimental data representative of a field measurement. Instead, MCNP6 was used to develop a simulation that would generate the response of the 18 tubes to the measured ^{252}Cf source such that in a second phase of this project, this model could be used to simulate partial defect detection scenarios in various fresh fuel assemblies with greater confidence.

An original UNCL-I MCNP model in fast Pressurized Water Reactor mode, developed by Anthony Belian of NA-241 for the separate Neutron Rodeo Campaign, was modified to match the active configuration of the Canberra Industries JCC-71. The JCC-71 dimensions and geometry were modeled based on Canberra specifications and technical drawings, and the cadmium liners and AmLi source within the HDPE slab were removed. The output of the MCNP model was then analyzed in-depth and compared to the experimentally measured spatial response results presented in the previous section. The physics of the simulated counter was validated using the comparison, ensuring that this model can accurately represent the experimental behavior of the JCC-71, laying the foundation for future analysis work to meet the ultimate goals of the List Mode Response Matrix project.

A small ^{252}Cf source was simulated and moved to three of the positions measured in the previous section for comparison, as shown in **Figure 4.13- Figure 4.15**. A cumulative probability distribution was used to represent the spontaneous fission of the ^{252}Cf source, the spontaneous fission yield was directly specified, and the typical parameters of the Watt spectrum were entered into the source definition, as stated by the MCNP User's Manual [80]. Various tallies were recorded to study the count rate responses across these different source positions using the spontaneously fissioning source. Singles tallies, infinite gate tallies, ungated coincidence capture tallies, and coincidence capture tallies with various timing windows were produced through the MCNP simulation. The gated coincidence capture tallies, FT8, in each of the individual 18 ^3He tubes for a predelay of 4.5 μs and a gate width of 64 μs are specified. Using the CAP keyword with 2003 on the input, the ^3He is indicated as the location for the captures of interest. The GATE keyword applies the correct gate structure, following shift register logic. Variance reduction is not possible with multiplicity problems. MCNP does not place the starting trigger events onto a timeline, which LMDA does to form the neutron pulse train, so it does not need to deal with overlapping events and Accidentals; the output of MCNP is then a series of well isolated launch events. The capture tallies may be written to a PTRAC file, mimicking the pulse trains produced through LMDA, but external codes are necessary to process and analyze these pulse trains.

Histograms are then produced for each specified tally. The number of neutron captures, in terms of neutron multiplicities, are grouped together and the histograms are used to produce the moments of the

neutron distribution. All values are given for events recorded over all time, not as a rate; this must be done offline. For the end goal of the list mode response matrix, the neutron coincidence rate would be the signature of focus. Using the neutron creation source track number, the ^{252}Cf average neutron number per fission $\bar{\nu}$, the run time, the number of captures within the ^3He in all tubes without any timing windows, the first factorial moment recorded for an infinite gate width, and the first factorial moment recorded for the set predelay and gate width timing windows, the singles and doubles count rates can be calculated. To do this the total simulated count values must be converted to rates, and the simulated source strength must be normalized to the experimental source output rate in order to get comparable values to the measured data.

Performing this analysis for each of the 18 tubes results in similar trends across all three positions of the simulated singles data, and similar trends across the three positions of the simulated doubles data, compared to the measured data, but the values are not in agreement. The measured data is taken from the previous section, Positions 0, 3, and 4. The MCNP simulation underpredicts the Singles count rate that should be measured in these scenarios (**Figure 4.13 a**, **Figure 4.14 a**, **Figure 4.15 a**). The simulation overpredicts the Doubles count rate for the same positions (**Figure 4.13 b**, **Figure 4.14 b**, **Figure 4.15 b**). Many factors have been considered for their impact on these results; some of which include: MCNP's lack of electronic pulse processing losses and dead time contributions, background counts, geometric differences in the system and differences in the true source placement compared to what is simulated. None of these factors account for as large of a difference between the measured to simulated rates, and the fact that the measured singles count rates are larger than the simulation, but the measured doubles count rates are smaller than the simulation. After attempting to apply corrections for various factors, it became clear that the cause of the discrepancy was that the source information used throughout this analysis was not accurate. The true neutron output and the age of the source do not appear to match what is reported.

The original assay activity and current activity of the ^{252}Cf source used for these measurements are logged into a source control database. The current activity was recorded on the date of measurement and was used to normalize the simulated data to the source intensity used within the experiment. However, the difference in Singles rate indicates the activity of the measured source may be greater than what is given on its source certificate. It is not uncommon in a laboratory setting for a ^{252}Cf source to have an uncertainty of $\pm 15\%$ when its value is based off a nominal specification from the vendor; in a couple instances a measurement has shown that the neutron output of a source has an even larger variation than 15% of its quoted value. It is important to have source standards for these scenarios such that the true neutron output can be known to $\pm 1\%$, and better compared to simulated data. These standards are discussed in more detail in Chapter 7.

Because the simulated singles count rate is calculated by normalizing the factorial moment of the neutron capture in ^3He tally, independent of any timing gates, by the experimental source output value and the weight of the simulated source fission neutrons, a difference in the quoted source activity would have a large impact on these rates. Then, the doubles count rate in each tube is calculated using the gated neutron capture tallies, factorial moments, and the event rate. The event rate used in these calculations are based off of the average neutron number; changes to $\bar{\nu}$, the number of neutron tracks, or weight normalization by source fission neutrons has a significant impact on the simulated rate values. If the measured source is old, the ^{250}Cf contribution will be significant. The full implications of the presence of ^{250}Cf in a ^{252}Cf source is discussed in Chapter 7 but simply, it will alter the average neutron number per fission. The $\bar{\nu}$ for ^{250}Cf is 3.53 rather than 3.768 for ^{252}Cf ; this would therefore decrease the measured doubles rate. By simulating a pure ^{252}Cf , using its specific nuclear data, and then scaling that data using measured values obtained from a mixed source, there will undoubtedly be deviation in the comparison of those values.

It is possible to calculate the actual neutron output and the correct ^{250}Cf mass ratio of this source given the correct date of calibration and the associated output uncertainty. Then, the ^{250}Cf contribution, including the weight percent and its associated neutron spectrum, could be added into the simulation, but it is far better practice to repeat these measurements with a well-calibrated, young, certified source. This

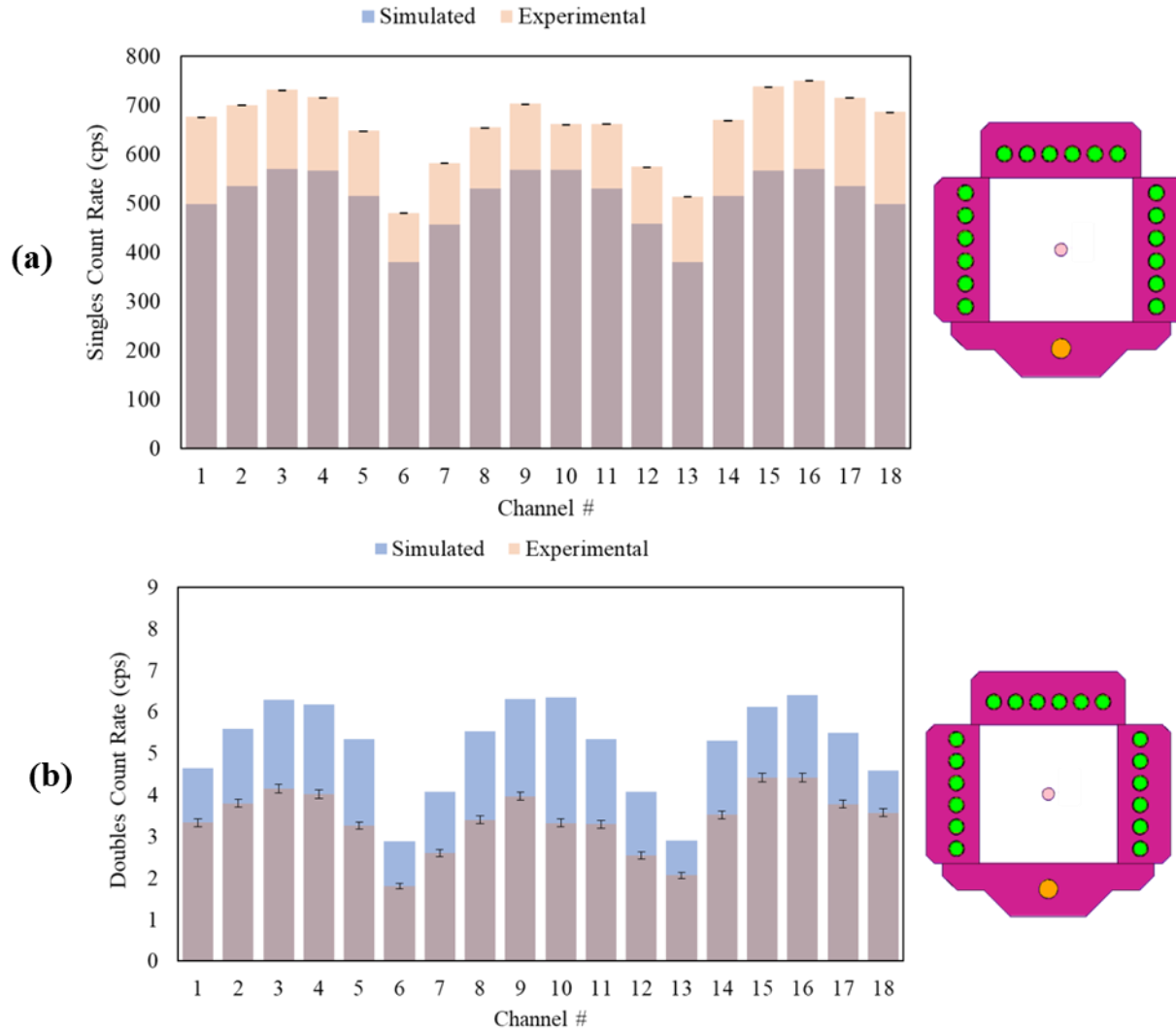


Figure 4.13. A comparison of MCNP simulated data and (a) measured singles count rate data and (b) measured doubles count rate data using a ^{252}Cf source placed at the center Position 0 of the modified JCC-71. The MCNP output data has been normalized to the experimental source strength.

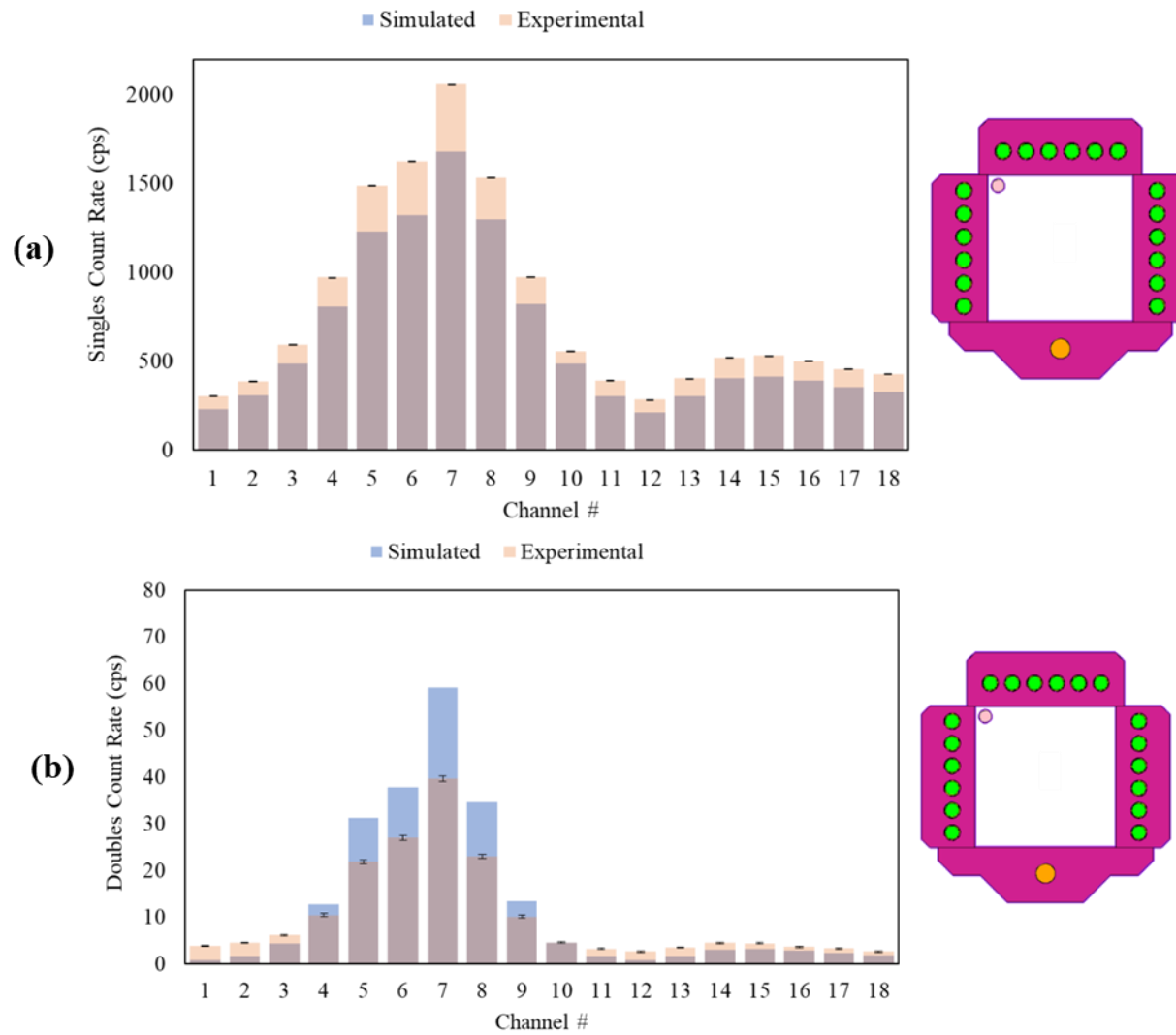


Figure 4.14. A comparison of MCNP simulated data and (a) measured singles count rate data and (b) measured doubles count rate data using a ^{252}Cf source placed at the top left Position 3 of the modified JCC-71. The MCNP output data has been normalized to the experimental source strength.

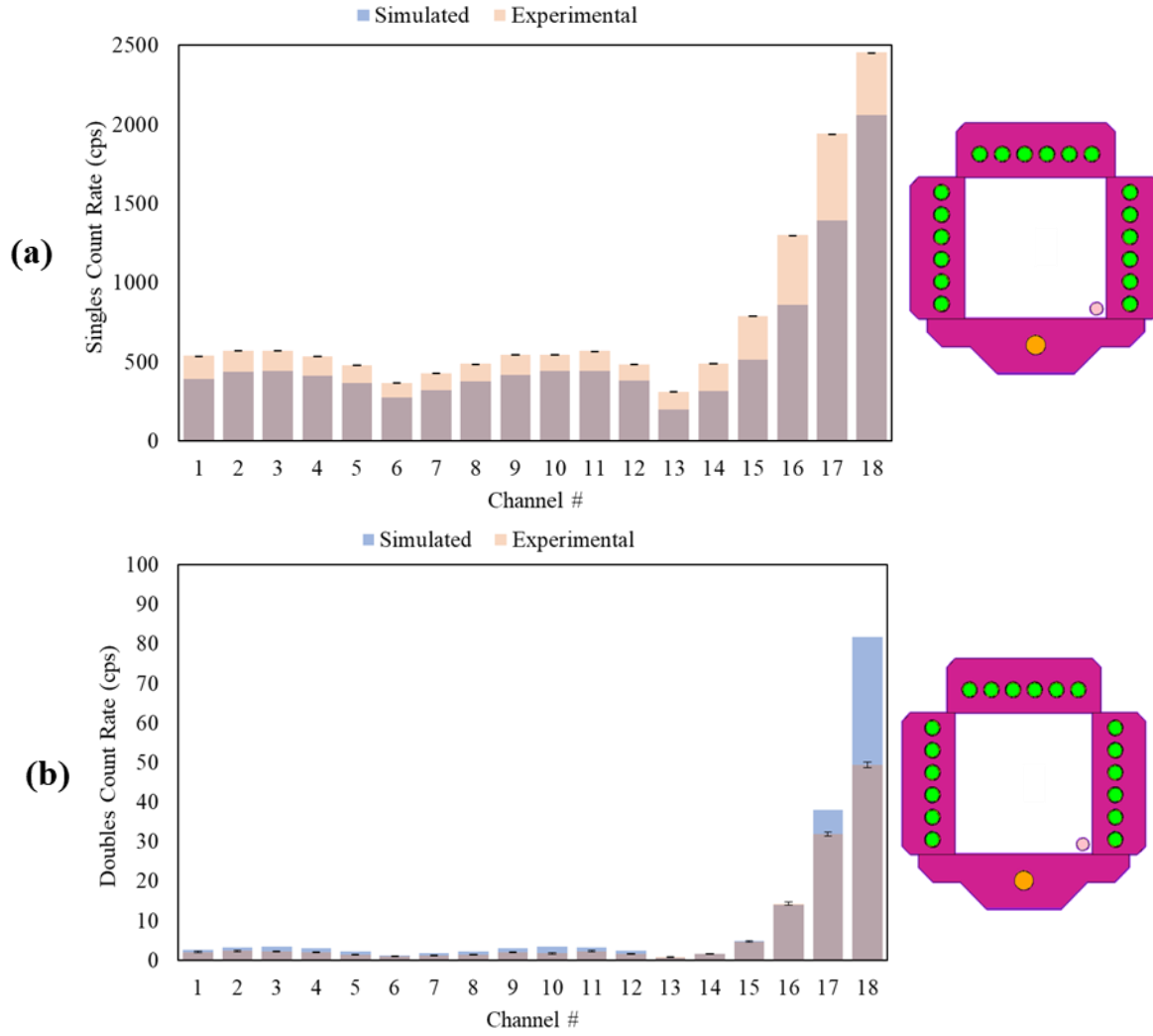


Figure 4.15. A comparison of MCNP simulated data and (a) measured singles count rate data and (b) measured doubles count rate data using a ^{252}Cf source placed at the bottom right Position 4 of the modified JCC-71. The MCNP output data has been normalized to the experimental source strength.

can be done using any of the certified sources presented in Chapter 7. The benchmarking simulation used for the List Mode Response Matrix needs to have better precision than what this current source certificate value can provide to allow credible count rate estimations for various source placement scenarios.

Despite the differences in value caused by the source output uncertainty, the trends of the simulated data coincide with the measured trends as a function of source position in the Collar. Examining **Figure 4.13** where the ^{252}Cf source is placed within the center of the well, tubes more centralized within the HDPE record higher count rates. Tubes closer to corners of the HDPE record lower count rates. When the source is then placed in the top left corner as shown in **Figure 4.14**, the range of rates is more drastic across the 18 tubes. A higher count rate is recorded in tubes surrounding the source's position, and the response can be distinguished from that recorded when the source is moved to the opposing corner in **Figure 4.15**. These trends validate that the model used here is reasonable and that it can accurately predict the neutron capture behavior across the 18 ^3He tubes. This is the crucial aspect of the spatial response matrix project goal, as ideally there would be reference matrices obtained through simulation, to which an experimentally acquired matrix would then be compared to that library of scenarios. Any deviations along an otherwise matched trend could indicate diversion. The sensitivity of the system response will need to be studied for detectable minimums. Therefore, using MCNP may allow the user to anticipate the spatial response in the modified JCC-71, and any deviation from this behavior would prompt further investigation for the true numerical values of count rate and source activity compared to declared values.

To eliminate the concern regarding the difference in quoted source strength and age, the simulated results for the top left and bottom right positions were normalized to the results obtained at the center position (**Figure 4.16** and **Figure 4.17**). This provides the spatial response in terms of a relative efficiency, which avoids the uncertainty in the original source strength. With this normalization, it is clear that the measured and simulated trends are nearly identical with the singles count rates in both source positions, within <1 cps difference (**Figure 4.16 a** and **Figure 4.17 a**). As for the doubles count rate comparison between measurement and simulation, the difference is slightly greater <2 cps difference (**Figure 4.16 b** and **Figure 4.17 b**), that could stem primarily from the positional difference between the true physical placement and the source location in the simulation.

There are numerous sources of uncertainty that could contribute to these slight differences as well. MCNP assumes perfect electronics. There is no dead time component nor any electronic artifacts incorporated in the simulation analysis. The doubles dead time is known to be characteristically longer than the singles count rate (see Chapter 6). Therefore, the measured singles count rate is not as greatly impacted as the doubles count rate by dead time, and the difference attributed to the presence of dead time in the measured rates compared to the simulated rates should be less for the singles response.

The code also assumes that every neutron capture event generates an electronic logic pulse that could be read by an associated software; i.e., the tubes are 100% efficient. However, there are slightly different thresholds set on the preamplifiers, within human tolerances, which change the trigger point at which a neutron event can generate a logic pulse and be recorded from tube to tube experimentally. Therefore, the simulated response will always differ slightly from true experimental values.

The MCNP simulation is given a fill pressure and atomic composition of the ^3He material within each tube. This is traditionally quoted by the manufacturer; as are the tube dimensions and any other dimensions provided in the technical drawings of the counter. It is not well known how accurate these values are in reality, as machining tolerances and slight uncertainties from tube to tube will cause slight deviations in experimental performance. Changes in the HDPE slabs would have an effect on the neutron thermalization within each bank. The fill pressure uncertainty would not be a large contribution to the overall measured count rate, but it should be considered. The dead layers, or the ends of the ^3He tubes where no captures will be recorded, are included in the MCNP model but may have varying impacts on the active volume tube to tube depending on its accuracy.

Depending on the physical placement of not only the source capsule relative to the banks in height and XY positions, but the ^{252}Cf active material within the source capsule, the loading on the tubes may vary slightly compared to its placement in the simulation. Within the source definition in MCNP the

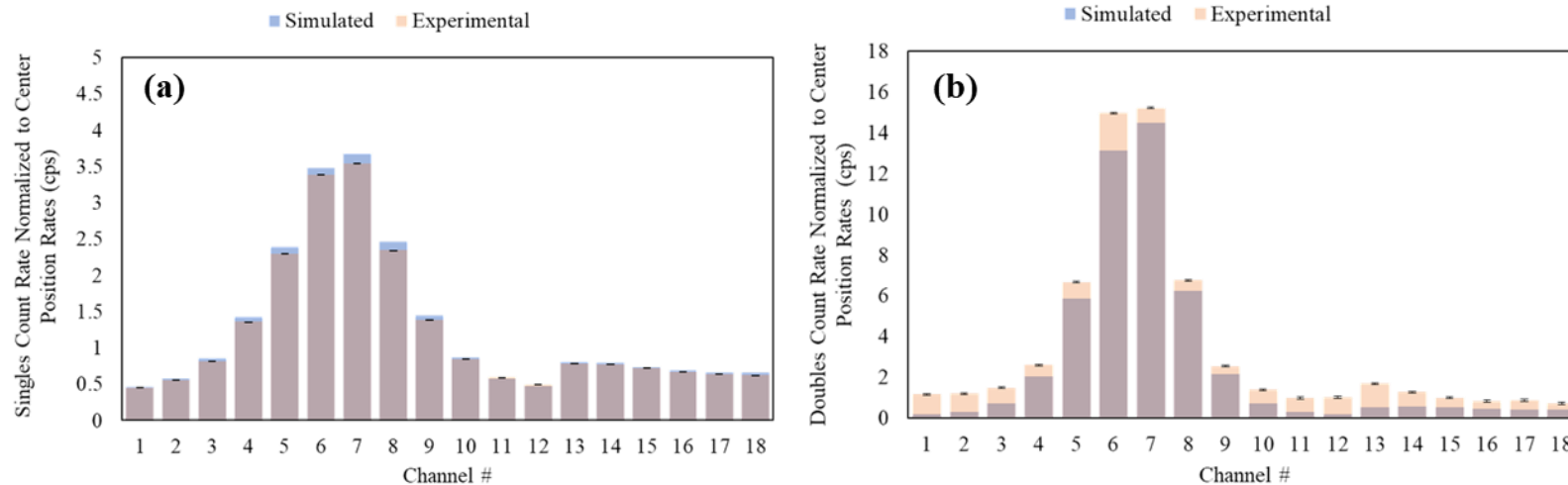


Figure 4.16. A comparison of MCNP simulated data and (a) measured singles count rate data and (b) measured doubles count rate data using a ^{252}Cf source at Position 3. The data has been normalized to the singles count rate measured and simulated for the central position 0 response.

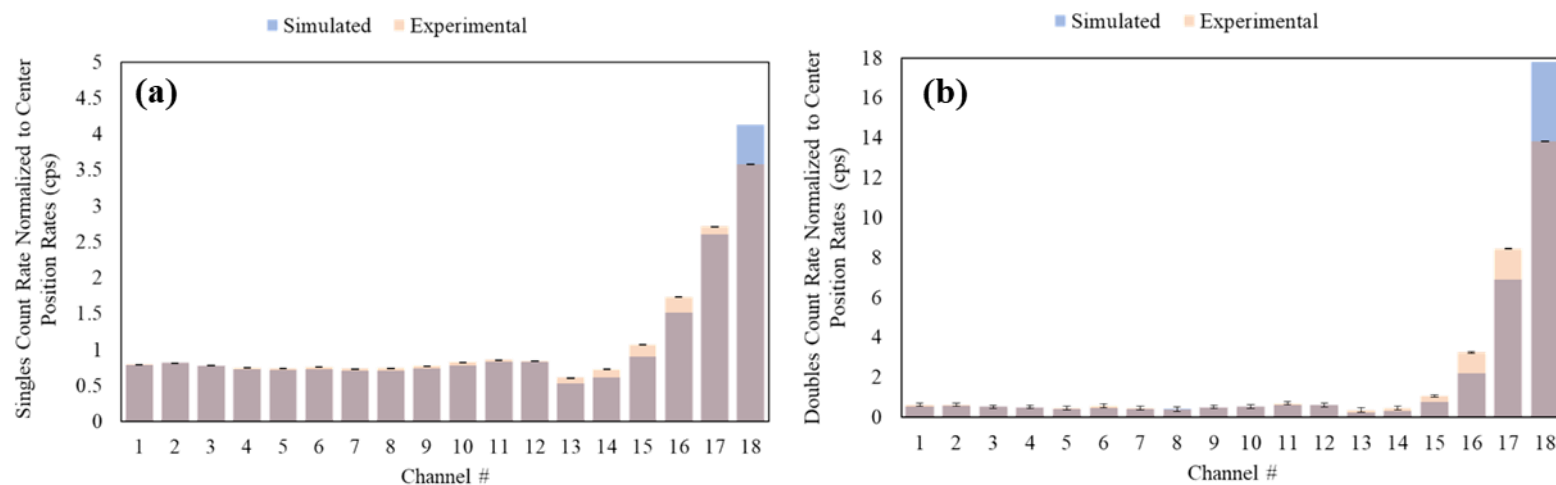


Figure 4.17. A comparison of MCNP simulated data and (a) measured singles count rate data and (b) measured doubles count rate data using a ^{252}Cf source at Position 4. The data has been normalized to the singles count rate measured and simulated for the central position 0 response.

^{252}Cf was roughly estimated as a point source and placed at set distances from the center. Uncertainty in the physical placement of the source could cause slight deviations in the measured count rates across the different tubes. Room return and scattering are not included in the MCNP model. Since these measurements were taken on a benchtop within several feet of a wall, the tubes do experience some events caused by this return, which is not accounted for in the simulated response. The model could be refined to accommodate a more accurate scatter environment such as incorporating the tabletop on which the Collar was placed for these measurements, including the neutron source stand that was used to suspend the ^{252}Cf in its various positions, and the nearby cement walls of the room. In reality, the environment of every fuel fabrication plant or laboratory environment will differ, so there will always be an associated uncertainty from simulation. Many of these contributions to uncertainty are studied in depth for their final impact on the MCNP simulation results in [81] Unfortunately, introducing a fresh fuel assembly in place of a ^{252}Cf point source only adds complexity to the problem as knowing the exact geometry and machine tolerances, exact source activity and location, full material compositions and introducing the AmLi interrogation source within the model adds more uncertainty in the rates.

To solidify confidence in the MCNP model, further investigation was performed using the simulation values compared to experimental values. Using the PTR-32 LMDA and MCNP output, the physical behavior of the simulated system was compared to that what was measured at the three simulated source positions. The die-away time of the measured and simulated systems were calculated for each of the three source positions using chi-squared analysis of minimizing the sum of squared errors of the doubles count rate across a range of gate width settings (**Figure 4.18 a**). This follows the analysis presented in Section 2.5.3. The die-away times at each position were in general agreement between the simulation and measurement (**Error! Reference source not found.**). In addition, the relative standard deviation (rsd) was analyzed for both the simulated and measured doubles count rates to identify the optimal operational gate width as presented in Section 2.5.2. The data showed the minimum relative standard error was achieved at the traditional operational gate width of 64 μs for both data sets (**Figure 4.18 b**), across all three source positions. Again here, the rates, such as R_0 and the rsd values, are not in agreement, due to the source certificate discrepancy, but the trends verify that the physical system behavior is well represented through the MCNP input. The behavior of the simulated counter was validated using the comparison of representative physics trends, ensuring that this model is performing as it should, and it can accurately represent the experimental behavior of the JCC-71. Therefore, there is confidence in expanding this model for future analyses.

Table 4.1. A comparison of experimental to simulated calculated system die-away times and fit parameter R_0

^{252}Cf Source Position	Experimental (LMDA)		Simulation (MCNP)	
	R_0 (cps)	τ (μs)	R_0 (cps)	τ (μs)
Center	1680.23	62.38	2189.16	60.69
Top Left	2850*	50*	4731.78	58.72
Bottom Right	2124.39	65.20	2487.00	66.40

*The chi-squared fit parameters were estimated by eye

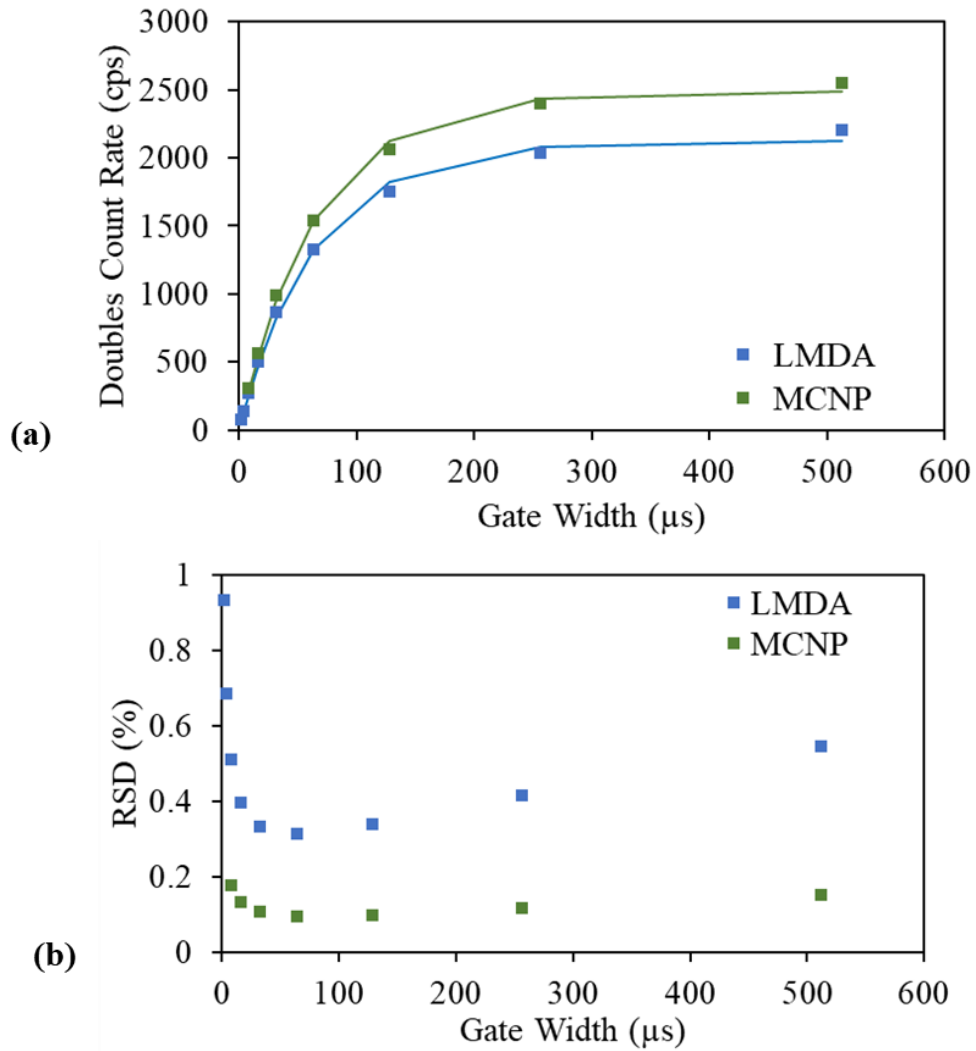


Figure 4.18. The comparison between LMDA measured data and MCNP simulated data used to determine the (a) neutron die-away time using the doubles count rate trends as a function of gate width and the (b) optimal operational gate width using the relative standard deviation as a function of gate width for the center source position. These values were verified for the other two source positions.

4.4 Conclusions and Further Work

This work has successfully addressed the objectives of the experimental testing and validation aspect of the List Mode Response Matrix project. The novel developments and necessary groundwork to complete the end goals of this project have been established here through this first phase of the larger picture of the LMDA spatial response matrix. This project has demonstrated that a historic system may be retrofitted with modern electronics on each of its original ^3He tubes. As a contribution to the overall project goal, this dissertation research has helped optimize those electronic settings over a couple prototype iterations through performance matching with associated software. It has also proven that the new electronics have equivalent performance to the existing electronics. Through extensive experimental testing, it has been shown that these electronics can then be used to provide detailed spatial response measurements for a neutron source.

An MCNP simulation has been developed and evaluated for its performance relative to the physical system when measuring a ^{252}Cf source. Despite uncertainties surrounding the measured source activity, which propagates through to deviations in the measured to simulated data comparisons, this model has demonstrated it is representative of the physics trends present in the JCC-71. A certified source should be measured and compared to simulated values to determine the final error associated with the calculations. The MCNP model can then be used in future work to simulate various fresh fuel assemblies and various diversion scenarios to test and optimize the algorithms for detection. In **Figure 4.19**, a general 17x17 pressurized water reactor fresh fuel assembly was designed within the well as an example of what could be done for future work. In this figure, the 17x17 array has several fuel pins removed, shown in white, centered in a circular arrangement. Within this MCNP model of the JCC-71, the cadmium sheets are included and the active AmLi interrogation source is also include with the correct geometries.

From the work I performed for this project, LMDA has been introduced and characterized as a fully suitable alternative to shift register based logic, and its additional capabilities in system calibrations and characterizations have been exploited and discussed in detail. Simultaneous multichannel acquisition and analysis will help further advancement in the field, while expanding the physics-based understanding of the behavior of these systems. Through this knowledge, better calibration and analysis procedures, grounded in first principles rather than empirical methods, may be introduced.

This work has also established a significant area for further development and improvement. Through the course of the project several challenges were identified, and a few limitations were encountered. These challenges include: the performance and reliability of the LMDA module PTR-32 (discussed intermittently throughout this dissertation), non-ideal behavior in the standard JAB-01 boards within the JCC-71 (as discussed in the following chapter), physical limitations of efficiency in the individual ^3He tubes that will impact minimal detectable rates, and overcoming the significant computational demand for multichannel analysis combined with logic coincidences performed in real time, overlaid with a easily referenced simulated spatial response matrix.

Then, introducing fresh fuel assemblies into the problem further complicates this analysis. With an average enrichment of around 3-5%, the activity of these fresh fuel assemblies are significantly less than that of the ^{252}Cf point source. Using a 42 μCi ^{252}Cf source at the center of the JCC-71 well, the average doubles count rate measured in all tubes was approximately 3 counts per second. Detecting small changes in the associated doubles count rate caused by the removal of few fuel pins at a time will be a significant challenge. Currently, with traditional methods, the standard deviation on an UNCL measurement falls around 5%; this is a significant number of fuel pins removed. The LMDA spatial response matrix project aims to identify the removal of 8 pins and, specifically, the location of their removal within the fuel assembly.

The logic coincidences would increase the effective efficiency of these tubes by combining the neutron pulse trains of the designated tubes to calculate the doubles count rate. This requires large computational power in real time in order to provide, at a minimum, over 150 different tube pair combinations from the system. Once this is overcome, it may be possible, then, that the measured count

rate would suffice for fuel pin diversion detection, yet at this point it is not possible to give quantitative conclusions.

The activity is also distributed throughout a highly complex fuel pin matrix that contains metal fuel rods, burnable poisons and neutron absorbers. These assemblies suffer from self-shielding, scatter, and a high singles count rate generated by the interrogation source that raises the percentage of false coincidence events. In terms of creating reliable MCNP inputs, not only are there complexities in simulating the base geometries of these arrays, but there is also the added contribution of the active interrogation source within the assembly. This is an extremely complicated problem to simulate. Each fresh fuel scenario must have a reliable reference simulation to benchmark the experimental results on to identify diversion scenarios. Future work for this project includes further development of the classification algorithms based on machine learning, and laboratory measurements of a mockup fresh fuel assembly that would be more representative of a field measurement.

This work has also introduced concepts that may be applied across all neutron coincidence counting systems to advance the field and improve the performance of historic systems without a large financial burden. With minimal overhead cost, preexisting systems may easily be retrofit with modern electronics, which not only updates these systems, but also expands the information generated by them. More detailed source profiles may be obtained on complex samples in the field by using preamplifiers on each of the ^3He tubes within any system, without changes to these system footprints or manufacturing processes.

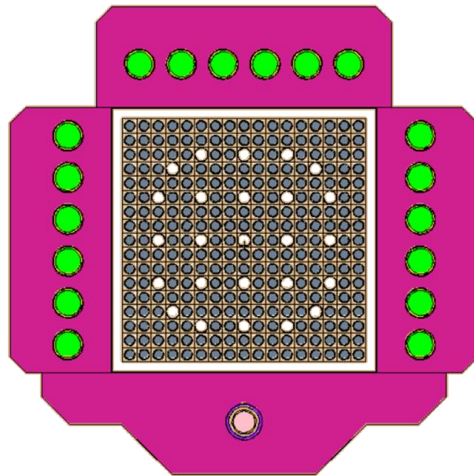


Figure 4.19. A MCNP model of the JCC-71 in active mode with Cd liners, the AmLi interrogation source, and a standard 17x17 pressurized water reactor fresh fuel assembly.

Chapter 5

Double Pulsing in the Amptek A111 Charge Sensitive Preamplifier & Discriminator Board–³He Proportional Counter Combination Used in Common Safeguards Neutron Coincidence Counters

5.1 Investigating the Non-Ideal Behavior Using LMDA⁵

5.1.1 Abstract

Neutron coincidence counting is a well-established technique used for the nondestructive quantification of special nuclear material during international safeguards inspections. The neutron counters are commonly designed with an annular body, centered about an inner well or cavity into which a measurement item is placed, and the moderating annulus is populated with ³He tubes connected to a varying number of preamplifiers. The Canberra Industries JAB-01 preamplifier/amplifier/discriminator board is employed within the company’s neutron coincidence counters, built for use by the International Atomic Energy Agency. Non-ideal behavior of these boards was identified during a detector characterization, using list mode data acquisition, of a Canberra Industries JCC-71 Neutron Coincidence Collar implementing four JAB-01 boards. List mode data acquisition and analysis reveals features that have commonly been overlooked by historic timing gate selection while using shift register data acquisition methods, which are routinely adopted in international safeguards. It has been shown that double pulsing effects are not fully captured within the predelay setting; therefore, they may influence the response of the system within the standard operating regime. We set out to identify and correct for double pulsing in our post analysis of neutron pulse trains, while isolating this behavior to the relevant system. To understand and potentially address these concerns, the responses of two different JAB-01 board systems—the JCC-71 Neutron Coincidence Collar and a modified JCC-51 Active Well Neutron Coincidence Counter—are compared with the responses of an AnTech Inc. N2071 Neutron Coincidence Collar that also uses an amplifier built on the Amptek A111 Charge Sensitive Preamplifier & Discriminator chip, and a JCC-71 that employs custom preamplifiers designed at Oak Ridge National Laboratory.

5.1.2 Introduction

Neutron coincidence counting is a well-established safeguards technique used for nondestructive analysis of fissioning samples of special nuclear material. It can exploit either passive or active

⁵ This section was originally published in a peer reviewed journal under the original title “Investigating the Non-Ideal Behavior of the Amptek A111 Charge Sensitive Preamplifier & Discriminator Board–³He Proportional Counter Combination Used in Common Safeguards Neutron Coincidence Counters,” A.T. Simone, S. Croft, C.L. Britton, R.D. McElroy, M.N. Ericson, and J.P. Hayward, Nuclear Instruments and Methods in Physics Research Section A: Accelerators, Spectrometers, Detectors and Associated Equipment, 2019. It is printed here with permission from the editors in its original form.

interrogation techniques to assay a range of Pu, U, and mixed oxide samples [4]. Commonly, arrays of ^3He gas proportional counters are placed within an annular system body, centered about an inner well or cavity to accommodate these samples. The induced current generated from the charge drift resulting from the $^3\text{He}(n,p)\text{T}$ capture reaction is collected over a period of time on the central anode wire of the ^3He proportional counter. This current is integrated and passed through the pulse processing chain containing preamplifiers and amplifiers to modify the signal into a useable shape and pulse height, so that the voltage signal may cross a threshold in the discriminator circuit and generate a logic pulse. The compatibility of the pulse processing chain with the operational application of the neutron coincidence counter is adjusted by the detector system manufacturers to optimize the triggering and filtering thresholds.

AnTech Inc. and Canberra Industries are the two main commercial suppliers of neutron coincidence counters to the International Atomic Energy Agency (IAEA). Both companies implement the Amptek A111 Charge Sensitive Preamplifier & Discriminator chip [31] in their system electronics. The A111 functions as a hybrid charge-sensitive preamplifier, discriminator, and pulse shaper. Therefore, the counters from both suppliers behave similarly, within design variations from their respective filtering networks. The A111 chip was developed in the mid-20th century for high-rate applications implementing short shaping times, ~ 200 ns, while adhering to specific design parameters for the original x-ray measurement application. It has since been adopted for use in the safeguards field among many other fields such as aerospace and portable instrumentation, mass spectrometers, particle detection, imaging, laboratory and research experiments, medical electronics and electro-optical systems. The AnTech electronics board, used on many of the company's neutron coincidence systems, is based on the Amptek A111 chip. The Canberra JAB-01 preamplifier/amplifier/discriminator board implements the Amptek A111 chip with a 74221 dual monostable multivibrator integrated circuit and a 74SI40 dual 4-input, Positive-NAND, 50-ohm line driver integrated circuit [30]. The Canberra JAB-01 board is employed within many of their own counters, including the JCC-51 Active Well Neutron Coincidence Counter (AWCC) model [33] and the JCC-71 Neutron Coincidence Collar (UNCL) model [30]. Both systems have been characterized at Oak Ridge National Laboratory (ORNL), and both have previously shown indications of non-ideal behavior, in particular double pulsing artifacts.

Triggering on, and successively processing, the individual proton and triton charge response peaks from a single neutron event as two separate neutron events, due to shaping time mismatch in the ^3He tube and associated electronics pulse processing chain, is known as double pulsing. It is an unwanted artifact of the electronics design and operation of these neutron detectors. Although it is a well-known problem to assay system designers, it is not widely acknowledged in the user community, as its effects have not been historically significant in standard operational regimes. Double pulsing increases the apparent number of measured neutron events from a source, but its origins lie within the electronics of the system. Therefore, it may contribute to a falsely increased count rate if present at the operational high voltage used when assaying samples, and it is therefore necessary to identify and characterize before accurate measurements can be taken—especially considering the future goals to perform absolute source measurements with these systems. If double pulsing is a fixed fraction of events, it may be incorporated into an empirical calibration. Setting a conservative predelay may also minimize the influence of this effect on a safeguards measurement by rejecting a majority of these pulses at shorter times, but the entirety of this effect cannot be captured as additional coincidences will be formed between the electronic feature and other true successive neutron events throughout the set gate width; the fraction of which is dependent on many factors, which will be discussed in this paper. However, this behavior will complicate system intercomparisons and comparisons to theory; and it is at odds with assumptions made in data interpretation, such as in rate loss corrections and coincidence counting used for absolute counting methods. Note that double pulsing is distinct from other problems—such as HV breakdown, electrical noise, and ringing from impedance mismatch—which can be eliminated by detector system design. Modifications to the time components of the electronic pulse processing chain must be made to resolve double pulsing effects on a measured neutron pulse train.

Therefore, to attribute this double pulsing behavior to either a counter system, the JAB-01 boards, or the Amptek A111 chip, four different systems were tested using a Hungarian Institute of Isotopes Pulse

Train Recorder (PTR-32) list mode data acquisition module [37]. The investigation began by obtaining a response from the UNCL, and then a response from the AWCC. The double pulsing behavior demonstrated by the UNCL and the AWCC ruled out that this is a model-specific behavior. Then, the response of an AnTech N2071 Neutron Coincidence Collar [32], using the A111 chip, illustrated that this behavior was A111-specific, not JAB-01-specific. Finally, the responses of the three previously listed systems were compared with the response of preamplifier prototypes, designed and built at ORNL, placed within the junction box of a single bank of the original JCC-71, which exhibited no signs of double pulsing within the operational regime. This paper outlines the comparison measurements among these systems, discusses double pulsing behavior, and attempts to apply a correction to the neutron pulse train data in post-analysis for these commonly used neutron coincidence counters.

5.1.3 Neutron Coincidence Counting Systems

Summary information for the Canberra Industries JCC-71 UNCL; the JCC-51 AWCC with its modified variant, the Large Volume AWCC (LV AWCC); and the AnTech N2071 UNCL is provided in Sections 2.1, 2.2, and 2.3, respectively.

Canberra Industries JCC-71 Neutron Coincidence Collar

The UNCL is designed to operate in two modes: active and passive. The active mode is used to measure the ^{235}U content per unit length in fresh fuel. The passive mode is used to measure ^{240}Pu in MOX. The system was designed to accommodate assemblies used in pressurized water reactors, boiling water reactors, or Canada Deuterium Uranium reactors. The rectangular detector body (**Figure 5.1 a**) consists of four individual banks, each containing six ^3He cylindrical proportional counters (“tubes”), with an active length of 33 cm [30], embedded in a single row within high-density polyethylene (HDPE) moderating slabs. The tubes and HDPE assembly are connected to a junction box panel containing a single JAB-01 preamplifier/amplifier/discriminator board per bank, which reduces the count rate burden and related pulse pileup on a single bank. The junction box transfers high voltage (HV) between the connected banks through “HV in” and “HV out” connections. The junction box also contains “Signal in” and “+5 V in” input connections and “Signal out” and “+5V out” output connections to interconnect the banks and communicate with an external data acquisition system.

The ^3He tubes are the GE Reuter Stokes model RS P4-0813-101, pressurized at 4 atmospheres (atm) with argon methane quench gas added, each having a 2.54 cm diameter. The six ^3He tubes per bank are processed by a single JAB-01, and the signal outputs from each of the four JAB-01 boards are ORed by the 74SI40 dual 4-input, 50-ohm line driver to provide a single total signal output when the UNCL is used in the field. The tubes are matched to operate at the same HV, and the threshold of the A111 preamplifier discriminator is set to match the gain and minimize the gamma-ray response before shipment of the systems. The 74221 dual one shot adjusts the digital output from the A111 discriminator to 52 ns, and requires no adjustment in the field.

Variant on the Canberra Industries JCC-51 Active Well Neutron Coincidence Counter

The AWCC is designed to operate in active mode, implementing an AmLi source within the HDPE end plugs, to interrogate and assay samples containing ^{235}U or ^{233}U . It can accommodate a large range of samples, such as bulk UO_2 samples, high-enrichment uranium metals, UAl alloy scraps, light water reactor fuel pellets, and ^{238}UTh fuel materials [33] within its well. The system can be operated in active fast, active thermal, and passive thermal configurations by adding or removing the AmLi or Cd inserts.

A LV AWCC (**Figure 5.1 b**) with 48 ^3He tubes, pressurized at 4.5 atm and arranged in two concentric rings surrounding a 27.9 cm diameter by 38.1 cm tall assay measurement cavity, was used for

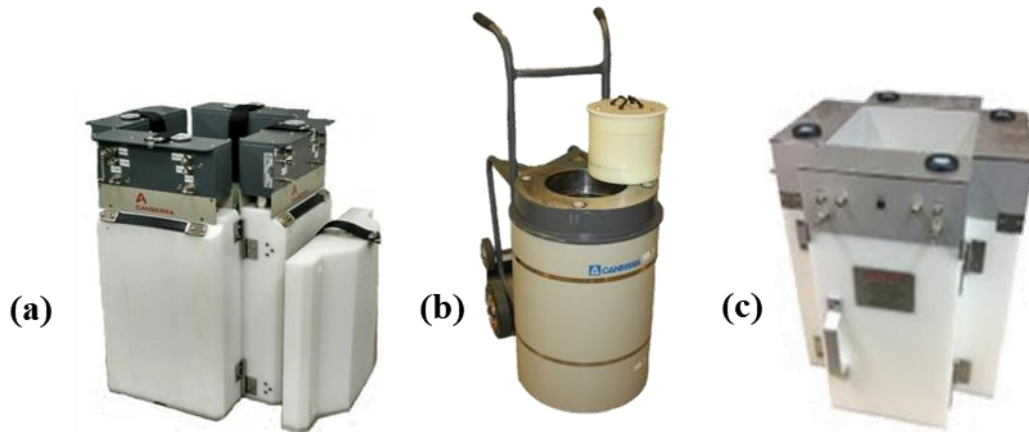


Figure 5.1. (a) Canberra Industries JCC-71 Neutron Coincidence Collar. (b) Variant on the Canberra Industries JCC-51 Active Well Neutron Coincidence Counter, the large-volume Active Well Coincidence Counter. (c) AnTech N2071 Neutron Coincidence Collar.

the measurements at ORNL. The tubes are GE Reuter Stokes model RS P4-0825-103, with an active length of 63.5 cm, and a quench gas composition of argon and methane [82]. The 48 tubes are organized into eight groups, with each group connected to a JAB-01 board. Transistor-transistor logic (TTL) logic pulses of 52 ns width are electronically summed and fed as a single pulse train for data acquisition. The LV AWCC provides three TTL outputs; one for each of the two rings plus the total summed signal output. Signals from both the inner and outer rings may be collected, but standard in-field use employs the total summed signal for analysis. Again, the ^3He tubes are matched to operate at the same HV settings, and the threshold of the A111 preamplifier discriminator is set to match the gain and minimize the gamma-ray response before shipment of the systems.

AnTech Inc. N2071 Neutron Coincidence Collar

Both the Canberra Industries JCC-71 and the AnTech N2071 UNCL systems must behave similarly within design variations from their respective filtering networks. Thus, the N2071 (**Figure 5.1 c**) has a very similar form factor at 23.5×23.5 cm for the larger configuration and 23.5×16.5 cm for the smaller configuration [32]. Each bank also houses six ^3He tubes, populated at ORNL with GE Reuter Stokes model RS P4-0810-116, pressurized at 4 atm with an argon methane quench gas. The signal is processed using Amptek A111 chips within each bank, producing a TTL pulse width of 50 ns. An externally mounted N1081 de-randomizing Mixer Buffer Counter reduces dead time and provides HV, +5 V, and signal out BNC connections for each detector bank.

5.1.4 Non-Ideal Behavior: Double Pulsing

During a list mode-based detector characterization campaign, the non-ideal behavior of a JCC-71 UNCL was revealed through investigation of the HV characteristic and the Rossi- α distribution (RAD) [4] produced from a ^{252}Cf source with a measured count rate of approximately $4 \cdot 10^4$ nps. Because the use of list mode data acquisition offers analysis with various timing gate parameters, it reveals features that have commonly been overlooked by historic timing gate selection while using traditional shift register data acquisition methods. These overlooked effects may have an impact on the results of coincidence timing analysis within the systems' operating regimes, as predelay values do not encompass

and exclude the totality of this effect due to coincidences formed between the electronic feature and other true successive neutron events throughout the pulse train [83]; the effect is dependent on the double pulsing ratio to true neutron events.

The JCC-71 doubles HV characteristic illustrates a plateau structure between 1680 and 1780 V, an increasing trend between 1800 and 1900 V, and a decreasing trend from 1900 to 2000 V (**Figure 5.2 a**). Once the system has reached the plateau region, it is expected that the count rate will remain stable until gamma breakthrough overtakes the trend, as shown at the **Figure 5.2 b**. The behavior measured with the JCC-71 suggests that the effective shaping time of the preamplifiers is short with respect to the signal formation within the operational range with associated threshold settings. The difference in count rate within the expected plateau region corresponds with triggering and processing individual proton and triton response peaks from a single neutron event; i.e. double pulsing. Double pulsing was briefly discussed in relation to Amptek circuit boards by Dytlewski et al in 1990 [84], and the cause for this phenomenon was later explained in detail by Fazzi and Varoli [85]. The cause will be discussed in detail later in this section.

When these data were analyzed to produce an individual RAD for each HV setting (**Figure 5.2 c**), a spike in the doubles count rate was observed to grow as a function of HV, which again indicates double pulsing [48]. The RAD serves as a histogram of double neutron events measured as a function of time in relation to the initial triggering neutron event. Based on the selected counter's timing gates, after an initial triggering neutron event, the frequency at which another neutron is measured, per selected timing bin width, is recorded over a range of times (e.g., a 1 μs binning structure from $t=0$ to $t=1024 \mu\text{s}$). This process is repeated for every neutron measured, where each can serve as the triggering neutron event to collect the total number of measured neutron coincidence events. The first few microseconds of the RAD suffer from charge collection and dead time effects, decreasing the measured count rate; this effect is not represented in **Figure 5.2 d**. It is expected that this distribution should follow an exponential decaying trend for a time-correlated (fissioning) source and a flat distribution for an uncorrelated source such as an AmLi (α,n). The peak in count rate measured at approximately 1 μs begins to build into the pulse train within the operational range between 1680 and 1720 V and is unmistakable at the higher HV settings.

Commonly, to determine the mass of the fissioning material, a sample is loaded into the central well of an annular neutron coincidence counter, and the emitted neutrons are captured by surrounding ^3He -filled tubes. The ^3He capture releases a proton and triton at different energies in a back-to-back orientation to conserve momentum. These particles travel through the ^3He gas, ionizing it into free electrons and positive ions which, in turn, ionize more gas atoms as they move through the electric field near the anode, resulting in an avalanche-like multiplication process. The average track of these particles is several millimeters depending on the gas pressure and quench gas composition. Together, these ionization tracks have the appearance of a dual-lobed cloud of charge. The electrons move ~ 1000 times faster than the positive ions; therefore, we can ignore the movement of the positive ions over the timescale in which the electrons are collected. The initial charge structure is dual-lobed, and not a single column of charge, because the degree of ionization changes along the charged particle's trajectories as a result of stopping power and Bragg peak effects. The current generated from the induced charge of the particle migrations is collected over a period of time on this central anode wire. The collection period of this charge cloud is influenced based on the particles' orientations relative to the anode (**Figure 5.3**), and it must be long enough to avoid double triggering on a single event. The induced charge signal is then modified, integrated, and differentiated as a function of the RC time constant in the preamplifier and the amplifier chips, respectively, to produce a voltage signal with suitable shape and pulse height for the discriminator [1].

If these back-to-back particle trajectories are parallel to the anode wire, a simple pulse collected over a short period of time is formed (**Figure 5.3 c**). However, if the trajectory is perpendicular to the anode wire (**Figure 5.3 d**), this dual-lobed cloud of charge will be accelerated toward the anode wire for collection as a function of initial position, i.e., the charge from one end of the lobe will reach the wire before the charge from the opposite end of the other lobe. The primary peak can be larger (**Figure 5.3 a**) or smaller (**Figure 5.3 d**) than the secondary peak, depending on whether the proton or triton was stopped

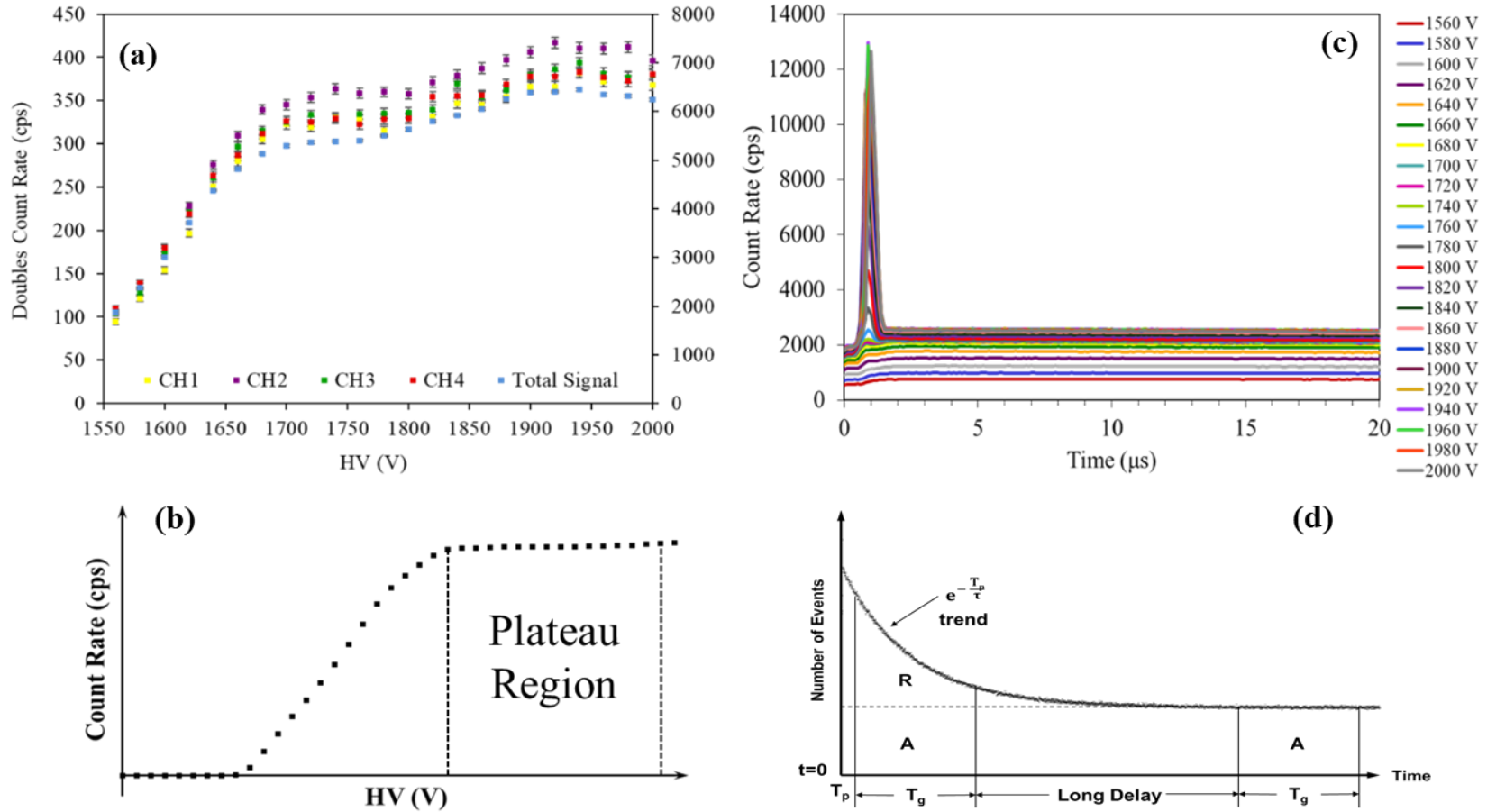


Figure 5.2. (a) Measured doubles count rate HV characteristic of the UNCL with individual channel count rate scale on the left and the total detector signal with scale on the right. (b) A measured HV characteristic for a well-behaved neutron coincidence counting system. (c) RAD for a ^{252}Cf measurement with the UNCL for HV range 1560–2000 V, revealing non-ideal behavior centered about 1 μs . (d) A measured RAD characteristic for a well-behaved neutron coincidence counting system.

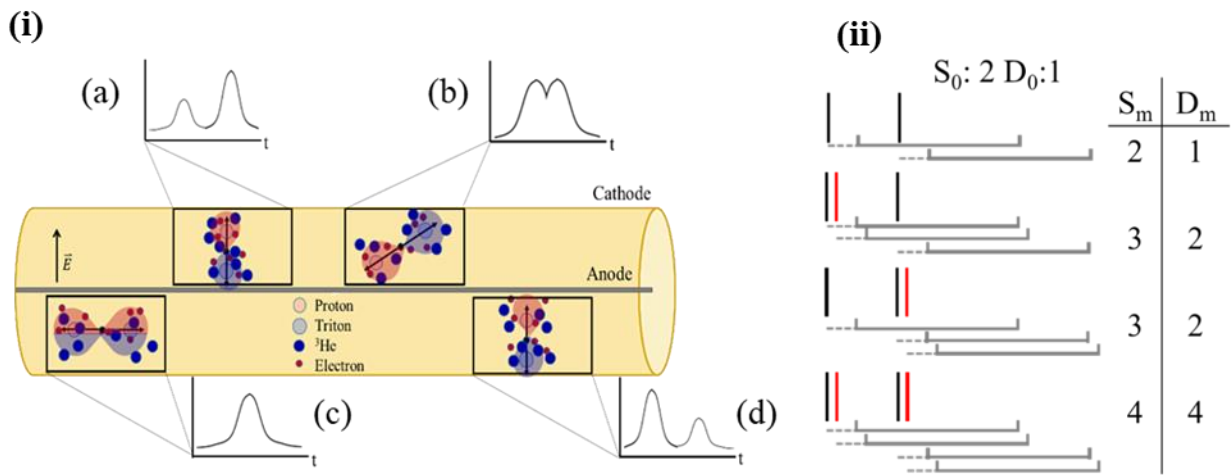


Figure 5.3. (i) An exaggerated representation of various pulse shapes collected on the central anode wire of a ^3He tube, caused by the positional dependence of the p and T-induced charge collection from the $^3\text{He}(n,p)\text{T}$ reaction. (a) Triton ionization trajectory is closer to the anode; collection of the triton-induced charge cloud is smaller and collected earlier in time than the charge cloud generated by the proton. (b) Charged particle trajectories at an intermediate angle; it is more difficult to resolve the two individual charge collection peaks. (c) The particles' trajectories are parallel to the anode; charge collection time is the same. (d) Proton ionization trajectory is closer to the anode; collection of the proton-induced charge cloud is larger and collected earlier in time than the charge cloud generated by the triton. (ii) An example neutron pulse train with red double pulsing, events highlighting the possible false counts that could be measured [48].

closer to or farther from the wire. This influences the charge collection process from a single neutron event, causing the induced charge waveform to appear bimodal with a portion of time between the peaks of the measured charge.

If the shaping time of the amplifier is much shorter than the charge collection time of the detector tube ($\sim 1 \mu\text{s}$ depending on the system), this bimodal pulse will be processed and sent to the discriminator, causing it to trigger on both peaks of the signal (**Figure 5.4**). If the digital output is also short, these pulses will be registered and counted as if they were two separate neutron events, causing this double-pulsing phenomenon to be observed in the count rate, as in the bottom three example pulse trains at right in **Figure 5.3** [48]. For example: assuming S_0 and D_0 are the true singles and doubles counts that should be measured by the system, respectively, and S_m and D_m are the singles and doubles counts actually measured by a system, the differences in these counts can be attributed to incompatibility of the pulse processing time settings, and thereby, double pulsing. For trajectories at intermediate angles, this separation in time is less, and it is much more difficult to resolve the two individual peaks (**Figure 5.3 b**); therefore, a majority of incoming signals are registered as a single pulse.

Ultimately, in a well-behaved pulse processing chain, one would expect the pulse from each neutron interaction to be of an amplitude great enough to be accepted by the discriminator, thereby eliminating gamma events and electronic noise, and for it to be registered as a single interaction event. As the gamma ray dose increases, more non-neutron events will be falsely registered as the gamma pulse height crosses the threshold more often because of pileup. Also, as the gain on the preamplifiers increases, the amplitude of lower-level noise is increased. By operating the counter at a higher than optimal HV for characterization and testing purposes, it is possible to induce and emphasize double pulsing that is present, but possibly not considerable, at lower voltages by effectively raising the gain. This means the discriminator is more likely to re-trigger on structures in the pulse shape. The threshold must be suitable to accommodate a wide range of conditions, but this is not always perfected. Matching the pulse processing chain with the application of the neutron coincidence counter and its associated gamma field and neutron background is done by the detector manufacturers before new systems are shipped for use; however, as has been shown, it may not always be optimized to fully account for double pulsing.

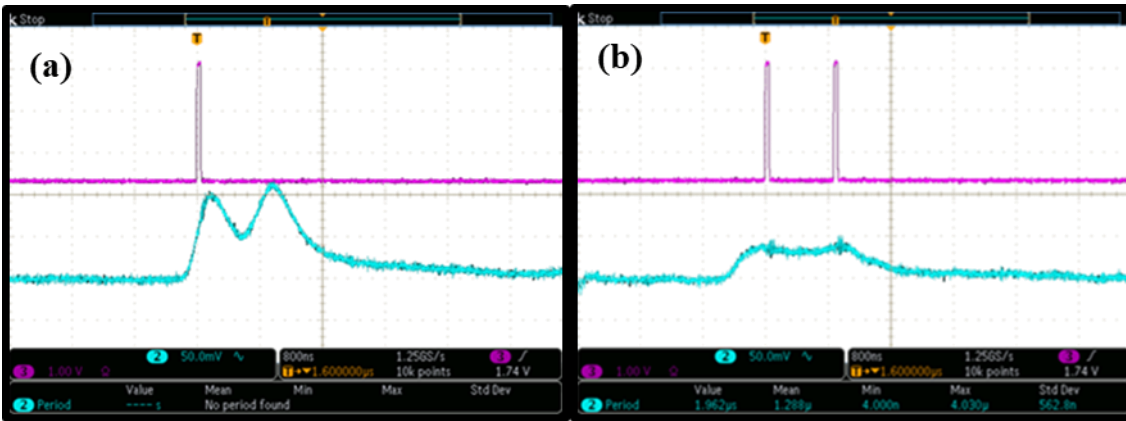


Figure 5.4. Oscilloscope captures of two different neutron events measured in the JCC-71 with ORNL preamplifiers before their optimization. These captures highlight the difference in the effects that pulse shape and amplitude can have on the number of events measured by the system, dependent on pulse shaping time and threshold settings. **(a)** The charge collection peaks for the proton and triton are distinguishable; however, because the measured voltage does not drop below the set threshold between the peaks, a single neutron event is measured. **(b)** The charge collection peaks for the proton and triton are marginally distinguishable and have a lower voltage amplitude than the previous pulse. Because the voltage signal dips below the threshold between charge collection peaks, two events are measured instead of one.

5.1.5 Isolating the Behavior: A Comparison between Systems

Because double pulsing was observed with the Canberra JCC-71, we set out to isolate this behavior to the relevant subsystem: the Canberra JCC-71 counter system, the Canberra JAB-01 boards, or the Amptek A111 chip. We did so by testing four different systems using the PTR-32 list mode data acquisition module. To first ascertain that double pulsing was not an isolated occurrence dependent on the number of detector channels analyzed or on the source type used, the neutron pulse train was obtained using an uncorrelated AmLi neutron source (compared with the previously measured correlated ^{252}Cf source). The resulting neutron pulse train was analyzed to produce a RAD for the total detector signal with the same measurable effect at $1\ \mu\text{s}$, followed by a RAD that was flat because an uncorrelated neutron source was used. This was done to justify that the double-pulsing behavior is source type-independent, as expected. The dead time was then determined for a combination of Channel 1; Channels 1 and 2; Channels 1, 2, and 3; and Channel 1, 2, 3, and 4, using the methods described in Croft et al. [73]. As expected, the dead time decreased as more preamplifiers were added to the pulse processing chain. However, when the RAD was analyzed for these four combinations of channels, the spike in the count rate was consistently measured at $1\ \mu\text{s}$, for all combinations of channels; this result indicated that the spike was not caused exclusively by dead time effects.

Variant on the JCC-51 Active Well Neutron Coincidence Counter: LV AWCC

The double pulsing response was also recognized in the RAD of the LV AWCC using a ^{252}Cf source with a measured count rate of $8 \cdot 10^3$ nps, with the spike in count rate again resolved at $1\ \mu\text{s}$ (Figure 5.5 a), eliminating the possibility that this effect was detector-specific. With this system, however, the double pulsing did not have a visible contribution until the bias was increased to 1820 V.

N2071 Neutron Coincidence Collar

Expanding the investigation of this behavior, the same measurements were performed once again on an AnTech N2071 Neutron Coincidence Collar, which implements the Amptek A111 chip. This time, the structure within the HV characteristic was not initially apparent; but when the RAD was analyzed for each HV setting, the spike at $1\ \mu\text{s}$ was again seen, with slight variations in the shape and magnitude due to the difference in the two companies' filtering networks (Figure 5.5 b). The double pulsing effect begins around the operational HV of 1680 V and increases as the HV increases. These findings eliminated the possibility that this effect was JAB-01-specific.

JCC-71 implementing ORNL Preamplifiers

Finally, a HV characteristic and RAD analysis were performed using prototype preamplifiers that were designed at ORNL and placed on six ^3He tubes within a single bank of the original JCC-71. These preamplifiers are independent of any A111 electronics, and they therefore provide an unbiased comparison. The RAD (Figure 5.6) shows no indication of a spike in count rate throughout the entire $1024\ \mu\text{s}$ range tested for all HVs listed, and it follows an obvious exponential decaying trend. For this HV characteristic, the stable plateau region extends from 1680 to 1980 V, illustrating ideal behavior for a preamplifier system. Therefore, it can be reasoned that the cause of the double pulsing in these three counting systems is the Amptek A111 Preamplifier and Discriminator chip.

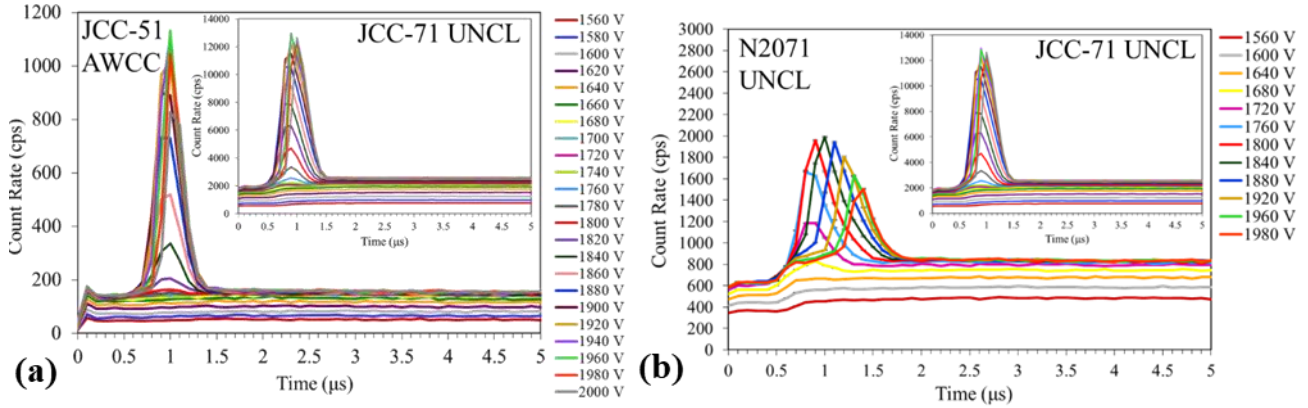


Figure 5.5. (a) A comparison of the RAD of the large volume JCC-51 AWCC compared with that of the JCC-71 UNCL. The spike is again measured at 1 μs . (b) A comparison of the RAD of the AnTech N2071 compared with that of the JCC-71. The spike is again measured at 1 μs , but it drifts in time as the HV is increased.

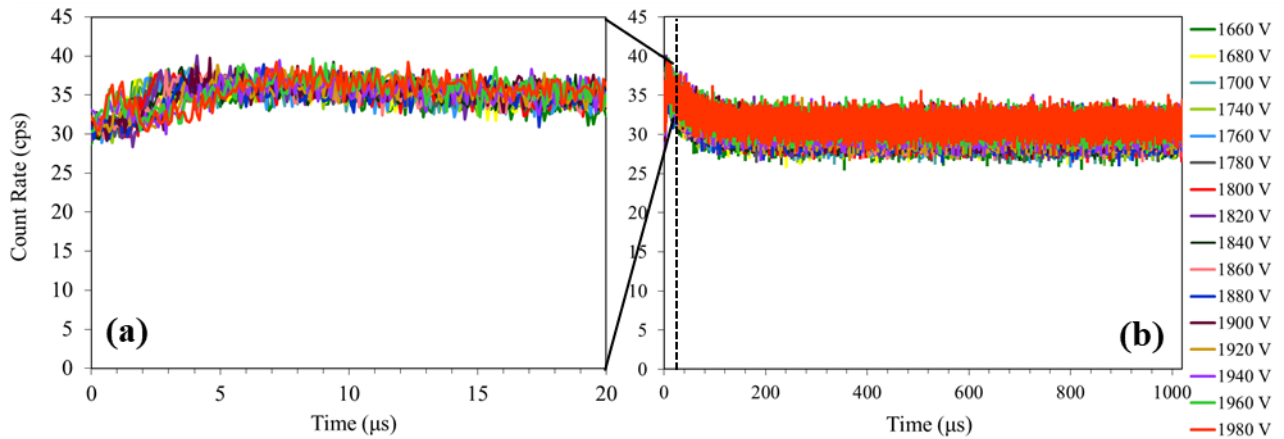


Figure 5.6. The RAD obtained from one bank of the JCC-71 retrofitted with ORNL-designed preamplifiers shown for HVs from 166 to 1980 V. (a) A 0–20 μs subsection of the 0–1024 μs bin range shown at the right (b).

5.1.6 ORNL Preamplifier Design

The ORNL preamplifier design is based on modern commercially available components, using the latest-generation, low-voltage, commercial operational amplifiers. The general electronics chain is based on printed circuit board technology, a motherboard, and a converter box. The operational amplifier packages are standard 8-SOIC packages (EIA-481-D). All six prototype preamplifiers were fabricated to fit within the existing junction box of the JCC-71 to maintain the overall system footprint (**Figure 5.7**). The preamplifiers have a unipolar input, rather than a bipolar input as with the A111. The ORNL preamplifiers do not output TTL pulses (+5 V, 52 ns) directly (as in the case of the JAB-01 board) but instead use low-swing logic (low-voltage differential signals). Fully differential, low-swing logic results in faster signal processing, reduced injected electrical interference, and less ground-induced current noise—ultimately looking toward the use of FPGA (field programmable gate array)–based signal processing. This helps make each channel independent of the others and eliminates daisy chains, which enables single-channel analysis through list mode data acquisition. The goal of this prototype design was to match and, in the instance of double pulsing, improve upon the performance of the JAB-01 board while benefiting from the same form factor and an affordable cost.

As discussed earlier, the ORNL preamplifier response did not indicate any double pulsing behavior within the relevant operating regime at 1680 V or higher as the electronics implementing the Amptek A111 chip did. The gain, shaping time, and discriminator threshold settings are well defined for the ORNL prototypes, for a total charge integration time of ~200 ns, but these values are not well documented for the A111 for comparison. **Figure 5.8** illustrates a comparison between the total signal responses from one bank of the JCC-71 with an original JAB-01 board and another bank of the JCC-71 with the six ORNL preamplifiers summed as one output, using a 50.6 μCi ^{252}Cf source. In the image at left, the HV characteristic supports the claim that the ORNL boards achieve similar performance to the JAB-01 board; however, it also highlights the difference in performance between the two electronics in the 1680–1980 V range attributed to double pulsing. The ORNL preamplifier response is similar to the expected performance of a ^3He tube throughout the plateau region; once the characteristic begins to plateau, the measured count rate remains stable with slight increases due to a marginally increasing charge collection efficiency. The RAD was already shown to behave ideally for the full HV range measured. When the RAD is analyzed for each individual HV measurement (**Figure 5.8 c**), the lack of double pulsing is evident in the ORNL board, in contrast to the JAB-01 systems. The ORNL prototype does suffer from charge collection time and dead time effects, as exposed in the decreased measured count rate between 0 and 1.6 μs . Beyond the double pulse centered about 1 μs in the JAB-01, both preamplifier designs achieve similar performance.

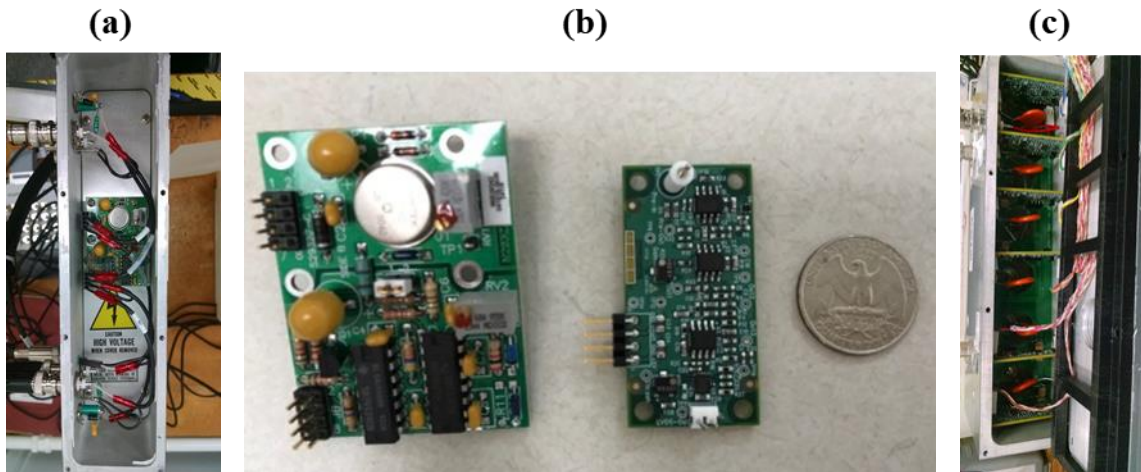


Figure 5.7. (a) Original JAB-01 board within the JCC-71 junction box. (b) A comparison between the JAB-01 circuit board and the new ORNL board (right). (c) Six ORNL boards placed within the JCC-71 junction box.

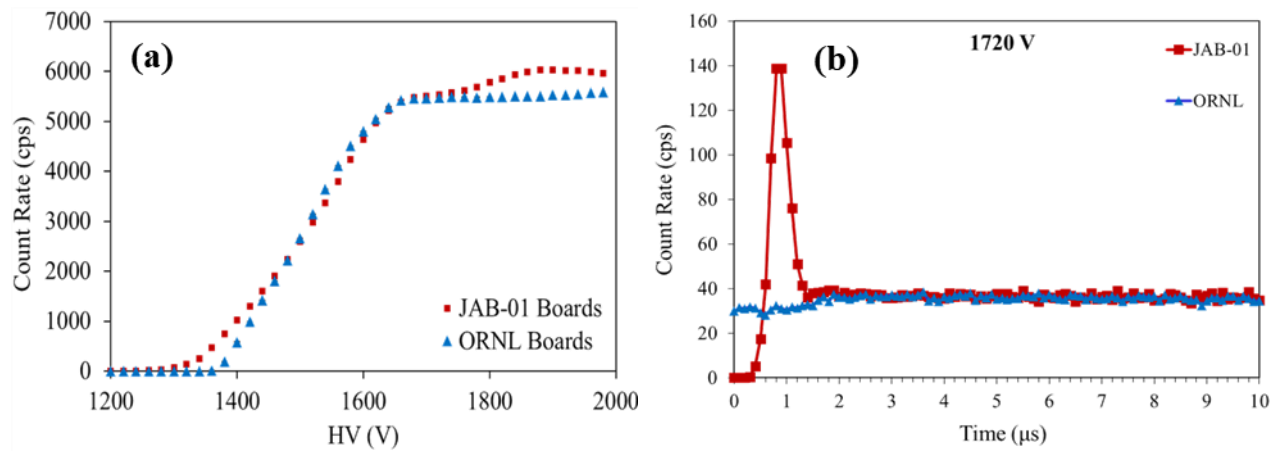


Figure 5.8. (a) The HV characteristic comparison between the JAB-01 boards and the ORNL boards. (b) A RAD produced for both electronic systems at 1720 V to highlight the lack of double pulsing measured in the ORNL boards.

5.1.7 Double Pulsing Correction for Common A111–based Systems

Previous work has been done to derive and apply a double pulsing correction to neutron data acquired using an AWCC at Los Alamos National Laboratory by Koehler et al. [48]. In terms of the common systems discussed in Section 2, we set out to quantify the double pulsing in each and correct for it in post-analysis using this approach. Koehler et al. provide several equations that may be applied to a neutron pulse train to determine the double pulsing fraction. This fraction, r , is the number of pulses measured under the peak in the RAD attributed to double pulsing, A_p , compared with the true singles counts that should be measured by the system if no double pulsing was present, S_0 (Eq. [5.1]). To calculate A_p , a difference in counts may be taken between a pulse train at a HV where double pulsing is present and a pulse train at a HV where negligible double pulsing is measured. The singles counts measured at the HV of interest where double pulsing is measured is referenced as S_m , and the singles counts measured at the HV with negligible double pulsing may be assumed to be approximately the true singles counts that should be measured by the system. Once the double pulsing fraction is determined, and knowing the measured singles, S_m , and the measured doubles, D_m , the true singles and doubles may be calculated using Eq. [5.2] and [5.3].

$$r = \frac{A_p}{S_m - A_p} = \frac{A_p}{S_0} \quad (5.1)$$

$$S_m = S_0(1 + r) \quad (5.2)$$

$$D_m = D_0(1 + r)^2 \quad (5.3)$$

The double pulsing correction for the JCC-71 UNCL with the JAB-01 board was achieved by first identifying the last HV setting where negligible double pulsing was observed in the RAD. For this system, with measurements taken every 20 V from 1580 to 1980 V, the HV selected was 1640 V. Recall that the standard operational HV for field measurements with the UNCL is 1680 V. The neutron pulse trains at 1660, 1680, 1720, 1760, 1800, 1840, 1880, 1920, and 1960 V were then analyzed to determine their double pulsing fractions. This range of HV illustrates the magnitude of the effect of double pulsing through their RADs in selected operating regimes, as well as in more extreme regimes (**Figure 5.9 a**). To do this analysis, the pulse train at 1640 V was subtracted from each pulse train of the HVs listed above over the full time range of 0-1024 μ s between the triggering neutron event and the successive coincident event (**Figure 5.9 b**); i.e. not considering a predelay setting. This assumption is somewhat faulted because of a slightly higher efficiency at the analyzed HV regions compared with the efficiency at 1640 V. However, this difference in measured counts related to the lower efficiency is difficult to resolve from the difference in measured counts caused by the double pulsing effect.

The total number of doubles counts under this subtracted RAD response was obtained as a sum, and taken as A_p . Because the starting and ending boundaries of the peak in count rate shifted as a function of HV, we elected to take A_p as the entire difference in count rate between the two neutron pulse trains to avoid any ambiguity, assuming the difference would encompass the double pulsing effects and the slight increase in efficiency. The singles count rate was given in the PTR-32 RAD data file output. The dead time may be estimated by visually inspecting the pulse train for the point in time when the measured count rate changes from 0 cps to several cps and is estimated at an average of 0.3 μ s for the JCC-71 system throughout the HV range. By applying a standard dead time correction to the singles count rate, and knowing the measurement time, the double pulsing fraction was determined. The results are given in **Table 5.1**, with associated error propagated through the related variables such as A_p , the singles count rate, and the dead time. The double pulsing percentage at the operational HV of 1680 V is calculated to be 1.75% and is as large as 5.41% at 1960 V. This means that under the standard operational HV of this particular system in the field, without any predelay selected, 1.75% of all measured counts will be generated by electronic artifacts. Since the greatest effect on the count rate is measured at 1 μ s, operating

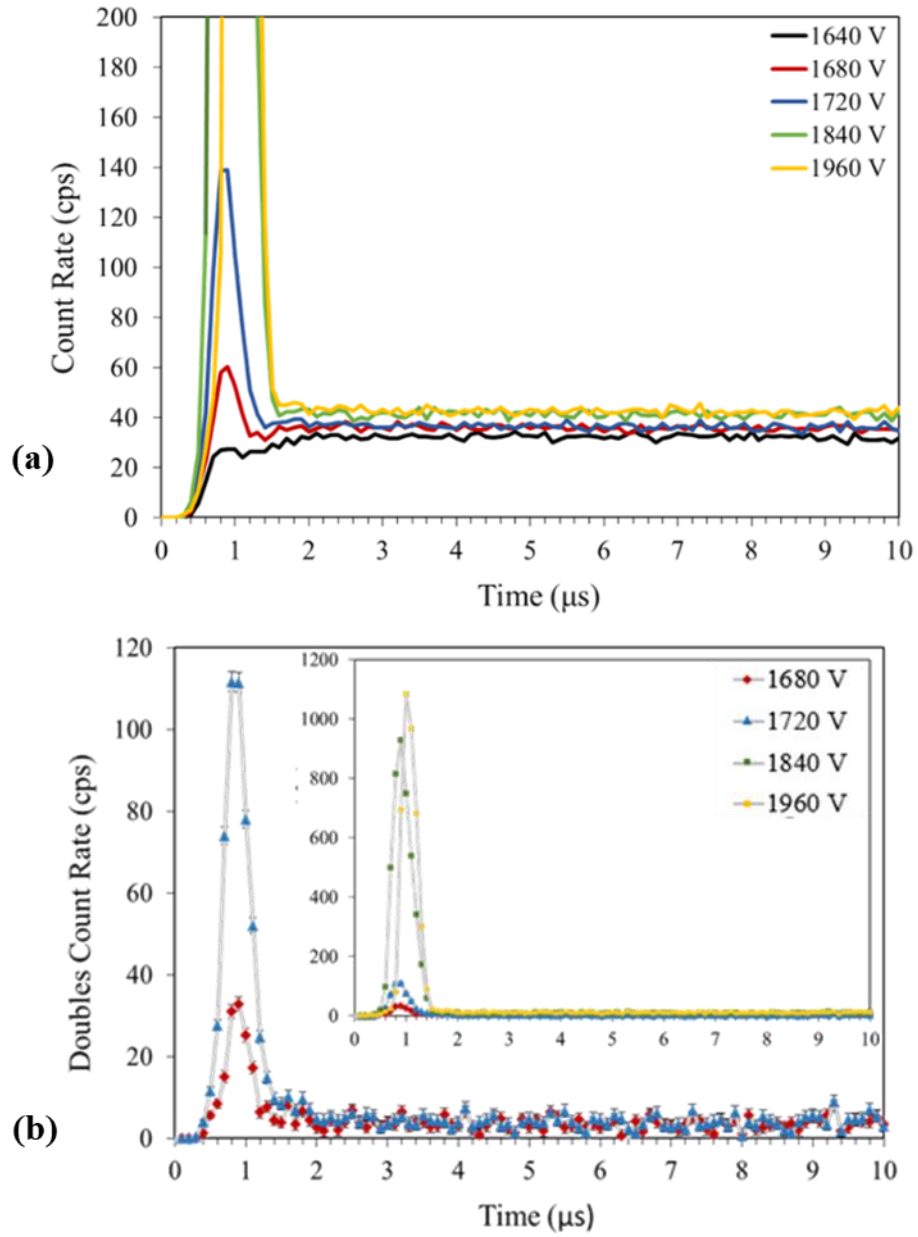


Figure 5.9. (a) RAD for several HVs within the operating regime and beyond, illustrating the effect of double pulsing. (b) RADs normalized to the RAD at 1640 V without double pulsing.

the system with a 4.5 μ s predelay will lessen this percentage, but as has been shown by Nguyen et al. [83], the totality of this effect cannot be absorbed by the predelay setting due to additional coincidences formed between the electronic feature and other successive events throughout the pulse train.

Table 5.1. Canberra JCC-71 Collar Double Pulsing Normalized to 1640 V, measured source strength: ~40, 500 nps

	1660	1680	1720	1760	1800	1840	1880	1920	1960
r	0.01144	0.01748	0.02202	0.02810	0.03966	0.05100	0.05785	0.05711	0.05411
\pm	0.00018	0.00026	0.00032	0.00040	0.00055	0.00070	0.00080	0.00079	0.00074

The same analysis was performed for the N2071 UNCL. In this case, the last HV setting where negligible double pulsing was observed in the RAD was at 1660 V; therefore, all successive neutron pulse trains were normalized to the pulse train at 1660 V. This normalization should have a smaller discrepancy in counts because of a slightly greater efficiency and its location on the HV plateau. The dead time was estimated at an average of 0.4 μ s for the system throughout the HV range. The double pulsing fraction found for this system, however, is much greater than that of the JCC-71 UNCL, as shown in **Table 5.2**. At 1680 V the double pulsing percentage was calculated to be 4.16%, with no predelay setting, and at 1960 V the percentage was calculated as 15.9%. This large contribution may be due to the fact that the N2071 was populated with ^3He tubes at ORNL that may or may not have been fully compatible with the timing components on the preamplifier circuit, to differences in the filtering network between the AnTech and Canberra electronics, and/or to differences related to source strength effects.

Table 5.2. AnTech Collar double pulsing normalized to 1660 V, measured source strength: ~26, 000 nps

	1660	1680	1720	1760	1800	1840	1880	1920	1960
r	0.0000	0.04165	0.10315	0.13371	0.1486	0.1574	0.1580	0.1572	0.1586
\pm	0.0000	0.00029	0.00073	0.00096	0.0011	0.0011	0.0011	0.0011	0.0012

Finally, the double pulsing fraction was determined for the JCC-51 AWCC. Recalling that the AWCC RAD did not show any visible contribution of double pulsing until 1820 V and higher, the neutron pulse trains at 1840, 1880, 1920, and 1960 V were normalized to the pulse train obtained at 1820 V. Because the standard in-field operating voltage is 1680 V as well, this correction is not as relevant as those done for the UNCL designs. Nonetheless, it is important to understand how a counting system is behaving and how it may influence other analyses. The dead time was estimated at an average of 0.1 μ s for the system throughout the HV range. The percentage calculated is much lower than those for the other two systems; this may be due to better matching between the ^3He tubes used and the JAB-01 used, and/or the source strength used (**Table 5.3**).

Table 5.3. LV AWCC variant on the Canberra JCC-51 double pulsing normalized to 1820 V, measured source strength: ~8,000 nps

	1840	1880	1920	1960
r	0.00641	0.00630	0.00623	0.00622
\pm	0.00009	0.00009	0.00009	0.00009

5.1.8 Discussion

The double pulsing correction values described cannot be generalized and applied to all UNCL systems nor all AWCC systems, but they indicate what others should expect to see in their own common systems. This analysis must be performed on a system-by-system basis, as many factors may contribute to the overall double pulsing fraction. Some of these include: threshold settings on the preamplifier, tube diameter and length, gas mix, applied HV, gain, pulse shaping time, electronics layout and associated capacitance across cables and connections, system dead time, and source strength. The Amptek A111 has also been modified throughout its several-decade history of use, so the generation of the chip may also influence the double pulsing fraction. Furthermore, any additions to the circuitry beyond the A111 chip made by manufacturers such as Canberra or AnTech, will also influence this behavior. The measured effect will be influenced by the predelay settings selected and the operational HV used. Initial plans for this work also included increasing the shaping time on the A111 to help mitigate some of the double pulsing effects in these systems, i.e. minimize by design. However, the A111 chip is a sealed hybrid unit and, therefore, no modifications can be made to minimize double pulsing because access to the components is restricted. Instead, we relied on quantifying the double pulsing fraction on a system-by-system basis to better understand its contribution to the counter's response. We propose that others characterize this behavior over the full HV range of interest and calibrate or correct for this behavior as needed; note that using neutron coincidence counting for any absolute source measurements requires that double pulsing is negligible.

5.1.9 Conclusions

Double pulsing was found to be present in a Canberra Industries JCC-71 Neutron Coincidence Collar, a variant on the Canberra Industries JCC-51 Active Well Neutron Coincidence Counter, and an AnTech Inc. N2071 Neutron Coincidence Collar—but not in independent preamplifiers designed and built at ORNL. After a series of characterization measurements, the cause of the double pulsing was isolated to the Amptek A111 Charge Sensitive Preamplifier, Discriminator, and Pulse Shaper. The A111 chip is used in both Canberra JAB-01 preamplifier/amplifier/discriminator boards and the AnTech preamplifier boards, but it is not present in the ORNL preamplifier prototype. The causes of this behavior are discussed with mention of how to avoid these issues in future designs through better compatibility matching. As modifying the A111 was not feasible because of its design structure, a double pulsing correction was applied to the JCC-71, JCC-51, and N2071 neutron pulse trains in post-analysis using the approach described in Koehler et al. A range of double pulsing percentages were found for the three systems, ranging from 1.7 to 4.2% at the operational voltage of 1680 V with no predelay setting in the UNCLs, from 2.2 to 10.3% at this work's chosen operational voltage of 1720 V in the UNCLs, and reaching a maximum at ~16% for the N2071 at 1880 V under the specified conditions and assumptions. Double pulsing is important to understand and quantify, as its influence on the neutron pulse train could affect the nuclear material mass measurement of a sample during a nondestructive assay. The study of this effect through to the final sample assay values is a topic for future work, including the effect as a function of predelay. This double pulsing correction will also be incorporated in future absolute source measurements that rely on knowing the behavior of the pulse train at a 0 predelay and infinite gate width. We recommend that future neutron counter designs could incorporate the custom ORNL preamplifier in place of the A111. Furthermore, future work could study the ORNL preamplifier performance in the higher gamma fields encountered in waste assays.

5.2 Methods for Diagnosing and Quantifying Double Pulsing Using Shift Register Logic⁶

5.2.1 Abstract

Double pulsing in neutron coincidence counters is the result of a pulse processing chain—³He proportional counter timing incompatibility well known to nondestructive assay system designers. It is not currently widely acknowledged, or accounted for, in the safeguards user community. However, it is gaining attention as list mode data acquisition and analysis becomes more commonly used for system diagnostics, revealing features that have been overlooked by historic timing gate selection using traditional shift register data acquisition methods. Double pulsing increases the apparent number of measured neutron events from a source. Therefore, it may contribute to a falsely increased count rate if present at the operational high voltage used when assaying samples, even with set predelays. The authors have previously studied the effects of double pulsing on neutron pulse trains in three common neutron coincidence counting systems used in routine measurements for international safeguards—a Canberra Industries JCC-71 Neutron Coincidence Collar, a variant on the Canberra Industries JCC-51 Active Well Neutron Coincidence Counter (the Large Volume Active Well Neutron Coincidence Counter), and an AnTech Inc. N2071 Neutron Coincidence Collar—using list mode data acquisition and analysis. This non-ideal behavior was isolated to the Amptek A111 Charge Sensitive Preamplifier & Discriminator chip used in both the Canberra Industries and Antech systems. The double pulsing fraction was calculated in post-analysis for various high voltage settings in these A111-based systems, assuming no predelay settings. In this work, the authors expand upon this identification and analysis to make it more translatable between list mode data acquisition and analysis and shift register-based analysis. By investigating the double pulsing fractions in a JCC-71 Uranium Neutron Collar as a function of predelay settings, as well as describing and performing alternative tests and analyses to diagnose and quantify the double pulsing using shift register logic, this work hopes to complete the picture of double pulsing identification and analysis.

5.2.2 Introduction

Neutron coincidence counters are used widely in international safeguards for nondestructive assay verification measurements of uranium and plutonium. They typically comprise moderated ³He proportional counters arranged in some geometry around a centralized well to detect thermalized neutrons emitted from the sample under question. The pulse processing chain of common International Atomic Energy Agency (IAEA)-approved counters is based around the commercially available Amptek A111 Charge Sensitive Preamplifier & Discriminator chip [31], as implemented by both Canberra Industries and Antech Inc [35]. The signals are then acquired and processed by shift register-based technologies, such as the Canberra Industries JSR-15 [60], based on Los Alamos National Laboratory Handheld Multiplicity Register concepts, to calculate neutron multiplicity rates used for further evaluation. This paper elaborates on prior work (Section 5.1), which identified double pulsing in three systems containing the A111: the Canberra Industries JCC-71 Neutron Coincidence Collar [30] and Large Volume JCC-51

⁶ This section is under review to be published in a peer reviewed journal under the original title “Methods for Diagnosing and Quantifying Double Pulsing in a Uranium Neutron Collar System Using Shift Register Logic,” A. S. Moore, S. Croft, R. D. McElroy Jr., and J. P. Hayward, Nuclear Instruments and Methods in Physics Research Section A: Accelerators, Spectrometers, Detectors and Associated Equipment, 2019. It is printed here with permission from the editors in its original form.

Active Well Coincidence Counter [33] [82], and the Antech N2071 Neutron Coincidence Collar [32]. That work set out to: identify double pulsing in a neutron pulse train using list mode data acquisition (LMDA) and analysis, isolate the behavior to the relevant component in the pulse processing chain—which turned out to be the A111, and calculate the double pulsing fractions in each of these systems across a range of high voltages (HVs). This work explores various alternatives to identify and quantify double pulsing using more traditional shift register–based data acquisition and analysis, specifically under historical timing gate selections. This will help determine the impact double pulsing may have on practical in-field measurements.

Double pulsing is the result of the mismatch between the charge collection time through the $^3\text{He}(n,p)\text{T}$ capture reaction and the electronic pulse processing shaping time. It is strictly an unwanted electronic artifact. The current generated by the ionized gas is integrated and passed through the preamplifiers and amplifiers to modify the signal into a usable shape and pulse height. Based on the amplitude of this pulse, the signal may cross a threshold in the discriminator circuit and generate a logic pulse. This logic pulse is then read by either a shift register or list mode module, indicating a neutron interaction [1]. Individually triggering on and successively processing the two ionized charge response peaks (generated by the movement of both the proton and triton through the gas) from a single neutron event is double pulsing. It is a function of the position of the particles' trajectories relative to the central anode wire; the measured charge, and its difference in time, is proportional to that trajectory [85]. It is common for double pulsing to be present in ^3He -based systems, simply based on the physics of charge collection and electronic pulse processing characteristics. In a properly designed safeguards system, double pulsing is nonexistent or negligible in the operational HV regime. Some forms of double pulsing, such as reflections of the logic pulses formed between the counting system and pulse processing system, are easy to eliminate by termination. Here, we are discussing an intrinsic effect that may be insidious to some systems.

It is possible that this effect has always been present in these coincidence counters. It could have been disguised by empirical calibration methods and historic timing gate selection while using shift register data acquisition methods, which are routinely adopted in international safeguards. Or, it is possible that previous systems did not suffer from this effect and, as modifications have been made to these components over decades of production, double pulsing has since been introduced. The problem is also likely to stem from the fact that the same preamplification system, the A111, is used across a range of ^3He proportional counters in practice. The A111 is approved for general use by the IAEA and Euratom due to its reliability, radiation tolerance, and count rate capabilities. However, the same performance cannot be achieved across all counting systems using the same timing settings when the A111 is connected to different systems with varying fill pressures, gas compositions, and tube diameters.

Standard operation of these A111 systems, with predetermined HV settings and timing windows, does not imply that there is a problem with the historical design. However, in certain conditions—such as cases of the A111 paired with the systems studied—as the HV increases, the double peaks become increasingly amplified above threshold because of the greater gain. This allows a larger double pulsing fraction to be measured, revealing the underlying non-ideal behavior and indicating further investigation may be necessary. Although this behavior is not always obvious at operational HV settings, it may nonetheless be present. For systems that have double pulsing present within the operational HV range where the timing gate settings do not encompass the totality of this effect, it is important to characterize, quantify, and understand the influence of this behavior on a measurement.

It is also essential from a practical standpoint to identify when a system is behaving correctly, and when it is not. It is crucial to establish that the standard assumptions of the coincidence counting system behavior hold true for the operational conditions so that they may be used to accurately perform the specified measurement. Because double pulsing effects are not included in traditional coincidence system models, or in physical assumptions made in solving the point kinetics equations, this behavior is not currently corrected for in neutron coincidence counting measurements [5].

As these systems are modernized and their applications are expanded as a result of new list mode capabilities and associated theory, double pulsing continues to be a hindrance. Dead time behavior cannot

be fully described in common systems implementing the Amptek A111 because of the double pulsing present within this timing regime. These effects cannot be separated, and generalizations must be made for the best approximation. Overall system efficiency is also affected as the measured neutron count rate is falsely elevated due to these electronic artifacts. In addition, as the field is motivated to use neutron coincidence counting for absolute source measurements—as an alternative to certify neutron emission rates independent of the national MnSO_4 bath program [86] [87] [88] (Chapter 7)—estimating the neutron count rate independent of any coincidence timing windows becomes increasingly challenging when double pulsing is present. The closer the proximity of the double pulsing events to the triggering event (i.e., location in time relative to $0 \mu\text{s}$), the more difficult it is to estimate the expected neutron coincidence rate at $0 \mu\text{s}$ predelay without dead time, charge collection effects, and spurious electronic artifacts. In addition, the count rate at long gate widths is subject to large increases due to double pulsing, which would influence this calculation as well. Therefore, having a detailed methodology to identify, quantify, and correct double pulsing effects is essential as the applications of neutron coincidence counting expand. It is important to provide several different methods—both for LMDA and analysis and for traditional shift register data acquisition and analysis techniques—for ease of use and for cross verification and confidence that the calculated double pulsing fraction values are correct before they are applied to a system.

This paper will focus on the double pulsing behavior measured in a Canberra Industries JCC-71 UNCL (Uranium Neutron Coincidence Collar). This is a fairly typical system configuration of tube pressure, diameter, fill gas composition, and grouping ratio to the number of preamplifiers. Therefore, this study is applicable to a wide audience, and these methods may also be extended to other system configurations. It investigates and quantifies the double pulsing fraction for various predelay settings and gate widths, and it verifies consistency between the previous LMDA calculation and additional methods of determining the double pulsing fraction. The results of these studies support the idea that double pulsing effects are not fully captured within the predelay setting within the standard operating regime. These overlooked effects do impact the results of coincidence timing analysis due to coincidences formed between the electronic feature and other true successive neutron events throughout the pulse train, the magnitudes of which are quantified for specific timing windows. Using the general procedures outlined in Sections 3 and 4, the authors hope to encourage neutron coincidence counting users and manufacturers to check and quantify their systems for this behavior using shift register data acquisition and analysis, since double pulsing remains a significant hindrance for LMDA, system characterization, neutron multiplicity counting, and future research and development focused on expanding the scope of neutron coincidence counting.

5.2.3 Established Methods of Identifying Double Pulsing

As was shown in previous work (Section 5.1), only when a full system characterization was performed using LMDA was double pulsing first identified within several IAEA-approved neutron coincidence counting systems. This behavior manifested as a spike in count rate centered about $1 \mu\text{s}$ in the Rossi-alpha distribution (RAD) of three different Amptek A111-based systems: the JCC-71 [30], LV JCC-51 [82], and N2071 [32]. This was the first indication that the JCC-71 UNCL was not behaving as it should historically. This result attracted our attention and encouraged type-testing to identify the origin of this behavior. An in-depth investigation was conducted, including a comparison with electronics that did not show signs of double pulsing. This investigation resulted in identifying this behavior as a product of the Amptek A111 Charge Sensitive Preamplifier & Discriminator chip- ^3He combination. The qualitative contribution of this double pulsing fraction to the entire neutron pulse train was estimated for the JCC-71. The JCC-71 is populated with GE Reuter Stokes model RS P4-0813-101 ^3He cylindrical proportional counters (“tubes”), pressurized at 4 atmospheres (atm) with argon methane quench gas added, with an active length of 33 cm, and a 2.54 cm diameter. At the historical standard operational HV of 1680 V,

applying no pre-delay and making several other systematic assumptions for the normalization, the double pulsing fraction was found to be $1.748 \pm 0.026 \%$ (**Table 5.4**). However, it was shown that in this standard operational regime, the Large Volume JCC-51 Active Well Coincidence Counter with GE Reuter Stokes model RS P4-0825-103 tubes, pressurized at 4.5 atm with a quench gas composition of argon and methane, an active length of 63.5 cm, and a 2.54 cm diameter, did not exhibit significant double pulsing fractions. Instead, double pulsing became evident only at 1840 V, well beyond the operational regime. Its fraction was calculated to be $0.641 \pm 0.009 \%$ (Section 5.1) — well below the UNCL double pulsing fraction.

Table 5.4. Canberra JCC-71 Collar Double Pulsing RAD approach, no timing settings (Section 5.1)

HV (V)	1660	1680	1720	1760	1800	1840	1880	1920	1960
r (%)	1.144	1.748	2.202	2.810	3.966	5.100	5.785	5.711	5.411
\pm	0.018	0.026	0.032	0.040	0.055	0.070	0.080	0.079	0.074

The RAD, generated using LMDA, facilitates identifying the double pulsing present in a system by providing a histogram of double neutron events measured as a function of time in relation to the initial triggering neutron event. RADs commonly use small timing windows for better response resolution. After an initial triggering neutron event, the frequency at which another neutron is measured, per selected timing bin width, is recorded over a range of times (e.g., a $1 \mu\text{s}$ binning structure from $t=0$ to $t=1024 \mu\text{s}$). This process is repeated for every neutron measured, where each serves as the triggering neutron event. Ultimately, the total number of coincidence events is collected over the duration of a measurement. The first few microseconds of the RAD suffer from charge collection and dead time effects, decreasing the measured count rate. Beyond this, it is well known that this RAD follows an exponential decaying trend, related to the neutron die-away time of the system. Because of different fast and delayed components, multiple exponentials can be fit to this distribution for an accurate representation of the neutron die-away time. This exponential behavior represents a greater probability that successive neutron coincident events will be detected closer in time to the triggering event. The die-away time of the system is typically on the order of 20–100 μs across the full range of neutron correlation counters, but more closely approximated to 50 μs across neutron coincidence well counters and collars. Beyond the neutron die-away time of the system, accounting for room return and reflected neutrons to also die-away, future events can be attributed to background, or accidental, coincident neutron events.

When double pulsing is present, a peak will manifest in the first few microseconds of the RAD (**Figure 5.10**). The time at which this peak manifests is dependent on system parameters such as tube diameter, fill pressure, gas composition, electronic shaping time, and so on. It may also be caused by easily changeable factors such as cable length, reflection, impedance mismatch, and termination. When the cause is the electronic timing settings, not much can be done on a commercially available system with restricted access to the components, such as the case of the A111. It is important to note that the accidentals count rate will also be influenced by double pulsing. This complicates any background (chance coincidence), or accidental, subtraction that is traditionally performed on a RAD. Double pulsing events are also recorded as event triggers, which then form future false coincidence events, which ultimately elevate the count rate level along the full RAD. This elevated accidentals behavior is masked unless the full RAD is compared and normalized across a range of HVs, with settings that suffer from double pulsing and settings that do not, along the HV plateau.

The RAD can be a comprehensive LMDA diagnostic to identify double pulsing, to test whether it is rectifiable, to quantify its effect, and to see at what point in time the double pulsing takes place. However, it is not easy to produce a RAD using shift register logic, as a new measurement would have to take place for every time bin desired (e.g., 1024 separate acquisitions in the example given). Therefore, one must rely on more simple diagnostics when using traditional shift register-based data acquisition and analysis.

Double pulsing can be identified by simple investigations of an amplifier's pulse output on an oscilloscope. After triggering on a charge collection pulse, another pulse caused by double pulsing will appear close in time. Its frequency may be estimated by turning up the persistence and identifying the point at which there is a greater saturation of events compared with the more Poisson-like distribution of true neutron events. However, this is not a very quantitative approach, so more advanced diagnostics and analysis techniques are necessary. Specifically, diagnostics within typical operating procedures and characterization testing of these neutron coincidence systems are needed to avoid significant resource investments.

Using standard neutron coincidence characterization parameters, such as the HV characteristic, double pulsing can be initially identified during system testing. The HV characteristic is a visual representation of the system's behavior over a range of applied HV settings. It may be generated by LMDA or by shift register-based acquisition and analysis—making it a simple, universal diagnostic for neutron coincidence counting systems. The HV characteristic is one of the basic characterization measurements conducted, so using it as a diagnostic does not add resource investments during performance testing. A pre-delay and gate width setting are selected and the neutron multiplicity rates are acquired within those regimes for each HV setting desired. These rates are then plotted and visually inspected. For a ^3He counter, the measured neutron count rate begins at 0. Then, at some threshold the current generated from neutron interactions in the $^3\text{He}(n,p)\text{T}$ reaction begins to be collected on the anode and processed by the electronics chain. The effective efficiency increases as the bias is increased, as more charged particles can reach the anode and allow a related logic pulse to be measured. Finally, at some value intrinsic to the system, the charge collection saturates around the anode. This efficiency then remains relatively constant across a range of HV settings ($<+1\%/100\text{ V}$ slope due to small amplitude wall effect pulses being amplified above threshold by the increasing gain), known as the HV plateau [1]. A counter is operated at a point along this plateau; it is standardly selected at 40 V above the inflection point, known as the knee. Typically, there will be gamma breakthrough at high HVs beyond the plateau where, because of pulse pileup, a gamma event can be falsely measured as a neutron event. This saturation of the anode wire causes runaway behavior of the charge collection response as HV increases. It is important to operate the counter away from this region, accounting for HV drift. When the ^3He HV characteristic does not have a plateau region, it may indicate that electronic artifacts are present which are overpowering the physical behavior of the system. For the UNCL, the operational HV is selected to be 1680 V off the singles HV plateau. It has been argued that since the UNCL exploits the doubles neutron count rate rather than the singles neutron count rate in a measurement, the instruments should be characterized by the doubles HV plateau [89] (Chapter 2), resulting in an operational HV of 1720 V to meet the criteria described. Both settings will be evaluated in this work.

As in the HV characteristic in **Figure 5.10**, the neutron count rate continues to increase in the historical plateau region between 1680 V and 1980 V. The count rate increases from 1560 V to approximately 1660 V, reaches a plateau between 1680 V and 1780 V, increases again between 1800 V and 1900 V, and then decreases through 2000 V. This structure appears to follow the double pulsing assumption that as the HV increases, the system is more likely to trigger on the structure in the pulse shape, resulting in two measured neutron events from one physical one. The decreasing trend beyond 1920 V is consistent with the theory that the gain begins to reach a value large enough that both peaks have an increasing probability of remaining above threshold, decreasing the double pulsing probability. The plateau region is measuring a greater neutron doubles count rate than is physically present, but it is not obvious from the characteristic what the true value should be because the base count rate is fundamentally elevated. Therefore, although the HV characteristic is a good visual diagnostic, it cannot be used in this context to quantify a double pulsing fraction.

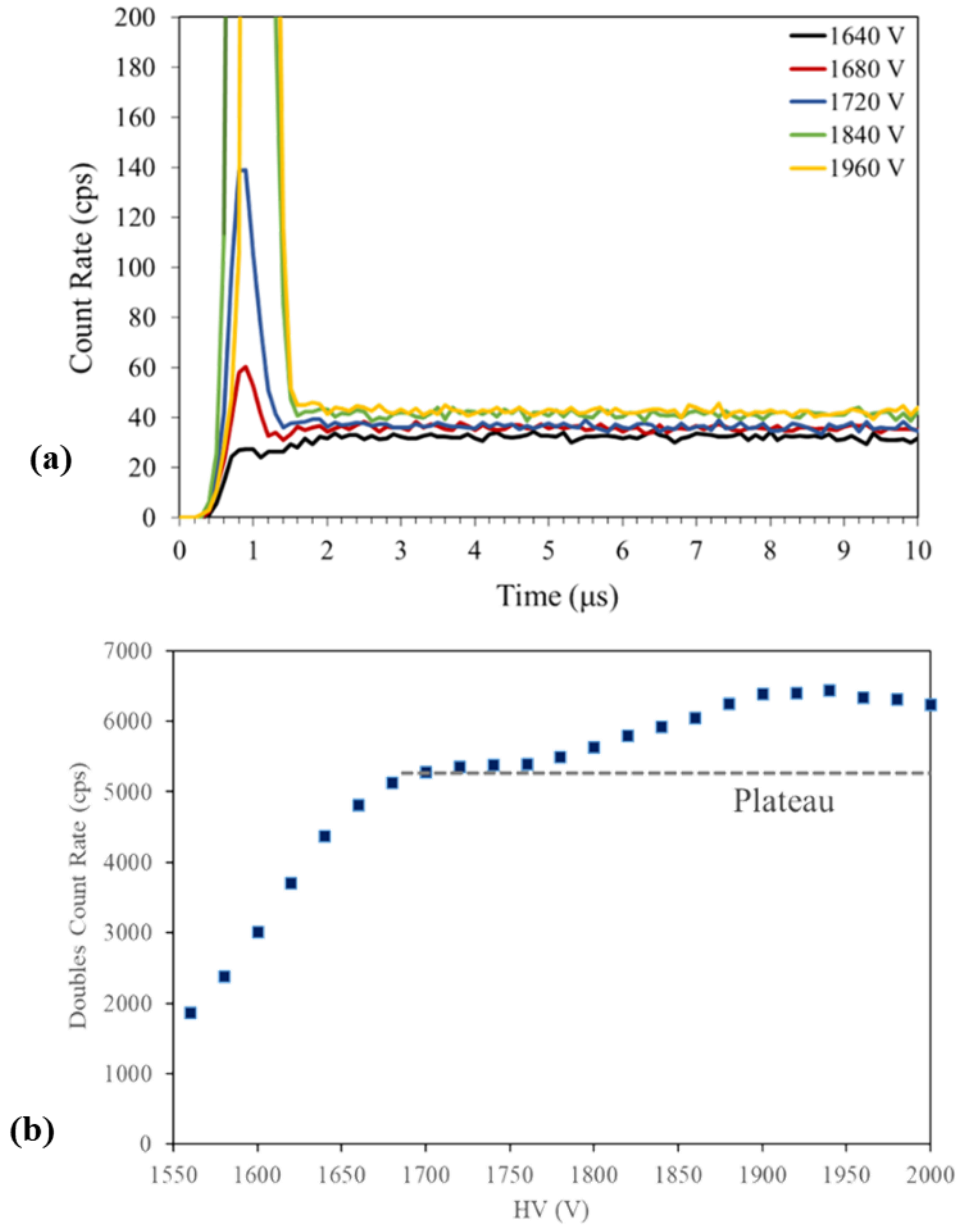


Figure 5.10. (a) RADs produced for a range of HVs RAD within the operating regime and beyond, illustrating the effect of double pulsing (Section 5.1). (b) A HV characteristic produced using the JCC-71 UNCL and PTR-32 LMDA module. The expected “plateau” region is depicted for a coincidence system without double pulsing.

5.2.4 Double Pulsing Fractions Determined for Various Time Gate Settings

Using a 1-D RAD, the same approach initially described by Koehler et al. [48], was used to calculate the double pulsing fraction, r , in the JCC-71 UNCL for various predelay settings. This was previously done for the JCC-71 using 0 predelay (Section 5.1). A neutron pulse train was acquired with a ^{252}Cf and the IAEA– approved Hungarian Institute of Isotopes’ Pulse Train Recorder-32 (PTR-32) [37] LMDA module software. The double pulsing fraction is taken as the number of pulses measured under the peak in the RAD attributed to double pulsing, A_p , compared with the true singles counts that should be measured by the system if no double pulsing was present, S_0 (Eq. [5.1]). To calculate A_p , a difference in counts is taken from a RAD at a HV where double pulsing is visually evident, compared with a RAD at a HV where double pulsing is not visually evident (**Figure 5.10**). The singles measured at the HV of interest where double pulsing is seen are referenced as S_m . The singles counts measured at the HV with negligible double pulsing are assumed to be the true singles counts that should be measured by the system. This analysis was performed on the RADs for 1680 V and 1720 V, both compared with the RAD at 1640 V, for predelays ranging from 0 to 6 μs in 0.5 μs increments. 1640 V is the last HV setting where negligible double pulsing effects are seen.

The argument must be made that because 1640 V is not in the HV plateau region (**Figure 5.10**), but instead is the beginning of the knee (or cusp of the plateau), these calculated double pulsing fractions also include minor effects of an increased count rate caused by a difference in the charge collection efficiency at the relevant HV compared with that at 1640 V. It is not possible with this method to separate these effects from the effects caused by double pulsing. Because 1680 V and 1720 V settings should historically fall within the HV plateau region, the same contribution of this difference in efficiencies should apply to the calculations at both 1680 V and 1720 V. As shown in the HV characteristic in **Figure 5.10**, however, the measured count rates at both settings are not consistent; the inconsistency is attributed to the increasing double pulsing fraction as HV increases.

The predelay was applied by excluding the counts in each 0.1 μs time bin of the RAD from the sum A_p , through to the specified predelay value. This was first done for an effectively infinite gate width, where the doubles count rate is summed from the specific predelay until 1024 μs (**Table 5.5** and **Table 5.6**). This analysis was then performed over a typical gate width of 64 μs following the predelay (**Table 5.7** and **Table 5.8**). As the predelay increases, fewer events are counted in the sum, and the double pulsing fraction decreases slightly. However, this decrease is not significant enough to conclude that setting a conservative predelay, such as the traditional 4.5 μs setting, will encompass and mitigate the double pulsing behavior. If this were true, we would expect a greater decrease in the double pulsing fraction once the predelay exceeded 1 μs , where the double pulsing–induced spike in count rate was recorded. Instead, this result supports the notion that the double pulsing effects have an impact on coincidence timing analysis, despite predelay settings, due to coincidences formed between the electronic feature and other true successive neutron events throughout the entire pulse train. However, in the operational HV range of 1680–1720 V, the double pulsing contribution is approximately 0.122% of the pulses at 1680 V, with a 4.5 μs predelay and a 64 μs gate width (**Table 5.7**), and 0.146% at 1720 V (**Table 5.8**). The double pulsing fraction at the standard operational timing gates of the JCC-71 over a range of HVs is reported in **Table 5.9** for comparison.

The same analysis was subsequently conducted for various gate widths using the standard predelay setting of 4.5 μs (**Table 5.10** and **Table 5.11**). The double pulsing fraction increases with increasing gate width, since a larger time window will allow more false coincidences to be measured between a single neutron event from the source or from background in combination with the electronic artifact.

These tables indicate that the double pulsing fraction in the JCC-71 may not be significant when considering a traditional nondestructive assay coincidence measurement. However, this effect will be significant if greater multiplicities are used. Because triple events are not measured by neutron multiplicity counters but are derived and calculated from factorial moments, any electronic artifact will

manifest with greater impact in higher multiplicity calculations, thereby influencing the point kinetic equations. The effect of double pulsing in a multiplicity measurement will be studied in the future. For other non-JCC-71 systems, this double pulsing percentage may be determined to be greater due to system characteristics or the operational timing windows selected. Therefore, there may be a significant impact on coincidence timing analysis using other systems, but this possibility must be evaluated on a system-by-system basis, as many factors contribute to the percentage (Section 5.1). The discovery of double pulsing is also significant for modeling and understanding the behavior of these systems from first principles. It will also influence any proposed extension of use of these systems in more extreme timing regimes. For example, the pulse train analyzed at a 0 predelay and infinite gate width will not be known with certainty due to this effect, as is necessary for absolute source measurements.

Table 5.5. JCC-71 UNCL Double Pulsing Normalized to 1640 V for various predelays; HV: 1680 V, Tg: 1024 μ s- T_p

Tp (μ s)	0	0.5	1	1.5	2	2.5	3	3.5	4	4.5	5	5.5	6
r (%)	1.748	1.748	1.741	1.738	1.737	1.736	1.734	1.733	1.732	1.731	1.730	1.729	1.728
\pm	0.026	0.026	0.026	0.025	0.025	0.025	0.025	0.025	0.025	0.025	0.025	0.025	0.025

Table 5.6. JCC-71 UNCL Double Pulsing Normalized to 1640 V for various predelays; HV: 1720 V, Tg: 1024 μ s- T_p

Tp (μ s)	0	0.5	1	1.5	2	2.5	3	3.5	4	4.5	5	5.5	6
r (%)	2.202	2.201	2.176	2.169	2.166	2.165	2.163	2.162	2.161	2.159	2.158	2.157	2.156
\pm	0.032	0.032	0.031	0.031	0.031	0.031	0.031	0.031	0.031	0.031	0.031	0.031	0.031

Table 5.7. JCC-71 UNCL Double Pulsing Normalized to 1640 V for various predelays; HV: 1680 V, Tg: 64 μ s

Tp (μ s)	0	0.5	1	1.5	2	2.5	3	3.5	4	4.5	5	5.5	6
r (%)	0.1301	0.1305	0.1245	0.1228	0.1224	0.1220	0.1220	0.1218	0.1214	0.1215	0.1213	0.1209	0.1209
\pm	0.0029	0.0029	0.0028	0.0028	0.0028	0.0028	0.0028	0.0028	0.0028	0.0028	0.0028	0.0028	0.0028

Table 5.8. JCC-71 UNCL Double Pulsing Normalized to 1640 V for various predelays; HV: 1720 V, Tg: 64 μ s

Tp (μ s)	0	0.5	1	1.5	2	2.5	3	3.5	4	4.5	5	5.5	6
r (%)	0.1771	0.1770	0.1537	0.1480	0.1470	0.1465	0.1466	0.1464	0.1463	0.1459	0.1457	0.1452	0.1452
\pm	0.0033	0.0033	0.0030	0.0030	0.0030	0.0030	0.0030	0.0030	0.0030	0.0030	0.0030	0.0030	0.0030

Table 5.9. RAD-based Double Pulsing Percentage, with 4.5 μ s predelay and 64 μ s gate width

HV (V)	1680	1720	1760	1800	1840	1880	1920	1960
r (%)	0.1215	0.1459	0.2703	0.4259	0.5763	0.6524	0.6334	0.5775
\pm	0.0028	0.0030	0.0043	0.0061	0.0079	0.0088	0.0086	0.0079

Table 5.10. JCC-71 UNCL Double Pulsing Normalized to 1640 V for various gate widths; HV: 1680 V, Tp: 4.5 μ s

Tg (μ s)	2	4	8	16	32	64	128	256	512	1019.5
r (%)	0.00430	0.00832	0.01660	0.0319	0.0638	0.1218	0.2298	0.4453	0.8728	1.7311
\pm	0.00042	0.00060	0.00085	0.0012	0.0018	0.0028	0.0044	0.0075	0.0134	0.0254

Table 5.11. JCC-71 UNCL Double Pulsing Normalized to 1640 V for various gate widths; HV: 1720 V, T_p: 4.5 μs

T _g (μs)	2	4	8	16	32	64	128	256	512	1019.5
r (%)	0.00502	0.00983	0.01996	0.0404	0.0782	0.1479	0.2844	0.5529	1.0992	2.1858
±	0.00043	0.00060	0.00087	0.0013	0.0019	0.0030	0.0050	0.0087	0.0163	0.0315

5.2.5 Double Pulsing Disguised in Traditional Shift Register Measurements

LMDA may not always be accessible in a field measurement or in a laboratory setting. Thus, alternative tests and procedures to the RAD analysis must be developed to diagnose and quantify double pulsing effects using shift register–based techniques as well. If traditional characterization measurements that are routinely used and easily conducted can be exploited to identify double pulsing, a better understanding of each system may be obtained with little demand. Less traditional shift register–based measurements can also be conducted and used with new procedures for better identification and quantification of double pulsing effects. These tests are described in detail below.

This section discusses traditional shift register–based system characterization measurements currently performed to evaluate system performance. It also investigates whether these measurements suffice for revealing double pulsing behaviors. As seen in the RAD produced through LMDA (**Figure 5.10**), a greater concentration of electronic coincidences is measured around 1 μs. This should also be the case in performing similar analyses using shift register data acquisition and analysis. However, because the data are standardly acquired on a wider time interval scale (compared with the 0.1 μs time bins with the PTR-32 LMDA), there will be some smoothing of these effects. With shift register–based analysis using a JSR-15, we no longer have access to the neutron pulse train as a function of time, but instead we are given the multiplicity rates per cycle measured at the specified timing windows. A value for the singles, doubles, and triples will be reported for each measurement cycle using the JSR-15. These values can be used for external comparative analysis across various timing settings and cycles to study any non-ideal behaviors. A new measurement must be conducted for every timing setting, however.

In traditional shift register–based neutron coincidence counter characterization analysis, many measurements are made of a neutron source in the same configuration for varying predelays and gate widths to identify the optimal timing gates. However, this is only standardly done for operational HV at 1680 V, and not for multiple HV settings. These doubles count rate data are then plotted as a function of predelay with set gate width (**Figure 5.11**), and again as a function of gate width with a set predelay value (**Figure 5.12**). The optimal settings may be chosen based on historical selection or by visual inspection of the stability of the count rate response. The neutron counting system die-away time may be extracted by applying two different fits to these data. One fit is a decaying exponential, and the other a saturating exponential, respectively. The values obtained from these two methods should be in agreement, and the die-away time should be independent of HV settings. If they are not, the disagreement is an indication of non-ideal behavior influencing the system response as a function of HV.

A neutron pulse train was taken at different HV settings using the UNCL and a ²⁵²Cf source. The PTR-32 LMDA was used to emulate a shift register by sampling each HV pulse train for various predelay and gate width settings, and the singles and doubles count rate values were recorded for each setting. The same could be done with a JSR-15, by performing separate measurements at every setting for every HV. Using the doubles count rate for the different predelay settings, a neutron die-away characterization time plot was produced for three different HV settings: 1680 V, 1720 V, and 1840 V (**Figure 5.11**).

For the doubles count rate data acquired as a function of predelay, the gate width was set at 64 μs, and data were taken from 0 to 10 μs in 0.25 μs intervals. On short time scales the die-away behavior may be approximated as linear, beyond the dead time and charge collection effects measured in the first few microseconds; these effects may differ slightly based on the HV applied. Double pulsing may be entwined

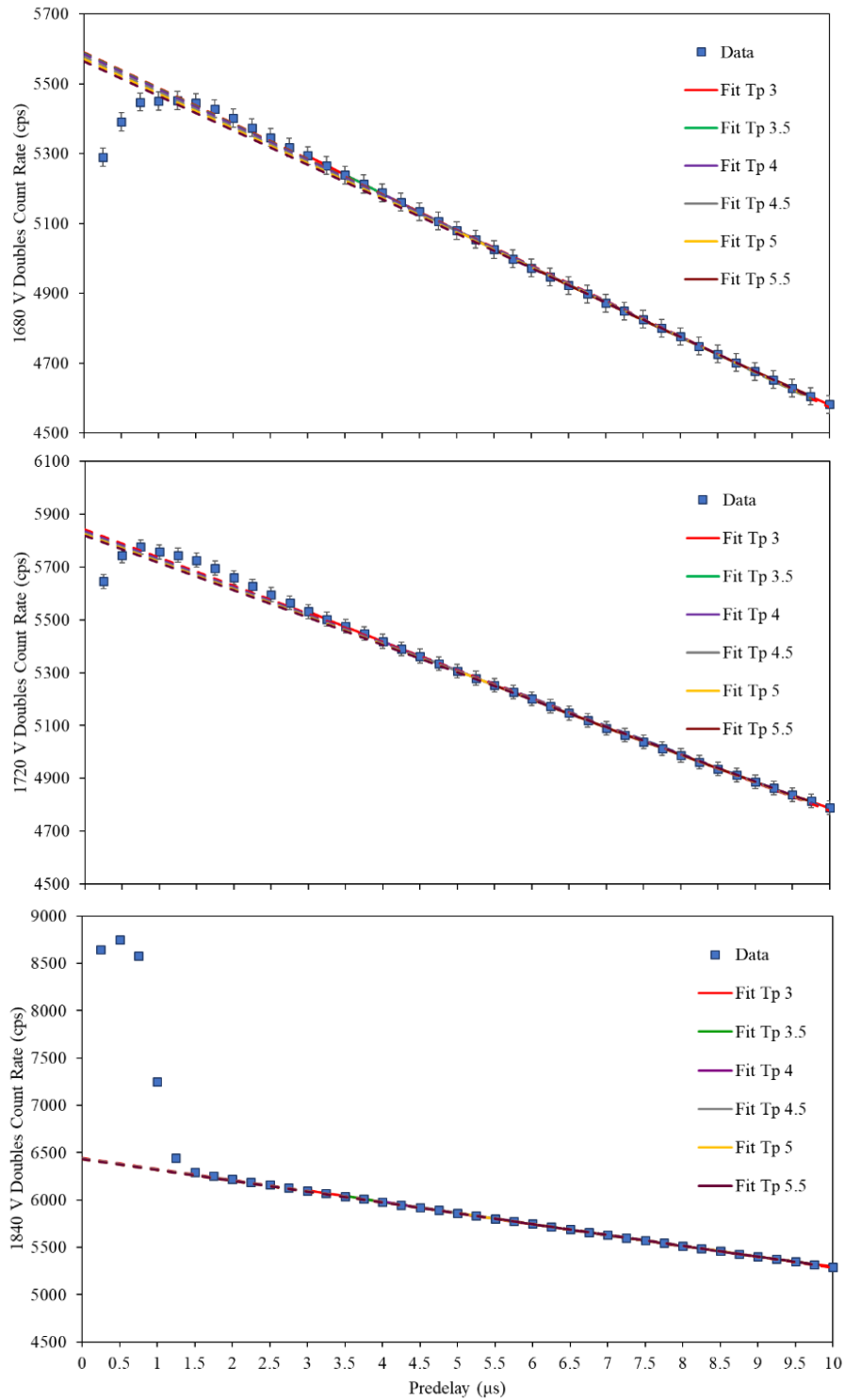


Figure 5.11. The measured doubles count rate values as a function of increasing predelay, with set gate width of 64 μs for 1680 V, 1720 V, and 1840 V.

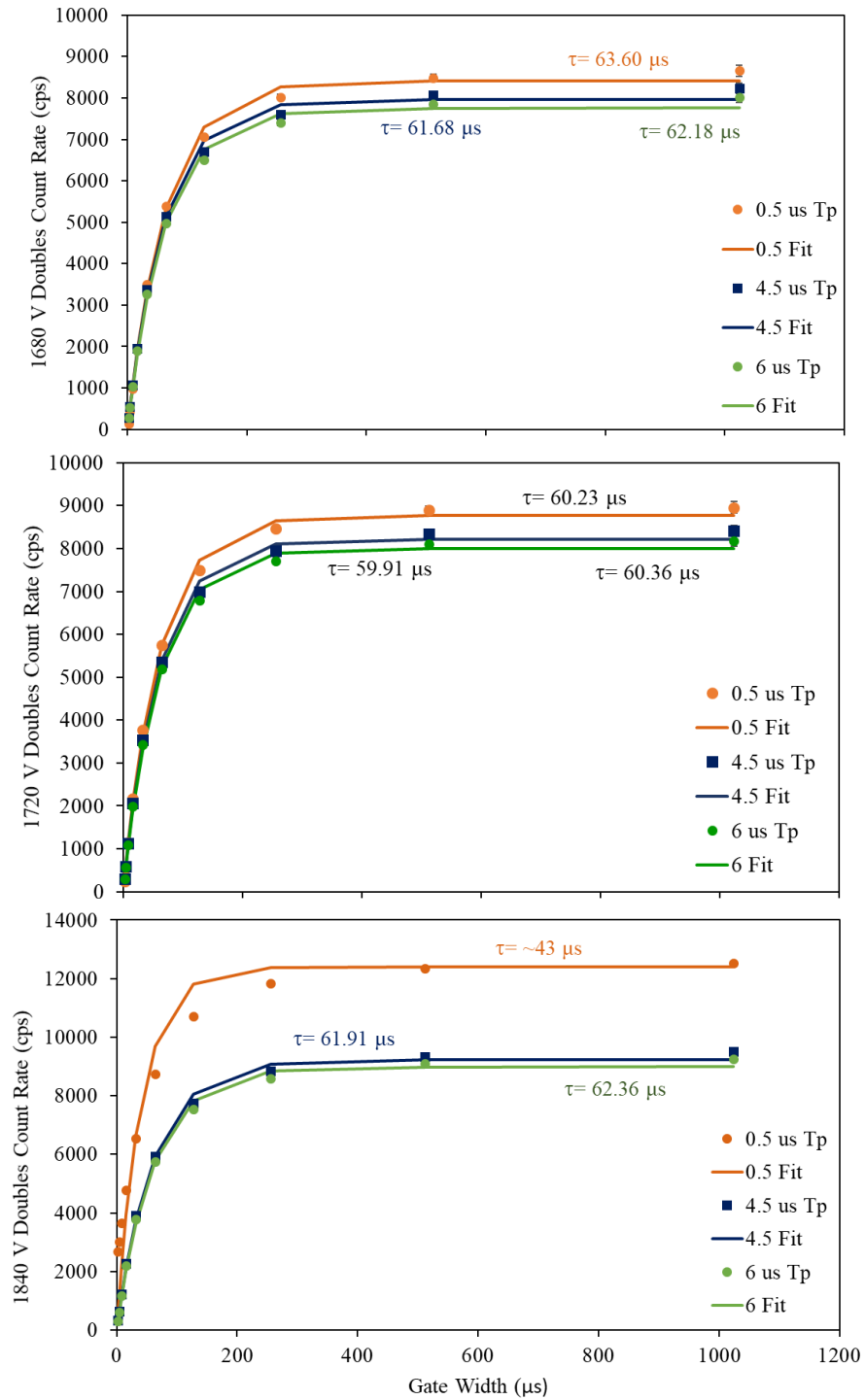


Figure 5.12. The measured doubles count rate values as a function of increasing gate width, with set predelay of 4.5 μs for 1680 V, 1720 V, and 1840 V. Counting statistic error bars are smaller than the data points. The calculated die-away times are also reported for each fit.

with the dead time and charge collection effects, but this study does not allow the opportunity to individually discern these different factors' effects on the measured rates at these scales. Therefore, analyzing these data at different starting predelays should help distinguish the predominant electronic artifact influencing the pulse train at that point in time.

The dead time and charge collection effects between 0 and approximately 2 μs are evident in the decreased doubles count rate responses for 1680 V and 1720 V (**Figure 5.11**); double pulsing is not evident. Double pulsing clearly dominates in this timing regime for 1840 V, as shown by the increased count rate. Recall that the double pulsing fraction increases with each HV setting, allowing a greater contribution of double pulsing in these similar measurements. However, because it is not standard to perform this analysis at 1840 V once the HV characteristic has identified the operational HV of 1680–1720 V, the double pulsing contribution would not historically be revealed. It is possible that the overshoot in count rate between 1 and 2.25 μs at 1720 V above each of the linear fits may be the influence of double pulsing, but this is not obvious for diagnosing the non-ideal behavior. It is also noticeable that the measured count rates increase significantly as the HV increases, despite historical justification that all 3 HV settings should be along the plateau. Although this finding would be difficult to quantify in relation to a double pulsing fraction, it is the result of false coincidences measured related to the electronic artifact.

A linear fit was applied to the data in the ranges of 3–10 μs , 3.5–10 μs , 4–10 μs , 4.5–10 μs , 5–10 μs , and 5.5–10 μs for 1680 V, 1720 V, and 1840 V (**Figure 5.11**). Each of these predelay-based linear fits has a slightly different slope due to the influence of these competing electronic effects. These slopes differ across a single HV measurement, by fitting a different time range, and they also differ between the 3 HV settings. It is expected that the neutron counting system will have the same die-away time for various HVs, i.e., the same slope at short time lengths. A difference in HV should not change the neutron transport behavior through the system; that is, the physical die-away should not be affected by a 40 V increase in applied bias. The die-away times, τ , were calculated using chi-squared analysis of the sum of errors squared between the measured doubles rate and this traditional fitting equation:

$$R_G = R_0 \left(\text{Exp} \left(-\frac{T_p}{\tau} \right) \right), \quad (5.4)$$

where R_0 is the maximum estimated doubles count rate value, T_p is the predelay, and R_G is the calculated doubles value expected with the determined die-away time. The die-away times for the 3–10 μs regime are in agreement, within one standard deviation, despite the slightly varying slopes calculated from these various time interval fits.

However, the calculated maximum doubles count rate varies substantially among the different timing ranges. Including the count rates measured between 2 and 3 μs up to 10 μs changes the slope more drastically than the inclusion and exclusion of any of the points from 3 to 10 μs . This result is consistent with the trend of the double pulsing fraction given in **Table 5.7** and **Table 5.8**—where the greatest double pulsing fraction is calculated with a 0 predelay, and then decreases from 1 to 2 μs , and finally remains stable from 2 μs forward through the 6 μs predelay range studied. However, as mentioned, it is not possible to fully discern if this behavior is caused strictly by double pulsing, or by a combination of double pulsing and charge collection effects; so, fitting through this region may not be reliable. Therefore, a standard study of the doubles count rate values as a function of predelay and set gate width may not be a clear indicator of double pulsing.

In addition, each of these count rate values is correlated, as they are all derived from the same neutron pulse train. A study of this correlation and how it propagates into the uncertainty of the doubles value and associated fit is a topic for a tangential work. However, because this is not well known, die-away time uncertainty values cannot be provided with confidence.

The system die-away time is also traditionally determined using a saturating exponential fit,

$$R_G = R_0 \left(1 - \text{Exp} \left(-\frac{T_G}{\tau} \right) \right), \quad (5.5)$$

and performing chi-squared analysis to minimize the sum of squared errors. R_G as a function of increasing gate width (T_G) is used here. Both R_0 and τ may be calculated. Using this method, and sampling the neutron pulse train for the different gate widths, it is obvious that not only do shorter pre-delay settings result in greater measured doubles count rates, but also they result in different die-away times (**Figure 5.12**). This finding could prompt further investigation into the behavior of the system. At longer pre-delays, such as the operational value of $4.5 \mu\text{s}$, the calculated die-away time is similar across the three HVs investigated. But the doubles count rate at $1024 \mu\text{s}$ is approximately 1000 cps greater at 1840 V than at 1680 V or 1720 V, and at $64 \mu\text{s}$ there is an increase of several hundred cps between each of the three HVs sampled (relating to the trends seen in **Table 5.10** and **Table 5.11**). Again, this test would not standardly be performed across several different HV settings, so these differences would be undiscovered. Ultimately, these measurements are very important to a system characterization, but they may not be sensitive enough, as currently applied, to diagnose double pulsing in the system.

The system bias parameter is used to identify the optimal pre-delay operation setting. The pre-delay must be long enough to avoid dead time and charge collection effects, but not so long as to lose a significant number of correlated events relative to the triggering event. A study of this parameter can also be used to identify non-ideal performance. The doubles count rate in both the (R+A) and A timing gate of a RAD are compared to calculate the bias. These count rates are automatically generated by a shift register measurement. The (R+A) timing window corresponds to the specified gate width following the pre-delay setting. Within this time region, all correlated (doubles/reals) neutron events are expected to be measured, with a background plateau of accidental coincidence events. After this timing window completes, a long delay relative to the operating timing windows (such as $4096 \mu\text{s}$) is then started, and the system does not record any events. During this time all correlated neutron events, including reflected neutrons, are expected to have quiesced, leaving only background (or accidental) coincidences. Afterward, these accidentals are measured in the A gate, which is the same time length as the (R+A) gate. This value is subtracted from the (R+A) total to get the true number of neutron coincidence events.

The bias is typically evaluated using uncorrelated neutron AmLi sources. AmLi produces random-in-time neutrons, so only a singles neutron count rate should be recorded; there should be no true neutron coincidence events. The accidentals rate then dominates the net doubles count rate. Therefore, there should be no statistical difference between the (R+A) and (A) gate values with a properly set pre-delay; i.e., the bias should be statistically consistent with 0. If the count distributions are not equal between these gates, the inequality may indicate the presence of electronic artifacts or non-ideal behavior in the system. If double pulsing is present, it is anticipated that the bias would be able to reveal this behavior.

Typically, the bias is calculated at a set HV for a range of pre-delay settings. This would be done for the operational HV selected for the system. Calculating the bias for varying pre-delays ranging from $0-6 \mu\text{s}$ at 1680 V and 1720 V using PTR-32 software does not indicate any concerning non-ideal behavior. The bias is not consistent with 0 for these HVs at these time settings, yet, its difference would not prompt further investigation. The bias calculated at 1840 V for different pre-delays is approximately 2% for $<1 \mu\text{s}$ pre-delays, with a higher bias beyond this setting compared with 1680 V and 1720 V. Those results could draw attention that some non-ideal behavior was occurring at this setting prompting further investigation, but again it is not conclusive nor quantitative. This data would also not be standardly acquired at a HV beyond the operational setting.

Because double pulsing is ever present in a system, and manifests with a probability relative to the charge collection position and amplitude for all events, these effects are continuous along a RAD. Therefore, the effect of double pulsing should also be equal between the (R+A) and A gates (beyond the spike at $1 \mu\text{s}$), and bias will therefore not reflect the underlying non-ideal behavior with traditional operational timing settings, even as the double pulsing fraction increases as a function of HV. The bias

was calculated using the (R+A) and A values given for each HV setting at the 4.5 and 64 μs windows to show this effect (**Figure 5.13**).

The trend of the bias over the HV range also does not support the fact that double pulsing is present in the system and is increasing as HV increases. However, there is a surprising response across the HVs studied. The bias is clearly negative, within uncertainty, up through 1660 V. This would mean that the accidentals count rate later in time (predelay + gate width + long delay) is greater than the (R+A) count rate measured. If we hold true the assumption that double pulsing is ever present across the RAD (i.e., with equal probability of its effects manifesting in the R+A and A gates outside of the double pulsing peak and charge collection physics), the difference between the two gates should still be consistent with zero. Within the region of 1680–1800 V, a statistically equal rate is measured to result in a bias consistent with zero. Then, from 1820 to 1860 V, the bias increasingly becomes more negative again, reaching a minimum at 1860 V. This trend is consistent with the maximum double pulsing fraction calculated in **Table 5.4** but its physical justification is lacking. Beyond 1860 V, the bias begins to trend toward zero again. There are stronger trends when the bias is evaluated for a shorter predelay, but it is not common to do so across a range of HVs in the field with these systems. Therefore, although bias could be a preliminary indicator of non-ideal behavior, within the standard 4.5 μs / 64 μs settings, it is not an obvious diagnostic, nor quantitative.

As has been shown, double pulsing does not clearly manifest in standard shift register–based data acquisition and analysis methods; and if it did, it is quite difficult to quantify. Because measurements are routinely conducted at a set predelay value and set gate width setting at a set HV, the double pulsing effects have traditionally been masked by the historical timing gates selected and specific analysis procedures. Longer gate widths, such as those used for operation of the UNCL (64 μs) aid in smoothing out this behavior while intrinsically elevating the measured count rates, further complicating its identification and quantification. This response is a main reason why double pulsing may not be widely acknowledged in the user community. Although the double pulsing contributions are not large, they are still present. The only clear indication that could be determined through standard measurements appears to be an increased count rate across plateau HV settings, which would be difficult to discern if a HV characteristic did not exist from a properly behaving system for comparison. Therefore, typical investigative measurements may not be adequate for easily identifying double pulsing using shift register logic and set predelay time intervals.

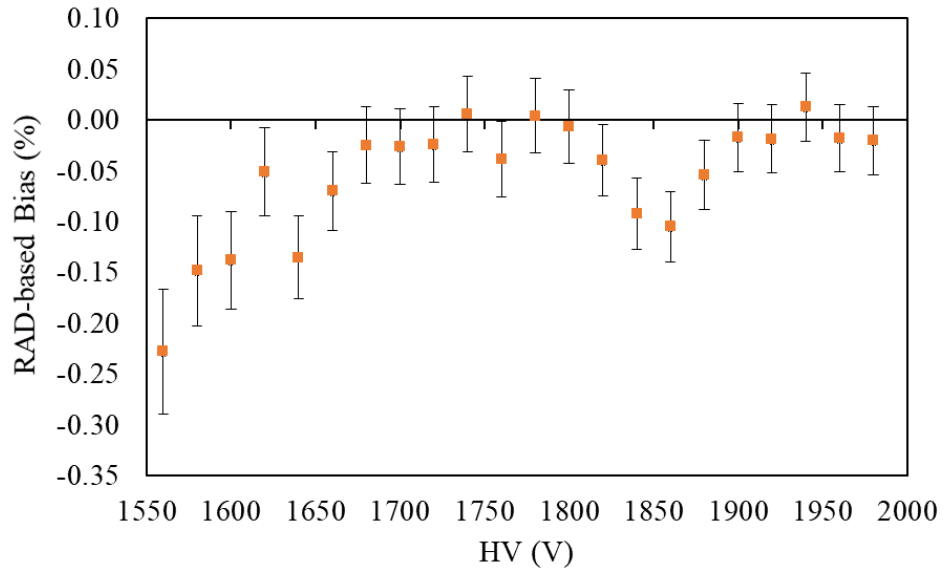


Figure 5.13. The calculated bias from the RAD (R+A) and A gates, of 64 μ s, across a range of HVs.

5.2.6 Double Pulsing Revealed with Non-Traditional Shift Register Measurements

Some nontraditional analysis of common shift register–based measurements may be more effective at revealing double pulsing effects if LMDA is not accessible. If shift register analysis is going to successfully diagnose double pulsing, users must be open to expanding how, and at what timing and HV regimes, measurements are taken at. The count rate data can still be obtained in a traditional matter, but additional analyses of these data may be performed offline to gain an expanded knowledge of the system’s behavior. Measurements must be taken using both a spontaneously fissioning neutron source and random–in–time neutron sources to reveal these features. In this case, LMDA was again used to sample the neutron pulse train as a shift register would to save measurement time.

A measurement of the ratio of doubles count rate to singles count rate squared was taken at a predelay of 4.5 μs and gate width of 64 μs . Because doubles scales as efficiency squared, and singles as efficiency, this ratio eliminates the count rate dependence on differences in efficiency as a function of HV. It also highlights differences generated by system performance abnormalities. This ratio should be equal for all HVs, as the doubles should trend with the singles equivalently across all settings. All HVs along the HV plateau region should certainly be in agreement as long as no non-ideal behavior is present. This analysis would also validate that efficiency differences are not mistaken as double pulsing contributions in Section 3 if the doubles to singles squared ratios were not the same for 1640, 1680, 1720, and 1840 V. The behavior illustrated in **Figure 5.14** was first introduced in [89] (Chapter 2). It is obvious that this behavior is not consistent across all HV settings, especially across the HV plateau settings. Since these ratios are different, it reveals underlying non-ideal behavior across these different settings. This approach would be the first, simplest, and most accessible diagnostic for any non-ideal behavior, as these rates are already obtained in a traditional system characterization when collecting the HV characteristic. This result appears to follow a similar trend to that shown in **Figure 5.13**.

By simple inspection of **Figure 5.15**, it is evident that there is some discrepancy in the system’s response as a function of predelay between all three HV settings, as was also shown in the traditional analysis of **Figure 5.11**. Fits are applied to the data within the 3–10 μs region with slightly varying slopes and intercepts. Again, all rates generated for the different predelay settings are correlated because the same pulse train is sampled. However, like **Figure 5.14**, the important aspect of this plot is the relationship of the ratios at the different HVs. The largest difference in behavior is highlighted in the region between a 0–1.25 μs predelay for 1840 V. This is consistent with the spike in doubles rate seen centered about 1 μs in the RAD.

The doubles rate at 1840 V dominates the doubles to singles squared relationship at short predelays because the double pulsing peak is large and is not excluded by these settings, which is a clear indicator of abnormal behavior. After the predelay encompasses the double pulsing peak at 1 μs , this ratio stabilizes and resembles the trends at both 1680 V and 1720 V, but its value is consistently lower. This would seemingly indicate a decreased double pulsing fraction relative to 1680 V and 1720 V as less counts are measured, implying there are less false triggers. As has been shown in previous sections, this is not the case.

The decrease in this ratio at 1840 V relative to 1720 V may be explained by the fact that an average singles count rate is being used across all timing settings for these HVs. The singles rate is not subject to predelays or gate widths. The singles rate would be both higher and lower than this average at different points across the full measurement time because of the determined probability of double pulsing occurring. However, the overall singles rate would be significantly greater at 1840 V than at 1720 V or 1680 V, because the greater double pulsing probability would cause a greater number of electronic events. As the predelay increases, and the doubles count rate decreases with the exclusion of the double pulsing peak at 1 μs , the singles rate remains at the elevated value because it is an average across the entire measurement. The resulting ratio is therefore less than that calculated for 1720 V. This resulting decrease

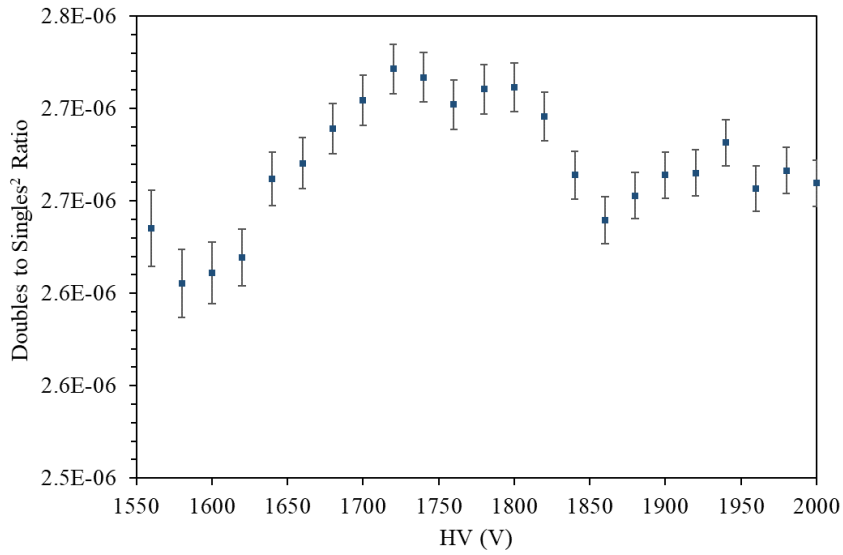


Figure 5.14. The ratio of double neutron count rate to single neutron count rate squared as a function of increasing HV, illustrating inconsistencies in system response due to double pulsing. [89]

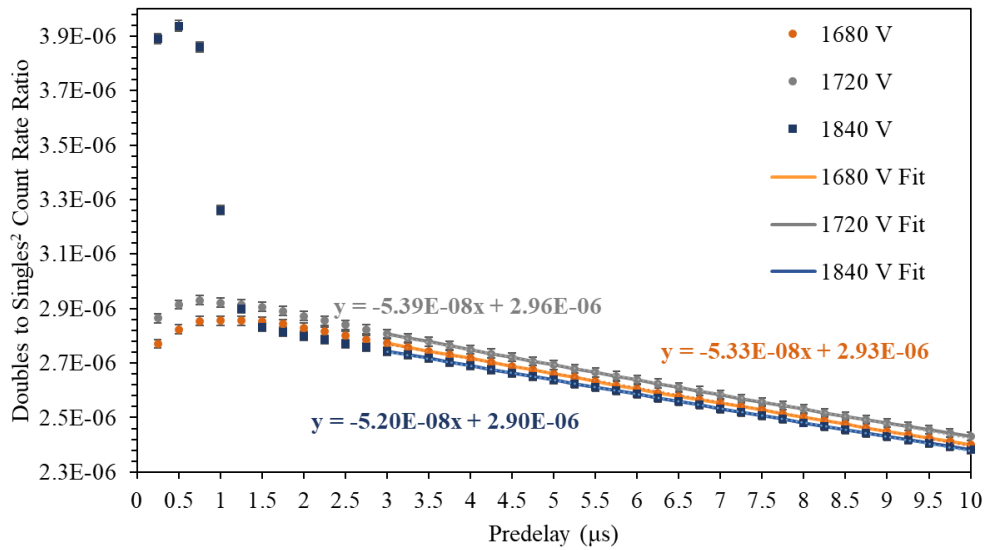


Figure 5.15. The measured doubles to singles squared count rate ratio values as a function of increasing predelay, with set gate width of 64 µs for 1680 V, 1720 V, and 1840 V.

in the ratio is a product of how this analysis is performed. Because of this, this diagnostic cannot be used quantitatively, but rather to indicate further investigation into the system is necessary.

For this to be a successful diagnostic, multiple HV settings would need to be sampled and compared for the different timing settings. Doing so would be quite time-intensive but worthwhile in a system characterization and a search for non-ideal behavior if efficiency differences are of concern. Even if the structure below 1.25 μs were not studied, the difference in ratios along the HV settings, as with **Figure 5.14**, would indicate concerning behavior for further investigation.

As has been stated, both the singles and doubles rates suffer from the effects of double pulsing (as does the triples count rate, but that is more complicated and not considered here), but there is no way to experimentally determine what the true rates should be. From Koehler et al. [48], the double pulsing correction factors for the singles and doubles rates are given by Eq (5.2) and (5.3). The measured singles, S_m , and the measured doubles, D_m , are used with the double pulsing fraction, r , to calculate the true singles and doubles rates. These true rates, S_0 and D_0 , respectively, would be measured by the system if no double pulsing were present. Rearranging and taking $\frac{D_0}{S_0^2}$ for the above relationship, results in an equation that is equal to $\frac{D_m}{S_m^2}$; this equation does not include r to allow any correction to these rates. This means that this plotted ratio will exhibit the influences of double pulsing on the measured rates across the different settings, but it is not clear how to quantify this effect using this diagnostic.

Another straightforward diagnostic for double pulsing involves measurements performed with very short timing gates to encompass the double pulsing peak, and not much else. A pre-delay of 0.5 μs and a gate width of 1.5 μs were used to acquire the measured doubles count rates from both ^{252}Cf and AmLi neutron sources as a function of HV applied to the system. Examining this behavior on a short time scale with a correlated ^{252}Cf neutron source and uncorrelated AmLi neutron source accentuates the double pulsing as a function of HV. This time range, from 0.5 μs to 2 μs , would capture a majority of the primary double pulsing events (and not the successive coincidences formed between a true event, another electronic event, or a background event with the electronic trigger), while also limiting the effects of dead time and charge collection behavior in the system. With these short timing windows, it can be assumed that the probability of detecting correlated neutron events produced from the ^{252}Cf is small and increases slightly with HV. There should be no truly correlated neutron events measured with the AmLi source. Nevertheless, low count rates are traditionally measured with the AmLi due to background events measured in coincidence with the single random-in-time neutron events from (α ,n) reactions. Because the plateau region of the JCC-71 should extend from approximately 1680 to 1980 V, the efficiency should be equal across the region. Therefore, the detection probability of these events should be equal throughout this region. These data should then reflect a stable low count rate attributed both to background events counted in coincidence in this short timing window, and to the small probability of detecting some correlated neutrons for the ^{252}Cf .

At lower HV settings (1560–1740 V), dead time effects within the first few microseconds of the (R+A) gate decrease the measured count rate (**Figure 5.16**). These dead time effects do not extend into the A gate. This allows more events to be measured here, resulting in a negative value when the (R+A)-A subtraction is performed to get the doubles count rate. The relatively high count rate measured between 1740 V and 1960 V can be attributed to double pulsing. This is emphasized in the AmLi random neutron response, as no net double neutron events should be measured, within counting statistics. Although this is a simple measurement, it is quite informative.

The double pulsing fraction may be calculated using the double pulsing fraction equation (Eq [5.1]) presented earlier. However, since the timing windows are significantly different from those used in a traditional in-field assay measurement, these fractions are not highly relevant to further measurements. As is shown in Section 3, the double pulsing fraction is heavily dependent on the timing settings selected. Since no counter is operated with these settings for a true measurement, and therefore this fraction cannot be applied as an accurate correction factor, this method serves best as simply a diagnostic of double pulsing behavior when using shift register logic.

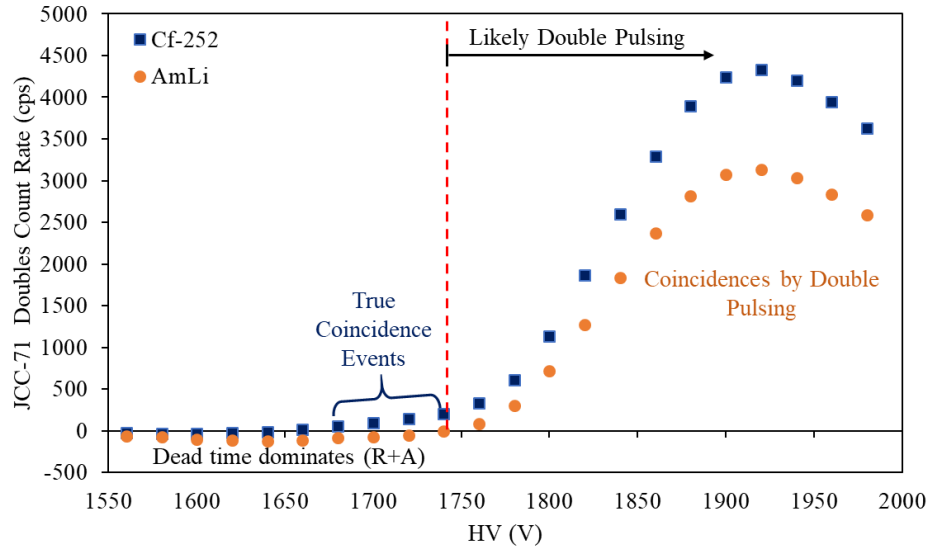


Figure 5.16. The doubles count rate measured with a 0.5 μs predelay, and 1.5 μs gate width for both a ^{252}Cf source and an AmLi source to reveal double pulsing. Error bars are smaller than the data points.

The same analysis may be done using applicable timing windows, 4.5 μs and 64 μs , but this analysis does not provide an obvious trend that may serve as a useful diagnostic because of statistical fluctuations dominating the double pulsing effect over this time regime (**Figure 5.17**). The doubles count rates at these settings are also compared between LMDA-generated RAD values for the net reals (~net doubles) count rate, as provided by PTR-32's Rossi Alpha subprogram, and the doubles count rate as reported by PTR-32's SDT subprogram, using the typical shift register gating structure on the same neutron pulse train. The (R+A) and A values given by SDT are not used since they are not given with an associated uncertainty. Instead the (R+A) - A subtraction for the net reals is calculated from the counts per bin given in the Rossi Alpha file for the 4.5 μs predelay and 64 μs gate widths. The large error bars allow these values to agree for most HV settings, but this difference in doubles rates indicates that there is some discrepancy between how these two subprograms of PTR-32 perform their calculations on the neutron pulse train, which will need to be investigated further as the choice of analysis package appears to affect results when using PTR-32. Because the documentation of the software and analysis used within PTR-32 routines is not well reported, we speculate that the discrepancy stems from the specification of the long delay used, the full acquisition time recorded, and the tagging of the events relative to the triggering event in the Rossi Alpha subprogram.

Therefore, including a doubles to singles squared analysis into a system characterization procedure would reveal the presence of non-ideal behavior, without large resource investments. But it cannot provide a quantitative analysis of the double pulsing fraction. It can instead be used to highlight the behavior of the system across a range of HVs, independent of efficiency contributions, as well as across a range of pre-delay settings, to isolate the primary contributing electronic effect at that setting. This would then prompt further investigation using LMDA methods. In addition, an analysis of a ^{252}Cf and AmLi source response in the system at short time gates would also emphasize the HV regime in which these effects are most prominent. An accurate double pulsing correction factor cannot be obtained by this method.

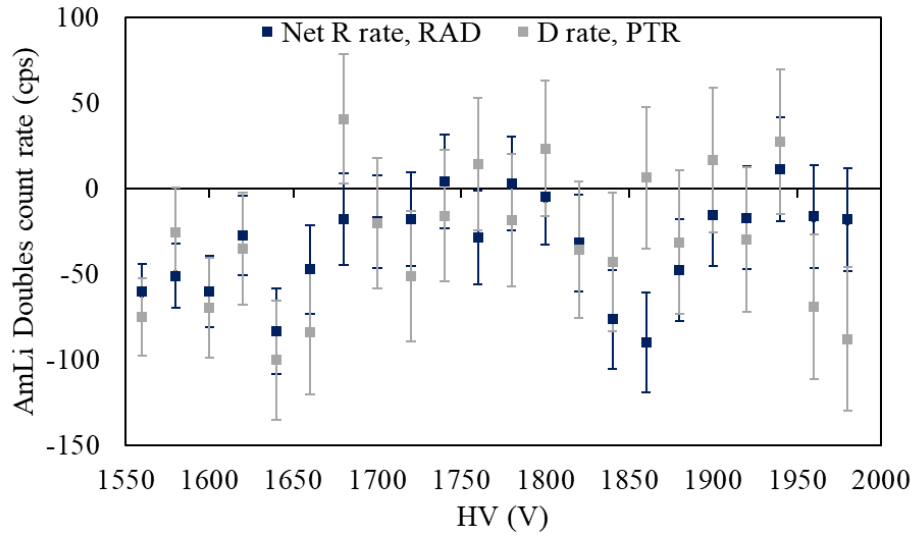


Figure 5.17. The doubles count rate measured with a 4.5 μs predelay and 64 μs gate width for an AmLi source, as determined through LMDA RAD values and shift register based analysis using PTR-32 timing windows.

5.2.7 Double Pulsing Fractions Determined Using a Comparison of High Voltage Characteristics

A final method to identify and quantify the double pulsing fraction at various HVs is done by comparing the HV characteristic of two equivalent banks of a neutron coincidence counting system simultaneously. These banks would need to have different electronics, with and without double pulsing, and the differences in measured count rates along the plateau would then be used to calculate the double pulsing fraction in that system. It is not common to have the opportunity to simultaneously measure the response from one bank of a neutron coincidence counting system with one set of electronics producing double pulsing effects, and measure a duplicate bank of the system with another set of electronics without any double pulsing effects. Therefore, this section serves more to validate the previously calculated RAD-based double pulsing fractions—since the methods described in Sections 5.2.4 and 5.2.5 were diagnostic and not quantitative in nature—rather than to propose a common diagnostic method that can be routinely used. However, this is a straightforward analysis method that could, in practice, be applied if a similar situation were available (e.g. if historical data were available using a system without double pulsing in comparison with a modern system with double pulsing).

One bank of the JCC-71, containing preamplifiers designed and built in-house at Oak Ridge National Laboratory (ORNL), was placed on a benchtop opposite another bank of the JCC-71 containing the A111-based board (the JAB-01). The ^{252}Cf source was suspended equidistant between both banks, and a simultaneous measurement was conducted using PTR-32 to obtain both signal sums of the respective banks. A HV characteristic was produced using a 4.5 μs predelay and a 64 μs gate width for 1200–1980 V in 20 V increments (**Figure 5.18**). The ORNL electronics have no double pulsing within the operational regime, and their performance has been optimized to match the response of the previous A111 electronics outside the double pulsing regions. The efficiency of both banks should be equal because of their replicate geometries. This measured count rate should then be constant along the HV plateau region. Thus, there should be a negligible increase in the measured count rate due to the increase in HV and the effective gain. Because the A111-based bank does not exhibit this HV-independent behavior, the difference in measured count rate can be assumed to be due to double pulsing effects. Note that the authors are not claiming superiority for the ORNL design against alternative designs [75] [76] in high-rate or fast-recovery situations. It simply provides a useful comparison for our purposes, especially because the shaping time could be readily tailored on the bench to better match the charge collection characteristics of the particular ^3He proportional counters and wiring configuration used.

The difference between the A111-measured count rate (S_m) and the ORNL-measured count rate (S_0) was taken as A_p for this calculation: i.e., the number of counts generated by double pulsing. The difference in this count rate is illustrated in **Figure 5.19**. Below 1680 V, the difference in count rate is negative. This finding can be primarily attributed to the slight difference in the charge collection and pulse processing chain performance of the two boards in this HV regime and not double pulsing effects. It is assumed that beyond this regime, the performance of the A111-based board is matched by the ORNL boards, so the difference in measured count rate is caused by the presence/lack of double pulsing in the circuits, respectively. At 1680 V, the difference in measured count rate was positive, which was also the HV at which double pulsing was first clearly evident on the neutron pulse train through RAD analysis. As the HV increased, the difference in count rates, A_p , increased. Therefore, the double pulsing percentage calculated also increased between 1680 and 1880 V. Beyond 1880 V, the difference in measured count rates decreased, as shown in **Figure 5.19**. This finding was again reflected in the calculated double pulsing percentage. The decrease can be credited toward the high gain at these HVs. With a sufficiently high gain, despite the double peak structure of the $^3\text{He}(n,p)\text{T}$ charge collection, the total pulse shape remains above threshold for the duration of the timing window, preventing the electronics from triggering twice for one single neutron event. As the HV increased, the amplitude of the signal increased. This allowed a greater fraction of the double peaked pulses to remain above threshold, which decreased the additional measured counts beyond 1880 V. Theoretically it is possible that if the gamma breakthrough

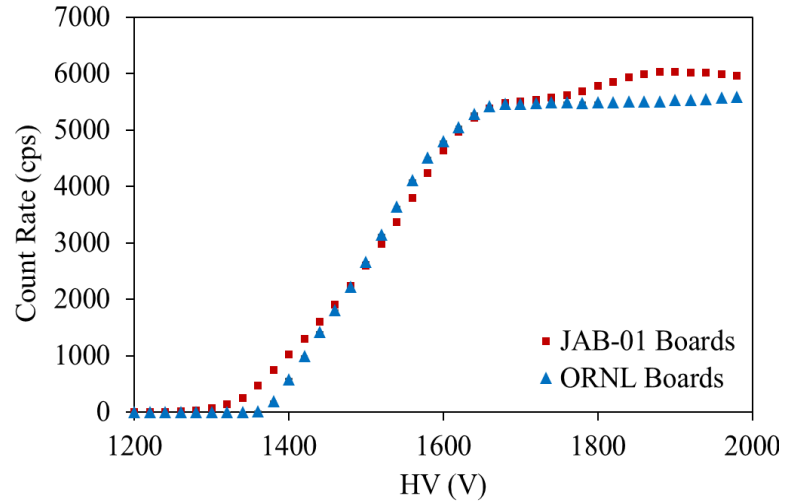


Figure 5.18. The HV characteristic (Section 5.1) produced for a simultaneous measurement of one JCC-71 bank with A111 electronics and another bank with ORNL electronics with the given experimental setup. The difference in performance across the HV range is attributed to double pulsing in the A111 and lack of double pulsing in the ORNL boards.

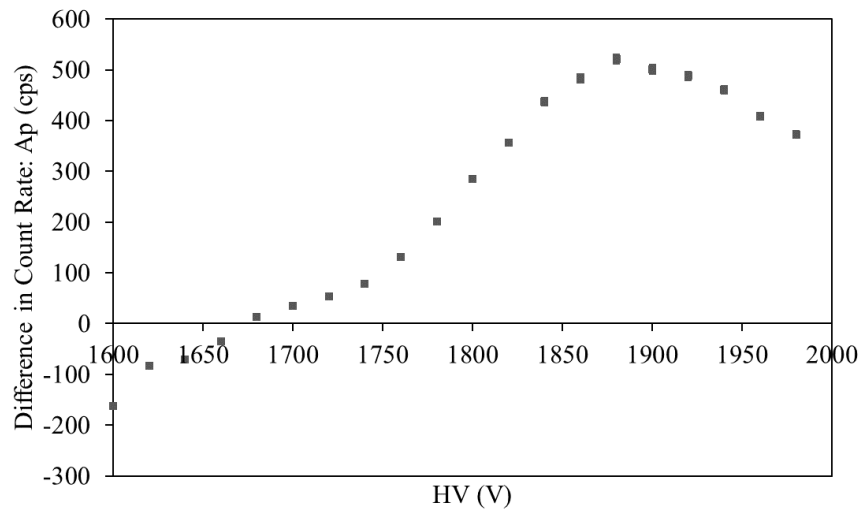


Figure 5.19. The difference in count rate measured between the double pulsing bank and non-double pulsing bank of the JCC-71 for various HVs.

Table 5.12. HV Characteristic-based Double Pulsing Percentage, with 4.5 μ s predelay and 64 μ s gate width, subtraction of singles neutron count rate values

HV (V)	1680	1720	1760	1800	1840	1880	1920	1960
r (%)	0.243	0.983	2.386	5.198	7.945	9.461	8.814	7.332
\pm	0.117	0.117	0.117	0.118	0.119	0.119	0.118	0.117

point were well beyond this regime, and the system could be biased beyond 1980 V, the measured count rate might reach a plateau once the double peak charge collection structure was above threshold for all pulses.

Using Eq (5.1), and these count rate differences, the double pulsing fraction, r , was determined as reported in **Table 5.12**. The difference in singles count rates, as measured between the A111–based bank and ORNL bank, are used in this expression. This is different from Section 3 where the doubles count rate difference is used to calculate A_p . These values were first compared with the results given in **Table 5.7**, **Table 5.8**, and **Table 5.9** using the RAD–based approach. **Table 5.7** and **Table 5.9** report the double pulsing percentage calculated at 1680 V with a 4.5 μ s predelay and 64 μ s gate width to be (0.1215 ± 0.0028) with the same ^{252}Cf source measured in this section. **Table 5.12** reports a double pulsing percentage of (0.243 ± 0.117) at 1680 V for this HV characteristic approach, with a 4.5 μ s predelay and 64 μ s gate width. Again, the results given in **Table 5.8** and **Table 5.9** for the 4.5 μ s predelay and 64 μ s gate width at 1720 V have a lower calculated percentage: (0.1459 ± 0.0030) compared with those given in **Table 5.12** (0.983 ± 0.117) , and the discrepancy between these two tables grows as HV increases.

This approach is quite different from the RAD–based approach. Instead of analyzing the neutron pulse train as a function of time, it takes two measured values—the average singles count rate for the A111–based bank and for the ORNL bank—and subtracts them. This uncertainty is then dictated by the measurement time. Subtracting two values at the same HV in the same measurement configuration with the same system efficiency does eliminate any efficiency dependence that may be entangled within double pulsing effects. Despite the challenge of separating the variation in performance between the two electronic systems due to fundamental processing differences from double pulsing effects, this approach is quite straightforward for analysis.

Interestingly, when the same analysis was performed again—this time taking the doubles neutron count rate values from the A111–based boards for S_m and the doubles neutron count rate values from the ORNL boards for S_0 to calculate A_p , but maintaining the singles neutron count rate as the denominator to determine r —the double pulsing fraction was in much better agreement with the RAD–based approach in **Table 5.9**. This is logical since the RAD subtraction uses doubles count rate values for A_p . Recall, the RAD is a histogram of double neutron events measured as a function of time in relation to the initial triggering neutron event. Therefore, when one RAD is normalized to another RAD, it is the subtraction of two separate doubles count rates, which is not outwardly stated in Koehler et. al [48]. So, instead, taking the values from the doubles HV characteristic results in the **Table 5.13** values. This approach then compared (0.016 ± 0.117) to (0.1215 ± 0.0028) for 1680 V, (0.146 ± 0.117) to (0.1459 ± 0.0030) for 1720 V, and (0.411 ± 0.119) to (0.5763 ± 0.0079) for 1840 V.

Table 5.13. HV Characteristic–based Double Pulsing Percentage, with 4.5 μ s predelay and 64 μ s gate width, subtraction of doubles neutron count rate values

HV (V)	1680	1720	1760	1800	1840	1880	1920	1960
r (%)	0.016	0.146	0.106	0.399	0.411	0.532	0.536	0.369
\pm	0.117	0.117	0.117	0.118	0.119	0.119	0.119	0.118

The ORNL doubles count rate values were not as stable across the plateau region as the singles count rates, as a result of the length of measurement and efficiency, and therefore, the double pulsing fractions were not as reliably determined as through the RAD–based approach. The ORNL preamplifiers are currently in the prototype phase, and they are undergoing optimization testing for better HV filtering and stabilization. This approach is therefore a proof of concept for a similar diagnostic tool and method. It also serves as validation that the previously calculated double pulsing fractions are the correct order of magnitude when determined either by the LMDA RAD approach or by shift register–generated neutron count rates.

5.2.8 Conclusion

As it has been shown, it is quite difficult to produce quantitative values for double pulsing fractions in a neutron coincidence counting system when shift register acquisition and analysis is used. Not only are the measurement requirements much more time-intensive than those for LMDA, but also the information gained by acquiring data at set timing windows inhibits easy identification of the behavior because of smoothing of effects over long durations (relative to 0.1 μs binning resolution or similar). The best diagnostic tools lie with LMDA, specifically through RAD normalization. However, it is possible to identify double pulsing when using shift register analysis if additional measurements are added into the typical characterization procedure of neutron coincidence counting systems. The most effective shift register-based analysis of double pulsing incorporates referencing historic data taken with a system known and proven to be double pulsing-free and comparing that with data taken with a modern system of the same model known to have double pulsing in mirroring conditions. Or, if the situation is available, an effective analysis incorporates taking a simultaneous HV characteristic measurement using identical banks with different electronics within them and comparing the count rate data for a quantitative analysis. A useful diagnostic measurement to identify whether double pulsing is present, and if so, in what HV regime—using shift register data acquisition and analysis—is measuring a spontaneously fissioning neutron source and a random-in-time neutron source at short time windows such as a 0.5 μs predelay and 1.5 μs gate width with the A111 to predominantly capture double pulsing events and no true coincidence events. In addition, plotting the doubles to singles squared count rate ratio for varying predelay values over several different HVs is also enlightening if any electronic artifacts are present in a system, as this ratio is self-normalizing. The singles and doubles should trend together at the same HV, and any differences across these HVs would indicate non-ideal behavior.

Although LMDA is gaining traction and its use is expanding in the field of international safeguards, it is still much more widely used in research and development applications at laboratories than for in-field measurements. Therefore, it is still necessary to provide effective shift register-based characterization tools that can, at a minimum, indicate to a user or manufacturer of a coincidence system that the behavior and performance should be investigated further. The tests outlined in Sections 4.2 and 4.3 would suffice for identification of non-ideal behavior using a shift register, which could then be followed up using LMDA for quantification.

The double pulsing fraction in the UNCL is also specifically evaluated for various timing windows using the LMDA-based RAD approach to quantify how this effect influences correlation timing analysis used in the field. At a standard operational HV of 1680 V and timing windows of 4.5 μs predelay and 64 μs gate width, the double pulsing fraction in this system configuration is approximately 0.12%. This added error is not large enough to be alarming for restructuring a safeguards measurement using the UNCL when considering other sources of error during a nondestructive assay that exceed several percent. The double pulsing fraction does change as predelay increases and as gate width increases over the range of HV plateau settings, since a different number of neutron events are included in the pulse train analysis. Therefore, a correction may become more relevant to A111-based systems that traditionally operate at short predelays and/or long gate widths, or higher HVs. This effect would also be much more significant for neutron multiplicity counters as the triples rate would be impacted to a greater degree by double pulsing than lower multiplicities.

This effect also becomes relevant as the applications of neutron coincidence counting are expanding. In terms of absolute source measurements, dead time calculations, physical assumptions made about the system when solving the point kinetic equations, and an overall understanding of the efficiency and charge collection process of these systems, double pulsing continues to be a hindrance. Unfortunately, these tests and evaluations of double pulsing at various timing windows must be performed on a system-by-system basis, as many factors contribute to this double pulsing fraction, so a general correction cannot be applied. Using the procedures outlined here and in (Section 5.1) the authors hope to encourage the users and manufacturers to check and quantify their systems for this behavior.

Chapter 6

Neutron Coincidence Counting System Dead Time Calculations

Neutron coincidence counting depends on the accurate measurement of fission neutrons as a function of time to correctly determine the quantity of nuclear material within the measured sample. As each neutron is captured and processed by the ^3He tube–electronics chain system in these counters, that chain remains busy, and “dead,” for a length of time. This means that any neutrons captured during this dead period are not counted and do not contribute to the total neutron pulse train. The resulting neutron count distribution histograms are perturbed due to this dead time, which influences assay values. The count rate response behavior can no longer be assumed to follow Poisson counting statistics, as the width of this distribution decreases due to the dead time [90]. Because of this influence on the neutron pulse train, another correction for the dead-time-related losses in the system is required.

A significant contribution to the uncertainty introduced during pulse processing by the data acquisition electronics is due to dead time effects. Dead time is generated in a combination of different components; there are contributions from the charge collection time in the proportional counters, the shaping time of the preamplifier to convert the analog signal into a TTL logic pulse, losses due to coincident signals falling within busy amplifiers, and processing time in the shift register or LMDA module. The dead time is rate and sample dependent, and it depends on the degree of correlation in the pulse train. Typically, a dead time value, or dead time parameters, are reported for a system using a range of commonly–used source types and activities, but it may vary slightly if a sample differs significantly from that range. This dead time is inherent to the system, and is characteristic of the tube diameter, bias applied, neutron and gamma count rate, and the electronic settings such as thresholds, shaping time, filtering networks, and derandomizer used. The dead period is related to the processing and recovery time of the electronics used and applies to each tube–electronic system within the counter. The more preamplifiers present in a system, the shorter the dead time for these ^3He counters. Using LMDA, the dead time can be determined for each individual ^3He tube–preamplifier system, a combination of a number of these systems, or the neutron coincidence counter as a whole. This value must be well-known to accurately adjust the respective measured neutron singles and doubles count rates for the true emitted rates to perform an accurate analysis.

It has been a great challenge to accurately describe the dead time in neutron coincidence counters. It requires extensive knowledge about the system behavior, well–understood neutron pulse train analysis methods and doubles multiplicity histograms, and an in-depth measurement campaign exploiting multiple sources. The long-standing and widely-used approach for totals and reals (singles and doubles) relies on empirical methods [91] rather than first principles. This method is essentially the only method used in routine system characterizations applied for NDAs. It will be described in detail below. Work by Dytlewski further develops this empirical method to incorporate triples count rate dead time analyses [92], and a recent paper discusses the challenges and limitations of these empirical methods to experimental scenarios that must be addressed and overcome in addition to extension of this method to all orders [93]. Others have also built on these methods over the last several decades. There is currently a revival of interest in better quantifying and modeling the dead time of neutron coincidence and multiplicity systems in terms of physical parameters. As technology improves, understanding the dead time of a system should not be the limiting factor in using these counters. These additional works derive alternative approaches to singles dead time corrections [72] [90] and investigate the effect of correlation in the neutron pulse train due to varying sources [94] [95], while also trying to simplify the theory and expressions for easy adaptation. This list is certainly not exhaustive, and it illustrates the revived drive to

accurately, precisely, and easily represent detector dead times based on true physical models. Generally, the final expressions and implementation of these theories to experiment are complex in these methods, and, as a result, they have not been adopted in favor of the older simplifications.

Currently, theoretical models of the dead time of neutron coincidence counters are based on the well-defined paralyzable (or updating) model. This model assumes that not only will a neutron captured during the dead period of the tube not be counted towards the total neutron pulse train, but that a neutron event will extend the dead period for a characteristic length of time. Each neutron event does this whether it's from the same fission event, background, or a successive fission event (**Figure 6.1**). Therefore, if this behavior is not taken into account when designing the circuit, the dead time may extend indefinitely, and no successive events may be recorded. Another assumption is that the neutron counter behaves as a single effective counting chain. Although this model has been assumed for neutron coincidence counting, it has not been fully verified. This compares to the non-paralyzable dead time model, where, following a detected neutron event, the dead time will be induced and occur for its characteristic duration. According to this model, if successive events are detected during this time, they do not extend the dead time beyond this set duration.

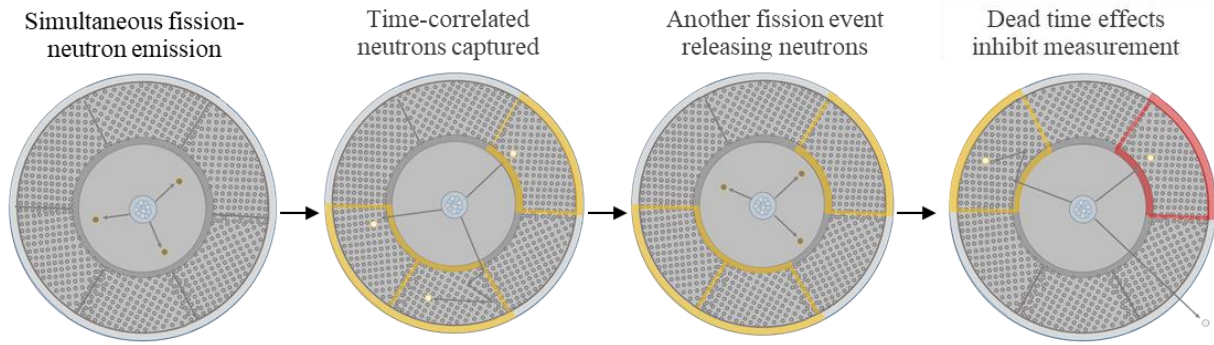


Figure 6.1. An illustration exaggerating the response of a neutron coincidence counting system to separate fission event neutrons. An example neutron coincidence counter is drawn here with 6 separate banks, each with their own preamplifier, separated by the dark gray lines. The yellow and red highlights indicate that the specific bank has captured a neutron and its associated preamplifier electronics are busy processing that event. For the red highlight, the preamplifier was already busy when the second neutron was captured, therefore this event will not be recorded. In reality, dead time may be induced through multiple fission events, or the detection of multiple neutrons from one fission event.

6.1 A Comparison of Methods Using a Boron Coated Straw–Based, High–Level Neutron Coincidence Counter¹

With current neutron coincidence counting data acquisition widely in the form of shift register logic, there are several options to determine effective dead time model parameters. A customary approach consists of incrementally overwhelming the counting system with various sources to generate different count rates for analysis. An empirical fit to these data can then produce a dead time parameter for correction to the measured rates. This method makes use of the expectation that the doubles to singles count rate ratio, after dead time correction, should remain fixed for the same isotope and counting system pairing, irrelevant of source strength. The common experimental approach to measure the dead time with this method makes use of multiple ²⁵²Cf sources of increasing strength to determine two dead time parameters. Another experimental approach for this method makes use of random-in-time neutrons produced by AmLi (α, n) sources— in conjunction with a single ²⁵²Cf spontaneous fission neutron source— to increase the uncorrelated single neutron events while maintaining the doubles neutron rate. For an uncorrelated neutron source, where the emitted neutrons have no time-dependent pattern (as a fissionable source would have), there is a very low probability that emitted neutrons will be counted as doubles. Therefore, the Reals + Accidentals count rate should be approximately equal to the Accidentals count rate in a RAD. A number of AmLi sources can be used with a single ²⁵²Cf source to incrementally overwhelm the detection system to generate different singles count rates for a similar analysis. The number and/or strength of the sources chosen should correlate with the full count range expected to be measured with the system in the field.

This traditional, and most commonly used, approach was established decades ago, and extended to greater multiplicities by Dytlewski in 1990 [92], assuming the paralyzable dead time model. This methodology was then applied for use in neutron coincidence counters such as the ³He-based High–Level Neutron Coincidence Counter (HLNCC) models [35] [70]. The combination of these works implements the following equations for the doubles (D) and singles (S) dead time correction factors (CF):

$$CF_D = e^{\delta_D \cdot S_m} = e^{(a+b \cdot S_m) \cdot S_m} \quad (6.1)$$

$$CF_S = e^{\delta_S \cdot S_m} = e^{\frac{1}{4}(a+b \cdot S_m) \cdot S_m} = CF_D^{1/4} \quad (6.2)$$

$$S_{DTC} = CF_S \cdot S_m, D_{DTC} = CF_D \cdot D_m \quad (6.3)$$

where δ_D is the dead time for the doubles, δ_S is the dead time for the singles, S_m is the measured singles rate, and a and b are the dead time parameters which are empirically determined for a specific detection system using various sources. Equation 6.1 represents the dead time correction factor for the doubles rate, and Equation 6.2 represents the dead time correction factor for the singles rate. Equation 6.3 is used to apply the dead time correction onto the measured rates. These three equations were previously given and used in Chapter 2 for the JCC-71 system characterization.

A chi-squared analysis is performed by minimizing the sum of squared errors between the measured doubles-to-singles, dead-time-corrected values to the calculated ratio. The free parameters a and b are determined by a quadratic fit using Equations 6.1 and 6.2 for these corrected doubles-to-singles count rate ratios as a function of increasing singles rate. It is common for counters of the same model to keep the ratio of a/b constant across all systems during characterization and calibration measurements,

¹ Aspects of this section are published elsewhere in a full journal article as A.T. Simone, J. P. Hayward, S. Croft, and A. Favalli. "A Comparison of Approaches to Determine Dead Time Parameters Using a Boron-Coated-Straw High-Level Neutron Coincidence Counter." ESARDA Bulletin 54 (2017): 6-13.

aiding in this analysis. The dead-time-corrected rates are then determined by multiplying the measured rate for the respective multiplicity by the appropriate correction factor.

Another more recently developed approach consists of utilizing the neutron count number distribution produced in a basic measurement using shift register or LMDA-based acquisition, for a number of counting cycles, to permit a statistical analysis and subsequent determination of the dead time along with a robust estimate of the statistical uncertainty. Using the approach laid out by Menaa [69], based on the theory outlined by Foglio Para and Bettoni [96], random-in-time neutrons produced by AmLi sources are used to obtain a neutron-count distribution. Then, a statistical analysis is performed on this distribution over many cycles. Moments of several orders can be used; therefore, several estimates of the effective dead time parameter are obtained [73]. With this analysis, the dead time parameters for second, third, and fourth order factorial moments can be determined, enabling an inter-comparison of values from a single data acquisition. These multiple samplings also allow for a robust estimate of the statistical uncertainty.

The equations presented in [96], under the assumption of a paralyzable not-free counter (the system starts counting the initial neutron pulse while it may be dead), represent the mean value of the count distribution and the variance of that distribution. They are then used by Menaa et al. [69] to derive expressions for the dead time, δ , in terms of the gate width, T_g , and the statistics of the neutron count distribution:

$$\varphi = 1 - \sqrt{1 - \frac{[\langle i \rangle - \sigma_i^2]}{\langle i \rangle^2}}; \quad \varphi = \frac{\delta}{T_g} \quad (6.4)$$

with $\langle i \rangle$ representing the mean value of the neutron count distribution as

$$\langle i \rangle = \frac{\sum_i i \cdot A_i}{\sum_i A_i} \quad (6.5)$$

and σ_i^2 representing the variance of the distribution as

$$\sigma_i^2 = \frac{\sum_i [i - \langle i \rangle]^2 \cdot A_i}{\sum_i A_i}. \quad (6.6)$$

Croft et al. [73] reviewed this method in detail and built upon this work to extend the same methodology to higher order moments of the neutron count distribution. This equation may be applied to third, fourth, and higher order moments if the precision on these measured rates suffices. This can all be done from a single measurement producing the neutron count rate distributions for each cycle. Typically for a neutron coincidence counter in a laboratory-based setting, triples may be acquired, using LMDA or the JSR-15, but they are not used in the field. Therefore, the second order moment is primarily used in the analysis of a neutron coincidence counter dead time here. Through simple measurement of an AmLi source, all necessary variables can be obtained in a short period of time.

Because the bias (previously defined in Chapter 2 and 5) should be approximately zero for an uncorrelated neutron source, the neutron count distributions should be roughly equal between the Reals + Accidentals and the Accidentals gates. To test this theory, the (R+A) and (A) neutron count distributions were analyzed separately to produce individual dead time values, checked for bias, and then combined into a single 48 cycle dataset for an additional dead time determination.

The importance of this method from a safeguards inspection perspective relates to the availability of sources for in-field measurements; AmLi sources are present for active interrogation in neutron coincidence counters. Meanwhile, it is uncommon for a facility under inspection to have ^{252}Cf source standards at that location. The strength of the AmLi is not crucial, as the values are derived from the measured neutron count distributions from the respective sources and not the given source activity. The stronger the sources, the better the statistics and the shorter the counting time, but the calculation of the

dead time parameter is not intimately dependent on the source strengths selected. Compared to the traditional method, the AmLi sources allow for shorter acquisition times with similar precision, and they do not have to be replaced as frequently due to the long half-life of Am isotopes.

Here the traditional approach and the statistical approach are implemented and compared using data obtained with a novel boron-coated-straw (BCS) High-Level Neutron Coincidence Counter (HLNCC) prototype. The same analysis procedures would apply to a ^3He -based neutron coincidence counter. These two methods are compared for the first time using the same system in an attempt to bridge the gap between the traditional empirical method, and a more modern calculation using measured neutron count distributions. Distancing neutron coincidence counter characterization procedures from empirically determined methods aids in furthering the field's physics-based understanding of the system behavior and hopes to lead to further developments in the modeling of this behavior from physics first principles.

The BCS HLNCC contains preamplifiers designed in-house by its manufacturer, Proportional Technologies Inc. Through extensive characterization of the system, it was determined that these electronics did not suffer from double pulsing in the relevant HV region. Because of this, the neutron pulse train is not obscured at short time lengths, and the dead time is not convoluted with non-ideal effects. This allows a detailed study of the dead time to be performed with confidence. Because these custom preamplifiers also had their own filtration networks, PTR-32 LMDA was used to bias, record, and analyze the neutron pulse train for each of the six counter channels (**Figure 6.2**). PTR-32 can produce output files in a form similar to those output by INCC (Chapter 1), including a neutron count distribution per every cycle recorded, in addition to neutron count rate analysis. The optimal timing gates for this system were determined to be 2 μs for the predelay, 48 μs for the gate width, and 4096 μs for the long delay. The total neutron signal was used for this analysis.

To determine the dead time parameter through the traditional empirical method, a single, newly-acquired, NIST-traceable ^{252}Cf source, with a known neutron emission rate around 94,000 cps and 1.10% relative standard error, was placed in the center of the BCS HLNCC. A 7200 s acquisition, using only the ^{252}Cf source, was obtained to ensure good counting statistics on the doubles count rate. Then, it was successively combined with a number of AmLi (α,n) sources in separate acquisitions of the neutron pulse train. The next measurement taken was of the ^{252}Cf along with two AmLi sources. These two AmLi sources had measured strengths around 7,300 cps with a count rate uncertainty of 0.11% with the selected timing gates. Because of the greater singles count rate, the acquisition time for this data collection was reduced to 1800 s. A third AmLi source, with a measured strength around 10,200 cps and a count rate uncertainty of 0.11%, was then added. Data were taken again for 1800 s. A fourth, and final, AmLi source, with similar strength to the third, was then added. For this run, the acquisition time was increased to 2700 s to give a greater certainty of the count rate, as this is crucial for producing an accurate fit using the endpoint. The time-correlated fission neutrons from the ^{252}Cf are recorded in these timing gates and the random-in-time neutrons produced from the multiple AmLi sources provide excess counts on which to trigger. This method benefits from the convenience and availability of using one ^{252}Cf source, while still having the ability to determine the dead time corrections for both the singles rate and the doubles rate.

From these acquisitions, the doubles-to-singles ratio was calculated from the measured rates as a function of singles rate (which is dependent on the number of sources used). This trend is shown in **Figure 6.3**, and the empirical fit, reflecting the ratio of the dead time-corrected rates calculated using Equations 6.1 and 6.2, is shown with the dotted red line. From these fit values and chi squared analysis, the a and b parameters are determined. For a set of standard counters, the ratio of b/a has typically been determined previously using a large number of ^{252}Cf sources; but for this new BCS HLNCC, there is no predetermined ratio. Instead, assuming that $b = \frac{a^2}{4}$ as outlined in the literature [72] [90], the fitting parameters were found to be $a = 6.53 \cdot 10^{-8}$ and $b = 1.066 \cdot 10^{-15}$, resulting in an average dead time of (0.0653 ± 0.0054) μs . The uncertainty in this value was determined through chi-squared analysis of minimizing the sum of squared error and is relatively large due to the reasons discussed previously. Next, b was constrained to 0, as is oftentimes done, and a was found to be $6.199 \cdot 10^{-8}$, producing a dead time



Figure 6.2. The BCS HLNCC showing (a) the six detector bank outputs; (b) the BCS HLNCC-specific conversion box containing electronics to shape and amplify the output signals, resting on the external power supply used for the +5 V; (c) the output signal cables of the conversion box; and (d) PTR-32.

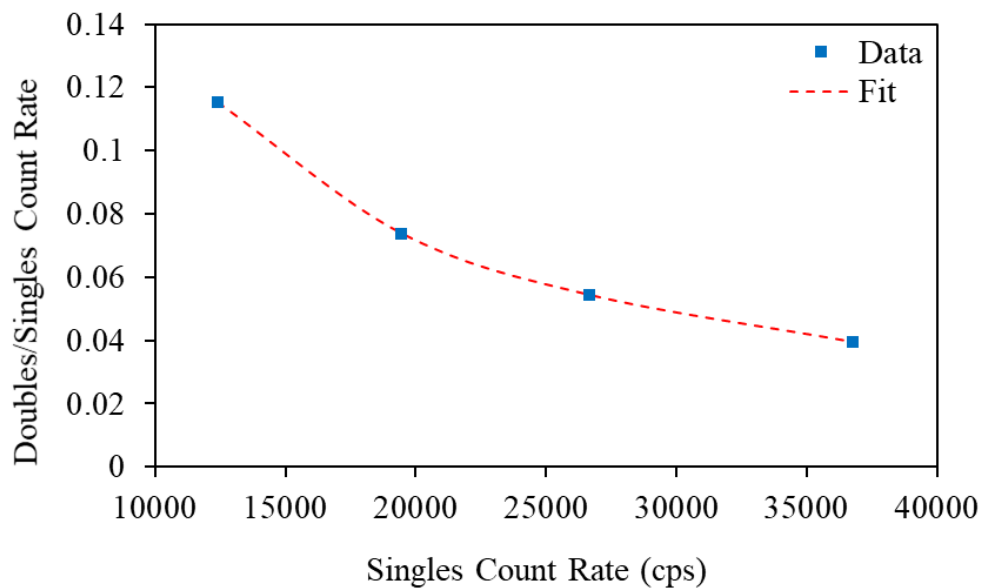


Figure 6.3. A plot of the measured doubles-to-singles count rate ratio as a function of the measured singles count rate. An empirical fit used to determine the dead time parameters is shown as the dotted red curve. The error bars are smaller than the markers.

of (0.0620 ± 0.0077) μs . The dead time values found are within error using the different empirical constraints, due to the insensitivity of the equations to b over a wide range of values.

This empirical dead time correction method is not robust, as it relies on a user to manipulate the terms to produce the best fit. This method is also sensitive to the number of data points acquired, and length of acquisition, thereby increasing the total experimental time and number of sources needed for a more accurate result. Because of this, there can be several values which minimize the sum of squared errors of the deviation between the dead-time-corrected doubles-to-singles ratio to the uncorrected ratio with respect to a and b .

Then, the dead time parameter was determined through the statistical method of analysis on multiple data acquisition cycles outlined by Equations 6.4-6.6. Twenty-four cycles of 300 s data acquisition runs were taken to randomly sample the neutron count distribution, produced by the AmLi sources previously listed, a large number of times. The AmLi sources were centered vertically and radially within the well to load an approximately even count rate on each of the six detector banks. Two separate acquisition runs were taken, one using two AmLi sources for a combined measured singles count rate of approximately 14,000 cps with a standard error of 0.02%, and the other using all four AmLi sources for a combined measured singles count rate of 33,500 cps with a standard error of 0.016%. The total neutron pulse train recorded in PTR-32 was exported to INCC format to produce the count distributions. As is customary with shift register electronics and INCC software, the neutron distributions in each of the cycles are reported as a function of multiplicity for both the (R+A) and (A) gates. Detected neutron multiplicities can range up to, on average, approximately 10 neutrons per cycle due to background events falsely measured in coincidence with AmLi single neutron events. These count distributions were analyzed using the second order moment expressions to determine the dead time and verify that the bias was consistent with 0 in support of the combined dead time values. The results are reported in **Table 6.1**.

As expected, there is less uncertainty in the dead time calculated for the measurement using four AmLi sources rather than just two sources, due to better counting statistics. However, as is typical for in-field measurements, two AmLi sources may be more readily available and still provide accurate evaluations of the detector dead time. The bias is consistent with 0, the individually calculated dead time values are consistent within counting precision across sources, and, therefore, the average dead time values between (R+A), (A), and the combined gates are also in agreement.

The comparison of the dead times determined from both the traditional and statistical methods are shown in **Table 6.2**. The traditional approach values are reported for two different empirical fits: where $b = \frac{a^2}{4}$ and when b was constrained to zero. The combined gate average dead time value, obtained from both the two source and four source measurements, are reported for this comparison. The dead time values are in agreement within uncertainties (**Table 6.2**) across all calculations. It is evident that the uncertainty in the neutron count distribution analysis approach is much less than the uncertainty associated with the traditional approach. This is due to the traditional method's insensitivity to b in its equations over a wide range of values, and the number of experimental data points used to find the empirical fit.

This result verifies that the statistical approach of dead time analysis is robust and appropriate as an alternative to the empirical approach. Compared to the empirical method of dead time parameter determination, the statistical method is more heavily grounded in true physical parameters that may be measured with the system; this compares to the user-manipulated fits that are dependent on the constraints selected for analysis. It provides an experimentally determined approximation to the neutron multiplicity counter's dead time which may be simpler to grasp and implement, returning values with greater confidence due to the robust uncertainty calculations. This alternative method may allow neutron coincidence counter characterization procedures to rely more heavily on physics-based understanding of each system's behavior and also lead to further developments in the modeling of this behavior from physics first principles.

Table 6.1. Total detector dead time values calculated using the second order factorial moment.

Number of AmLi Sources	$\delta(R+A)$ (μs)	\pm	$\delta(A)$ (μs)	\pm	$\delta(\text{Combined})$ (μs)	\pm	Bias (%)	\pm
2	0.0669	0.0050	0.0657	0.0054	0.0663	0.0036	0.0008	0.0197
4	0.0641	0.0015	0.0652	0.0018	0.0646	0.0012	0.0060	0.0069
Average	0.0655	0.0052	0.0654	0.0057	0.0654	0.0038	0.0034	0.0209

Table 6.2. Comparison of total detector dead time values using the traditional method and the statistical approach.

Method	δ (μs)	\pm
Traditional- $b=a^2/4$	0.0653	0.0054
Traditional- $b=0$	0.0620	0.0077
Statistical- 2 sources	0.0663	0.0036
Statistical- 4 sources	0.0646	0.0012
Statistical- Average	0.0654	0.0038

6.1.1 Dead Time as a Function of Preamplifier Number

It is well known that the dead time varies based on the number of preamplifiers used within a system. The more ^3He tubes (or BCS) connected to a single preamplifier, the longer the effective paralyzable dead time is since the likelihood of a neutron capture increases with an increasing number of ^3He or ^{10}B atoms. This would subsequently occupy the electronics of that system with the pulse processing for each capture event for the characteristic duration. But if numerous preamplifiers are placed within a system, this tube-preamplifier pairing ratio decreases, and it is less likely that a pairing will encounter two successive neutron events over the dead period due to the isotropic behavior of emissions from a fission event. This means it is less likely that the pairing will be busy processing a previous capture event when another neutron is captured. Less events will then be lost. If there are multiple channels, even if some channels are occupied processing an event, there are others that may not be dead that can simultaneously record a capture, which decreases the effective system dead time. The more pairings, the lower the effective dead time becomes. This behavior is studied across a various number of preamplifier combinations contributing to the total measured neutron pulse train. For each combination of preamplifier number, the effective dead time is calculated.

The statistical approach of dead time analysis was used here. The results in **Figure 6.4** show calculated values for the combined (R+A) and A gate dead time. For this analysis, a single measurement was taken and a variety of channel number combinations were analyzed offline with LMDA. Initially, the dead time for all six individual channels of the BCS HLNCC was calculated. This results in the characteristic dead time of a single preamplifier, or a readout subsystem dead time. This value is understandably the greatest dead time value as there are no alternative tube-preamplifier pairings to capture and process another neutron event while this one pairing is dead. Every neutron coincidence counting system should have a slightly different characteristic channel dead time based on the electronic settings used, tube pressure and diameter, and applied HV.

Then, the neutron pulse trains from two detector banks, channels 1 and 2, channels 3 and 4, and 5 and 6, were summed and analyzed. There is a very small difference in the calculated dead time values across these different combinations. This may be due to small variations in the geometry or electronics across the different channels. Combinations for channels 1, 2, and 3 then 4, 5, and 6 were used for the

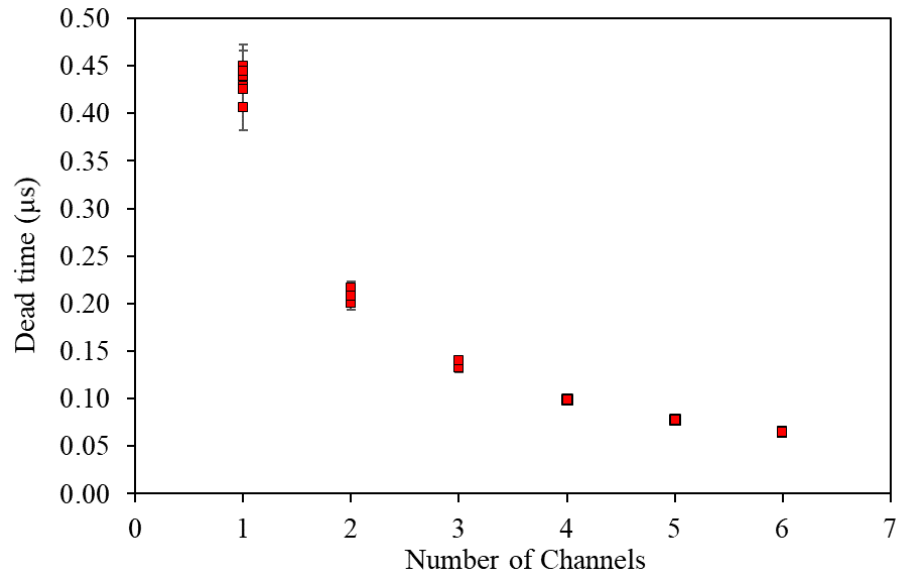


Figure 6.4. The dead time determined using the statistical analysis approach is shown for a variety of channel combinations in the BCS HLNCC.

dead time value for three channel sums. Insignificant differences in the dead time values between these two different combinations were recorded. For the four channel result, channels 1, 2, 3, and 4 were used and finally for the five channel dead time calculation channels 1, 2, 3, 4, and 5 of the BCS HLNCC were used. The total summed pulse train returns the minimal dead time value calculated across all combinations. It is shown in **Figure 6.4** that the more channels used in a system, the lower the system dead time is. The dead time decreases from an average single preamplifier dead time of (0.4229 ± 0.0153) μs to the total system dead time, using all 6 preamplifiers, of (0.0646 ± 0.0012) μs . This is due to the likelihood that even while one preamplifier may be busy, there are increasingly more preamplifier–bank systems that will not be busy and can detect successive events during that time.

Therefore, not only do additional preamplifiers help with the spatial response signature of a source, as presented in Chapter 4, they also fundamentally lower the system dead time to allow a more in–depth study of the other system parameters. With a lower effective system dead time, less events will be lost during an NDA and a smaller correction factor may be applied with lesser uncertainty. This would effectively increase the system efficiency without changes to the system geometry or composition. With LMDA, the additional channel signals are easily recorded and analyzed. In addition, without dead time behavior convoluting other behavior at short time bins, diagnosing and quantifying double pulsing may be more straightforward. This would also allow for more reliable studies of the system behavior at short predelays with a more well defined, and shorter, dead time duration. Finally, the system dead time may then be better studied and modeled to isolate to the correct behavior and calculation method on a more fundamental scale. Once this is done, more accurate dead time corrections may be applied to existing systems. Or, if the addition of multiple preamplifiers in current neutron coincidence counting systems may be done at an affordable cost, the additional benefits of their inclusion would also be reflected in aspects of system design, analysis procedures, and final NDA results.

6.2 A Difference in Values Due to Double Pulsing Using a JCC-71 Neutron Coincidence Collar

The same statistical dead time analysis methods and channel–by–channel combination analysis may be applied across a wide range of neutron coincidence counters. However, for systems such as the original JCC-71 with the four JAB-01 boards, and any other systems with double pulsing present within the HV operational region, dead time methods are not in agreement due to the effect that double pulsing has on the neutron pulse train and any affiliated analysis performed on it. Since the previously discussed traditional method and statistical method rely on different information from a measurement, they return different dead time values when characterizing the JCC-71.

It is important to note that since the JCC-71 UNCL is designed for low count rate applications of measuring fresh fuel assemblies, there is no dead time correction applied in the field. Instead, the dead time effect on the measured rates is included empirically in the doubles versus ^{235}U g/cm calibration curve, alongside the efficiency and die-away time values. Therefore, this deviation is not significant to the UNCL’s application, but stands as a representation and common model of other A111–based neutron coincidence counters that may have double pulsing present in their HV operational region.

Referencing the dead time parameter characterization originally presented in Section 2.5.5, the traditional empirical analysis was performed using the a and b parameters given by Canberra Industries during their system characterization. Given $a = 1.07$ μs and $b = 0.53$ ps with an a/b ratio set at $2 \cdot 10^6$ from historical data, the system coincidence dead time was found to be 1.1 μs . The dead time parameter for the singles count rate can therefore be approximated as $a/4$ (Equation 6.2), resulting in a system dead time of 0.27 μs . The same neutron pulse train was analyzed four ways: the previously described method with $a = 1.07$ μs and $b = 0.53$ ps , with $a = 1.07$ μs and $b = a^2/4$ [72], along with b set to 0, and, finally, eliminating a data point from the fit to study the sensitivity. This study of dead time values revealed that this data set did not generate a precise result, with final dead time values ranging by

approximately 20%. This result is as expected when using the empirical method since it is highly insensitive to the selection of b , is manipulated by hand by the user, and is strongly dependent on the number and strength of the sources used. The statistical dead time analysis was performed on a neutron pulse train acquired similarly to that acquired with the BCS HLNCC using AmLi sources. Using LMDA, the total system coincidence dead time was found to be 0.1648 μs , with individual channel dead times ranging from 0.685-0.717 μs (**Table 6.3**). These values are clearly not in agreement. However, these two methods previously produced values that were in assured agreement for the BCS HLNCC and the ^3He -based LV AWCC; both of which did not have double pulsing present at the HV used for the measurement.

The full system behavior, including dead time effects and double pulsing, may be revealed through the RAD produced from the measured neutron pulse train. This is reflected in its structure, including zero count rates measured across a range of time bins and the spikes in count rate compared to surrounding bins. The RAD provides a cursory visualization of the dead time and electronic stability of a system by binning the coincidence neutron events into small time dwell bins. For the PTR-32, the smallest time bins achievable are 0.1 μs , which suffices to resolve features attributed to these effects to a high level of fidelity. The RAD is true measured data and does not rely on approximations or assumptions of the behavior of the system, therefore what it reveals is difficult to dispute. Both discussed calculation methods return experimental approximations for the dead time values, and, therefore, may be slightly different than what is observed in the RAD.

Figure 6.5 shows RADs produced for each of the four JAB-01-based JCC-71 channels at 1720 V, and the total summed signal from these banks on different scales. When examining the individual detector bank RAD responses, zero counts per bin are recorded between 0 μs and 0.4 μs ; this is consistent with dead time, where no coincidence events can be registered successive to the triggering neutron event. Then, between 0.4 μs and roughly 0.7 μs , the drastic increase in count rate signifies the recovery of the preamplifier system combined with charge collection effects in the ^3He tubes (Chapter 3 contains a discussion of the JAB-01 electronics specifications). A small double pulsing peak is measured between 0.5 μs and 1 μs (see Chapter 5). After this artifact, more structure can be observed until the signal stabilizes around 2 μs . This may be related to ultimate charge drifting and collection effects and the further stabilization of the electronics. Then, the count rate begins to follow the expected exponentially decreasing trend of a RAD. The RAD produced from the total signal data reinforces these claims. From the 0-0.1 μs time bin, there is an increase in count rate. Between 0.1 and 0.4 μs , there is approximately $\frac{3}{4}$ of the count rate measured at 2 μs and beyond, which supports one of the four detector banks being dead over this duration. Because the total signal relies on all four channels, it will still register neutron events in three out of the four banks while a neutron event is being processed in the last bank; as was shown in Section 6.1.1, the dead time of a total system is much less than the dead time of a single preamplifier chain (JCC-71 values reported in **Table 6.3**). Then, following the same trend as each individual channel, the count rate increases between 0.4 μs and 0.7 μs , followed by the double pulsing peak, before reaching the stable decreasing exponential trend at 2 μs .

Depending on how the traditional and statistical dead time calculation methods isolate the values for their results, the dead times could, in principle, be justified between the range of 0.4 μs up to 2 μs for an individual channel coincidence dead time and the range of 0.1 μs up to 2 μs for the total summed signal. A 1.1 μs total system dead time may indicate that the traditional method is sensitive to the effects of double pulsing, as following 1.1 μs the total signal RAD no longer decreases but increases until it reaches a more stable response. As for the statistical approach, the total system dead time was determined to be 0.16 μs . The lowest doubles count rate in the RAD is measured between the 0-0.1 μs time bin. Beyond the 0.1 μs time bin, a decreased stable count rate is measured between 0.1-0.4 μs , indicating one of the four banks is dead. Following this range, a double pulsing peak can be resolved and the total measured signal reaches a stable value below 2 μs . Resolving this behavior may be subject to the time bin resolution available in the PTR-32 analysis software, limiting the ability to further discern the system response at short time intervals; but this cannot be investigated as the bin values are not adjustable by the user. The individual channel dead time values determined through the statistical approach may also be

Table 6.3. The dead time values calculated for the JAB-01–based JCC-71 using the statistical analysis method

Channel	$\delta_{(R+A)}$ (μs)	$\delta_{(A)}$ (μs)	$\delta_{(Combined)}$ (μs)
1	0.699 ± 0.012	0.666 ± 0.014	0.6824 ± 0.0092
2	0.685 ± 0.012	0.688 ± 0.014	0.6865 ± 0.0091
3	0.717 ± 0.011	0.701 ± 0.013	0.7091 ± 0.0085
4	0.615 ± 0.010	0.622 ± 0.011	0.6187 ± 0.0075
Total	0.1648 ± 0.0021	0.1635 ± 0.0022	0.1641 ± 0.0015

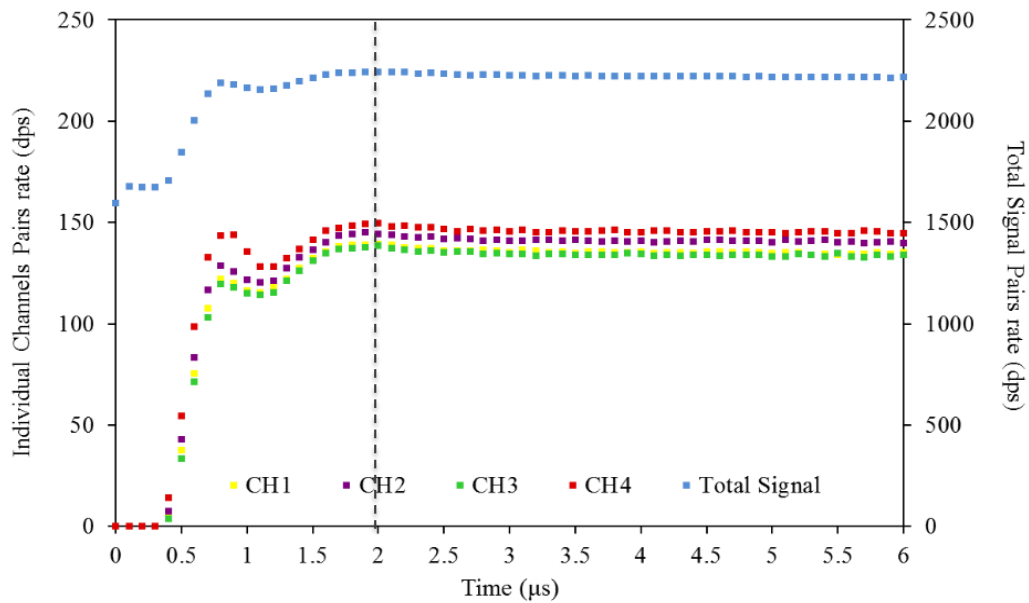


Figure 6.5. The RADs produced for the four individual JCC-71 banks and the total summed signal. The dotted black line indicates where the measured count rate stabilizes.

justified by their respective RADs. The contribution of double pulsing clearly convolutes and obscures the dead time behavior within this region, but dead times ranging between 0.685-0.717 μs coincide with the point where a majority of the expected count rate is being recorded. There is an increase in measured rate within the double pulsing peak following these dead time values, which then decreases, increases, and reaches a stable value around 2 μs . This complicates the interpretation and modeling of this behavior, to ultimately deceive dead time analysis methods.

Although both the statistical experimental approach and traditional experimental approach to dead time analysis provide consistent results when characterizing a system that does not suffer from double pulsing, they break down when double pulsing is present. They no longer provide reliable dead time values that can be traced back to physics first principles. This would affect any dead time parameter calculation performed on a system with unknown double pulsing. The speculation surrounding how the calculated dead time values relate to what is seen on an experimentally obtained RAD, for a system with double pulsing, indicates a need to be able to simulate the effects of dead time within a system with confidence. Simulated neutron pulse trains should be analyzed to produce their own RADs with the various dead time values across different models such that the intricate response may be compared to experimentally obtained RADs.

Beginning with the first principles of the neutron capture in a ^3He tube or a BCS, it would be extremely beneficial to track the formation of each neutron pulse, its resulting pulse processing and induced dead time, and the final time stamp on each event forming a simulated neutron pulse train. This would require extensive simulation packages including gas capture physics and simulations for the charged particle clouds, an electronics pulse processing simulation software, and neutron pulse train analysis software that could analyze the output of these combined simulations. Several existing codes that may be suitable for this analysis are discussed in the Future Work section of Chapter 8.

Chapter 7

Absolute Source Measurements

Neutron coincidence counters capture neutrons released by fission reactions in an item and convert the current generated through their related ionization interactions into logic pulses as a function of time. These detected neutron events, and their correlation over time, may be used with the point kinetic equations (PKE) to calculate the relevant sample effective mass in an NDA. When these neutrons are collected over a period of time using LMDA, a neutron multiplicity histogram can be generated from the frequency of the number of time correlated measured neutrons; where the number of zero neutron events measured in a set timing window following the initial triggering event, one neutron event in that timing window (singles), two neutron events in that timing window (doubles), etc. are summed over the measurement time [4]. Each isotope has a unique signature through this analysis, which allows for mass identification when paired with gamma spectroscopy.

However, it is not simple to perform this NDA analysis. The PKEs are dependent on many potentially unknown parameters that must be determined by system characterization and calibration using standard sources in a laboratory or industry setting, and at the time of the NDA measurement in the field using the item under question. Some of these parameters include: the source's spontaneous fission rate, the source's induced fission rate (or sample self-multiplication, and its variation across the sample), the (α ,n) reaction rate in the sample, the neutron capture in the sample, the spatial variation in neutron detection efficiency, the energy spectrum effects on detection efficiency of the system, and the neutron die-away time in the detector [4]. These parameters are taken from nuclear data, with associated uncertainties, through simulation, extensive characterization and calibration, and from estimates from fissioning source standards as a representation for ^{240}Pu . It is therefore crucial to have reliable source standards and calibration methods with low associated uncertainties for a quantitatively accurate NDA. The strengths and characteristics of the source standards must be known to a high precision to avoid propagating significant errors further into the final determination of effective mass.

Typically, ^{252}Cf source standards are used. They are often certified sources, calibrated using a MnSO_4 bath at a national standards laboratory [86] such as the National Institute of Standards and Technology (NIST) [97]. The accuracy of the national standards laboratory measurement emission is of the order of $\pm 1\%$. A counting system's efficiency can then be calibrated using the known ^{252}Cf neutron emission rate, and then scaled for a ^{240}Pu source using known nuclear data (energy spectra and multiplicity distributions) [4], and so a calibration for ^{240}Pu neutrons can be obtained with a somewhat higher uncertainty. Other standards would suffice, and other calibration methods are possible [98], but the most commonly used approach implements ^{252}Cf standards and relates the counting system's performance to that expected when measuring ^{240}Pu . Unfortunately, certified ^{252}Cf sources typically require a several month lead time with high associated costs to produce and measure in the MnSO_4 bath and have an approximate 2.65 year half-life so they must be replaced frequently. Also, numerous certified sources are necessary in facilities where a large variety of sample activities are used.

Instead, an alternative method for self-certification of a ^{252}Cf source using an in-house procedure to determine the absolute neutron output has previously been proposed and tested using neutron multiplicity counters [87] [88] [99]. This passive counting Absolute Californium Determination (ABCD) method utilizes commonly-available safeguards resources to obtain a source strength estimation precision on par with national standard facilities' capabilities. This is achieved by long measurement times, which are possible in a research laboratory, with low associated costs. In this approach, the correlated neutron counting technique is applied absolutely. This means that for the ABCD, the doubles neutron count rate

must be obtained at an effectively infinite gate width relative to the operating gate width of the system, and at a zero pre-delay; i.e., the measurement is independent of any timing settings traditionally set with these counters to collect the total number of neutron events interacting with the system.

The neutron coincidence counting used for this analysis must also be characterized for dead time, die-away time, and any non-ideal behavior. Combining these system parameters, nuclear data for the ^{252}Cf source neutron output properties, and applicable counting rates at the operational timing windows, provides the absolute determined neutron source output of the ^{252}Cf in question.

This has previously been achieved using traditional shift register logic, where multiple measurements were obtained independently and recorded for each of the different time windows selected [99], in addition to LMDA where a single pulse train was obtained and various timing settings were applied to the neutron pulse train in post-analysis [87] [88]. An in-house LMDA unit, the LMMM, was used for this testing at LANL [87] [88] in addition to the JSR-15 at ORNL [99].

This chapter investigates if this procedure can be extended from high efficiency neutron multiplicity counters to neutron coincidence counters, since the previous works used counters with some of the highest efficiencies of all safeguards counters, such as the Epithermal Neutron Multiplicity Counter [66]. Here a less efficient traditional safeguards counter, a variant of the Active Well Coincidence Counter [33], the LV AWCC, with the PTR-32 LMDA module is used. Using neutron coincidence counters also restricts the data acquisition and PKE analysis to using the singles and doubles rates, rather than the singles, doubles, and triples as with neutron multiplicity counters. The procedure for this LMDA absolute measurement and extrapolation analysis is summarized, and the results of 3 separate ^{252}Cf sources are compared to the NIST certificate. It also tests the precision of results found using the pairing of the neutron coincidence counter and LMDA.

Because the same pulse train is sampled for the different timing windows using LMDA, unlike with a shift register measurement, the extrapolated count rate results are innately correlated. This complicates the uncertainty estimation, which influences the precision of the absolute source rate determination. For the first time various uncertainty estimations are proposed to account for this correlation. The impact of characterization parameter uncertainties is studied, in addition to the validity of the extrapolation analysis provided by the PTR-32 software. The uncertainty contributions generated by assumptions and approximations made throughout this procedure are also investigated.

7.1 Absolute Source Measurement ^{252}Cf Certification Procedure

The idea of ABCD is centered around determining the expected doubles count rate output from a neutron source, independent of any counting system timing parameters. To calculate these values, a zero pre-delay must be used to avoid eliminating relevant neutron events following the triggering event (**Figure 7.1**). In addition, an effectively infinite gate width must be used to ensure that all neutron coincidence events are recorded relative to the triggering event (**Figure 7.1**). Then, an estimated value for the true doubles count rate can be obtained, as $D(0, \infty)$. When these rates are known, they can be used with ^{252}Cf nuclear data, and the doubles count rate at the standard operational timing settings, to calculate the absolute neutron output of the source. The absolute measurement result is ideally independent of the counting system used and therefore, the final value can be compared between detection systems assuming all detection parameters are understood and properly adjusted for in the calculation.

The LV AWCC has been shown to have double pulsing, but it is not measurable until 1820 V which is well above the operational setting of 1700 V (Chapter 5). The LV AWCC is used in this work to perform the ABCD on three different ^{252}Cf sources. These sources are referenced as FTC-CF-1830, FTC-CF-3010, and FTC-CF-7009 and have source strengths of 222,528.323 nps with a rsd of 1.063%, 91,136.480 nps with a rsd of 1.061% and 245,772.459 nps with a rsd of 1.074%, respectively, on their dates of relevant measurement. Source FTC-CF-1830 is certified through the NIST MnSO_4 , and Sources FTC-CF-3010 and FTC-CF-7099 have been cross-calibrated at ORNL using FTC-CF-1830; they have

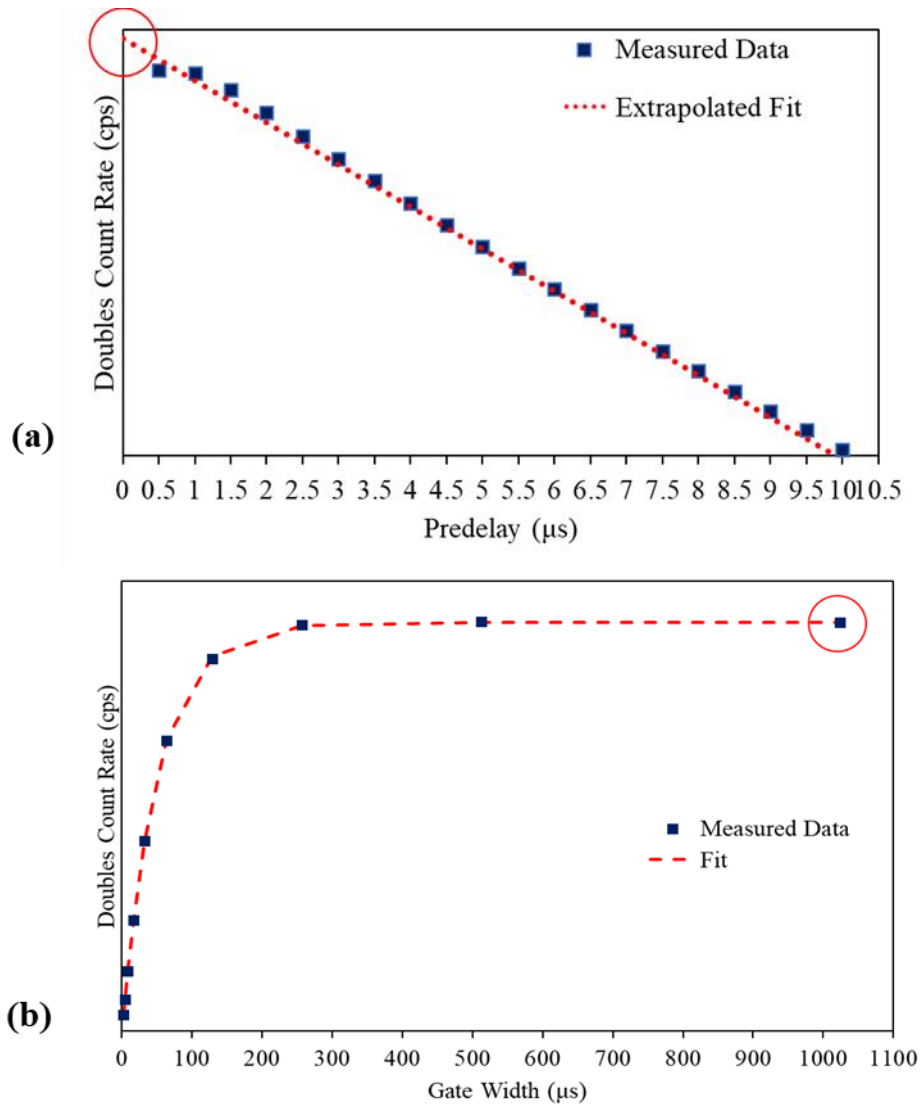


Figure 7.1. (a) Extrapolated doubles count rate estimated for a 0 μs predelay with set gate width by fitting a range of measured data, ignoring charge collection and electronic effects. The structure seen between successive predelay settings is described in the next section. (b) Extrapolated doubles count rate estimated for a 1024 μs gate width with set predelay.

not been NIST certified. To the knowledge of the author, the multiplicity counters used in previous works [87] [88] [99] have not been studied for evidence of double pulsing behavior in their A111-based boards (Chapter 5).

The LV AWCC differs from the neutron multiplicity counters used in the previous works for this analysis [87] [88] as its design purpose is coincidence counting not multiplicity counting, its efficiency is approximately half that of the neutron multiplicity counters used, and its dead time is an order of magnitude longer. This analysis tests to see if the ABCD method is translatable between neutron coincidence counters and neutron multiplicity models.

The equations for calculating the absolute source output are developed in [87] and summarized in [88]. They consist of expressions for a lightly encapsulated ^{252}Cf source, that with known system parameters and nuclear data, can be used to extract its yield, Y . The focus here is on the expression that is only dependent on the singles and doubles count rates, as neutron coincidence counters are used. With LMDA or modern multiplicity shift registers, triples data is easily measured in neutron coincidence counters, but the counting time required for suitable precision is much longer.

$$Y = \frac{1}{r^2} S \left(\frac{S}{D(0, \infty)} \right) \left(\frac{\nu_2/2}{\nu_1} \right) \quad (7.1)$$

$$\frac{1}{r^2} = \frac{\left(1 + \frac{\nu_d}{\nu_1} \right)}{\left(1 + \frac{\varepsilon_d \nu_d}{\varepsilon \nu_1} \right)^2} \quad (7.2)$$

In these equations: S is the dead time corrected singles rate; $D(0, \infty)$ is the extrapolated doubles count rate at zero predelay and infinite gate width; ν_1 is the first factorial moment of the ^{252}Cf spontaneous fission neutron distribution (i.e. the mean number of prompt fission neutrons emitted per fission); ν_2 is the second factorial moment of the ^{252}Cf spontaneous fission neutron distribution; ν_d is the mean number of delayed neutrons emitted per fission; and $\frac{\varepsilon_d}{\varepsilon}$ is the ratio of the system's detection efficiencies of delayed neutrons to prompt fission neutrons, which should be close to unity for a carefully constructed counter.

As described in [87], a majority of these values are well known through nuclear data references and can easily be entered into this calculation. Referencing the well-established work of [100] [101], ν_1 is given as (3.757 ± 0.010) prompt neutrons per fission produced for ^{252}Cf . The experimentally determined estimate of the delayed neutron yield is taken from [102] [103] where ν_d is (0.0086 ± 0.0011) delayed neutrons per fission with a rsd of 0.27%. This results in a $\frac{\nu_d}{\nu_1}$ ratio of (0.00229 ± 0.00029) with a rsd of 13% and a $\left(\frac{\nu_2/2}{\nu_1} \right)$ ratio of (1.5901 ± 0.0043) , with a rsd of 0.27%, using a ν_2 value of 11.953. Note, it is important that a physically small, fresh ^{252}Cf source is used, such that the neutron production is dominated by ^{252}Cf spontaneous fission and there no position-sensitive efficiency differences in the system influence the final analysis. Then, the nuclear data given for ^{252}Cf may be applied with certainty to the expressions above.

The singles count rate is obtained directly from the neutron pulse train. It is independent of any timing windows set for coincidence analysis, so it only needs to be determined once per measurement. The measured singles count rate must be dead time corrected before it is used to determine the absolute yield of a source. A dead time correction must also be made to the measured doubles count rate. This can be done by using the equations given in Chapter 6 (Eq.6.1-6.3), so these parameters must be well defined through in-depth system characterization. These equations show no dependence of the dead time parameter on gate width, so a universal doubles dead time parameter can be applied, regardless of predelay and gate width used. In reality, this may not fully represent the dead time behavior, but this needs to be explored further through simulation. This is the assumption made here. The dead time of the LV AWCC was previously determined using the traditional empirical method of analysis presented; the

values of both the singles and coincidence dead times are reported in **Table 7.1**. Due to the insensitivity of the dead time calculation to variations in the determined dead time parameters, a conservative systematic 5% uncertainty is assigned to this calculation. The dead time can be applied directly to the extrapolated doubles count rate determined for zero predelay rather than each of the calculated doubles rates in the 3.0-10.0 μs fit region. This is justified as the dead time correction is applied directly as a scaling factor to the measured rates, as given in Eq.6.3. With this linear extrapolation, the correction factor would have the same effect if applied to each of the measurement points, or directly to the extrapolated value. It was verified that both methods return the same extrapolated rate.

The extrapolated doubles count rate at a zero predelay is used in combination with the calculated doubles count rate at an infinite gate width to ultimately determine the doubles count rate independent of timing windows, $D(0, \infty)$. This can be done by first extrapolating to an infinite gate width with set predelay, determining the saturation gate width setting, and then using that gate setting combined with varying predelay settings to extrapolate to zero predelay. It can also be done by taking the doubles count rate measured at the counter's standard operational time windows, $D(4.5, 64)$, the calculated doubles count rate at infinite gate width and set predelay, $D(4.5, 1024)$, and the extrapolated doubles count rate at $D(0, 64)$, as shown in Eq. 7.3 [99].

$$D(0, \infty) \approx D(4.5, 1024) \cdot \left[\frac{D(0, 64)}{D(4.5, 64)} \right] \quad (7.3)$$

This relationship may be justified through the gate utilization factor (GUF) parameter, which represents the fraction of neutron coincidence events recorded in the specified gate window compared to that which would be recorded over all time in a measurement [104]. Here, the goal is to obtain a GUF of unity. The GUF is influenced by both the predelay and gate width timing windows set for the acquisition. A different neutron coincidence count rate will be recorded if either timing window is changed. Therefore, the GUF for a particular measurement can be described by both a predelay component contribution and a gate width component contribution. The first component is representative of the fraction of neutron coincidence events recorded when using the specified predelay setting, and the second component is representative of the fraction of neutron coincidence events recorded when using the specified gate width setting. This is reflected in Eq.7.3. This equation incorporates the calculated doubles count rate determined at the standard operating predelay value and infinite gate width, encompassing all possible coincidence events that could be recorded when using the system at a 4.5 μs predelay; the extrapolated doubles count rate determined at a zero predelay and standard operating gate width of 64 μs , which incorporates all neutron events that could be obtained in that set gate width; and normalizes these two rates to the doubles count rate that would typically be measured when using the system in a measurement at its standard operating time windows.

Because the final source measurement uncertainty must be comparable or lower than what is achieved in the national certification programs, it is important to also take background measurements surrounding the long counts of the neutron source. Using the background singles and doubles count rates, a subtraction may be applied to the singles and doubles count rates measured with the ^{252}Cf source. The reported doubles count rate is already a net value through the PTR-32 software subtraction of Accidentals, but a background count rate from the room and cosmic events also be accounted for. While neutron background is minimal in most laboratory measurement scenarios, it is still important to consider. This background subtraction will introduce an additional statistical uncertainty; therefore, the counting time should span for several hours for multiple acquisition cycles to minimize this contribution.

It is also necessary to account for the differences in the efficiency of the counting system for both prompt and delayed neutrons such that an accurate correction may be applied using Eq.7.2 for the true absolute source output. These parameters can be obtained from measured data. It has been shown that the mean energy of the AmLi spectrum can approximate the average spectrum of delayed neutrons well [105] [106]. By measuring certified AmLi sources in the well of the LV AWCC, and using the well-known

source strength, the delayed neutron efficiency can be calculated for the system. AmLi has a very long half-life so the decay correction is minimal and introduces a small uncertainty. Then, for the ^{252}Cf source an efficiency can also be measured. This efficiency is calculated for all 3 ^{252}Cf sources, and averaged, to ensure consistency and accommodate the slight calculated differences into the uncertainty. These two values are reported in **Table 7.1**. Then using these values, $\frac{\epsilon_d}{\epsilon}$ is calculated to be (1.135 ± 0.027) and used in Eq. 7.2 for the final analysis. This ratio provides a small, but important, correction factor into the analysis to compensate for the slight differences in detection efficiency due to the energies of delayed neutrons also produced in measurement scenarios.

It was mentioned that it is important that a fresh ^{252}Cf source is used in these measurements. The half-life of ^{252}Cf is 2.645 years. As ^{252}Cf ages, ^{250}Cf builds in. The average neutron number produced by ^{250}Cf differs from that produced by ^{252}Cf . This would affect the nuclear data parameters used in these equations, and the associated measured doubles count rate, if the source contains a significant amount of ^{250}Cf . Therefore, the ^{250}Cf contribution to the neutron output must be corrected for when using aging sources. For all three sources used, the ^{250}Cf to ^{252}Cf mass ratio were, 0.105 for FTC-CF-1830, 0.101 for FTC-CF-3010, and 0.136 for FTC-CF-7009. The known source strength values for each respective date of measurement, based on the given nuclear data certificate values, were all adjusted for the decay of ^{252}Cf and build in of ^{250}Cf contributions. The ^{250}Cf contribution correction factor is very small. The nuclear data parameters used in Equations 7.1 and 7.2 are not changed from their original ^{252}Cf values given.

In addition, due to slight differences in the emitted neutron energy spectrum between ^{250}Cf and ^{252}Cf , it is possible the detection efficiency of the system may be impacted by the presence of ^{250}Cf . It is important to identify if this will influence measurements. The average energy of these neutrons may be estimated using [107] paired with system efficiency data obtained across a variety of sources having different mean energies. Since the ratio of estimated $\frac{\epsilon_{250}}{\epsilon_{252}}$ is (1.004 ± 0.004) , this contribution can be assumed to be insignificant in this instance. Even if the ^{250}Cf concentration was large, it wouldn't seem to be significant in terms of a correction factor to the calculated system efficiency due to the small difference in average energy values. If the average energy of various isotopes' spectra differ significantly in another source undergoing certification, both efficiencies will have to be taken into account.

Table 7.1. LV AWCC characterization parameters

	Value	Uncertainty
System Singles Dead time (μs)	0.218	0.011*
System Doubles Dead time (μs)	0.870	0.044*
Delayed Neutron Efficiency (%)	39.51	0.40
^{252}Cf Neutron Efficiency (%)	34.81	0.75

*A 5% systematic uncertainty is assigned to the dead time due to insensitivity of dead time parameters to slight variations

7.2 Neutron Pulse Train Extrapolation to Zero Predelay and Infinite Gate Width using PTR-32 List Mode Data Acquisition and Analysis

LMDA has the ability to emulate the same analysis performed by a shift register to determine singles and doubles count rates for neutron coincidence counters. LMDA records the total number of neutron events as a function of time over the full duration of measurement. In offline analysis, this neutron pulse train is then analyzed with relevant timing windows to determine rates and produce multiplicity histograms, if desired. A single measurement can be analyzed countless times with any combination of timing windows to generate the associated count rate for that combination, which saves valuable measurement time both in the field and in a laboratory setting by not having to repeat individual measurements for every timing window sampled, as would have to be done with a shift register. LMDA also allows for a greater in-depth study of the behavior of the counting system as each channel output may be studied for performance and individual characterization. By doing so, the efficiency, neutron die-away time, and dead time can be well described and understood such that multiple channels of one system may be used as a cross verification in a single measurement.

An extrapolation to zero predelay is used from measured data obtained with longer predelays (**Figure 7.1 a**). Then, the doubles count rate can be calculated at an effectively infinite gate width while keeping the predelay constant (**Figure 7.1 b**); the predelay selected is the value traditionally used with the system in shift register analysis, e.g. 4.5 μs for D(4.5, 1024). The effectively infinite gate width should be chosen relative to the neutron die-away time of the system to ensure that all correlated neutrons will be captured in that timing gate. The neutron die-away time is the amount of time it takes a neutron to either get captured by the system or escape, and is typically on the order of 50 μs for standard well or collar neutron coincidence counters. For this work, 1024 μs is taken as the infinite gate width, but it will be shown later that the doubles count rate reaches a saturation value between 512 and 1024 μs that could instead be used as approximately infinite relative to the die-away time. There is little difference between the rates at these two settings; the slight variation stems from more accidental counts recorded in the longer gate width.

Using the PTR-32 LMDA it is notionally possible to sample the pulse train with a predelay of 0 μs , but that was discovered to be problematic. Entering 0 μs in the PTR selection window for the extrapolation to zero predelay allows the program to run, but it is clear that this analysis is not reliable at this setting based on the drastic increase in rate from a 0.25 μs predelay to no predelay (**Figure 7.2**). The calculated doubles count rate reported at this setting is also more than the singles count rate measured for the run, which is not physical.

Therefore, it is necessary to extrapolate backward to a zero predelay from confidently reported, physically validated values. The measured doubles count rate can be obtained by sampling the pulse train at different short predelay values, ranging from 2.0-10.0 μs , while keeping the gate width constant (**Figure 7.1 a**). The gate width selected is the value traditionally used with the system in shift register analysis, e.g. 64 μs for D(0,64). Then, a trend may be applied to that data and extended backward to intercept at a 0 μs predelay. This trend comes from the traditional equation used in die-away determination,

$$R_G = R_0 \text{Exp}\left(-\frac{T_p}{\tau}\right) \quad (7.4)$$

where R_G is the gated doubles count rate, R_0 is the maximum calculated doubles count rate, T_p is the predelay setting, and τ is the die-away time of the system. By minimizing the sum of squared errors between this fit's R_G and the calculated doubles count rate given by PTR-32 software, in a chi squared analysis where R_0 and τ are the free variables, an accurate fit may be applied to the PTR-32 calculated data. The fit may, in principle, be generated from any number of data points across the desired range of

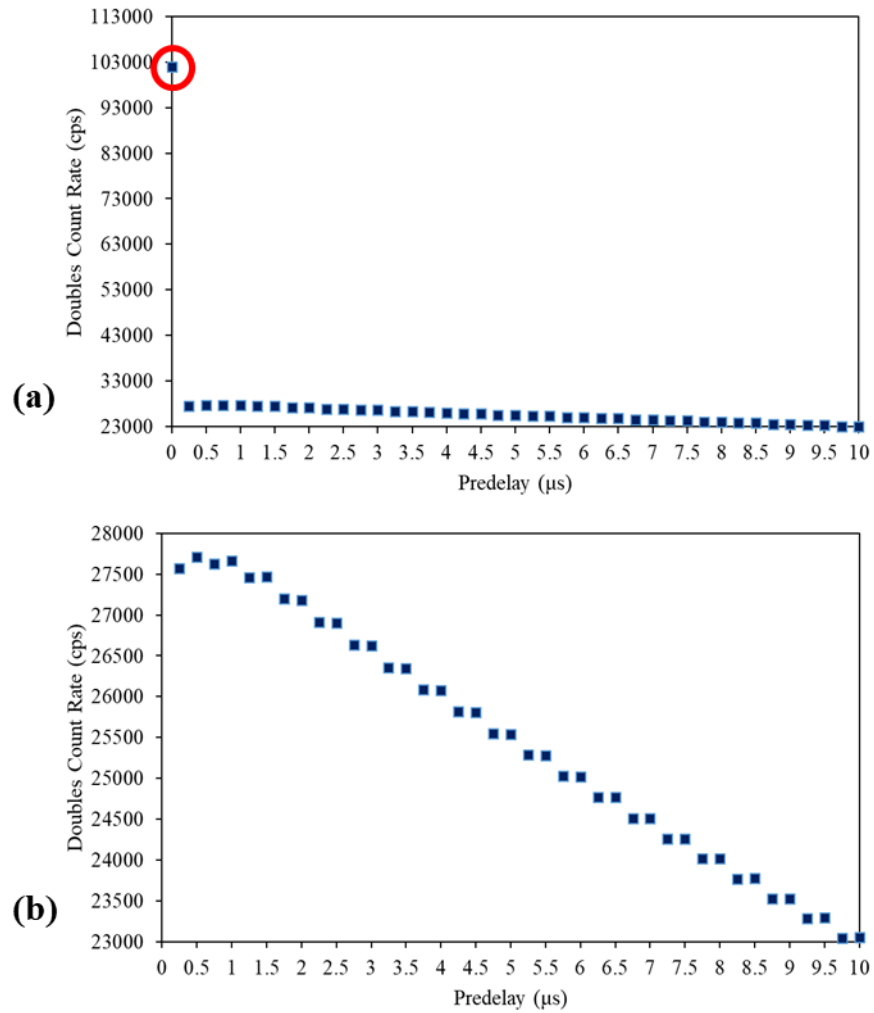


Figure 7.2. (a) Doubles count rate values over a range of predelays, including the PTR-32 calculated value at 0 μs illustrating non-physical behavior. (b) Doubles count rate values from 0.25 μs-10 μs, showing an expected count rate trend.

short predelay settings. This fit may then be extended backward using a linear trendline to a zero predelay intercept.

The behavior of the doubles count rate over this short predelay range can be approximated as linear as

$$R_G \sim R_0 \left(1 - \frac{T_p}{\tau} \right) \quad (7.5)$$

through the Taylor expansion of Equation 7.4, or through taking the logarithm such that

$$\ln R_G = \ln R_0 - \frac{T_p}{\tau} \quad (7.6)$$

if the system die-away time can be verified to have a single exponential decay trend, which is a good approximation for most common systems, and the predelay range used for this analysis is short relative to this die-away time.

The calculated difference between setting a 0 μs predelay in PTR-32 and extrapolating to a zero predelay in an example 3.0-10.0 μs range, using Equation 7.3, is then given in **Table 7.2**. Additionally, the doubles count rate provided for a 0.01 μs predelay entered in PTR-32 is also compared. It is clear that these three methods of estimating an approximate D(0,64) provide values that are not in agreement within uncertainty, as may be anticipated by using different predelay settings which omits part of the neutron pulse train. However, one would imagine that the values determined by PTR-32 for D(0.01, 64) and by the least squares fit for D(0,64) may be in better agreement. The difference across these three approaches is caused by competing electronic effects in these respective time ranges, and the behavior of PTR-32's analysis algorithms.

Table 7.2. The different doubles count rate values estimated for an approximately zero predelay

D(0.01,64) (cps)	\pm (cps)	σ	D(0.25,64) (cps)	\pm (cps)	σ	Extrapolated D(0,64) (cps)	\pm (cps)	σ
27631.09	23.95	22.47	27549.46	23.93	24.01	28043.34	12.78	23.85

In addition, when studying the results of PTR-32's neutron pulse train analysis using 0.05 μs increments, it became evident that the doubles rates generated by the software exhibits non-physical microstructure. There is a very clear oscillation between the calculated doubles count rate across the different predelay settings. This behavior is shown in **Table 7.3**. This behavior results from the analysis software programmed within PTR-32 and will need to be addressed by its developers.

The challenge with using PTR-32 is that there is no documentation on how the software performs its analysis. The user manual does not provide algorithms, nor how the pulses are handled along the pulse train. Although its performance has been characterized in depth relative to a common shift register module, as discussed in Chapter 2, there are instances where the validity of the PTR-32 results raise further questions, like at the 0 μs time setting and with these small changes in predelay settings. The same challenges are not reported, nor is data shown for a 0 μs setting or in 0.05 or 0.25 μs increments, in the LANL LMMM analysis for their absolute measurements [87] [88]. This software is an in-house LANL unit that is not available for this study. Because PTR-32 is the only current IAEA-approved LMDA module, it is used in this work, but in the future as more LMDA for neutron coincidence counters are developed, there may be opportunity for improvement.

Table 7.3. Doubles count rates for various predelay settings in 0.05 μs increments

T_p (μs)	D (cps)	\pm	Difference from previous value
3.00	26629.58	23.654	-----
3.05	26476.08	23.609	-153.500
3.10	26575.21	23.638	99.130
3.15	26421.05	23.592	-154.160
3.20	26520.46	23.622	99.410
3.25	26366.06	23.576	-154.400
3.30	26465.18	23.605	99.120
3.35	26311.66	23.559	-153.520
3.40	26411.17	23.589	99.510
3.45	26258.13	23.543	-153.040
3.50	26357.45	23.573	99.320
3.55	26203.63	23.527	-153.820
3.60	26303.39	23.557	99.760
3.65	26149.45	23.511	-153.940
3.70	26249.30	23.541	99.850
3.75	26095.73	23.495	-153.570
3.80	26195.61	23.525	99.880
3.85	26041.70	23.479	-153.910
3.90	26141.48	23.509	99.780
3.95	25988.28	23.463	-153.200
4.00	26087.98	23.493	99.700
4.05	25935.10	23.447	-152.880
4.10	26034.90	23.477	99.800
4.15	25881.53	23.431	-153.370
4.20	25981.03	23.461	99.500
4.25	25827.63	23.415	-153.400
4.30	25927.43	23.444	99.800
4.35	25773.68	23.398	-153.750
4.40	25873.40	23.428	99.720
4.45	25720.75	23.382	-152.650
4.50	25820.72	23.412	99.970
4.55	25667.60	23.366	-153.120
4.60	25767.71	23.397	100.110
4.65	25614.49	23.350	-153.220
4.70	25714.90	23.381	100.410
4.75	25562.05	23.335	-152.850
4.80	25662.03	23.365	99.980
4.85	25509.71	23.319	-152.320
4.90	25609.50	23.349	99.790
4.95	25457.73	23.303	-151.770
5.00	25558.30	23.334	100.570
5.05	25405.01	23.287	-153.290

Examining this behavior in larger increments of 0.25 μs , it is shown that each 0.50 μs multiple has a difference from its previous predelay setting of under 10 cps (**Table 7.4**). This means that two successive predelay settings are producing nearly identical count rates through this analysis; this is visualized in **Figure 7.2 b**. Specifically, it appears that the data follows a step trend between the 0.5/1.0 μs predelay settings and the 0.25/0.75 μs predelay settings where the count rate will drop significantly between this range, and then the successive 0.5/1.0 μs predelay data point measures a similar value to that value. Therefore, on the average the trend with predelay is correct as the doubles count rate is linearly decreasing. To proceed, then, we ignore this instrumental artifact in short predelay increments, and the extrapolation is sustained using data in 0.50 μs increments.

One remaining point to be addressed is which 0.50 μs increments to use. For the 0.25 and 0.75 μs settings, the calculated doubles count rate is lower than what is calculated for the 0.50 and 1.0 μs predelay settings. Although using either grouping results in a consistent difference in count rate from setting to setting (**Table 7.4**), the extrapolated D(0,64) value will differ depending on the grouping selected. This difference is illustrated in **Figure 7.3**. However, this difference in the final effective D(0, 64) value is not large, 95 cps, so either choice would suffice. Thus, every 0.50 and 1.0 μs predelay settings is used in the following analysis.

Table 7.4. Doubles count rates for various predelay settings in 0.25 μs increments

T_p (μs)	D (cps)	\pm	Difference from previous value	Difference in 0.50 μs steps
3.00	26629.58	23.654	-----	-----
3.25	26366.06	23.576	-263.52	-----
3.50	26357.45	23.573	-8.61	-272.13
3.75	26095.73	23.495	-261.72	-270.33
4.00	26087.98	23.493	-7.75	-269.47
4.25	25827.63	23.415	-260.35	-268.10
4.50	25820.72	23.412	-6.91	-267.26
4.75	25562.05	23.335	-258.67	-265.58
5.00	25558.30	23.334	-3.75	-262.42

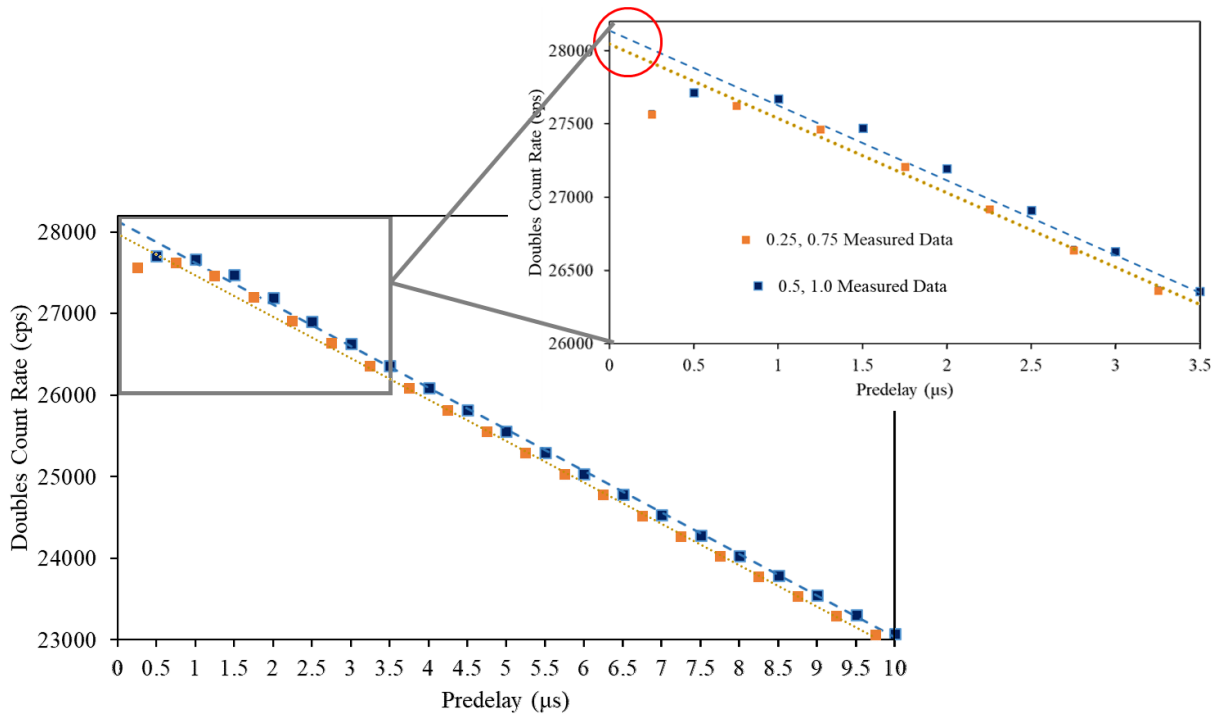


Figure 7.3. The PTR-32-calculated doubles count rate for various predelays. The orange and blue data points show the oscillating values as given by PTR-32: orange is for every 0.25 and 0.75 μs predelay setting, blue is for every 0.50 and 1.00 μs predelay setting. Their extrapolation difference for the zero predelay intercept is highlighted.

Extrapolating to zero predelay is victim to dead time and charge collection effects. Dead time on the microsecond scale is unavoidable in ^3He -based systems due to charge collection physics and the pulse processing time of associated electronics, and it is therefore always relevant in these systems, as discussed in the previous chapter. As the predelay decreases with a set gate width, the system starts collecting data closer to the triggering event which incorporates some of the dead period where the system cannot record any events. The averaged count rate then decreases with shorter predelays, compared to the same data at settings with a longer predelay which are not subject to dead time effects, as more of the dead period is included in the measurement time. This causes a “rolling over” behavior of the count rate (**Figure 7.4** a and b), which further complicates applying an accurate fit to these data for D(0,64). To avoid these effects, the fit must be applied to data beginning at longer predelays. This introduces more uncertainty in the D(0,64) estimation as the extrapolation extends backwards over a greater range than if the fit could be used from 0.25 μs to estimate 0 μs .

To study this behavior, the FTC-CF-1830 neutron pulse train was analyzed with different predelay values, ranging from 2.0-10.0 μs , while keeping the gate width constant. The results are reported in **Table 7.5**. These values, and their associated uncertainties, are the average doubles count rate values and uncertainties calculated by PTR-32 across 20 cycles of acquisition, of 1 hour each, where the source placement and system placement remained constant. The uncertainties are low due to the high count rate and long measurement time. This was done, like in [87] [88], as a basic form of uncertainty estimation, to determine the statistical spread in the data as a check of self-consistency in the values generated. The decay of the ^{252}Cf over this time range is verified to be negligible for this analysis. The average extrapolated D(0,64) value is obtained from the intercept calculated by a least squares fit applied to each cycles’ doubles count rate data for the fits.

Table 7.5. The effective doubles count rate estimated for fits to the measured data in different predelay intervals

Fit interval (μs)	Eff. D(0,64)	\pm
2.0-10.0	28,090.149	13.020
2.5-10.0	28,066.572	12.908
3.0-10.0	28,043.336	12.781
3.5-10.0	28,020.026	12.634
4.0-10.0	27,996.495	12.460
4.5-10.0	27,972.419	12.252
5.0-10.0	27,948.843	12.013

As the starting predelay setting included in the fit increases in length, the final estimate of the effective D(0,64) decreases (**Figure 7.4** c). Despite this change in D(0,64), the overall difference from the 2.0-10.0 μs fit to the 5.0-10.0 μs fit is 141 cps (**Table 7.5**). Therefore, relative to the total count rate, this difference is not significant. For this analysis, then, the 3.0- 10.0 μs fit interval is used.

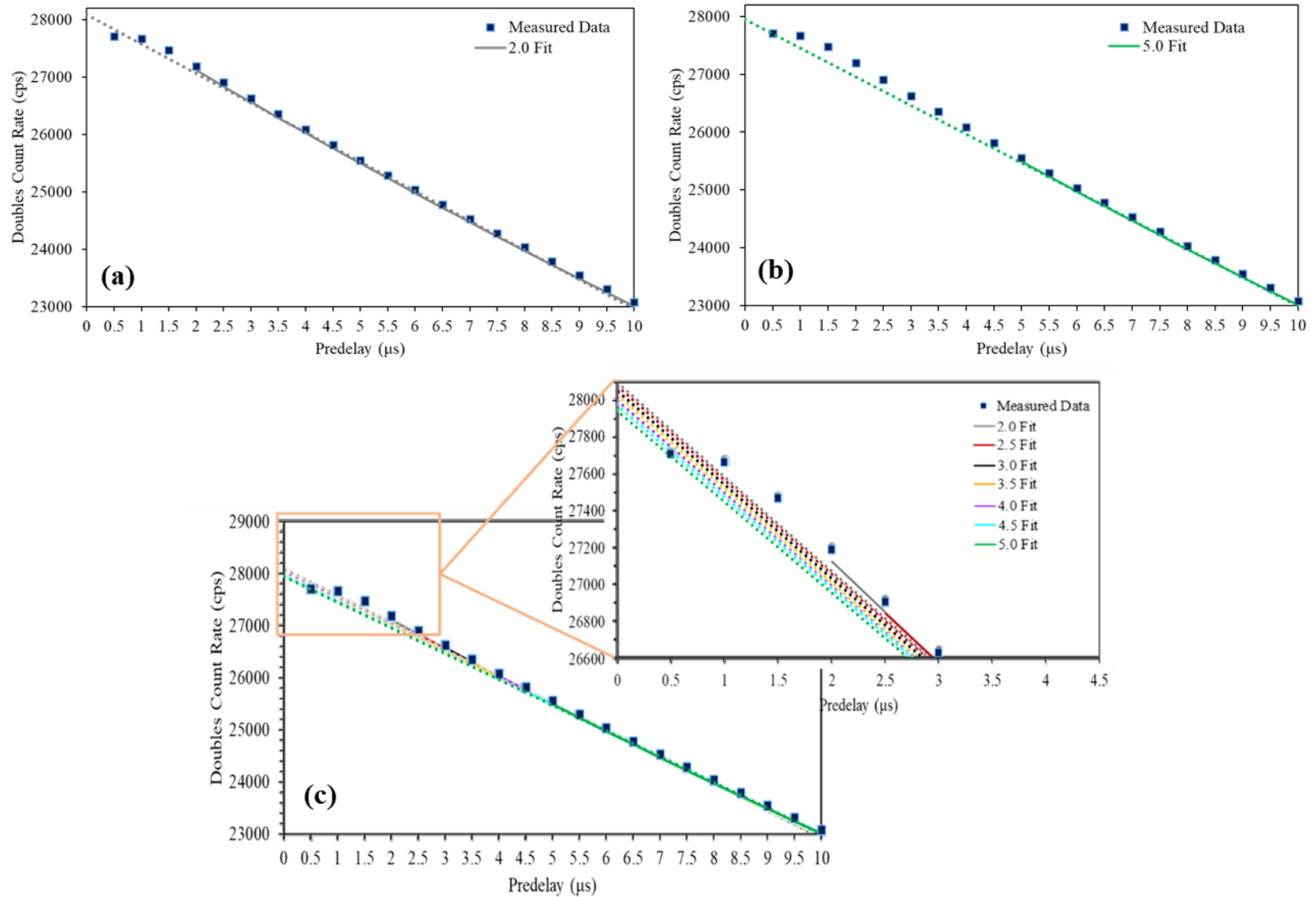


Figure 7.4. (a) Doubles count rate data as a function of increasing predelay setting with a fit applied from 2.0 μs - 10.0 μs and extrapolated backwards to determine the intercept for D(0,64). (b) Doubles count rate data with a fit applied from 5.0 μs - 10.0 μs . (c) The deviation of intercepts generated by different fits applied between a starting predelay range of 2.0 μs and 5.0 μs to 10.0 μs .

7.3 Comparison of Neutron Coincidence Counting Absolute Source Measurements to NIST Certificate Values

Data were collected in two hour acquisitions for each of the three sources: FTC-CF-1830, FTC-CF-3010, and FTC-CF-7009. Recall, at the date of measurement, the calculated source outputs were 222,528.323 nps with a rsd of 1.063%, 91,136.480 nps with a rsd of 1.061% and 245,772.459 nps with a rsd of 1.074%, respectively. The NIST certificate output for FTC-CF-1830, and the associated cross-calibrated output values for FTC-CF-3010 and 7009, were decay corrected and the ²⁵⁰Cf contribution was accounted for in these values.

Each measured pulse train was then extrapolated to a zero pre-delay using linear fits to the data ranging from 3.0-10.0 μs, and to an infinite gate width at 1024 μs (**Figure 7.5**). The final $D(0, \infty)$ were used with Equations 7.1 and 7.2, the nuclear data given in Section 7.1, and the specific LV AWCC characterization parameters given in **Table 7.1**. The final calculated yields are reported in **Table 7.6**, with their ratios to the respective calculated source outputs. The ratios range from 0.9415 with the weakest source FTC-CF-3010 up to 1.0014 with the strongest source FTC-CF-7009. It is believed that FTC-CF-3010 is older than it is quoted and has a much more significant ²⁵⁰Cf contribution. This would affect the comparison of the yield to calculated source output values if the proper ²⁵⁰Cf correction cannot be applied.

Error is propagated through each calculation for all parameters involved that have an associated uncertainty. Source FTC-CF-1830 is analyzed across twenty cycles for an additional statistical contribution to its uncertainty. This is discussed in detail in the next section. For FCT-CF-3010 and FTC-CF-7009, one two-hour measurement was obtained and the error from that measurement is propagated through. With all factors considered, these equations and the final yield result precision are ultimately governed by the confidence in the extrapolation fit parameters and assumptions made, and the counting precision. The calculated rsd for each source is less than that typically quoted on a NIST certificate. This is achieved by the long measurement time, and the in-depth LMDA characterization and associated analysis of the neutron coincidence counting system behavior.

Table 7.6. Absolute source measurement yield comparison to the NIST certificate value

	Y (nps)	± (nps)	rsd (%)	Calculated output (nps)	± (nps)	rsd (%)	Ratio Calculated output/Y
FTC-CF-1830	219,649.34	*1,211.36	0.55	**219,716.12	2,339.26	1.06	1.0003
FTC-CF-3010	96,794.97	422.76	0.44	91,135.51	967.34	1.06	0.9415
FTC-CF-7009	245,426.19	1,149.42	0.47	245,772.46	2,638.41	1.07	1.0014

*The uncertainty term for FTC-CF-1830 also includes the standard deviation of the extrapolated doubles count rate across 20 cycles of data described in the next section

**FTC-CF-1830 has an associated NIST certificate from which the other 2 sources were cross-calibrated. The output value calculated here is from that certificate

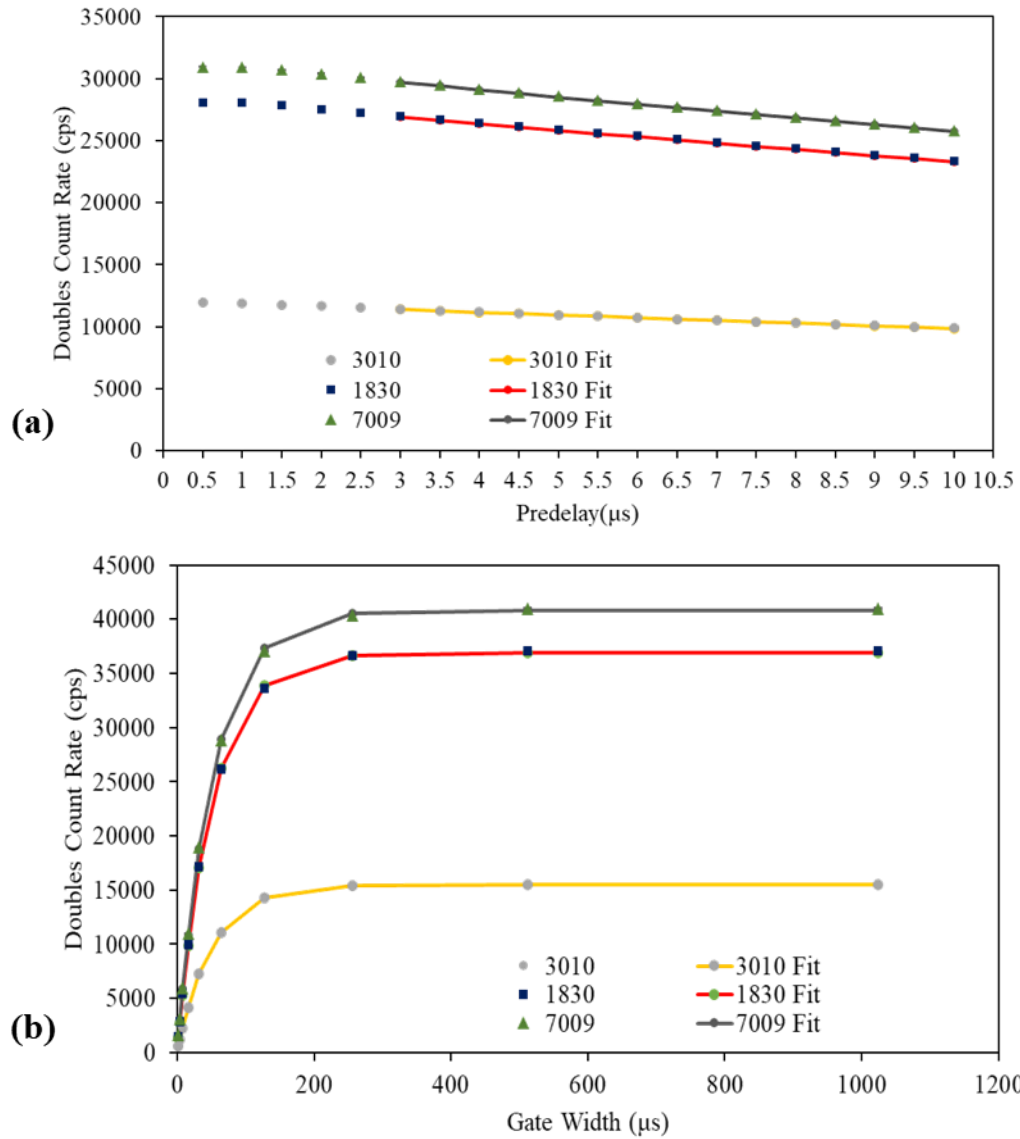


Figure 7.5. (a). The measured doubles count rates obtained for various predelay settings for all three ^{252}Cf sources. A linear fit is applied to each source's data from which the $D(0,64)$ count rate value is calculated. **(b).** The measured doubles count rate data obtained for an infinite gate width, $D(4.5,1024)$, for all three ^{252}Cf sources.

7.4 Uncertainty Determination

The final uncertainty value incorporates many different sources of error and uncertainty produced throughout this analysis. Beginning with the initial measured doubles count rate at the specific predelay and gate width settings, there is an affiliated counting statistics uncertainty. Then, with the LMDA analysis of these rates and the associated extrapolation to a zero predelay, there are additional uncertainty factors that must be considered.

To test the relationship of the fit interval and the calculated yield, the ratio of the expected neutron output of FTC-CF-1830 to the NIST certificate values were analyzed using the different $D(0,64)$ count rates estimated from the various fits presented in **Table 7.5**. Here, the impact of these differences is propagated through to the final calculation of the yield. The $D(0,64)$ value, in combination with the constant PTR-32-calculated $D(4.5,1024)$ and $D(4.5,64)$ count rates were used to calculate $D(0, \infty)$. All other factors in Equations 7.1 and 7.2 were kept constant for this comparison. The differences in the final ratio values are then due to the differences in the extrapolated values (**Table 7.7**). As reflected in this table, the omission of data in $0.5 \mu\text{s}$ predelay increments provides a 0.001 ratio change, in most cases, of the NIST certificate output to that which is calculated through the ABCD method. Therefore, it is necessary to include the uncertainty involved with the fit selection into the extrapolated doubles count rate. The associated doubles count rate difference across these different settings is propagated into the uncertainty. It is possible that in unfolding the different electronic contributions (dead time, charge collection effects, double pulsing) at short predelays through neutron pulse train simulation, and determining at what predelay setting there is still confidence in the resulting behavior of the doubles count rate, an optimal fit range can be specified in future work. This may improve the precision of the final yield.

It is also shown that the selection of either a $512 \mu\text{s}$ infinite gate width or a $1024 \mu\text{s}$ gate width provides a $D(4.5, \infty)$ doubles count rate that is in agreement within counting statistic uncertainty. Due to tradition, $1024 \mu\text{s}$ is used. Since the die-away is on the order of $50 \mu\text{s}$, performing this analysis at $512 \mu\text{s}$ is long enough such that the doubles count rate behavior is saturated (**Table 7.8**), acting as an infinite gate width as well. The data analyzed with a $1024 \mu\text{s}$ gate width has a higher counting statistics uncertainty due to the greater contribution of Accidentals, which propagates through to the final uncertainty analysis. Although the doubles count rate at $D(4.5,1024)$ is used in the above analysis, the doubles count rate at $D(4.5,512)$ could also be used and provide a slightly smaller uncertainty.

Because this extrapolation method for an absolute source measurement utilizes the same neutron pulse train for list mode analysis with various predelay and timing gates, unlike with a shift register measurement, the data points are inherently correlated. This influences the fits applied to these data, which ultimately impacts the $D(0,64)$ values. This complicates the uncertainty estimation for these calculated values, and the added uncertainty caused by this correlation must be taken into account in the final yield precision. However, reflecting this uncertainty is not straightforward. There are several methods that may be used to further determine uncertainties associated with the LMDA analysis and propagate them into the final ABCD calculation.

The most commonly used method when working with list mode data, and the method used here, is performing statistical analysis of independent replicate counts. This is achieved by obtaining data in multiple cycles of acquisition without changing anything about the measurement system. The source and counter remain in place, and PTR-32 records data for the duration of the specified count time and iterates through the number of cycles specified by the user. With a shift register, it is necessary for the user to manually set the time settings before initiating a run; therefore, each measurement is independent of any other measurements taken across other settings. Although the calculated doubles count rates across a single pulse train have an inherent correlation, the values obtained at a specific setting are independent from cycle to cycle. These multiple cycles provide a spread in measured doubles count rate that is used to calculate an additional uncertainty term, as any measurement of that source at that setting could be expected to fall within this range of data, despite the correlation from point to point on one pulse train.

Table 7.7. A summary of the different doubles count rates of FTC-CF-1830 and associated yields calculated for various predelay range fits

Fit interval (μs)	Eff. $D(0,64)$ (cps)	$D(0, \infty)$ (cps)	$D(0, \infty)_{\text{DTC}}$ (cps)	Calculated Y (nps)	Ratio NIST output/Y
2.0-10	28090.149	39783.266	40432.967	219143.181	1.003
2.5-10	28066.572	39749.874	40399.030	219327.270	1.002
3.0-10	28043.336	39716.965	40365.583	219509.005	1.001
3.5-10	28020.026	39683.951	40332.031	219691.616	1.000
4.0-10	27996.495	39650.625	40298.161	219876.265	0.999
4.5-10	27972.419	39616.528	40263.507	220065.508	0.998
5.0-10	27948.843	39583.138	40229.571	220251.144	0.998

Table 7.8. Doubles count rate values for two effectively infinite gate width settings at 4.5 μs predelay

	512 μs		1024 μs	
	Doubles	\pm	Doubles	\pm
FTC-CF-1830	36,436.91	87.71	36,314.60	126.38
FTC-CF-3010	15,608.58	26.93	15,569.29	38.73
FTC-CF-7009	40,969.79	69.50	40,961.13	100.30

Using FTC-CF-1830, twenty cycles of one hour counts were obtained using PTR-32 and the LV AWCC. Each of these neutron pulse trains was then analyzed to determine the doubles count rate with predelay settings ranging from 3.0-10.0 μs at a 64 μs gate width, a predelay of 4.5 μs with a 64 μs gate width, and a predelay of 4.5 μs with a 1024 μs gate width. The scatter in these rates is not large (**Figure 7.6**); over all 20 cycles the doubles count rate at $D(2.5,64)$ has a rsd of 0.086 %. The scatter increases as the gate width increases; at $D(4.5,1024)$ the rsd is 0.400 %. This helps show that the correlation associated with using list mode analysis to sample the same pulse train for various rates does not greatly impact the determined rates compared to the effect of counting statistics, but it is still something that should not be ignored when operating on a sub 1% precision measurement. For the $D(0,64)$ total uncertainty, the counting statistics uncertainty, the fit range uncertainty, and the statistical spread across multiple cycles are added in quadrature to determine a combined value. For the $D(4.5,64)$ and $D(4.5,1024)$ total uncertainty, the counting statistics uncertainty and the standard error across these multiple cycles are added in quadrature and propagated through to the final yield uncertainty. The decay of the ^{252}Cf source over this acquisition time had a negligible impact on the measured values, so it is not included in the uncertainty analysis.

For the final calculation of the $D(0, \infty)$ uncertainty rates performed here using the multicycle LMDA data, an extrapolated fit was applied to each of the twenty cycle's data across the 3.0-10.0 μs predelay setting range, and an associated zero predelay value was recorded. An average extrapolated doubles count rate was taken across all cycles and the standard error was taken as the associated uncertainty. Therefore, it is important to have a large number of cycles for this analysis. This standard error is added in quadrature with the counting statistics uncertainty and the different fit range uncertainty to finalize a total count rate-LMDA uncertainty term. There is then dead time uncertainty, efficiency uncertainty, and nuclear data uncertainties, as they were all specified in the previous section, incorporated into the final yield uncertainty value.

As an alternative to the multicycle acquisition, a single neutron pulse train could be separated into multiple cycles of data by dividing the measurement into shorter, multicycle neutron pulse trains. This could be done in software of the LMDA (not readily available with PTR-32 but it is available with other in-house LMDA modules), or possibly through bootstrapping the data. Bootstrapping the data could incorporate Monte Carlo sampling; the sequence of shorter count duration files could be analyzed by randomly picking some number of the cycles and analyzing the data for variation. The cycle lengths and the number of files analyzed could also be studied for their impact on the correlation analysis. Each of these new files can then be analyzed separately and their standard error could be propagated through to the final uncertainty analysis.

There are other methods beyond sampling that are under investigation for the interpretation and analysis of the correlation across the pulse train. One avenue of interest is analyzing a RAD. A calculation for $D(0, \infty)$ could be applied to the RAD using the PTR-32 0.1 μs time bins. The selected predelay can be applied such that data on the RAD below this setting is not included in the analysis, and data up through the desired gate width is summed. The RAD could then produce $D(4.5,64)$, $D(4.5,1024)$, and the doubles count rates obtained at a range of predelay settings for the extrapolation to zero. Through this analysis, including the successive summation of neighboring bins for a full gate width, it becomes clear that neighboring $D(T_p, T_g)$ settings, such as what is done for the extrapolation, share most data points and are therefore correlated. The goal of this method is to compute the full input covariance matrix for the linear fit that may be applied to these data for uncertainty analysis.

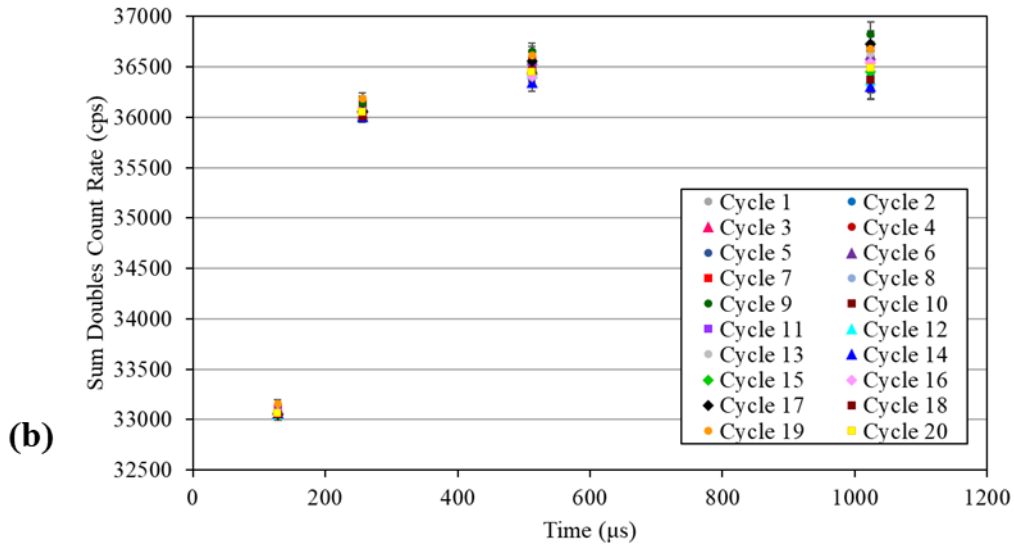
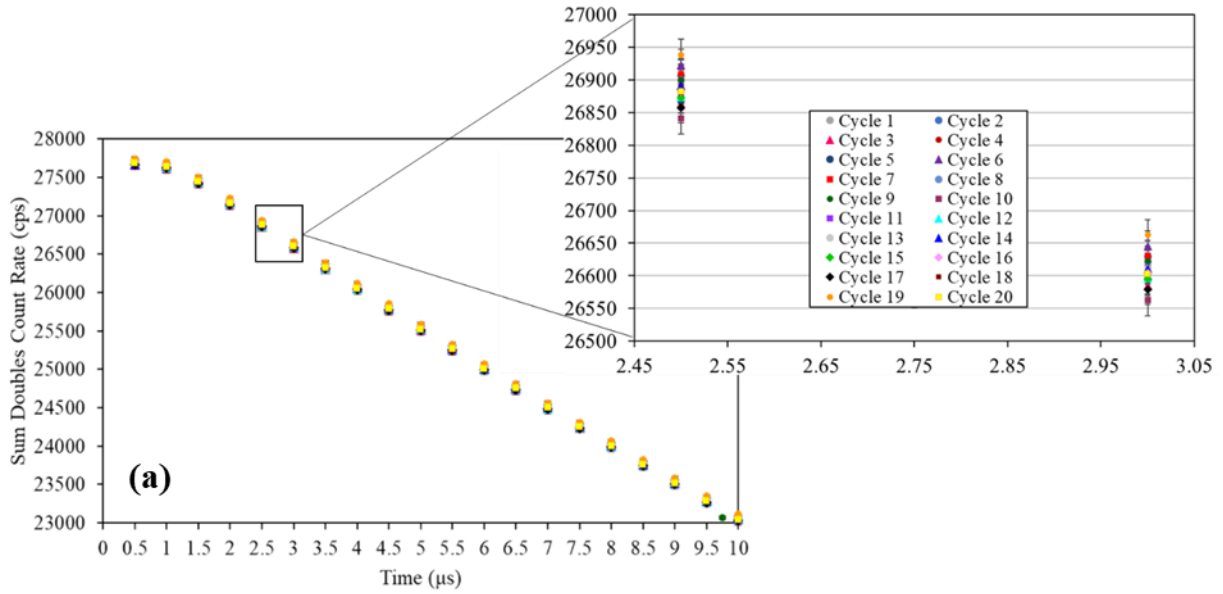


Figure 7.6. (a). The doubles count rate data for various predelay settings reported for twenty cycles of one hour acquisitions. The cut away investigates the scatter in the calculated doubles count rates over these multiple cycles for two specific predelay values. **(b).** The doubles count rate data for various gate width settings reported for twenty cycles of one hour acquisitions. The spread in the calculated doubles count rates increases with increasing gate width.

7.5 Conclusion

It has been shown that this previously developed ABCD method can also be used with readily available neutron coincidence counters and the commercially available PTR-32 LMDA module rather than expensive neutron multiplicity counters and in-house LMDA. These systems on average have half the efficiency and an order of magnitude longer dead time. It can be performed using either shift register-based logic [87] or LMDA-based logic [88] and allow a user to self-certify a ^{252}Cf neutron source in-house with precision surpassing national metrological laboratories such as NIST. This mitigates long lead times and expensive price tags associated with the use of certified neutron sources, which are necessary for the calibration and characterization of neutron coincidence counters and NDA measurements. With the validation that this procedure can be used in traditional NDA laboratories, further progress has been made to establish the various sources of uncertainty contributing to the final certification precision, including correlations caused by list mode analysis of a single neutron pulse train.

The applications of this approach extend beyond international safeguards or neutron time-correlation counters. Although a neutron coincidence counter must be present to perform this analysis, once the source strength is known it can be used in a variety of applications. One application could be calibrating other neutron detectors, for a wider neutron counting audience and metrology focus. Having the ability to self-check a source after certification, or after some time has passed since its manufacturing, is an added benefit to any laboratory, and this method lends itself for straightforward source checks as well.

Chapter 8

Summary of Research Findings

This dissertation proposes and addresses advancing the field of neutron coincidence counting for international safeguards through the characterization and implementation of a list mode data acquisition (LMDA) system and affiliated advanced data analysis techniques, in combination with an improved counter system design using modern prototype electronics. These modifications will improve the functionality of currently deployed systems by augmenting their measurement capabilities, in addition to enabling enhanced analysis techniques. This allows for in-depth detector characterization, calibration, and optimization procedures based on physics first principles rather than traditional empirical methods; ultimately leading to improved performance and more confidence in a system's reliability.

Others have focused their efforts on the design and evaluation of novel systems over the last couple of decades. The traditions associated with current systems, including the thousands of systems deployed worldwide, and their associated infrastructure and man hours dedicated towards training on them, do not readily lend themselves to the easy adoption of new technologies. Furthermore, today the amount of nuclear material and the number of nuclear facilities under IAEA safeguards is growing steadily, placing increasing demands on limited resources. Instead, this research addresses the need to do more with less. Drawing from advancements in other related fields, and commercial-off-the-shelf technology, cost-effective improvements are shown to be viable and beneficial to the operation of these systems. These upgrades may be incrementally introduced into existing systems in order to provide a complete refurbishment without large associated overheads.

The research topics presented in this dissertation to realize these goals include: substituting list mode data acquisition and analysis for shift register-based analysis, which enables simultaneous multichannel data acquisition and an in-depth investigation into the behavior and performance of the system; the testing, evaluation, and optimization of preamplifiers designed at ORNL as implemented on a Uranium Neutron Collar; using an advanced system design to perform 18 channel count-rate-based spatial response measurements; diagnosing and quantifying double pulsing in currently-used preamplifiers; calculating dead time for systems, with and without double pulsing, and for an increasing number of preamplifiers, using more physics-based approaches; and using these technologies to expand the applications of neutron coincidence counters to include absolute source measurements that allow for source certifications with a <1% relative standard deviation, a precision surpassing that of national metrological laboratories such as the National Institute of Standards and Technology.

A majority of the research presented here was in direct support of, or inspired by work performed for, a Department of Energy National Nuclear Security Administration Defense Nuclear Nonproliferation Research and Development funded project, the "List Mode Response Matrix for Advanced Correlated Neutron Analysis for Nuclear Safeguards." The new List Mode Response Matrix method provided an avenue for the study of the use of LMDA, modern electronics, and advanced measurement procedures, with a focus on source positioning location using a maximum number of counter system channel outputs.

During the first stage of this project, the use of the commercial-off-the-shelf PTR-32 LMDA was evaluated with the Mirion Technologies (Cannerra), Inc. JCC-71 UNCL [30]. A translatable counting system characterization procedure was developed here, for the first time, using LMDA. This involved work which expanded upon current traditional neutron coincidence counting characterization procedures, theory, and equations that the field is accustomed to, meanwhile exploiting the greater information revealed through LMDA for a detailed representation of system behavior. Through this research, it was shown that this procedure is compatible with traditional analysis methods performed, and ensures that the results acquired have the same, if not more precise, results as shift register-based analysis methods.

LMDA can also be used to gain more in-depth understanding of the system performance through individual channel characterizations as well. This LMDA procedure and analysis is published in a peer reviewed journal article in Nuclear Instruments and Methods in Physics Research Section A: Accelerators, Spectrometers, Detectors and Associated Equipment (NIM A).

Parameters such as coincidence time windows, dead time, efficiency, die-away time, and non-ideal double pulsing were explored in new ways through detailed analysis of the neutron pulse train using LMDA, that are not possible using traditional shift register logic due to the prespecified timing windows and number of signal inputs. This permits a high-fidelity physics-based understanding of these systems with a detailed representation of all the characterization parameters and their sources of error across all system channels.

This characterization analysis also led to the diagnoses of several non-ideal behaviors within the A111 preamplifier electronics present in most neutron coincidence counting systems, and the PTR-32 module. A HV instability was found within the PTR-32 module, which influences the measured count rates if insufficient filtering is present within the counting electronics. Double pulsing was measured in the Mirion Technologies JAB-01 preamplifier/amplifier/discriminator boards across different neutron coincidence counting systems, as well as in the Antech N2071 UNCL implementing the Amptek A111 chip, for a range of high voltage (HV) settings— including the operational HV in the UNCLs. Double pulsing falsely elevates the measured count rate and will affect a nondestructive assay measurement in addition to characterization and calibration measurements. Here, the source of this behavior was isolated to the A111 for the first time and new methods for diagnosing and quantifying this behavior in a system are provided using both LMDA and shift register–based analysis. These findings are presented in two other journal articles within NIM A.

During the second stage of the List Mode Response project, new preamplifiers were tested, evaluated, and optimized using the appropriate coincidence counting procedures and software. It was shown through extensive testing that these ORNL prototype boards match the performance of the JAB-01 board when used within the UNCL, can be made to fit within the existing counter footprint, are translatable and scalable to other neutron coincidence counting systems with few modifications (as verified with the evaluation of a prototype for a coincidence system implemented at the ORNL High Flux Isotope Reactor Neutron Activation Analysis laboratory), and do not contain double pulsing within the operational HV settings. These electronics may then be a suitable alternative to the JAB-01 or A111.

Count rate–based spatial response measurements were then successfully performed using the modified JCC-71 with the prototype electronics and a ^{252}Cf source. The 18 channel outputs were analyzed using PTR-32 for various source placements and compared to an MCNP simulation. The simulation results were used to show the physical performance of the simulated JCC-71 was in agreement with the true physical system, despite source certificate uncertainties, such that this simulation may be used as a benchmark after further optimization.

In addition, neutron coincidence counters have successfully been used to self–certify ^{252}Cf sources at ORNL with a precision surpassing that of national metrological laboratories using LMDA methods for the first time. Previously much more efficient multiplicity counters, with an order of magnitude less dead time, were used at LANL to perform these measurements. The experimental procedures, analysis methods, and results described for these absolute source measurements may expand the application of neutron coincidence counters and assist with addressing nuclear data uncertainty concerns. With a better understanding of the influence of dead time on the neutron pulse train, the precision of these certifications may be improved even further.

Currently, list mode capabilities are not being fully utilized in safeguards neutron coincidence counting systems or by corresponding analysis methods. LMDA is only used in research and laboratory environments and is not routinely used in the field by nuclear safeguards inspectors. With these new developments presented throughout this dissertation it is possible that LMDA may be more easily adopted for international safeguards inspection applications, and the additional capabilities of these analysis

procedures may be exploited for further advancement of these systems. Ultimately, the combination of these improvements and discoveries help achieve the goals of modernizing the field of neutron coincidence counting in a cost-effective manner. The research problems addressed throughout this work help reconcile the current limitations facing both inspectors and researchers and lead to further avenues for development and expansion of the relevance of neutron coincidence counting beyond international safeguards applications.

8.1 Recommendations for Future Work

8.1.1 Absolute Source Measurements

The ability to self-certify any neutron source using a neutron coincidence counter and LMDA, as an extension of the absolute source method presented here for ^{252}Cf sources, would make system calibrations for NDA measurements more straightforward because representative source standards are not easily accessible in either inspection applications or laboratory settings. By having a ^{240}Pu source standard with a neutron output known to $\pm 1\%$, the efficiency of a neutron coincidence counting system no longer needs to be calibrated using a ^{252}Cf standard and then scaled for a ^{240}Pu source response using known nuclear data (energy spectra and multiplicity distributions). This allows the NDA calibration procedure, using the point kinetic equations, to be independent of any associated nuclear data uncertainties that often contribute to an overall measurement. The absolute source method may therefore be extended to self-certify well-known ^{240}Pu sources in future work. The absolute source method may be applied to certifying other neutron sources as well, based on interest.

8.1.2 The List Mode Response Matrix

Although the work presented in this dissertation provides a successful experimental proof of concept, in order to complete the List Mode Response Matrix project goals, a second phase will be necessary. This phase will have a strong computational focus including machine learning and sizeable MCNP components in order to accurately develop a library of fresh fuel pin diversion scenarios such that a measurement could, in live time, correlate decreased count rates with a localized position within a complex assembly related to the diversion. This will also require the development of an external pulse train processing code that can efficiently perform all combinations of channel logic coincidences in software. Then, the measured matrix will have to be compared to the simulated expected matrix for that particular fresh fuel assembly and measurement condition, to compare if there is a localized difference in count rate. The minimum detectable differences will also have to be studied for their application and relevance.

8.1.3 A New List Mode Data Acquisition System

Through the extensive use and study of the PTR-32 LMDA module for this work, it has become evident that it will be necessary to either improve the current, or design a new, LMDA module. Several significant shortcomings of the PTR-32 hardware and software were revealed in different facets of its use and testing. Currently, PTR-32 is the only IAEA-approved LMDA hardware and software. Although there are several other functioning in-house LMDA modules, such as the List Mode Multiplicity Module [38] at LANL, many are laboratory-specific, and are not well documented for use, nor commercially available. Over the duration of this research more LMDA modules have been under development, such as

the Antech N2000 Universal Neutron Counter [108]; however, none of which have been characterized alongside the PTR-32, nor any shift register, for performance testing and none have yet been approved for use by the IAEA. Unfortunately, due to the untimely death of PTR-32's designer, Jozef Huszti, it is uncertain at this time if the company will maintain his work and continue to make improvements on this module in collaboration or not.

First and foremost, it is imperative to have sufficient documentation regarding a data acquisition module and its affiliated software. There were many instances during the use of PTR-32 where questions would arise regarding its capabilities and the actual mathematics surrounding an analysis subroutine in its software. Oftentimes this would result in directly contacting Dr Huszti. As discovered in Chapter 3, the HV supply provided by PTR-32 is unstable. When used with a system with minimal filtering, the instabilities become evident and clearly interfere with the measured neutron signal. Although current JAB-01 boards appear to have sufficient filtering that make them immune to the fluctuations in HV during a measurement, this behavior is not acceptable for a commercialized system. The hypothesized Cockcroft-Walton circuit providing the HV could be replaced by a more stable design. There are other deficiencies in the analysis subroutines, ranging from simple limitations such as file path input lengths to complex limitations such as the user manipulation required to unfold, subtract, or place in logic coincidence, individual channel neutron pulse trains. In addition, there are several supplemental functions and features of analyses that would benefit the community and expand the applications of LMDA. This would incorporate the work of an electrical engineer to design the circuitry, a neutron coincidence counting expert to outline all of the mathematics and analysis procedures that the module must accomplish, and a computer scientist who can efficiently program and execute these analyses into routines and subprograms within a user-friendly software. This prototype would then need to undergo extensive testing and evaluation for robustness and completeness compared to other LMDA modules.

8.1.4 Modern Electronics and Advanced System Designs

The prototype electronics presented here may undergo further development such that they could be readily adopted into preexisting systems without a large overhead burden. Since they rely on modern commercial-off-the-shelf products, they are easily accessible and are designed to be affordable. In doing so, the more preamplifiers used in a system, the smaller the ^3He tube groupings, and the more detailed information may be obtained of a system's performance in a characterization and calibration measurement. Then, using these advanced system designs, neutron coincidence counting may be more widely applied to measure complicated items, with better calibration procedures; ultimately leading to improved performance and spatial response measurements. In addition, the more preamplifiers used, the shorter the system dead time. This will effectively improve system efficiencies without modifications to the system geometry, as more counts can be recorded due to less loss. More dead time simulation, from physics first principles, will be necessary to quantitatively assess these improvements and evaluate how best to characterize this parameter fundamentally.

8.1.5 Dead Time Modelling Using Monte Carlo Simulation Codes

To first perform a reliable dead time simulation benchmark, it must be established that double pulsing will not be present. Once this is established, various dead time models and correction factors may be studied by applying them individually to a simulated neutron pulse train response. The simulated data can be compared to experimental data taken with the system to determine which model, if any, fully represents the physical behavior of the system. Once the correct model can be verified, successful corrections may be applied to the pulse train. Then, these simulation platforms may be modified to include a double pulsing contribution, in addition to a dead time contribution, to propagate through to the analysis. This would hopefully encompass the full behavior expected to be measured in a system and

provide a simulation benchmark to accurately characterize any neutron coincidence counting system's dead time prior to an NDA measurement—whether it contains double pulsing or not.

MCNP is the “gold standard” simulation package for safeguards studies. The source–counter interaction, including nuclear fission probabilities, neutron thermalization and the successive particle tracks throughout a volume can be simulated and the results reported in a readable format. The code depends on the correct geometry input, source definitions, and specified tallies. For neutron coincidence counters, spontaneous and induced fission sources may be included in the source definitions using nuclear data libraries, and the ^3He capture physics is modeled using the correct physics cards and system geometry across a wide variety of systems. Tallies can then be produced that indicate the desired interaction in the system, which can be related to the measured coincidence rates using timing windows. However, MCNP does not account for detector electronics effects, reporting answers assuming perfect electronics.

There have been several efforts over previous decades to develop and test various Monte Carlo codes for the applicability to neutron coincidence counter measurements [109] [110] [111] [112] [113] [114] [115] [116]. These various platforms seek to be directly compatible with MCNP while also introducing additional data and capabilities that are directly applicable to neutron coincidence counting for safeguards. They pair the preexisting capabilities and reliability of MCNP to simulate the neutron radiation transport within the sample plus detector system with external codes that allow simulation and analysis of this response into neutron pulse train data. These external codes, named differently across these various projects, have similar goals and functionalities. They may provide easily referenced multiplicity distribution nuclear data for ^{252}Cf and ^{240}Pu spontaneous fission sources for direct inclusion into the input file, and also incorporate the influence of the electronics pulse processing behavior on the pulse train. These data are then analyzed as they would be experimentally using shift register or LMDA logic with relevant timing windows. The success of these codes has been tested across their niches, but the platforms have not become readily available to the general safeguards community.

In more recent years, an example of a combination Monte Carlo code, the MCNP-PTA (Pulse Train Analysis) [115] [116] has been created and evaluated across various neutron coincidence counting systems. It adds a special module to MCNP to enable neutron coincidence counting while including the complete distributions of the neutron number probability to improve simulation precision to experimental values. It then uses the output from a successful MCNP run to form a Pulse Information File which is read into the Pulse Train Analysis file for final analysis. Here within the PTA the neutron pulse train is created. The program calculates the dead-time losses created through the electronic pulse processing chain, and finally performs the neutron analysis using predelays and gate widths for a direct comparison. The MCNP-PTA has been compared and its performance verified with experimentally obtained values obtained with various counters and sources: fresh fuel assemblies in a JCC-73 Collar and a low enriched uranium standard [115], MOX fuel assemblies, AWCC, and a High Efficiency Passive Counter [116]. However, the MCNP-PTA is used in-house at the JRC on their respective cluster and is not openly used across the community for similar simulations.

An MCNPX input deck paired with a bespoke C++ pulse analysis code were used and reported in [117] for dead time studies. The combination of the MCNPX PTRAC output analysis, and the C++ pulse train analysis/ shift register simulator, allowed the author to overlay perturbations on the simulated pulse train using a single system dead time parameter, according to the chosen model. This analysis was done considering either the paralyzable and non-paralyzable dead time models. New dead time correction approaches were also studied through these simulations, which would benefit the discussion in Section 7.2. Ultimately, the author suggests future areas of work with her code could address multiple channel analysis as would be available in the multi preamplifier neutron coincidence counter and ^3He pulse shape variation that would encompass double pulsing effects. These suggestions echo the needs that this dissertation outlines for future study and quantification.

The codes discussed here are not exhaustive of the efforts put forward by the community. Some of these codes may no longer be supported due to the new versions of MCNP. As discussed in [117], the ESARDA NDA working group held several benchmark exercises for the community to develop and test

the performance of various pulse train analyses programs, and additional work is consistently ongoing to better represent the dead time parameters for a system through theory and experimental analysis. MCNP is continuously improved, and in-house codes are made to address certain research challenges. However, the development and evaluation of these complete codes have formed several scientists' dissertations and various teams of scientist's efforts over years of work. Therefore, it is evident that further development of these codes, with the inclusion of double pulsing effects connected to dead time simulation, would require a lengthy effort and should be considered for future work. These particular codes are discussed here as feasible platforms to build this extended analysis from.

Alternative Monte Carlo codes have also been developed to perform similar analyses to MCNP. A program has been written by ORNL scientist Scott Stewart to address part of this challenge for safeguards. The Monte Carlo Simulator of Point Model Neutrons (MASTODON) Software Application [118] was written as a means to easily use the point model assumption of neutron behavior in a counter, for appropriate neutron sources, to generate a neutron list mode pulse train. Paired with the source specifications and system characterization parameters, the user may define input probabilities of various interactions based on the source desired. Multichannel systems with individual preamplifiers can be simulated individually, with known parameters, and included in the pulse train output. This software builds on the work of a previous application called Simple Neutron Simulation that LANL used to simulate pulsed neutron data [119]. In order to read out the neutron pulse train, an additional external code is needed to apply the appropriate timing windows for analysis. The simulated pulse train can then be compared externally with the measured neutron pulse train to draw comparisons in the external pulse processing code.

MASTODON outputs a neutron pulse train in a shorter time duration than full neutron transport codes. It also does not require extensive input decks, but rather user specified parameters that can be obtained from experimental setups and easily accessible nuclear data. It can be used in implementations where the application could still be studied using a point model assumption of neutron behavior, and it is not intended to serve as a replacement for MCNP simulations, but instead as an alternative simulation tool for the applications where the robustness of the codes is not needed. For the relevance to this section, MASTODON's primary purpose was to further the exploration and understanding of dead-time phenomena in neutron counting for safeguards applications. Currently, as it sits, MASTODON would need modifications to the code in order to allow for in depth analysis of dead time effects throughout the pulse train. Currently, the user inputs a set dead time value which is then applied to the program's analysis using the non-paralyzable assumption of dead time. It does not incorporate double pulsing contributions in its analysis.

Geometry and Tracking (GEANT) is another Monte Carlo simulation package that is more widely used outside of the field of nuclear safeguards, for in depth object-oriented radiation simulations [120]. GEANT is open source and based on C++ coding, with a more complex user interface than MCNP as essentially every parameter may be specified and modified by the user. It allows for simulating the passage of particles through matter through a range of functionality including tracking, geometry, physics models, and hits. The physics of the particle creations, interactions, captures, and digitizations are all incorporated in the code. However, the user must provide their own analysis of the detector response, specific to their electronics used, the application of their work, and the successive information desired. Here, it may be possible to include electronic artifacts in the final simulation output response, but the complex nature of GEANT is often a deterrent for more basic counter system modeling and performance testing.

Each of these codes may be possible avenues for future modification and in-depth studies of both the correct dead time analysis method, and the effect of double pulsing paired with dead time effects on the resulting neutron pulse train. Other platforms not discussed here may also be suitable with proper tailoring. With the ability to simulate the full lifetime of a neutron event within a neutron coincidence counter, from birth from the source to thermalization, capture, electronic pulse processing, and final record on the neutron pulse train, simulated data can be directly compared to experimental data taken. The RADs may be compared through this analysis, and the neutron pulse trains resulting from different dead

time approaches and models may be studied to determine the model that best represents these systems, independent of double pulsing effects. This behavior would then be grounded in physics first principles and not reliant on empirical methods. Then, the analysis could be extended to include the convolution between dead time effects and double pulsing effects. Having the additional ability to simulate multiple neutron pulse trains, for the multichannel preamplifier systems, allows an estimation of the optimal number of preamplifiers for the system to minimize dead time losses during a NDA.

References

- [1] G.F. Knoll, Radiation detection and measurement, John Wiley & Sons 2010.
- [2] J. Leake, S. Croft, R. McElroy, K. Lambert, Optimizing ³He tube design for various operational conditions: A review of the design parameters of ³He gas proportional counters used for neutron detection, Proceedings of the INMM 46th Annual Meeting, Phoenix, AZ, 2005.
- [3] M. Iliev, C.W. Mc Cluskey, D. Henzlova, M.R. Newell, H. Nguyen, K.D. Ianakiev, Study of the front end electronics contribution to the dead time in He3 proportional counters, Los Alamos National Laboratory 2011.
- [4] N. Ensslin, W.C. Harker, M.S. Krick, D.G. Langner, M.M. Pickrell, J.E. Stewart, Application guide to neutron multiplicity counting, Los Alamos Report LA-13422-M, (1998).
- [5] N. Ensslin, Principles of neutron coincidence counting, Passive Nondestructive Assay of Nuclear Materials, 1991, pp. 457.
- [6] IKI, Russian neutron detector HEND for the NASA space mission 2001 Mars Odyssey, Nuclear Planetology Department No63 <https://np.cosmos.ru/en-us/instruments/hend>.
- [7] N. Pacilio, REACTOR-NOISE ANALYSIS IN THE TIME DOMAIN. AEC Critical Review Series, Argonne National Lab., Ill. Comitato Nazionale per l'Energia Nucleare, Rome ..., 1969.
- [8] Safeguards Techniques and Equipment, International Atomic Energy Agency, 2003.
- [9] Safeguards Techniques and Equipment. , International Atomic Energy Agency, 2011.
- [10] R.D. McElroy, Private communication, 2019.
- [11] D. Reilly, K. Smith, Passive Nondestructive Assay Manual, Los Alamos National Laboratory Safeguards Science Technology Group, (1991).
- [12] B. Harker, M. Krick, INCC software users manual, Los Alamos National Laboratory, LA-UR-99-1291 (1998).
- [13] Passive Neutron Coincidence and Multiplicity Counting Techniques, Los Alamos National Laboratory, 2019.
- [14] H.A. Smith, The Measurement of Uranium Enrichment, Passive Nondestructive Assay of Nuclear Materials, (1991) 195.
- [15] Measurements of BWR Fuel Assemblies, Los Alamos National Laboratory, LA-UR-12-00574, 2019.
- [16] The Statute of the IAEA, International Atomic Energy Agency, <https://www.iaea.org/about/statute#a1-22>.
- [17] International Nuclear Verification Series 2, International Atomic Energy Agency, https://www-pub.iaea.org/MTCD/Publications/PDF/NVS2_web.pdf.
- [18] Treaty on the Non-Proliferation of Nuclear Weapons (NPT), United Nations Office for Disarmament Affairs, <https://www.un.org/disarmament/wmd/nuclear/npt/text>.
- [19] INFCIRC/153 (Corrected), International Atomic Energy Agency, <https://www.iaea.org/sites/default/files/publications/documents/infcircs/1972/infcirc153.pdf>.
- [20] Nuclear-Weapon-Free-Zones, International Atomic Energy Agency, <https://www.iaea.org/topics/nuclear-weapon-free-zones>.
- [21] S. Ciccarello, S. Lechner, Euratom Safeguards System, Springer Berlin Heidelberg, Berlin, Heidelberg, 2018, pp. 63-68.
- [22] Basics of IAEA Safeguards, International Atomic Energy Agency, <https://www.iaea.org/topics/basics-of-iaea-safeguards>.
- [23] IAEA Safeguards Serving Nuclear Non-Proliferation, International Atomic Energy Agency, https://www.iaea.org/sites/default/files/safeguards_web_june_2015_1.pdf, 2015.
- [24] STATUS LIST Small Quantities Protocols amendments, International Atomic Energy Agency, <https://www.iaea.org/sites/default/files/19/05/sg-sqp-status.pdf>, 2019.
- [25] Stages of the Nuclear Fuel Cycle, United States Nuclear Regulatory Commission, <https://www.nrc.gov/materials/fuel-cycle-fac/stages-fuel-cycle.html>.
- [26] J. Sprinkle, Total Neutron Counting Instruments and Applications, Passive Nondestructive Assay of Nuclear Materials, 1991, pp. 435.
- [27] International Nuclear Verification Series, International Atomic Energy Agency, <http://www-pub.iaea.org/books/IAEABooks/Series/100/International-Nuclear-Verification-Series>.

- [28] Mirion Technologies, <https://www.mirion.com/products>.
- [29] Antech Inc., <http://www.antech-inc.com/products/>.
- [30] Model JCC-71 Coincidence Counter Hardware Reference Manual, Mirion Technologies 2011.
- [31] A111 Charge Sensitive Preamplifier & Discriminator, Amptek X-Ray Detectors and Electronics, <https://amptek.com/products/a111-charge-sensitive-preamplifier/#4>.
- [32] Model N2071 Neutron Coincidence Collar, AnTech Inc, 2018.
- [33] Model JCC-51 Active Well Neutron Coincidence Counter, Mirion Technologies, 2009.
- [34] A.T. Simone, S. Croft, R.D. McElroy, L. Sun, J.L. Lacy, A. Athanasiades, J.P.J.I.T.o.N.S. Hayward, Performance of a Boron-Coated-Straw-Based HLNCC for International Safeguards Applications, 64 (2017) 2690-2697.
- [35] J.E. Swansen, Deadtime reduction in thermal neutron coincidence counter, Nuclear Instruments Methods in Physics Research Section B: Beam Interactions with Materials and Atoms, 9 (1985) 80-88.
- [36] Safeguards implementation in helping prevent the spread of nuclear weapons, International Atomic Energy Agency, <https://www.iaea.org/sites/default/files/18/04/sg-implementation-2017.pdf>, 2017.
- [37] J. Huszti, Development of a Pulse-Train Recorder for Safeguards, 2015.
- [38] D.C. Henzlova, H.O. Menlove, M.T. Swinhoe, J.B. Marlow, I.P. Martinez, C.D. Rael, Neutron data collection and analysis techniques comparison for safeguards, Los Alamos National Laboratory, 2010.
- [39] S.L. Cleveland, S. Croft, R.D. McElroy, J.A. Chapman, Comparison of Pulse Train Recorder Module (PTR) and shift register multiplicity measurements using the Large Active Well Coincidence Counter (LV-AWCC), 56th Annual Meeting of the Institute of Nuclear Materials Management, Indian Wells, CA, USA, 2015.
- [40] J. Bagi, L. Dechamp, P. Dransart, Z. Dzbikowicz, J.-L. Dufour, L. Holzleitner, J. Huszti, M. Looman, M.M. Ferrer, T. Lambert, Neutron coincidence counting with digital signal processing, Nuclear Instruments Methods in Physics Research Section A: Accelerators, Spectrometers, Detectors and Associated Equipment, 608 (2009) 316-327.
- [41] P. Peerani, M.J.E.B. Swinhoe, ESARDA Multiplicity Benchmark Exercise Final report-February 2006, 34 (2006) 2.
- [42] P. Peerani, M. Swinhoe, A. Weber, L.J.E.B. Evans, ESARDA Multiplicity Benchmark Exercise Phases III and IV, 42 (2009) 2-25.
- [43] R. McElroy, S. Croft, Comparison of list mode data acquisition and shift register measurements using the large epithermal neutron multiplicity counter (LEMC), Journal of Radioanalytical Nuclear Chemistry, 276 (2008) 725-730.
- [44] D. Henzlova, H.O. Menlove, M.T. Swinhoe, C.D. Rael, I.P. Martinez, J.B. Marlow, Epithermal neutron multiplicity counter (ENMC)-summary of measurement results, LA-UR-10-07089, Los Alamos National Laboratory, 2010.
- [45] D. Henzlova, H.O. Menlove, C.D. Rael, H.R. Trelue, S.J. Tobin, S.-H. Park, J.-M. Oh, S.-K. Lee, S.-K. Ahn, I.-C. Kwon, Californium interrogation prompt neutron (CIPN) instrument for non-destructive assay of spent nuclear fuel—Design concept and experimental demonstration, Nuclear Instruments Methods in Physics Research Section A: Accelerators, Spectrometers, Detectors and Associated Equipment, 806 (2016) 43-54.
- [46] A.M. LaFleur, S.-K. Ahn, H.O. Menlove, M.C. Browne, H.-D. Kim, Characterization and performance evaluation of a new passive neutron albedo reactivity counter for safeguards measurements, Radiation Measurements, 61 (2014) 83-93.
- [47] D. Henzlova, H.O. Menlove, S. Croft, A. Favalli, P. Santi, The impact of gate width setting and gate utilization factors on plutonium assay in passive correlated neutron counting, Nuclear Instruments Methods in Physics Research Section A: Accelerators, Spectrometers, Detectors and Associated Equipment, 797 (2015) 144-152.

- [48] K.E. Koehler, V. Henzl, S. Croft, D. Henzlova, P.A. Santi, Characterizations of double pulsing in neutron multiplicity and coincidence counting systems, *Nuclear Instruments Methods in Physics Research Section A: Accelerators, Spectrometers, Detectors and Associated Equipment*, 832 (2016) 279-291.
- [49] S. Croft, A. Favalli, D. Hauck, D. Henzlova, P.A. Santi, Feynman variance-to-mean in the context of passive neutron coincidence counting, *Nuclear Instruments Methods in Physics Research Section A: Accelerators, Spectrometers, Detectors and Associated Equipment*, 686 (2012) 136-144.
- [50] L. Holzleitner, M.T. Swinhoe, Dead-time correction for any multiplicity using list mode neutron multiplicity counters: A new approach—Low and medium count-rates, *Radiation Measurements*, 46 (2011) 340-356.
- [51] H.O. Menlove, S. Menlove, S. Tobin, Fissile and fertile nuclear material measurements using a new differential die-away self-interrogation technique, *Nuclear Instruments Methods in Physics Research Section A: Accelerators, Spectrometers, Detectors and Associated Equipment*, 602 (2009) 588-593.
- [52] X. Wen, J.G. Kavouras, D.R. Nakazawa, H. Yang, Simulation and measurement of delayed γ -rays after photon-induced fission, *Nuclear Instruments Methods in Physics Research Section A: Accelerators, Spectrometers, Detectors and Associated Equipment*, 729 (2013) 781-787.
- [53] M. Tornai, L. MacDonald, C. Levin, S. Siegel, E. Hoffman, Design considerations and initial performance of a 1.2 cm/sup 2/beta imaging intra-operative probe, *IEEE Transactions on Nuclear Science*, 43 (1996) 2326-2335.
- [54] A.J. Reader, S. Ally, F. Bakatselos, R. Manavaki, R.J. Walledge, A.P. Jeavons, P.J. Julyan, S. Zhao, D.L. Hastings, J. Zweit, One-pass list-mode EM algorithm for high-resolution 3-D PET image reconstruction into large arrays, *IEEE Transactions on Nuclear Science*, 49 (2002) 693-699.
- [55] C. Churms, J. Pilcher, K. Springhorn, U. Tapper, A VAX and PC-based data acquisition system for MCA, scanning and list-mode analysis, *Nuclear Instruments Methods in Physics Research Section B: Beam Interactions with Materials and Atoms*, 77 (1993) 56-61.
- [56] M.K. Khamzin, J.D. Valentine, A list-mode time stamping data acquisition module prototype for coincidence measurements, *IEEE Transactions on Nuclear Science*, 48 (2001) 570-574.
- [57] R. Kumar, M.Y. Ali, S. Degweker, S. Vishwasrao, R. Jadhav, Development and testing of neutron pulse time stamping data acquisition system for neutron noise experiment, *Nuclear Instruments Methods in Physics Research Section A: Accelerators, Spectrometers, Detectors and Associated Equipment*, 770 (2015) 8-13.
- [58] A. Oberstedt, F.-J. Hamsch, LISA—a powerful program package for Listmode and spectral data analysis, *Nuclear Instruments Methods in Physics Research Section A: Accelerators, Spectrometers, Detectors and Associated Equipment*, 340 (1994) 379-383.
- [59] W. Wagner, MPA4T, FAST ComTec—The worldwide leader in photon and ion counting technologies, <https://www.fastcomtec.com/products/mpa/mpa4t0/>.
- [60] JSR-15 Handheld Multiplicity Register (HHMR), Mirion Technologies, <https://www.mirion.com/products/jsr-15-handheld-multiplicity-register-hhmr>, 2017.
- [61] K. Böhnelt, The effect of multiplication on the quantitative determination of spontaneously fissioning isotopes by neutron correlation analysis, *Nuclear Science Engineering*, 90 (1985) 75-82.
- [62] W. Hage, D.M. Cifarelli, Correlation analysis with neutron count distributions in randomly or signal triggered time intervals for assay of special fissile materials, *Nuclear Science Engineering*, 89 (1985) 159-176.
- [63] D.M. Cifarelli, W. Hage, Models for a three-parameter analysis of neutron signal correlation measurements for fissile material assay, *Nuclear Instruments Methods in Physics Research Section A: Accelerators, Spectrometers, Detectors and Associated Equipment*, 251 (1986) 550-563.
- [64] H.O. Menlove, Description and performance characteristics for the neutron coincidence collar for the verification of reactor fuel assemblies, LA-8939-MS, Los Alamos National Laboratory, 1981.

- [65] P. Henriksen, H. Menlove, J. Stewart, S. Qiao, T. Wenz, G. Verrecchia, Neutron collar calibration and evaluation for assay of LWR fuel assemblies containing burnable neutron absorbers, LA-11965-MS, Los Alamos National Laboratory, 1990.
- [66] H. Menlove, C. Rael, K. Kroncke, K. DeAguero, Manual for the epithermal neutron multiplicity detector (ENMC) for measurement of impure MOX and plutonium samples, LA-14088, Los Alamos National Laboratory, 2004.
- [67] S. Croft, M.T. Swinhoe, V. Henzl, A priori precision estimation for neutron triples counting, *Advancements in Nuclear Instrumentation, Measurement Methods and their Applications (ANIMMA)*, IEEE, 2011, pp. 1-7.
- [68] Neutron counter checklist report, Canberra Industries, 2016.
- [69] N. Mena, S. Croft, S. Kane, S. Philips, M. Villani, L. Evans, Experimental determination of the multiplicity deadtime parameter, *Waste Management Symposia*, Tempe, AZ, 2008.
- [70] M.S. Krick, H.O. Menlove, High-level neutron coincidence counter (HLNCC): users' manual, LA-7779-M, Los Alamos National Laboratory, 1979.
- [71] A.T. Simone, J. Hayward, S. Croft, A. Favalli, A Comparison of Approaches to Determine Dead Time Parameters Using a Boron-Coated-Straw High-Level Neutron Coincidence Counter, *ESARDA Bulletin*, 54 (2017) 6-13.
- [72] S. Croft, L.G. Evans, M.T. Swinhoe, D.K. Hauck, P.A. Santi, Testing a alternative singles rate dead time correction algorithm for use in neutron multiplicity analysis, LA-UR-11-03761, Los Alamos National Laboratory, 2011.
- [73] S. Croft, S. Cleveland, A. Favalli, R.D. McElroy Jr, A.T. Simone, Estimating the effective system dead time parameter for correlated neutron counting, *Nuclear Instruments Methods in Physics Research Section A: Accelerators, Spectrometers, Detectors and Associated Equipment*, 871 (2017) 154-160.
- [74] PDT 110A, Precision Data Technology, <http://www.pdt-inc.com/products/100series/110a.htm>.
- [75] M. Iliev, K.D. Ianakiev, M.T. Swinhoe, KM200 Front-End Electronics for Thermal Neutron Detectors, INMM 57th Annual Meeting, 2016.
- [76] A. Fazzi, C. Pirovano, V. Varoli, A novel electronic chain for high level neutron coincidence counters, *IEEE Transactions on Nuclear Science*, 44 (1997) 557-562.
- [77] C.L. Britton, M.N. Ericson, Private communication, 2018.
- [78] J. Huszti, Private communication, 2018.
- [79] Cockcroft–Walton generator, Wikipedia, https://en.wikipedia.org/w/index.php?title=Cockcroft%E2%80%93Walton_generator&oldid=888009536.
- [80] MCNP6 Users Manual Version 1.0, LA-CP-13-00634, Los Alamos National Laboratory, 2013.
- [81] P. Peerani, A.-L. Weber, Analysis of uncertainties affecting the Monte Carlo simulation of a neutron multiplicity counter, *Radiation Measurements*, 47 (2012) 475-480.
- [82] Large Active Well Counter Hardware Reference Manual, Los Alamos National Laboratory, 1998.
- [83] T.C. Nguyen, J. Huszti, Q. Van Nguyen, Effect of double false pulses in calibrated neutron coincidence collar during measuring time-correlated neutrons from PuBe neutron sources, *Nuclear Instruments Methods in Physics Research Section B: Beam Interactions with Materials and Atoms*, 358 (2015) 168-173.
- [84] N. Dytlewski, N. Ensslin, J. Boldeman, A neutron multiplicity counter for plutonium assay, *Nuclear Science Engineering*, 104 (1990) 301-313.
- [85] A. Fazzi, V. Varoli, Signal shaping optimization with ³He tubes in high rate neutron counting, *IEEE Transactions on Nuclear Science*, 46 (1999) 342-347.
- [86] N. Roberts, L. Jones, Z. Wang, Y. Liu, Q. Wang, X. Chen, H. Luo, C. Rong, M. Králik, H. Park, International key comparison of measurements of neutron source emission rate (1999–2005): CCRI (III)-K9. AmBe, *Metrologia*, 48 (2011).

- [87] S. Croft, D. Henzlova, Determining ^{252}Cf source strength by absolute passive neutron correlation counting, *Nuclear Instruments Methods in Physics Research Section A: Accelerators, Spectrometers, Detectors and Associated Equipment*, 714 (2013) 5-12.
- [88] D. Henzlova, A. Favalli, S. Croft, In-depth evaluation of ^{252}Cf absolute calibration by passive neutron correlation counting method, *Metrologia*, (2018).
- [89] A.T. Simone, S. Croft, J.P. Hayward, L.G. Worrall, Using the JCC-71 neutron coincidence collar as a benchmark for detector characterization with PTR-32 list mode data acquisition, *Nuclear Instruments Methods in Physics Research Section A: Accelerators, Spectrometers, Detectors and Associated Equipment*, 908 (2018) 24-34.
- [90] L.G. Evans, M.T. Swinhoe, S. Croft, D.K. Hauck, P.A. Santi, Extension of ESARDA NDA Multiplicity Benchmark, LA-UR-11-03052, Los Alamos National Laboratory, 2011.
- [91] H. Menlove, J. Swansen, A high-performance neutron time correlation counter, *Nuclear Technology*, 71 (1985) 497-505.
- [92] N. Dytlewski, Dead-time corrections for multiplicity counters, *Nuclear Instruments Methods in Physics Research Section A: Accelerators, Spectrometers, Detectors and Associated Equipment*, 305 (1991) 492-494.
- [93] S. Croft, A. Favalli, Extension of the Dytlewski-style dead time correction formalism for neutron multiplicity counting to any order, *Nuclear Instruments Methods in Physics Research Section A: Accelerators, Spectrometers, Detectors and Associated Equipment*, 869 (2017) 141-152.
- [94] W. Hage, D. Cifarelli, Correlation analysis with neutron count distribution for a paralyzing dead-time counter for the assay of spontaneous fissioning material, *Nuclear Science Engineering*, 112 (1992) 136-158.
- [95] D.K. Hauck, S. Croft, L.G. Evans, A. Favalli, P.A. Santi, J. Dowell, Study of a theoretical model for the measured gate moments resulting from correlated detection events and an extending dead time, *Nuclear Instruments Methods in Physics Research Section A: Accelerators, Spectrometers, Detectors and Associated Equipment*, 719 (2013) 57-69.
- [96] A.F. Para, M.M. Bettoni, Counting statistics of nuclear detectors, *Nuclear Instruments and Methods*, 70 (1969) 52-56.
- [97] Radioactive Neutron Sources Emission Rates, National Institute of Standards and Technology, Radiation Physics Division, <https://www.nist.gov/sites/default/files/documents/2016/10/18/procedure13v500.pdf>.
- [98] A.T. Simone, S. Croft, R.D. McElroy, J.P. Hayward, How to Calibrate a Neutron Correlation Counter: Let Us Count the Ways, 59th Annual Institute of Nuclear Materials Management, Baltimore, MD, 2018.
- [99] S. Croft, Private communication, 2019.
- [100] M.S. Zucker, N.E. Holden, Parameters for several plutonium nuclides and ^{252}Cf of safeguards interest, *ESARDA Bulletin*, 17 (1984) 341-353.
- [101] N.E. Holden, M.S. Zucker, Prompt neutron emission multiplicity distribution and average values (Nubar) at 2200 m/s for the fissile nuclides, *Nuclear Science Engineering*, 98 (1988) 174-181.
- [102] S. Cox, P. Fields, A. Friedman, R. Sjoblom, A. Smith, Delayed Neutrons from the Spontaneous Fission of Cf ^{252} , *Physical Review A*, 112 (1958) 960.
- [103] A. Smith, P. Fields, A. Friedman, S. Cox, R. Sjoblom, An experimental study of fission in the actinide elements, 2nd International Conf. on the Peaceful Uses of Atomic Energy, United Nations, NY, 1958, pp. 392-397.
- [104] S. Croft, L. Bourva, The measurement of passive neutron multiplicity counter gate utilisation factors and comparisons with theory, *Nuclear Instruments Methods in Physics Research Section A: Accelerators, Spectrometers, Detectors and Associated Equipment*, 453 (2000) 553-568.
- [105] J. Owen, D. Weaver, J. Walker, Neutron spectra from Am/F and Am/Li (α, n) sources, *Nuclear Data for Science and Technology*, Springer, 1983, pp. 492-494.
- [106] G.D. Spriggs, J.M. Campbell, A summary of measured delayed neutron group parameters, *Progress in Nuclear Energy*, 41 (2002) 145-201.

- [107] J. Terrell, Prompt neutrons from fission, LA-DC-6675, Los Alamos National Laboratory, 1964.
- [108] 04 Universal Neutron Counter, N2000 Series, Antech Inc, <http://www.antech-inc.com/products/n2000-series-universal-neutron-counter/>.
- [109] J. MacDonald, Monte Carlo neutronic and electronic model for thermal-neutron coincidence counting, Transactions of the American Nuclear Society, 32 (1979) 635.
- [110] J. Stewart, Hybrid monte carlo/analytical model of neutron coincidence counting, Transactions of the American Nuclear Society, 53 (1986) 149.
- [111] T.E. Valentine, J. Mihalcz, MCNP-DSP: A neutron and gamma ray Monte carlo calculation of source-driven noise-measured parameters, Annals of Nuclear Energy, 23 (1996) 1271-1287.
- [112] T. Valentine, J. Mihalcz, Validation of the Monte Carlo code MCNP-DSP, Annals of Nuclear Energy, 24 (1997) 79-98.
- [113] A. Dodaro, F. Frazzoli, R. Remetti, Passive Neutron Assay of Plutonium Materials: Monte Carlo Procedures to Simulate Generation of Neutron Pulse Trains and the Application of the Neutron Coincidence Counting Method, Nuclear Science Engineering, 130 (1998) 141-152.
- [114] M.E. Abhold, M.C. Baker, MCNP-REN: a Monte Carlo tool for neutron detector design, Nuclear Instruments Methods in Physics Research Section A: Accelerators, Spectrometers, Detectors and Associated Equipment, 485 (2002) 576-584.
- [115] M. Looman, P. Peerani, P. Schillebeeckx, An overview of NDA instruments modeled with the MCNP-PTA code at the JRC Ispra, 23rd ESARDA Symposium on Safeguards & Nuclear Material Management, Bruges, Belgium, 2001, pp. 8-10.
- [116] H. Tagziria, P. Peerani, Monte Carlo modelling of neutron coincidence counting systems for nuclear safeguards, International Conference on Mathematics, Computational Methods & Reactor Physics, Saratoga Springs, NY, 2009.
- [117] L.G. Evans, Pulse train analysis applied to the re-evaluation of deadtime correction factors for correlated neutron counting, University of Birmingham, 2009.
- [118] S.L. Stewart, A.T. Simone, A.D. Nicholson, S. Croft, M. Swinhoe, Overview of the Monte Carlo Simulator of Point Model Neutrons (MASTODON) Software Application, 57th Annual Institute of Nuclear Materials Management Meeting, Atlanta, GA, 2016.
- [119] S.L. Stewart, M.T. Swinhoe, J.L. Thron, W.H. Geist, W.S. Charlton, Monte Carlo Modeling of Correlations in Pulsed Neutron Data, 53rd Annual Meeting of the Institute of Nuclear Materials Management, 2012.
- [120] S. Agostinelli, J. Allison, K.a. Amako, J. Apostolakis, H. Araujo, P. Arce, M. Asai, D. Axen, S. Banerjee, G. Barrand, GEANT4—a simulation toolkit, Nuclear instruments methods in physics research section A: Accelerators, Spectrometers, Detectors and Associated Equipment, 506 (2003) 250-303.

Vita

Angela Simone Moore was born Angela Tiffany Simone on June 16, 1993 in North Bellmore, New York. She earned her B.A. in Physics and Astronomy at the State University of New York at Geneseo in 2015. There, she worked within the Nuclear Physics Research Group on a $^{12}\text{C}(n,2n)^{11}\text{C}$ nuclear cross section measurement for an inertial confinement fusion diagnostic and helped design and fabricate a time-resolved faraday cup for target normal sheath accelerated particles for use at the University of Rochester's Laboratory for Laser Energetics. Throughout this research she gained the knowledge and skills to perform accelerator-based measurements and in-depth radiation detection characterization methods. In 2015, she began graduate school at the University of Tennessee Knoxville in the Radiation Instrumentation Research Group. Over the next four years she conducted her dissertation research within the Safeguards and Security Technology Group at Oak Ridge National Laboratory on modernizing neutron coincidence counting technologies. The culmination of these studies is provided in this work. She is first author on five peer reviewed journal articles related to the work presented here, and coauthor on five other peer reviewed journal articles both related and unrelated to this dissertation.

As a graduate student at the University of Tennessee Knoxville she was selected as the 2018 recipient of the Nuclear Engineering Department's Masters Graduate Research Excellence Award and as a recipient of the 2019 Chancellor Extraordinary Professional Promise Citation.